UNIVERSITY OF CALGARY

Assessing Solute Sources and Chemical Weathering Reactions in the Kettle River Basin, British Columbia

by

Leslie Laura Harker

A THESIS
SUBMITTED TO THE FACULTY OF GRADUATE STUDIES
IN PARTIAL FULFILMENT OF THE REQUIREMENTS FOR THE
DEGREE OF MASTER OF SCIENCE

DEPARTMENT OF GEOSCIENCE

CALGARY, ALBERTA
JANUARY, 2012

UNIVERSITY OF
CALGARY

Abstract

The sources and processes influencing solutes in surface waters and groundwaters in the Kettle River Basin, British Columbia, were investigated using major ion concentrations, stable isotope abundance ratios and geochemical modeling. The atmosphere, biosphere, pedosphere, lithosphere and anthropogenic activities were identified as sources of solutes in surface water and groundwater. A mass balance approach was used to quantify the proportion of ions derived from weathering of silicate bedrock. Results indicated that bedrock weathering primarily releases calcium, magnesium and sulfate, and lesser amounts of sodium and potassium. Ion exchange reactions between clay minerals and solution were investigated and found to exhibit controls on major ion chemistry. Consumption of CO_2 during silicate weathering, storage and subsequent export of carbon out of the Kettle River Basin was quantified and compared to major global carbon reservoir and flux estimates suggesting that terrestrial silicate weathering is an important component of the carbon cycle.

Acknowledgements

I thank my co-supervisors, Ian Hutcheon and Bernhard Mayer for the tremendous amount of support I have received throughout this project. This project was funded by Natural Sciences and Engineering Research Council (NSERC) grants held by Ian Hutcheon and Bernhard Mayer.

I also thank Ilana Fraser and Ian Hutcheon for assistance in the field, and Colleen McCechan and Ian Hutcheon for accommodation and fine dining during field work. Thanks to the residents of the Kettle River Basin who volunteered to participate in this project, and allowed me to collect samples from their groundwater wells.

Thanks to all members of the Applied Geochemistry Group for answering my many questions. Thanks to Maurice Shevalier for technical support and to Michael Nightingale and staff in the Isotope Science Laboratory for laboratory support.

Thanks to great friends at the University of Calgary - Anita Gue, Leanne Cantafio, Bernadette Prömse and Josh Bishop who have helped to make my time in Calgary enjoyable. Special thanks to Anita and Leanne for many coffee breaks and bike rides.

I also thank my fabulous housemates, and many friends for many great adventures throughout this project. Finally, thanks to my family for your non-stop support and of course, thanks to Matt

Table of Contents

List of Tables

List of Figures

Chapter One: Introduction

1.1 The Kettle River Basin

This study focuses on the chemistry of surface water and groundwater in part of the Kettle River Basin, which is located in south-central British Columbia (BC), Canada. In recent years, residents have expressed concern about the state of water quantity and quality in the Kettle River Basin (Regional District of Kootenay Boundary, 2011). In 2010 and 2011, the Outdoor Recreation Council of BC ranked the Kettle River as the most endangered river in BC, based on lower than previously recorded discharge rates and a high number of surface water license applications (Outdoor Recreation Council of BC, 2011). Decreases in the quantity of water are often correlated with decreases in water quality (e.g. Whitehead et al., 2009), which can adversely influence ecosystem health (Vitousek et al., 1997) and drinking water quality (Babiker et al., 2004).

1.2 Previous Research and Project Rational

There are no peer reviewed publications on the geochemistry or hydrogeology of the Kettle River Basin. Areas directly west and east of the Kettle River Basin have been studied in greater detail to address either water supply or water contamination issues. The hydrogeology and geochemistry of the Grand Forks Aquifer, located to the east of the Kettle River Basin, has been studied to address nitrate contamination issues associated with agricultural practices (Wei et al., 1993; Wei et al., 2010). To the west, near Osoyoos, in the Okanagan Basin, Wassenaar et al. (2011) established a local meteoric water line providing insight into sources and fluxes of water in this area of British Columbia. Nitrate contamination has also been identified in groundwaters and is suspected to originate from application of fertilizers (Athanasopoulos, 2009).

Between 1972 and 1975, there were five water quality stations on the Kettle and West Kettle Rivers, within the area of this project. The location of water quality stations was based on the location of mining operations, pulp mills or municipalities with the potential to affect the water quality (Rocchini et al., 1977). After 1975, there was no

available data on these sites, with the exception of the Midway station, which is still active today.

A water quality monitoring network was established in BC in the 1970's and in 1985 under the Canada–British Columbia Water Quality Monitoring Agreement, this network became jointly operated by the Provincial and Federal Governments (Environment Canada, 2010a). The water quality monitoring network began collecting data bi-weekly on the Kettle River at Midway in 1972 (Environment Canada, 2003). This station is considered to be a transboundary station due to close proximity to the Canadian-US border and was originally installed to document baseline water quality of the Kettle before it crossed the border (Environment Canada, 2003).

Since the inception of the monitoring network, several types of Water Quality Reports have been published on the Kettle River. To fulfil terms of the Canada-British Columbia Water Quality Monitoring Agreement, reports are co-published by the Ministry of Environment and Environment Canada summarizing the status of all stations within BC. The most recent of these reports state that the Midway station is active for trend monitoring because it is a transboundary river, upstream from a US mine; data are also used for fisheries (Environment Canada and BC Ministry of Environment, 2007). Collected data are compared to BC Ministry of Environment's *Approved Water Quality Guidelines, Working Criteria for Water Quality,* the *Canadian Council of Ministers of the Environment Guidelines for the Protection of Aquatic Life Guidelines* (Dessouki, 2009) and Health Canada's *Guidelines for Canadian Drinking Water Quality* (Health Canada, 2010).

Water Quality Assessments for the Midway station have been published, summarizing data from 1980 – 1994 (Webber and Pommen, 1996), 1972 – 2000 (BWP Consulting, 2003) and 1990 – 2007 (Dessouki, 2009). Results and recommendations from the Water Quality Assessment published by Dessouki (2009) are the most recent and include all historical water quality concerns. Aquatic Life standards were seasonally exceeded by total aluminium, total chromium, fecal coliform, dissolved fluoride and total iron. Dessouki (2009) concluded that seasonal exceedences are strongly correlated with increased flow and increased turbidity, indicating the higher total metal concentrations

may not be part of the dissolved fraction and so therefore are not bioavailable. This report recommended monitoring be continued on the Kettle "to assess the Kettle River as a source of drinking and irrigation water; and to monitor trans-boundary effects between British Columbia and Washington State" (Dessouki, 2009).

In 2007, Environment Canada, the BC Ministry of Environment and the Yukon Department of the Environment published a Water Quality Report with data collected between 2001 and 2004 which assessed the status of the health of the waterbodies and aquatic life, in BC and the Yukon, using the Canadian Water Quality Index – "a freshwater quality indicator endorsed by the Canadian Council of Ministers of the Environment (CCME). The Index ranks waterbodies as Excellent, Good, Fair, Marginal or Poor according to their suitability to support aquatic life" (Environment Canada, 2007). Overall 36 monitoring stations in BC and Yukon Territory were evaluated; 56 % were ranked as 'Good' or 'Excellent', 33 % were ranked as 'Fair' and 11 % were ranked as marginal. The Kettle River at Midway was ranked as 'Fair' based on seasonal guideline exceedences of phosphorous and fluoride and other parameters associated with high turbidity during high flows (Environment Canada, 2007). According to the CCME, 'Fair' indicates that measures sometimes exceed water quality guidelines and aquatic life is protected but at times may be threatened or impaired (Environment Canada, 2007).

Previous water quality monitoring and reporting has focused on the Midway station and no surface water data has been collected upstream of Midway after 1975. Groundwater chemistry and its influence on surface water chemistry have not been addressed previously. As part of this project, surface water and groundwater samples were collected throughout the Kettle River Basin, upstream of the Canadian – US border, to assess the state of water quality in the basin.

1.3 Project Description

In this thesis, sources of solutes in surface waters and groundwaters in the Kettle River Basin are investigated using major ion and stable isotope geochemistry. Variations in major ion concentrations are assessed spatially and temporally, and in relation to

groundwater chemistry. Stable isotope abundance ratios of oxygen and hydrogen are used to assess sources and fluxes of water in the Kettle River Basin. Stable isotope abundance ratios of dissolved inorganic carbon, nitrate and sulfate are used to determine the sources and processes influencing these ions. Possible sources of major ions in surface water and groundwater include the atmosphere, lithosphere, biosphere, pedosphere and anthropogenic activities (e.g. Drever, 1997).

In order to determine the role of bedrock weathering, a mass balance is completed for surface water and groundwater samples, taking into consideration sources of ions from the atmosphere, biosphere, ion exchange and anthropogenic activities (e.g. White and Blum, 1995). The geology of the Kettle River Basin is dominated by silicate lithologies (BC Geological Survey, 2005). Chemical weathering of primary silicate minerals produces secondary clay minerals and releases ions into solution. Ion concentrations in solution can also be controlled by ion exchange reactions with clay minerals, and precipitation reactions (Appelo and Postma, 2005). Controls on water chemistry in the Kettle River Basin are assessed using geochemical modelling.

Chemical weathering of silicate bedrock consumes CO_2 (Appelo and Postma, 2005), a greenhouse gas, which has been proposed to influence global climate (Walker et al., 1981). Ultimately, the CO_2 consumed during silicate weathering originates from the atmosphere (Meybeck, 2005), either through direct infiltration of precipitation water, or through uptake and release of CO_2 in the biosphere or pedosphere (Appelo and Postma, 2005). Since the onset of the industrial revolution, CO_2 concentrations have been steadily increasing, predominantly due to anthropogenic burning of fossil fuels and changes in land use (Sabine et al., 2004; Beaulieu et al., 2010). Of the carbon emitted from anthropogenic burning of fossil fuels, only about half has remained in the atmosphere with the remainder taken up by the oceans and the terrestrial biosphere (Sabine et al., 2004). The role of silicate weathering in consumption of atmospheric CO_2 is still not fully understood (Spence and Telmer, 2005; Moosdorf et al., 2011) and it is possible that silicate weathering may also consume a portion of anthropogenic CO_2. As part of this study, the amount of CO_2 consumed to reach partial pressures of CO_2 in equilibrium with

groundwater samples in both the Kettle River Basin and the Paraná Basin in Brazil is calculated using geochemical modeling. Results provide insight into the influences of temperature and lithology on the amount of CO_2 consumed during silicate weathering.

Consumption of CO_2 during silicate weathering produces HCO_3^-, which is subsequently stored in groundwaters or exported from the basin through rivers. The amount of HCO_3^- stored in groundwaters in both the Kettle River and Paraná Basin will be determined and compared to major global carbon reservoirs to assess the importance of carbon storage in aquifers. HCO_3^- transported in rivers eventually reaches the ocean and forms carbonate minerals (e.g. Bluth and Kump, 1994). The flux of HCO_3^- through rivers will be compared to the magnitude of other global carbon fluxes to assess the importance of silicate weathering as a global carbon sink. Rivers can also release carbon through degassing of CO_2, as the partial pressures of CO_2 in rivers are often higher than that of the atmosphere (Butman and Raymond, 2011).

1.4 Project Objectives

The objectives of this project were to determine the sources of solutes in surface water and groundwaters, identify the dominant chemical weathering reactions between minerals and solution, to quantify the amount of CO_2 consumed during silicate weathering and stored in groundwaters, and to estimate the flux of CO_2 exported out of the Kettle River Basin.

Chapter Two: Study Area

2.1 Location

The Kettle River Basin is located in south central British Columbia (BC), Canada. For this project, the area of focus was from the headwaters of the Kettle River and West Kettle River – a major tributary of the Kettle River, beyond their confluence, to the Canadian – US border, south of the town of Midway, BC. The headwaters of the Kettle River originate in the Monashee Mountains at an approximate elevation of 1350 meters above sea level (asl), while the headwaters of the West Kettle River are located at approximately 1285 meters asl, further to the southwest in the Okanagan Highlands (Dessouki, 2009). Both rivers flow in a southward direction and converge just south of the town of Westbridge, BC, where the river continues as the Kettle River. Beyond the confluence, the Kettle River flows south until the town of Rock Creek, where the river turns to the east towards Midway. Beyond Midway, the Kettle River flows south into the United States crossing the border at an elevation of 572 meters asl. The Kettle and West Kettle tributaries are 160 km and 105 km long, respectively. Beyond the confluence, the Kettle River flows for an additional 50 km before crossing the Canada – United States border. The Kettle River re-enters Canada at Carson, BC before crossing again into the United States. The Kettle River then continues south, draining into the Columbia River, which flows to the Pacific Ocean along the Oregon Coast. Figure 2-1 depicts the spatial extent of this watershed, Kettle and West Kettle Rivers and the confluence of these rivers.

2.2 Climate

There are four climate stations located within or near the study area (herein referred to as the Kettle River Basin), which were either historically active or are still actively recording temperature and precipitation data. The 'Beaverdell North' climate station, located at 830 meters asl, approximately 5 km from the town of Beaverdell (Figure 2-2), recorded temperature and precipitation data between 1975 and 2000, however this station is no longer active (Environment Canada, 2011a). A second climate

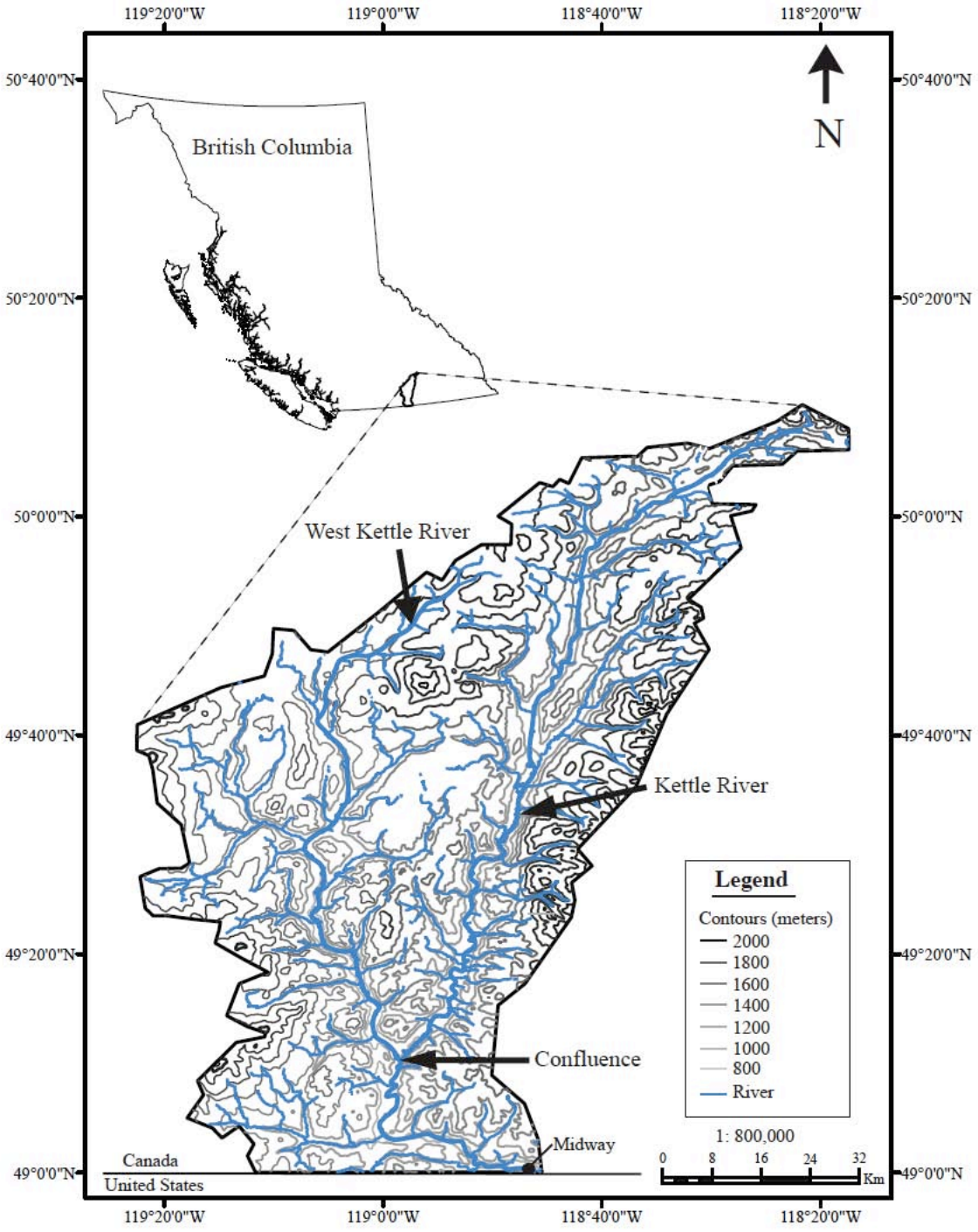

Figure 2-1: Location of the Kettle River basin, Kettle and West Kettle River and the Kettle River below the confluence. Map was created using ArcGIS using data obtained from the BC Geological Survey (2005) and Environment Canada (2011a,b).

station is located in Osoyoos, which is located 30 km west of Rock Creek, at an elevation of 297 meters asl. This station has recorded temperature and precipitation data since 1971 and is currently used for the Rock Creek weather forecast (Environment Canada, 2011a,b). Slightly south of the Canada – US border there is a hydrometric station at Ferry, which also records temperature; this station has been active since 1988 (United States Geological Survey, 2011). The fourth hydrometric station is located in Pentiction, BC, which is located at an elevation of 344 meters asl, approximately 20 km from the western boundary of the basin (Figure 2-2). This station has been actively recording temperature and precipitation data since 1941. Table 2-1 summarizes historical climate data and Table 2-2 summarizes climate data for 2009 and 2010.

Temperature and precipitation values vary depending on location. Historical average annual temperatures vary between 4.9 °C at the Beaverdell North station and 10.1 °C at the Osoyoos station. The historical total annual precipitation (sum of rainfall and snowfall) ranges from 318 to 482 mm at Osoyoos West and Beaverdell North, respectively. The area between Rock Creek (best represented by the Osoyoos station) and Ferry, is characterized by higher temperatures and lower amounts of precipitation, compared to the Beaverdell North climate station. Because there is not a climate station located in the basin of the Kettle River tributary, it is assumed that temperature and precipitation values are similar to values within the West Kettle sub-catchment, represented by the Beaverdell North station, as the two sub-catchments are located adjacent to each other. Comparison between historical average temperatures and average temperatures in 2009 and 2010 at Osoyoos, Ferry and Penticton, indicates that temperatures were lower in 2009, compared to the long term average, except at the Penticton station, and higher in 2010. Precipitation values recorded at the Penticton station in 2009 and 2010 were 5.1 % and 15.9 % higher, respectively compared to historical average values at this station.

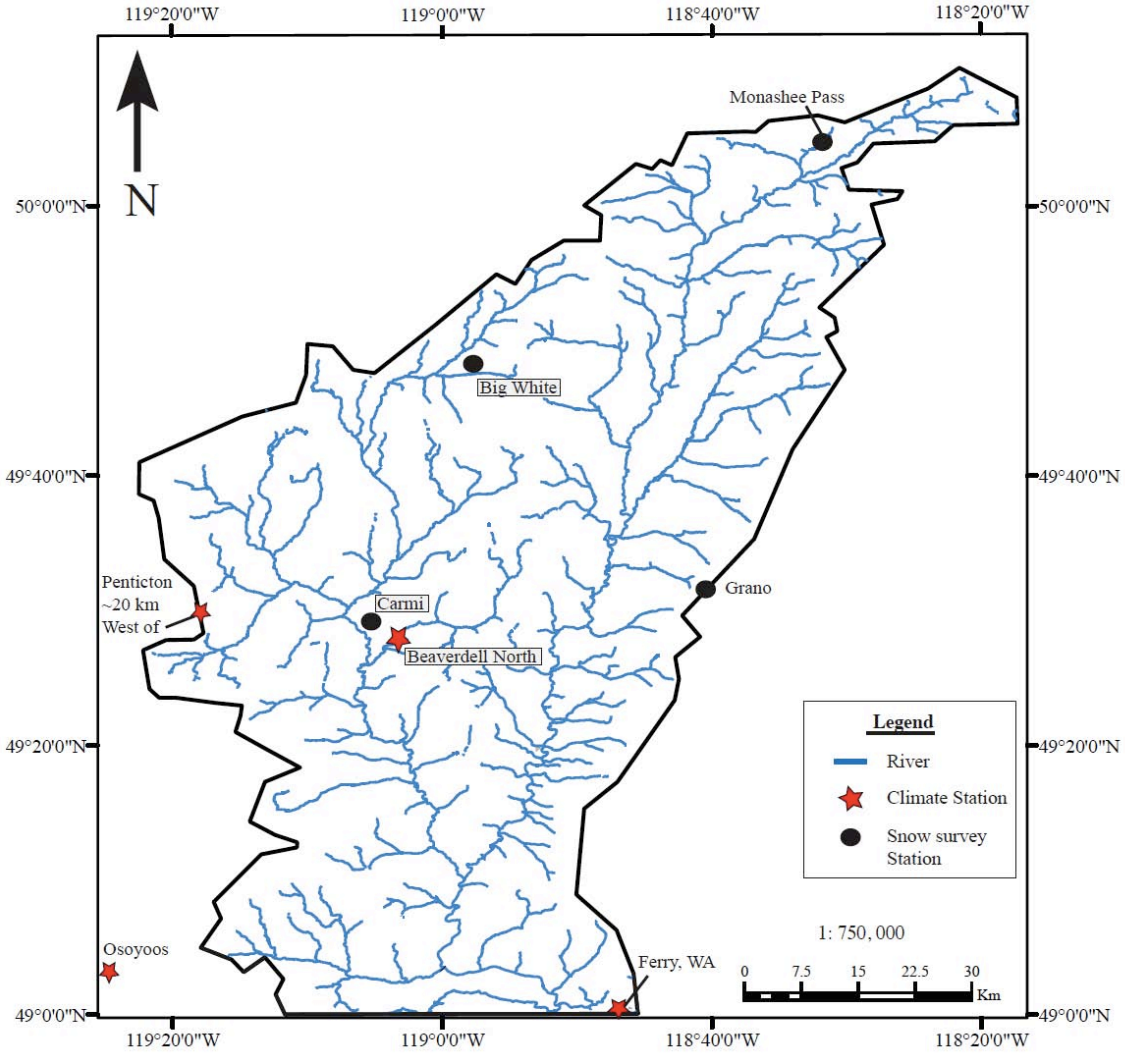

Figure 2-2: Location of climate stations and snow survey stations. Map was created using ArcGIS with data obtained from the BC Geological Survey (2005), BC Ministry of Forestry, Lands and Natural Resources (2011) and Environment Canada (2011a,b).

Table 2-1: Historical climate data from various climate stations within or near the Kettle River basin. Average temperature at Beaverdell North, Osoyoos and Penticton is the average of maximum and minimum temperatures recorded each day. At the Ferry station, average temperature is the average of values recorded throughout each day. The historical average temperature and average annual precipitation values were calculated for observations recorded between 1971 and 2000 (Environment Canada, 2011a; United States Geological Survey, 2011).

Climate Station	Observation Period	Average temperature (°C)	Average total annual precipitation (mm)
Beaverdell North	1975-2000	4.9	482
Osoyoos	1971-2000	10.1	318
Ferry	1988-2000	7.0	-
Penticton	1971-2000	9.2	333

Table 2-2: Climate data for 2009 and 2010 from climate stations within or near the Kettle River basin. Average temperatures at Osoyoos and Penticton are the average of maximum and minimum temperatures recorded each day. At the Ferry station, average temperature is the average of values recorded throughout each day (Environment Canada, 2011b; United States Geological Survey, 2011).

Climate Station	Observation Period	Average temperature (°C)	Total annual precipitation (mm)
Osoyoos	2009	10.0	-
	2010	10.9	-
Ferry	2009	5.7	-
	2010	8.3	-
Penticton	2009	9.3	350
	2010	10.0	386

In addition to spatial variation in temperature and precipitation, there are also seasonal variations. Figure 2-3 shows historical average monthly temperature and precipitation values for Beaverdell (1975 to 2000) and Osoyoos (1971 to 2000). At both the Beaverdell and Osoyoos stations, the highest average temperatures, up to 21.7 °C, are recorded in July and August and the lowest average temperatures, as low as -7.1 °C, are recorded in December and January. Precipitation data indicate that the months of May and June receive the most precipitation. Precipitation received in May and June is equivalent to 23.2 % and 19.9 % of the annual precipitation received at the Beaverdell and

Osoyoos stations, respectively. The Beaverdell climate station had consistently lower temperatures and received less precipitation in the summer and more precipitation in winter months compared to the Osoyoos station. Figure 2-4 indicates how temperature and precipitation in 2009 and 2010 compare to historical average climate parameters at the Penticton station. Temperatures in 2009 and 2010 were very similar to historical average values, whereas precipitation values differed markedly from historical average values. Precipitation values in 2009 were lower than historical averages through the first half of the year and were higher during the late summer and fall. In 2010, there was more precipitation in May, June and September and less precipitation during July and August, compared to historical averages.

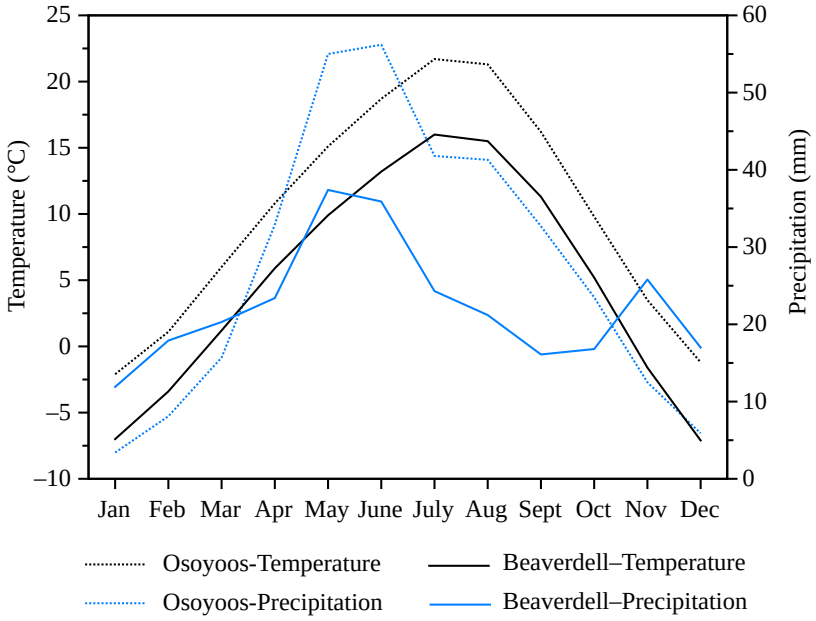

Figure 2-3: Historical average monthly temperature and precipitation values for Osoyoos (1971-2000) and Beaverdell (1975-2000) climate stations (Environment Canada, 2011a).

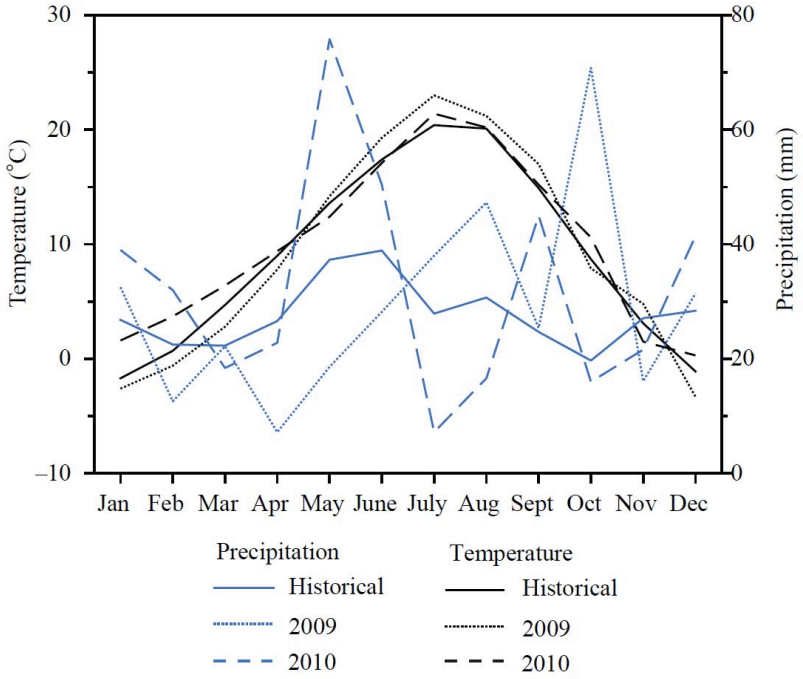

Figure 2-4: Average monthly temperature and precipitation values for 2009 and 2010 compared to historical values, at the Penticton climate station (Environment Canada, 2011a,b).

Snow Survey Stations

The River Forecast Centre, part of the Ministry of Forestry, Lands and Natural Resources, collects and interprets meteorologic and stream flow data to provide water supply advisories such as drought or flood warnings. The River Forecast Centre conducts monthly snow surveys throughout the winter months (January through June) to measure the amount of snow in selected areas. Both the depth and density of snow is measured and results are given as snow-water equivalent - the water content in the snow, expressed in millimetres as depth of water that would result from melting the snow.

Within the Kettle River basin there are four snow survey stations - from north to south these are: Monashee Pass, Big White, Grano and Carmi (Figure 2-2). The Monashee Pass station is located near the headwaters of the Kettle River, at an elevation of 1370 meters asl and has been active for 50 years. The Big White station is located near the Big White Ski Resort at an elevation of 1680 meters asl and the Carmi station is located at an elevation of 1250 meters asl. Both the Big White and Carmi stations are

located between the West Kettle and Kettle Rivers; they have been active for 44 and 46 years, respectively. The Grano station is located east of the Kettle, at an elevation of 1860 meters asl and has been active for 12 years.

Each station has different ranges and averages of snow-water equivalents throughout the winter. Stations at higher elevations have higher snow-water equivalent values compared to lower elevation stations (Table 2-3). Comparison of the average historical snow water equivalent values from each station to values from 2009 indicates that throughout the winter, there was above average amounts of snow at the Monashee Pass and Carmi stations, and below average amounts at the Big White and Grano stations (Figure 2-5). In 2010, all stations were below the average historical snow-water equivalent value throughout the winter, except in June, where the Big White and Grano stations exceeded historical average values.

Table 2-3: Snow-water equivalents at four snow survey locations between January 1st and June 1st. Historical normal values are calculated since the inception of the station (BC Ministry of Forests, Lands and Natural Resources Operations, 2011).

Snow Survey Station	Historical normal	2009	2010
	Snow-water equivalent (mm)		
Monashee Pass (1370 m asl)	270	296	185
Big White (1680 m asl)	404	326	366
Grano (1860 m asl)	440	333	345
Carmi (1250 m asl)	106	125	54

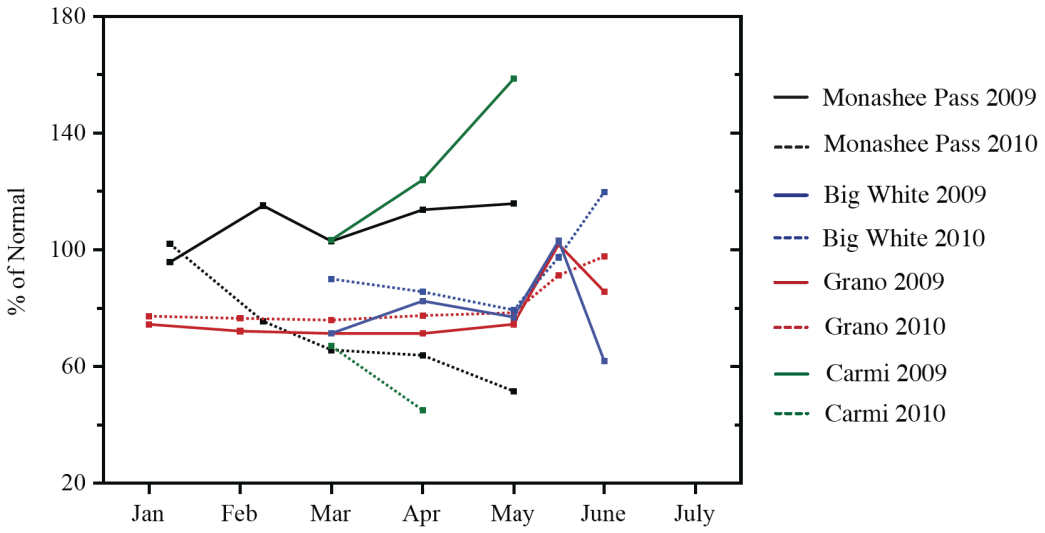

Figure 2-5: Percent (%) of normal average historical snow depth in 2009 and 2010 at four snow survey stations between January 1st and June 1st (BC Ministry of Forests, Lands and Natural Resources Operations, 2011).

2.3 Vegetation and Soils

The basin is densely forested with a variety of tree species including subalpine fir, coastal western hemlock, ponderosa pine, douglas fir, engelmann spruce and larch (BC Parks, 2011). Some sections of the rivers are bordered with willow, cottonwood and birch trees. In southern portions of the basin, especially on south facing slopes, there are fewer trees and more area is covered with open grasslands (BC Ministry of Environment, 1977).

The type of soils present is dependent on the factors that influence soil formation which are: geology, vegetation, topography and time (BC Ministry of Environment, 2011). There are five different soil types present in the basin, which are categorized into four soil orders – Chernozemic, Brunisolic, Luvisolic and Podzolic. The spatial distribution of these soils is shown in Figure 2-6. The following description of soil orders was obtained from the BC Ministry of Environment (2011), *Soil Landscapes of BC* publication. Soils from the Chernozemic order are associated with low rainfall, high summer temperatures, high evapotranspiration rates and grassland vegetation; this order corresponds spatially to the east-west corridor between Rock Creek and Midway. The Brunisolic order soils are moderately developed and found on young sediments such as alluvium, sand and gravel. There are two types of Brunisolic soils – Dystric and Eutric, which are classified based on pH. Dystric soils have pH values > 5.5, while Eutric soils have pH values < 5.5. Brunisolic soils cover areas of lower elevations in the Kettle River Basin. Luvisolic order soils are found in areas of higher rainfall or lower temperatures with less evapotranspiration. Because of the additional moisture, these soils are more developed and have undergone higher amounts of chemical weathering and clay formation. Luvisolic soils are found at moderate elevations between the two tributaries and in the upper portions of the Kettle River tributary. Podzolic soils typically have an abundance of water moving through the soil and are therefore well developed soils. The humo-ferric variety of the Podzoilic order, which is present in the Kettle River basin, commonly occurs in sub-alpine forests in the BC interior. As shown in Figure 2-6, Podzolic soils are found at higher elevations. The spatial distribution of soils was found to be primarily dependent on topography, but may also be influenced by underlying geology and by vegetation.

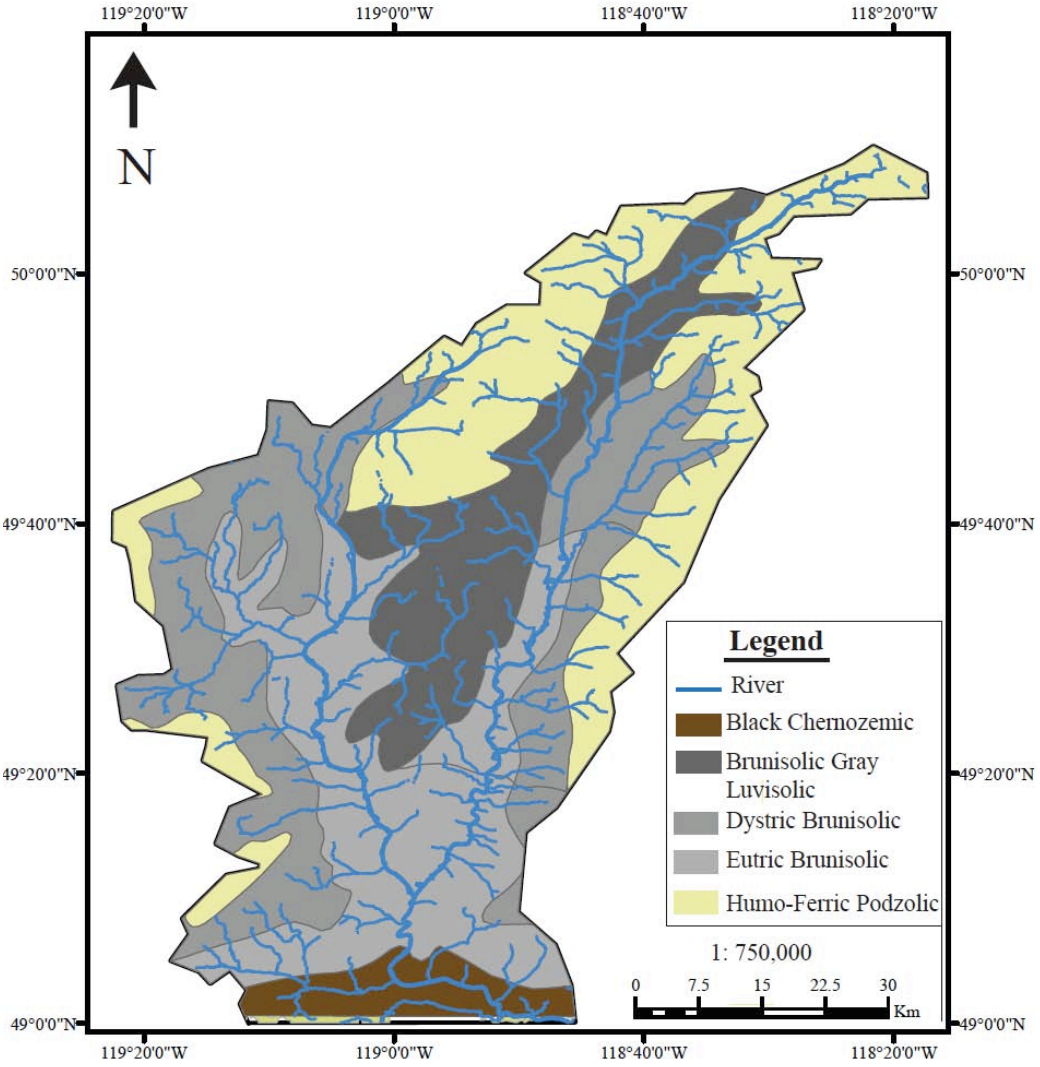

Figure 2-6: Soil types present in the Kettle River Basin. Map was created using ArcGIS and data was obtained from the BC Geological Survey (2005) and Agriculture and Agri-Food Canada (2011).

2.4 Geology

2.4.1 Bedrock Geology

The Kettle River Basin is located within the Canadian Cordilleran orogenic belt that extends from the Canada – United States border to the Canadian Arctic. The Canadian Cordillera is composed of an amalgamation of terranes - portions of the earth's crust, of varying size and thickness, which are geologically different from adjacent

terranes and are separated from adjacent terranes by major faults, intrusions or a cover of younger rocks (Monger et al., 1982, Gabrielse and Yorath, 1991). The proposed mechanism of orogenesis is subduction of oceanic plates, accretion of terranes and associated arc magmatism (Price and Monger, 2000). In addition to terrane accretion and arc magmatism, compressional and extensional tectonics as well as metamorphism have also contributed to the current geologic setting (Gabrielse and Yorath, 1991; Parrish et al., 1988). The Canadian Cordillera has been divided into five linear morphogeological belts based on rock types, metamorphic grade, structure and physiography (Price and Monger, 2000). These include, from east to west: Foreland, Omineca, Intermontane, Coast and Insular Belts.

The Kettle River Basin is located within the Omineca belt, which is described as "an uplifted region, extensively underlain by metamorphic and granitic rocks, which straddles the boundary between the accreted terranes and Ancestral North America (Foreland belt)" (Gabrielse and Yorath, 1991). The Omineca belt was structurally deformed by compression between the middle Jurassic and the early Tertiary, and by extension in the early Tertiary (Price and Monger, 2000). Underlying the Kettle River basin are two terranes – the Kootenay and the Quesnel Terrane, which are thought to have originated from similar geographic locations (Gabrielse and Yorath, 1991). The Kootenay Terrane is composed of Proterozoic to Paleozoic Shuswap Assemblage – undivided and orthogneiss metamorphic rocks. The Quesnel Terrane includes chert, siliclastic rocks, volcanics, volcanoclastics, mudstones, siltstones and greenschist metamorphic rocks from Paleozoic and Mesozoic mudstones, siltstones and volcanics. Since accretion of the Kootenay and Quesnel Terranes, these terranes have been intruded by mid to late Mesozoic intrusive rocks of both the Okanagan batholith and an unnamed Group, and by Cenozoic volcanics of the Penticton and Chilcotin Groups as well as the Coryell Plutonic Suite (BC Geologic Survey, 2005). Figure 2-7 indicates the spatial distribution of the Kootenay and Quesnel Terranes, and post-accretionary intrusions and volcanics.

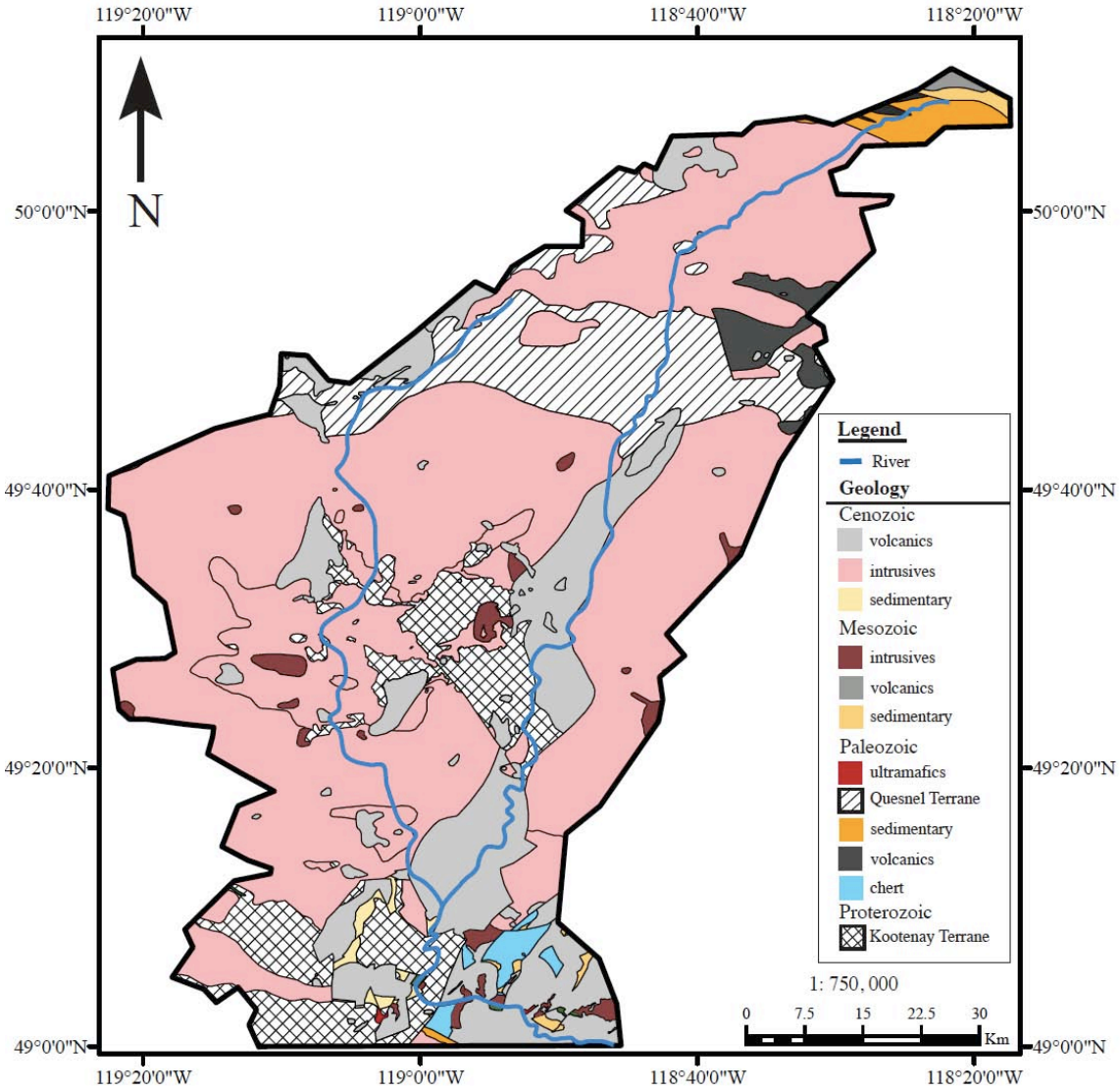

Figure 2-7: Simplified geological map of the Kettle River basin with tributaries and the Kettle River below the confluence overlain. Map was created with ArcGIS and data was obtained from the BC Geological Survey (2005).

2.4.2 Surficial Geology

The Kettle and West Kettle River valleys consist of flat valley bottoms, surrounded by steep bedrock hills, which rise 700 to 1500 meters above the valley bottoms. These valleys were formed by Pleistocene glaciers that were part of the Cordilleran ice sheet, which covered all of British Columbia, the southern Yukon and parts of Alaska (Clague and James, 2002). Advance and retreat of glaciers led to deposition of thick sequences of

glacial and fluvial materials in valley bottoms. The uppermost sections of the valley bottoms are comprised of fluvial materials, deposited by the Kettle and West Kettle Rivers. Unconsolidated materials of either glacial or fluvial origin are composed of sand, gravel, silt and clay (Wei et al., 2010). There is no information available on the provenance of glacial materials in the Kettle River Basin and it is difficult to hypothesize the provenance of glacial materials, due to the size of the Cordilleran ice sheet. Fluvial materials in the uppermost sections of the valleys are likely derived from within the basin.

2.5 Anthropogenic Activity

2.5.1 Population

Early settlement in the Kettle River Basin in 1858 was due to discovery of placer gold in Rock Creek, a tributary of the Kettle River. Over the next 50 years, population was transient as mining was ongoing in the Kootenays or Caribou Regions, or in the northwest United States (Sprout and Keeley, 1964). The Kettle Valley Railway was built in 1912, which allowed for continuous production from a silver-lead-zinc mine near Beaverdell, resulting in a more permanent population base. Midway was established in 1892 and by 1914, the population of Midway was around 300, but subsequently decreased due to the mining situation at that particular time (Sprout and Keeley, 1964). Historical population estimates at other times were not available.

Presently, there are people living throughout the Kettle River Basin – either in the small towns of Midway, Rock Creek, Beaverdell, Westbridge and Bridesville or in the rural areas surrounding these towns. The locations of these towns are identified in Figure 2-8. According to the 2006 Census, there are 621 people living in Midway (BC Stats, 2006). The other small towns in this area are not large enough to be included in the Canadian Census, however Canada Post provides a list of how many houses are in each Postal Code. As of September 2010, there are 255 houses in Rock Creek, 145 houses in Westbridge, 208 houses in Beaverdell and 66 houses in Bridesville, for a total of 674 houses (Canada Post, 2010). Overall, this area is very sparsely populated.

The town of Midway has three water supply wells for drinking water and a sewage treatment plant (Village of Midway, BC, 2009). Residents living in rural areas obtain drinking water from either surface water licenses or drilled water wells and have septic systems for wastewater. There was no available information for water supply or wastewater treatment systems for the small towns of Rock Creek, Beaverdell, Westbridge and Bridesville and therefore it is assumed these towns also rely on wells or surface water licenses and septic systems. Historic and current anthropogenic activities within the basin include mining, forestry irrigated agriculture and ranching (Dessouki, 2009).

2.5.2 Mining

Exploration for mineral resources in the study area began in the 1850's, initially due to discovery of placer gold, which lead to several mines that produced silver, gold, copper, cadmium, lead and zinc (Spout and Kelly, 1964; BC Ministry of Energy and Mines, 2011). Minerals such as molybdenite, pyrite, fluorite, magnetite, chalcopyrite and bornite have been identified. Minor calcite was also identified in volcanic lithologies and in veins within intrusive lithologies (Ewert et al., 2008). Currently there is one active mine and historically there have been several others in operation, the largest of which was the Highland Bell Silver-Lead-Zinc mine. There are several properties where exploration is currently active. The Kettle River – Buckhorn underground gold mine has been active since 2008 (Kinross Gold Corporation, 2009). It is located in the United States, within the Myers Creek watershed. Myers Creek flows north into Canada and joins the Kettle River upstream of Midway (Pommen Water Quality Consulting, 2003). The target production rate of ore is 900 tonnes per day; the ore is trucked outside of the Myers Creek drainage for processing (Kinross Gold Corporation, 2009).

The Highland Bell Mine was an underground silver-lead-zinc mine east of Beaverdell, which was in continuous production between 1913 and 1991 (BC Ministry of Energy and Mines, 2011). The ore was transported to the mill site, located west of Beaverdell, where the ore was crushed, screened and then further reduced in size with a wet grinding process, using various additives. The ore was then turned into a concentrate

and conveyed to flotation cells where the 'overflow' and 'underflow' or tailings were separated. The tailings were held in tailings ponds, which occupied 6.5 acres in 1977. Between 1950 and 1972, one of the tailing ponds failed frequently and effluents did occasionally reach the West Kettle River (BC Ministry of Environment, 1977). In total, the Highland Bell Mine produced 1,226,623 kg of silver, 544 kg of gold, 11,657 kg of copper, 12,965,868 kg of lead, 15,405,307 kg of zinc and 58,171 kg of cadmium (Intigold Mines Ltd., 2011). The location of the mine is shown in Figure 2-8. An air and water quality study was conducted by the BC Ministry of Environment in 1977 and concluded that the Highland Bell Mine and processing facilities had minimal impact on the West Kettle River. Since 1995, St. Elias Mines has owned this property and in 1996-1997, completed some basic mapping, sampling and drilling. More detailed exploration programs were conducted between 2007 and 2009 and there are plans for future exploration (Intigold Mines Ltd., 2011).

Close to the Highland Silver Bell Mine, is a molybdenum property known as the Carmi Deposit that has undergone extensive exploration activity between 1961 and 1990 including drilling, geochemical soil and stream surveys and mapping (Ewert et al., 2008) with some ore recovery. Since 1990, the property has changed ownership and the property has been an active site of exploration (St. Elias Mines Ltd., 2011); there are plans for additional exploration in the future (Hi Ho Silver Resources Inc., 2011).

In addition to Highland Bell and Carmi properties, there are several properties also close to Beaverdell, which have been previous sites of exploration, some of which were producing mines (BC Ministry of Environment, 1977; Ewert et al., 2008; BC Ministry of Energy and Mines, 2011). The location of these mines was determined from the BC Ministry of Energy and Mines MINFILE database and is shown in Figure 2-8. A uranium deposit, known as the Blizzard Project has also been identified and is located northeast of Beaverdell (Figure 2-8). The uranium deposit is hosted in sedimentary rocks and capped by Cenozoic plateau basalts (Christopher, 2005). In 2008, the BC Government issued an effective moratorium on uranium exploration, mining and

development in BC (Association of Mineral Exploration BC, 2009) and so there is currently no exploration activity in this area (Virginia Energy Resources Inc., 2011).

2.5.3 Forestry and Pulp Mills

As much of the basin is forested, logging has occurred since at least 1977 (BC Ministry of Environment, 1977) and is still active today. There is limited information available on the amount of the watershed previously logged, or which areas are currently being logged. There was a mill near Midway, active from 1969 until 2005 (Pope and Talbot, 2008).

2.5.4 Agriculture and Ranching

The onset of agricultural and ranching activities followed after mining attracted people to the area. In 1875, the first water license was obtained for irrigation purposes near Rock Creek (Sprout and Keeley, 1964). Similar to the mining industry, the intensity of agricultural activities varied through the first half of the 20th century. Animals such as cattle, sheep and swine were raised in varying numbers through this time (Sprout and Keeley, 1964). Animals are still being raised in the basin but estimates of the number of animals were not available. Currently, agricultural activities are concentrated between Midway and Westbridge. Land suitable for agricultural activities in BC has been identified and is known as the Agricultural Land Reserve (ALR) (Agricultural Land Commission, 2002). Land within the ALR is shown in Figure 2-8.

2.5.5 Recreational Activities

In the summer months, the Kettle River Basin is a popular spot for fishing, camping, canoeing or biking along the river (Dessouki, 2009). During the winter, skiing is popular at Big White Ski Resort or at Mt. Baldy (Figure 2-8). The Big White Ski Resort is located near the headwaters of the West Kettle River and is a significantly larger ski area compared to Mt. Baldy.

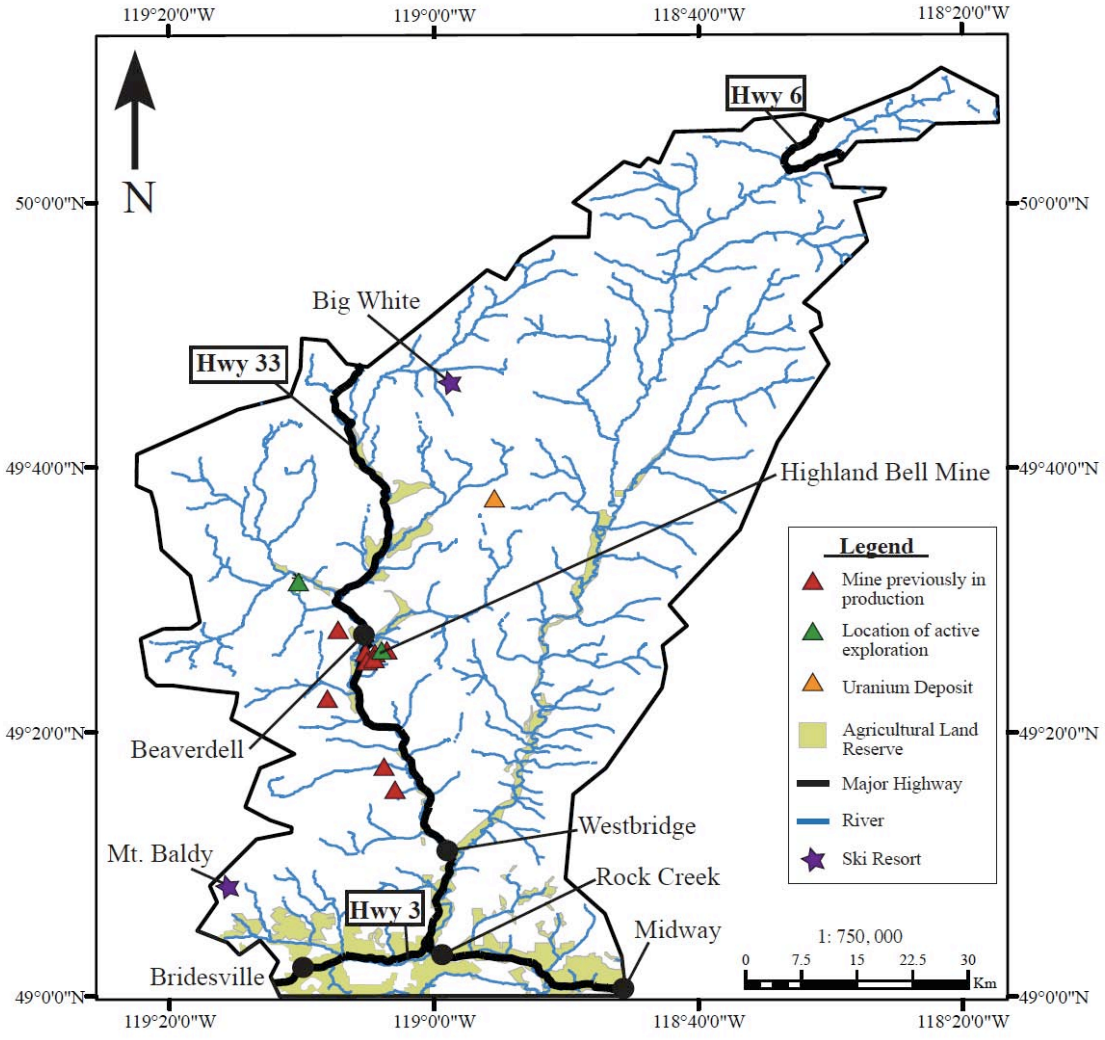

Figure 2-8: Current and historic spatial distribution of anthropogenic activities in the Kettle River basin. Map was created using ArcGIS and data was obtained from the BC Geological Survey (2005), Agricultural Land Commission (2011), BC Ministry of Energy and Mines (2011) and Christopher (2005).

Chapter Three: Hydrology, Hydrogeology and Anthropogenic Water Use

3.1 Introduction

Monitoring of water resources in the Kettle River Basin began in 1919 and therefore, there is much known about the historic and current hydrology and hydrogeology in parts of the study area. There are several hydrometric stations and a groundwater observation well, which monitors groundwater levels. Aquifers within the basin have been mapped and rated in terms of demand, productivity and vulnerability. In this Chapter, historical average discharge rates, groundwater levels and precipitation will be compared to conditions in 2009 and 2010, the years water samples were taken for this project, in order to determine whether samples were taken at times representative of average conditions. The types of anthropogenic water use will also be discussed, however there is not a monitoring system in place to quantify the amount of anthropogenic water use.

3.2 Hydrology

There are four hydrometric stations on the Kettle and West Kettle Rivers within the project area, three of which are jointly operated by the Provincial (Ministry of Environment - MOE) and Federal Government (Environment Canada - EC) while the other is jointly operated by EC and the United States Geological Survey (USGS) (Environment Canada, 2010a; United States Geological Survey, 2010). On the West Kettle River there are two stations - one close to McCulloch, close to the headwaters, and the other near the small town of Westbridge. On the Kettle River there is a station near Westbridge above the confluence of the two rivers, and a station near Ferry (located 2.1 km south of the Canada-US border), which is below the confluence (Environment Canada, 2010b,c). The Ferry station also includes Boundary Creek, a tributary that joins the Kettle River south of the border. Because Boundary Creek is not included in this project area, hydrometric data was examined in order to estimate how much this creek contributes to discharge values recorded at the Ferry hydrometric station. Hydrometric data on Boundary Creek was recorded sporadically from 1929 onwards, but currently this

station is not active. Average monthly discharge on Boundary Creek, compared to average monthly discharge at the Ferry station indicates that Boundary Creek contributes approximately 5 % to the flow in the Kettle River at the Ferry Station (Environment Canada, 2010b,c). Figure 3-1 shows the location of the hydrometric stations.

Historical hydrometric data is available from each station's inception to 2008 and real-time hydrometric data from 2009 and 2010 is available for three of four stations from either EC or the USGS (Environment Canada, 2010b,c; United States Geological Survey, 2010). The Westbridge and McCulloch stations on the West Kettle River have been active since 1919 and 1949, respectively. The Ferry and Westbridge stations on the Kettle River have been active since 1928 and 1975, respectively (Environment Canada, 2010b). The McCulloch and Ferry stations collect data for each day of the year, while the stations near Westbridge on the Kettle and West Kettle Rivers only record data between April and September. Historical data include daily maximum, minimum and mean discharge values. Real-time data is collected throughout each day. Historic and real time discharge data is shown in Figure 3-2 for the West Kettle River and in Figure 3-3 for the Kettle River. Real-time data is complimented with manual measurements, which are also included in Figures 3-2 and 3-3.

At each station, discharge rates begin to increase in early April, peak between late May and early June and decrease until late July. On the West Kettle River at McCulloch, daily mean peak discharge is approximately 20 m^3/s, while at Westbridge it is approximately 65 m^3/s. On the Kettle River, mean peak discharges at Westbridge and Ferry are 150 m^3/s and 220 m^3/s, respectively. Between August and March low flow rates are on average 0.75 m^3/s at McCulloch (between 1949 and 2008) on the West Kettle River and 9.42 m^3/s at Ferry (between 1928 and 2008), below the confluence.

On both the West Kettle and Kettle Rivers, the stations near Westbridge are located just above the confluence. Comparison of peak flow and low flow data indicates that the Kettle River sustains higher flows compared to the West Kettle River. When the mean daily discharge rates on the Kettle River (1975-2008) and West Kettle River (1914-2008) at Westbridge are combined to simulate flow at the confluence, these data indicate

that the Kettle River contributes 68 % of the flow beyond the confluence and the West Kettle River contributes 32 %.

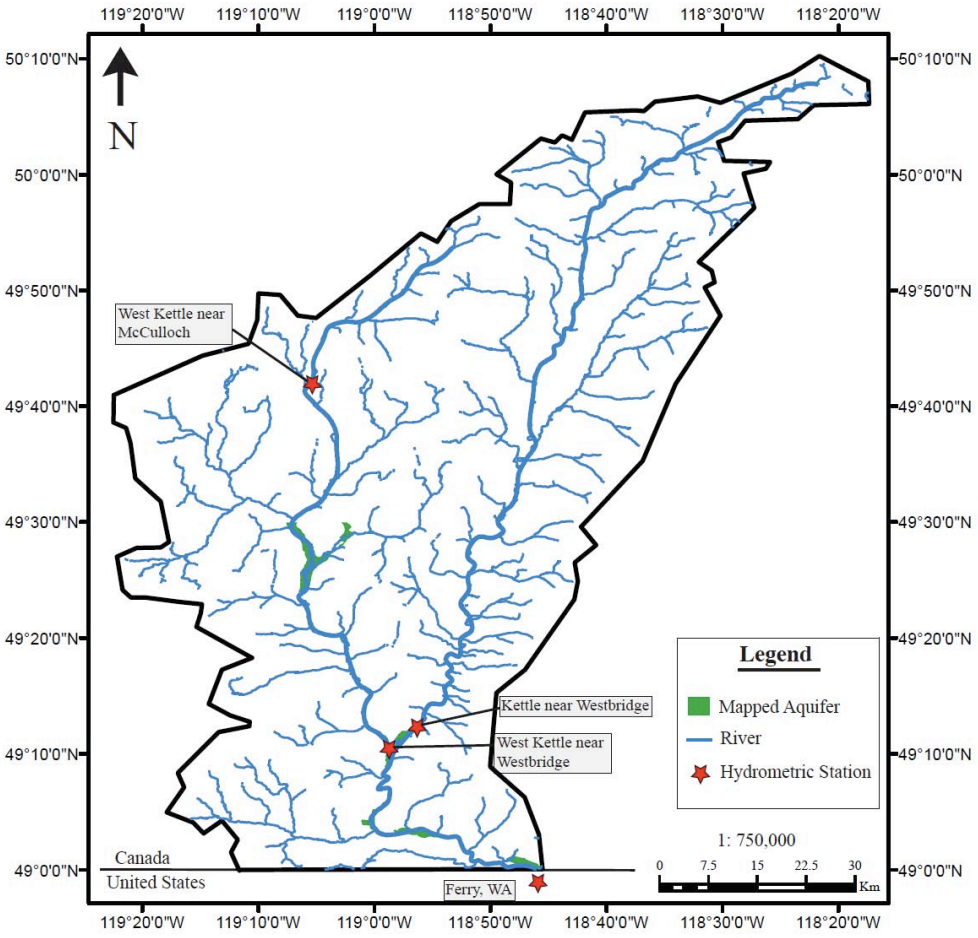

Figure 3-1: Location of hydrometric stations and mapped aquifers. Maps were created with ArcGIS using data obtained from the BC Geological Survey (2005), Environment Canada (2010b,c) and the BC Ministry of Environment (2007).

Real-time data from 2009 and 2010 compared to mean, minimum and maximum flows, in Figures 3-2 and 3-3 indicate that flow rates for these years were lower than average. At all three stations with real-time data, peak flow rates for 2009 and 2010 exceeded mean peak flow rates, at some point through the freshet. The percent decrease in in daily mean flow rate for each station and the average percent decrease for all stations for 2009 and 2010 are summarized in Table 3-1.

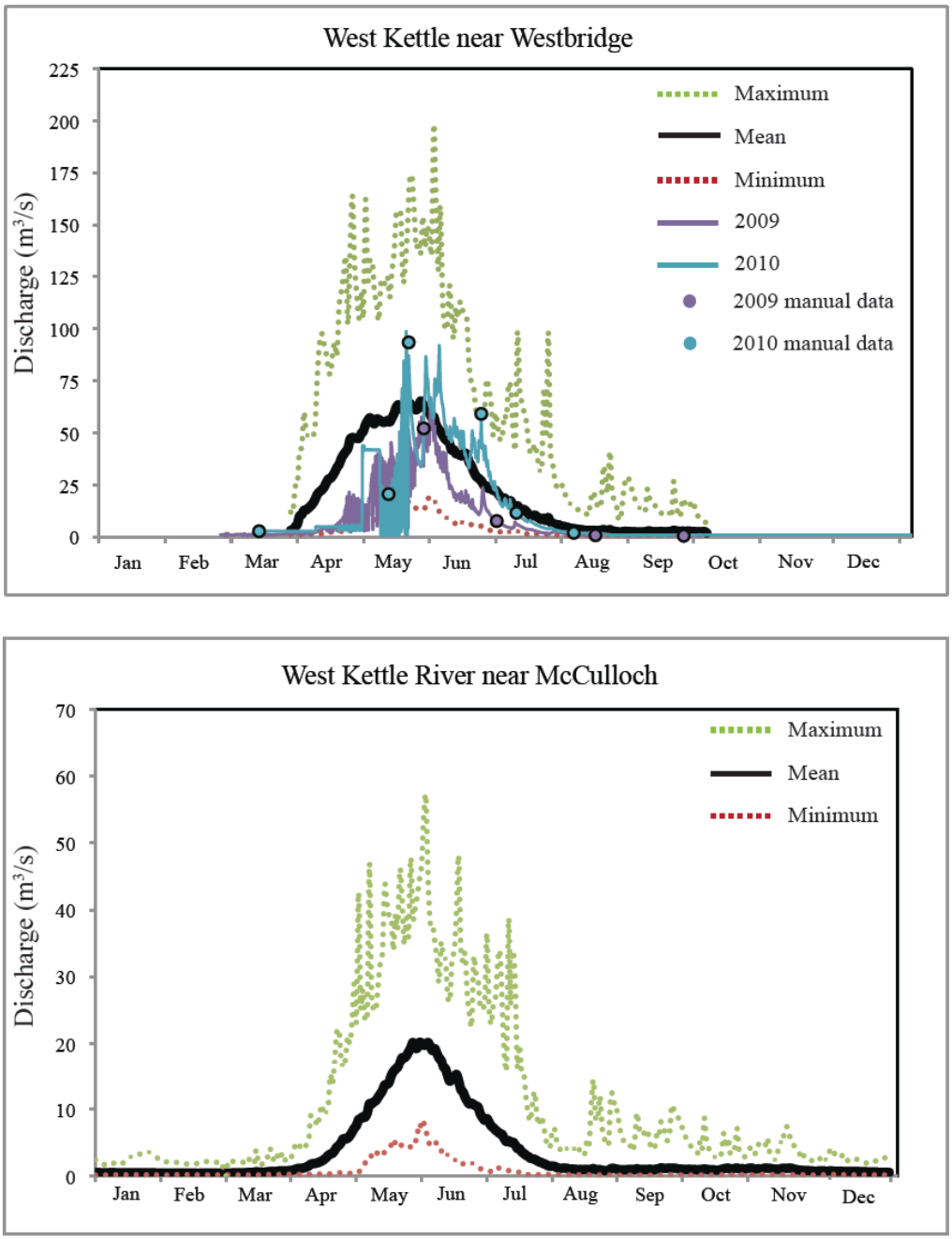

Figure 3-2: Historic and real-time hydrometric data for the West Kettle River at Westbridge and McCulloch. Historic data includes maximum, mean and minimum flow rates for Westbridge between 1914 and 2008 and for McCulloch between 1949 to 2008. Real-time daily discharge data from 2009 and 2010 is also included for the Westbridge station and is verified with manual measurements (Environment Canada, 2010b,c). Data from the Westbridge station in May is very sporadic, changing from 1 m^3/s to 22 m^3/s within a few hours, likely indicating there is a problem with the instrumentation recording data.

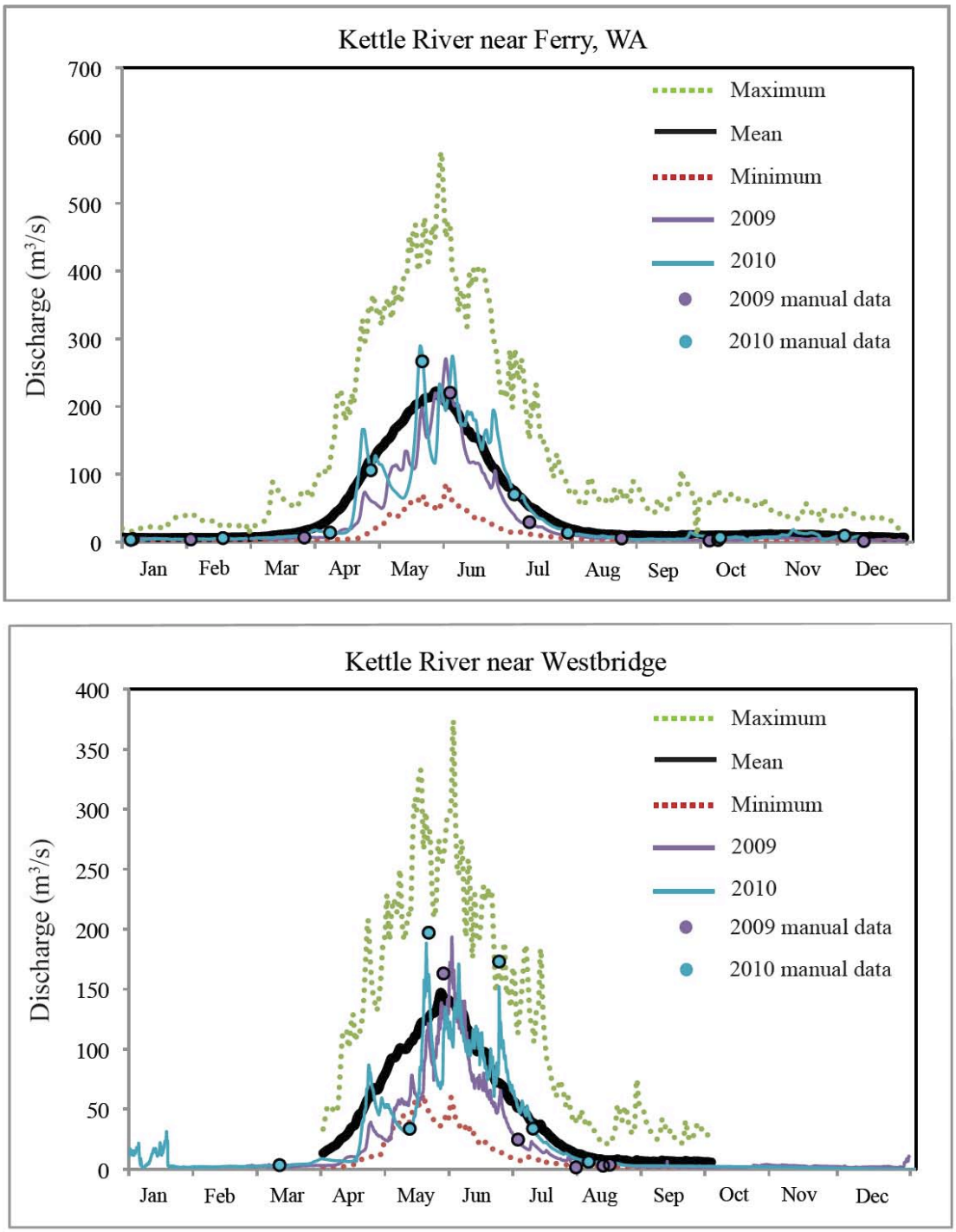

Figure 3-3: Historic and real-time hydrometric data for the Kettle River at Ferry and Westbridge. Historic data includes maximum, mean and minimum flows for Ferry between 1928 and 2008 and for Westbridge between 1975 to 2008. Real-time daily discharge data from 2009 and 2010 is also included and is verified with manual measurements (Environment Canada, 2010b,c; United States Geological Survey, 2010).

Table 3-1: Average annual percent decrease in mean daily discharge rates in 2009 and 2010 compared to daily mean values, from each stations inception to 2008. Data was obtained from Environment Canada (2010b,c) and the United States Geological Survey (2010).

Year	Kettle River at Ferry	Kettle River at Westbridge	West Kettle River at Westbridge	Average decrease
2009	49.1 %	51.6 %	65.4 %	55.4 %
2010	25.7 %	29.6 %	36.5 %	30.6 %

At each station, in 2009 and 2010, daily mean flow rates were 25.7 to 65.4 % lower compared to the historic mean flow rate. However in 2009 and 2010, there were less than 10 days of record low flows for each station. Record low flows are defined as a flow lower than the minimum value previously recorded on a particular day. On the Kettle and West Kettle Rivers at Westbridge, between April 1st and September 30th there were 9 and 7 days of record low flows, respectively in 2009 and 7 and 5 days, respectively in 2010. Because both stations near Westbridge only record hydrometric data between April and September, it is possible that there were other record low flows during the remainder of the year. On the Kettle River near Ferry, there were 5 days of record low flows in 2009 and no record low flow days in 2010.

3.3 Hydrogeology

The MOE has compiled water resource information such as mapped aquifers and registered well locations. There are four mapped aquifers within the study area – near Beaverdell, Westbridge, Rock Creek and Midway (BC Ministry of Environment, 2007). The location of these aquifers is shown in Figure 3-1. These aquifers are rated in terms of demand, productivity and vulnerability and are subsequently classified based on these ratings. 'Demand' refers to the amount of water currently withdrawn from the aquifer; the demand is ranked based on the density of domestic wells per square kilometer. 'Productivity' is the ability of the aquifer to supply water, which is ranked based on the following factors: aquifer materials, well yield, specific capacity and transmissivity. The demand and productivity ratings are combined and a "level of development" is assigned.

The vulnerability rating indicates how vulnerable the aquifer is to contamination introduced from the land surface and is based on the following factors: depth to water table, permeability, thickness of confining sediments and porosity. The 'level of development' and vulnerability ratings are then combined to rate the class of each aquifer (Berardinucci and Ronneseth, 2002). More information on the criteria for each of the different ratings and aquifer classes is available from Beradinucci and Ronneseth (2002). Table 3-2 summarizes size, materials and ratings of the aquifers in the Kettle River Basin.

Table 3-2: Characteristics of mapped aquifers in the Kettle River Basin (BC Ministry of Environment, 2007).

Location	**Beaverdell**	**Westbridge**	**Rock Creek**	**Midway**
Size (km^2)	15.9	6.1	5.8	3.6
Materials	sand and gravel	sand and gravel	sand and gravel	sand and gravel
Demand	low	low	moderate	high
Productivity	moderate	high	high	high
Vulnerability	high	moderate	high	high

The demand rating is based on how much water is withdrawn from the aquifer, which is related to the number of wells and the volume pumped from each well. The MOE has a voluntary program for water well drillers to submit data such as location, depth, lithology, and an estimate of flow rate, after drilling a well (BC Ministry of Environment, 2003), which is available on the WELLS database. A map of registered water wells is found on Figure 3-4. There are ~ 150 registered wells within the study area. Information from the well lithologies indicates surficial materials are composed primarily of sand and gravel with occasional boulders and minor amounts of silt and clay. Occasionally, lenses of finer materials (clay and silt), a few meters thick, were also recorded in well logs. Discussion of surficial geology in Chapter 2 indicated unconsolidated materials are either of glacial or fluvial origin and are deposited predominantly in the Quaternary. Well depths range between 3 and 250 meters. Of the ~150 registered wells, 30 % intercepted bedrock. The type of bedrock intercepted was not included in the well logs.

The aquifers discussed above are mapped because they are within close proximity to small towns, where population density is greater, compared to rural areas. There are other aquifers in rural areas, however they have not been mapped. Similarly there are many more wells drilled in the area, however because the WELLS database is voluntary, the wells discussed above only represent a portion of existing wells.

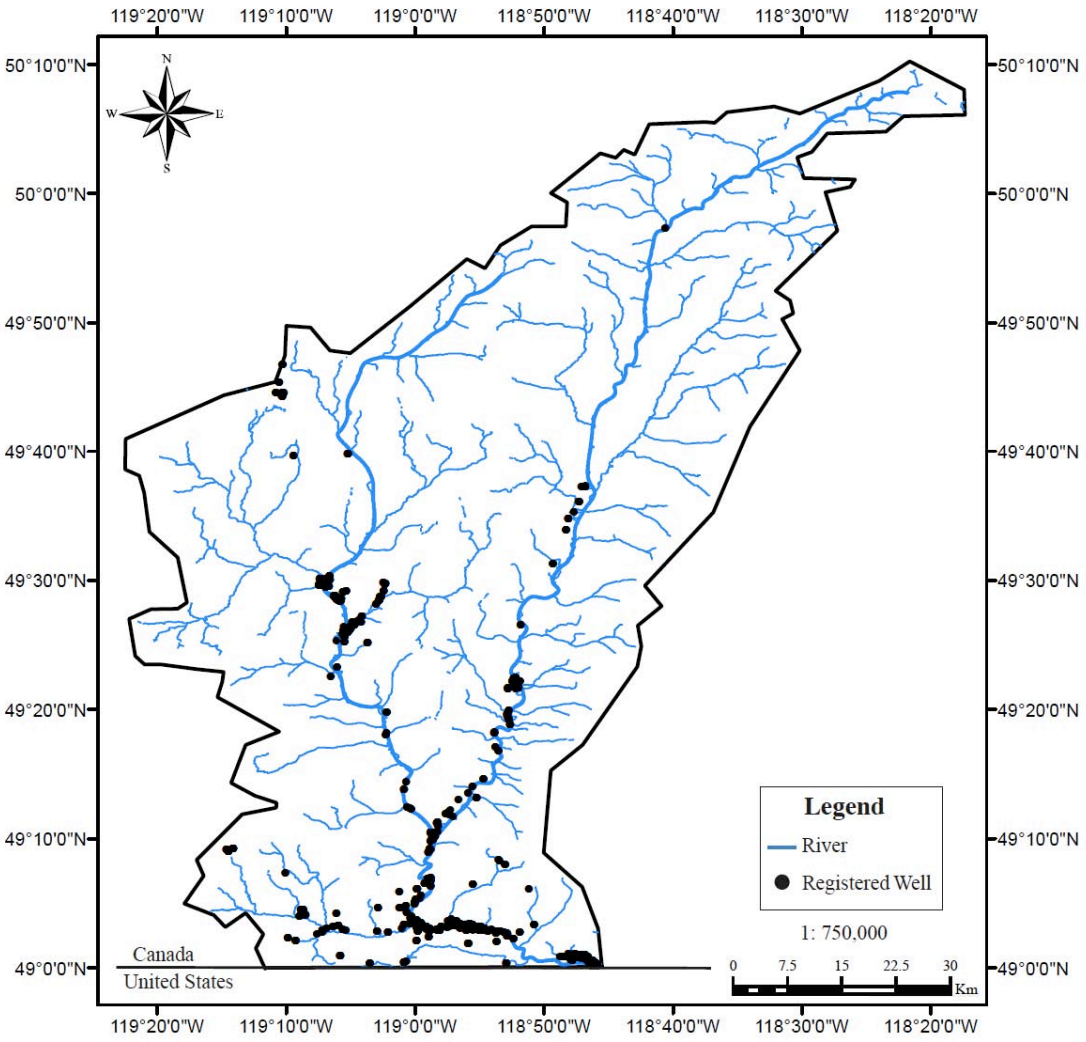

Figure 3-4: Mapped aquifers and wells registered in the Ministry of Environment WELLS database. The map was created with ArcGIS and data was obtained from the BC Geological Survey (2005) and BC Ministry of Environment (2003).

Mapped aquifers in the Kettle River Basin are moderately to highly productive sand and gravel aquifers. They have also been rated moderately to highly vulnerable to surface contamination. The Beaverdell and Westbridge aquifers have low demand ratings, compared to Rock Creek and Midway aquifers that have moderate and high demand ratings, respectively. The Rock Creek and Midway aquifers have both been rated highly productive and highly vulnerable, similar to the Grand Forks aquifer, located approximately 40 km east of Midway. Beyond Midway, the Kettle River flows into the United States for a short distance before it flows north back into Canada, near the town of Grand Forks. Surrounding the city of Grand Forks lies a unconfined sand and gravel aquifer. Groundwater studies have been on-going in this area since the 1960's, initially to address water supply issues and in more recent years, this aquifer has been investigated to address contamination issues (Wei et al., 2010). The population of the City of Grand Forks in 2006 was ~4000 (Wei et al., 2010), which is significantly higher compared to population in the study area of this project. Wei et al. (2010) released a report entitled: *State of Understanding of the Hydrogeology of the Grand Forks Aquifer*. As part of this project, a numerical groundwater model was created using MODFLOW to understand the current groundwater flow regime and estimate impacts of increasing groundwater demands. Lithologic data from well logs in the WELLS database were used to describe hydrostratigraphy and architecture of the aquifer in terms of six units (Wei et al., 2010). These six units are described in Table 3-3. The Midway and Rock Creek aquifers are located within close proximity to Grand Forks and have undergone similar glacial history and therefore are likely comprised of similar lithologic units. The glaciofluvial/fluvial gravel unit (Unit 1), closest to the surface is highly permeable and is therefore the reason for the high vulnerability rating of some aquifers. In areas overlying these high permeability gravels, anthropogenic activities have increased the potential to contaminate underlying aquifers (Wei et al., 2010).

Table 3-3: Description of hydrostratigraphy of the Grand Forks aquifer, modified from Wei et al. (2010).

Unit	Thickness (m)	Description	Hydrogeologic significance
1	Mean = 30	Glaciofluvial/fluvial gravel (along river channel) and minor colluvium	Vadose zone and unconfined aquifer when saturated
2	20-100	Glaciofluvial sand – aerially extensive, but varies in thickness	Unconfined aquifer
3	Mean = 40	Glaciolacustrine silty sand, silt and fine sand	Aquitard
4	unknown	Glaciolacustrine sand – spatial extent is unknown	Confined aquifer
5	unknown	Glaciolacustrine clay	Aquitard
6	unknown	Till	Aquitard, limited permeability aquifer

The MOE has a Groundwater Observation Network established in 1961 that monitors groundwater levels from observation wells remotely and/or manually on a daily basis (BC Ministry of Environment, 2010). Within the Kettle River Basin, there is one observation well (Well 306) in Beaverdell, which has monitored water level since 1989. As shown in Figure 3-5, the water level in Well 306 varied annually. The highest water level recorded was 4.2 meters below ground surface and the deepest water level recorded was 5.9 meters below ground surface, indicating water levels can vary up to 1.7 meters. Since 1989, it appears water levels have decreased slightly. In 2010, the maximum water depth recorded is less than 0.5 meters lower than the maximum water depth recorded in 1989. Figure 3-6 shows mean, minimum and maximum groundwater levels between 1989 and 2008 and groundwater levels during 2009 and 2010 for Well 306. Water levels from 2009 and 2010 are lower than average, with the exception of spring in 2010, which approaches the mean value in June. During fall of 2009, groundwater levels are particularly low and in some cases, are the lowest on record.

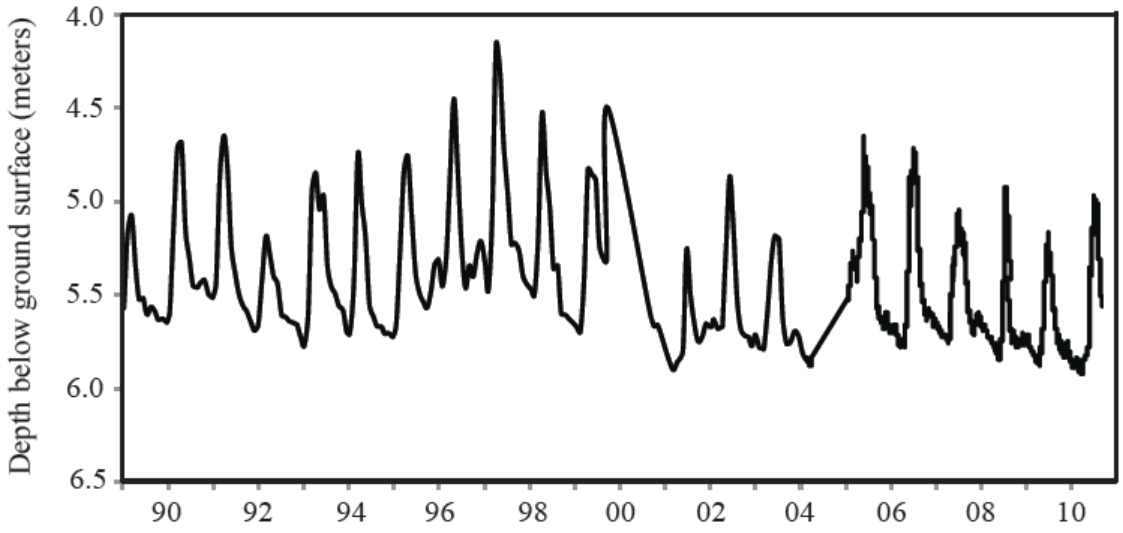

Figure 3-5: Historical groundwater levels in observation well 306 near Beaverdell between 1989 to 2010. Data from BC Ministry of Environment (2010).

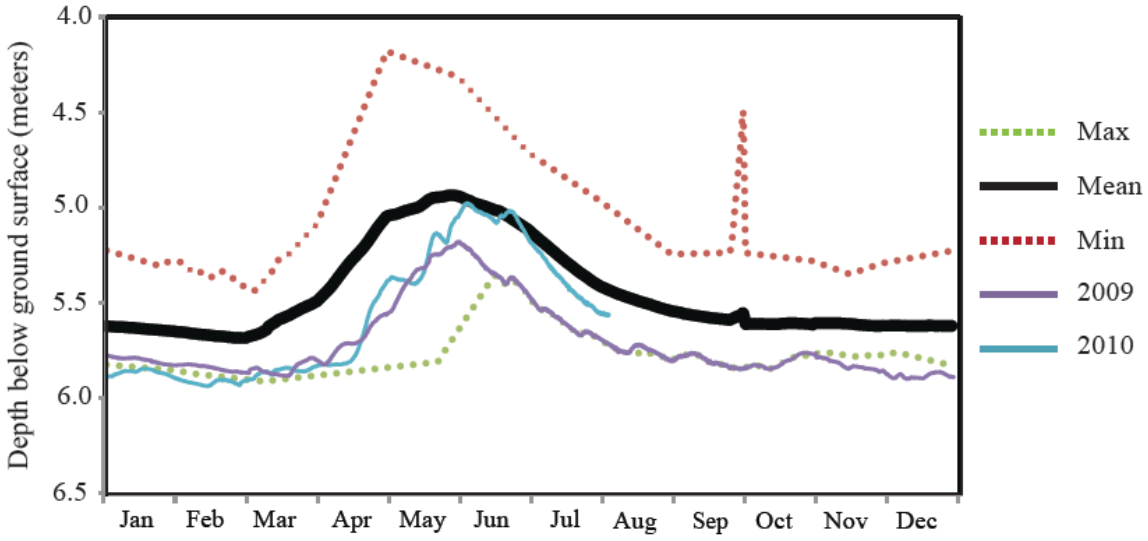

Figure 3-6: Groundwater levels in 2009 and 2010 compared to historical mean, maximum and minimum groundwater levels. Data for 2010 is only available until August (BC Ministry of Environment, 2010).

3.4 Hydrometric, Hydrogeologic and Climate Data: Historic vs. 2009 and 2010

Data from hydrometric stations indicate discharge rates from three stations in 2009 and 2010 were on average 55.4 % and 30.6 % lower, respectively compared to historic mean values, but there were only a few days of record low flows. Groundwater levels at the observation well in Beaverdell were lower than mean values throughout most of 2009 and 2010 and at times were lower than previously recorded values.

Comparison between historic and current climate data, discussed in greater detail in Chapter 2, indicated that average temperatures in 2009 were lower compared to average historic values, except at the Penticton station. In 2010, temperatures at all stations were higher than average historic values. The total annual precipitation (sum of rainfall and snowfall) at the Penticton station in 2009 and 2010 exceeded the historical average precipitation by 5.1 % and 15.9 %, respectively. Penticton was the only climate station with available historic precipitation data and data from 2009 and 2010. As mentioned in Chapter 2, this station is located approximately 20 km west of the western boundary of the Kettle River Basin and therefore may not be representative of precipitation rates in the basin. Comparison between historic snow survey values and values from 2009 and 2010, indicates that in 2009, values at half the stations exceeded the average historic snow-water equivalent values. In 2010, all the snow survey stations had snow-water equivalent values below average historic values throughout the winter until June, when values were higher than average.

Historical hydrologic, hydrogeologic and climate data compared to values in 2009 and 2010 indicate daily mean discharge rates and groundwater levels were lower than average. This may be due to climatic conditions – such as, lower rainfall and snow fall rates. However due to lack of precipitation data within the basin during 2009 and 2010, it is not possible to conclude with certainty that precipitation rates were lower. It is also possible there has been an increase in anthropogenic water use within the basin, which will be discussed in the following section.

3.5 Anthropogenic Water Use

Within the Kettle River basin, major water users include: municipal, domestic, agriculture (irrigation), ranching and mining (Dessouki, 2009). Rural residents, farmers, ranchers and industrial operations must either obtain water from surface water sources or groundwater wells.

Surface Water

In order to obtain water from surface water sources, a Water License must be obtained from the MOE. Water licences can be obtained for major rivers, such as the Kettle and West Kettle Rivers as well as smaller mountain streams. For each water license, detailed information is available, such as source name (stream or river name), purpose, quantity, licensee and issue date. The quantity is either the 'total demand for purpose' or the 'maximum licensed demand for purpose', neither of which indicate how much water is actually used. The Water Licensing system does not allow water use to be accurately monitored, but it does provide some insight into the major water users in the area. Within the Kettle River Basin there are two Water Districts for Surface Water Licences – McKinney and Westbridge. The McKinney district includes the southern part of the watershed, while the Westbridge district includes the northern portion of the watershed (BC Government, 2010).

There are seven different purposes for which a water license was issued in the Kettle Basin. These include, in order from largest to smallest volume, agricultural, industrial, power, storage, waterworks, institutional and domestic. The agriculture purpose includes irrigation or for stockwatering. The industrial purpose includes mining (hydraulic and placer), ponds, enterprises (businesses such as hotels and campgrounds which operate for a profit), work camps, camps (not for profit) and snow making (at Big White Ski Resort). The power licence refers to residential power licenses where water is used to produce power for residential use. The storage purpose includes the storage of water for non-power producing purposes. Waterworks refer to both local authorities and other authorities, which convey water to more than 5 dwellings. Institutional purposes

include fire protection and institutions such as schools and hospitals. Domestic water use includes water used in households as well as maintaining yards and gardens (BC Government, 2010). Figure 3-7 depicts the relative amount licensed for each purpose in the study area and Figure 3-8 details how much water is licensed for each purpose in both the McKinney and Westbridge districts. The greatest volume of water has been licensed for agriculture (59 %) and the majority of this (99.78 %) is used for irrigation, while the remainder is used for ranching/stockwatering. Other major water licenses include a hydraulic mining operation and four licences for residential power.

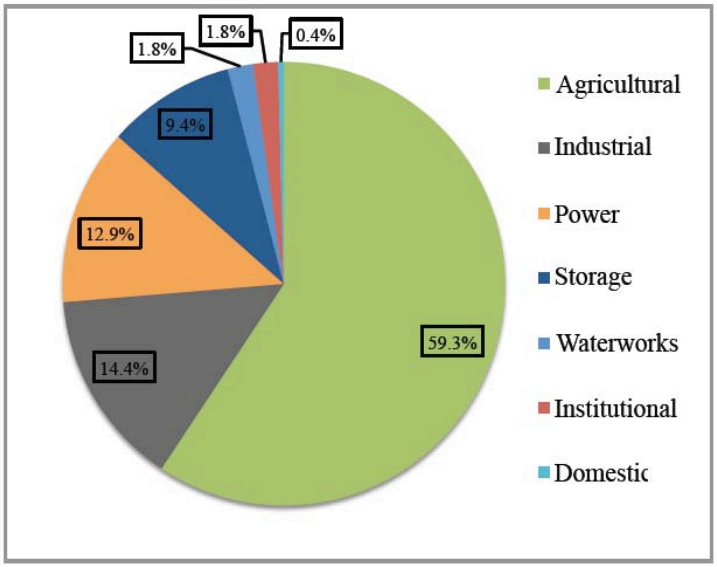

Figure 3-7: Relative amount of surface water licensed for different purpose in the study area (BC Government, 2010).

Big White ski resort has recently attracted attention in the media for submitting applications for several surface water licenses in 2007 on the West Kettle River and nearby streams. Big White is situated within the Westbridge District and currently holds water licences for enterprises, snowmaking, storage and waterworks purposes from Westbridge Creek, Trapping Creek, Hallam Creek and Skiing Brook. The current total water licence is 3.59 million L/day, 2 % of the total licensed water. On July 20, 2007, Big White submitted water license applications for an additional 26.1 million L/day from Trapping Creek, Hallam Creek and the West Kettle River (BC Government, 2010). The

water licenses have not been approved as of the date of writing. If approved, Big White would hold 17 % of the total surface water licenses in the Kettle Basin.

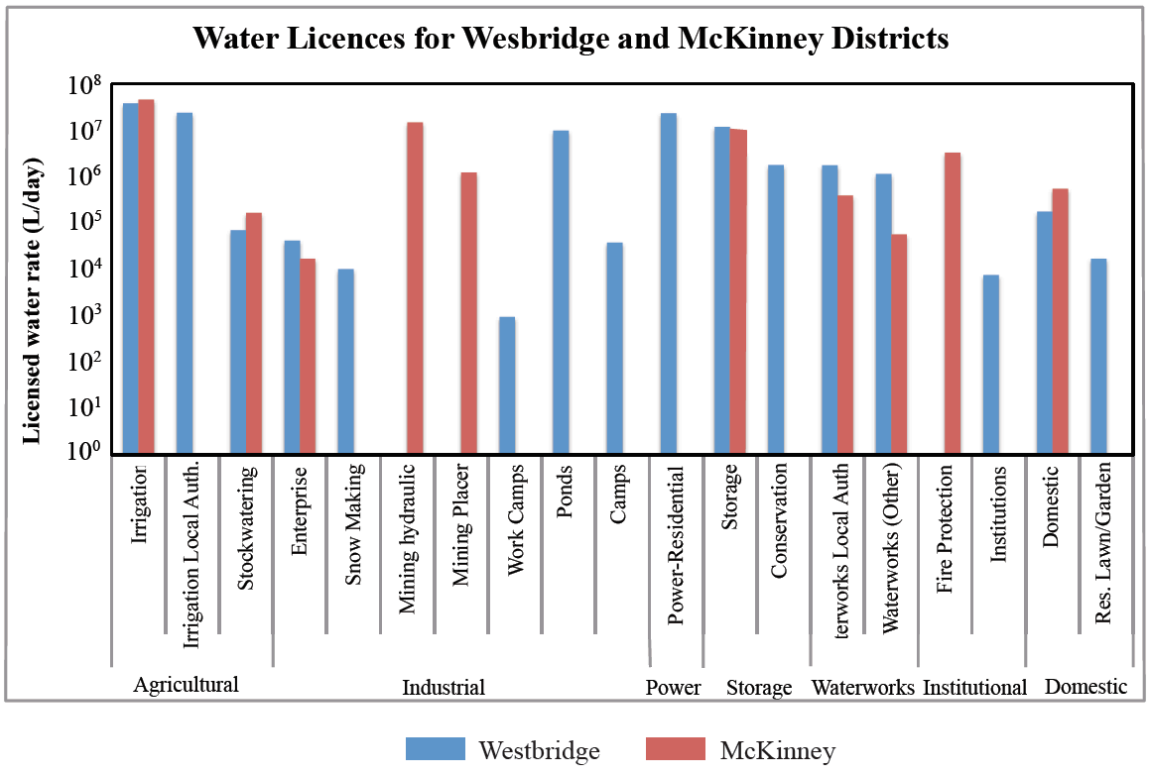

Figure 3-8: Types of water licenses for McKinney and Westbridge districts (BC Government, 2010).

Groundwater

In addition to surface water licenses, rural residents also use groundwater. The total amount of groundwater currently extracted is not known as it is not monitored. According to the BC Government, approximately 95 % of wells are used for single family homes, while the remaining 5 % are used for community water systems, municipalities, industry, agriculture and some other minor non-domestic uses such as geothermal.

Chapter Four: Field and Laboratory Methods

4.1 Sampling Campaigns

Surface water and groundwater samples were collected during three sampling campaigns, which occurred in October 2009, June 2010 and October 2010. The exact dates samples were collected are: October 30th to November 1st, 2009, June 17th to 21st, 2010 and October 15th to 18th, 2010. Precipitation samples were collected between June 8th and 18th of 2010.

4.2 Sampling Site Locations

Precipitation Samples

Four precipitation samples were collected near Rock Creek, BC. The location of the precipitation sampling site is shown in Figure 4-1.

Surface Water Samples

Surface water samples were collected from the headwaters of the Kettle and West Kettle Rivers, beyond the confluence of the two rivers, downstream to the Canadian – US border. Because anthropogenic activities increase with increasing distance downstream, a higher density of sampling sites were selected beyond the confluence of the two rivers. In October 2009, 22 surface water samples were collected and in June and October of 2010, 25 surface water samples were collected. Three more sampling sites were added in 2010, between Rock Creek, BC and the Canadian – US border, to ensure that potential anthropogenic influences on water chemistry were captured. Figure 4-1 shows the locations of surface water sampling sites. The sample numbers adjacent to the sampling locations correspond to sample numbers assigned during the June 2010 sampling trip. No samples were collected from site numbers 26, 28 and 35 in October of 2009.

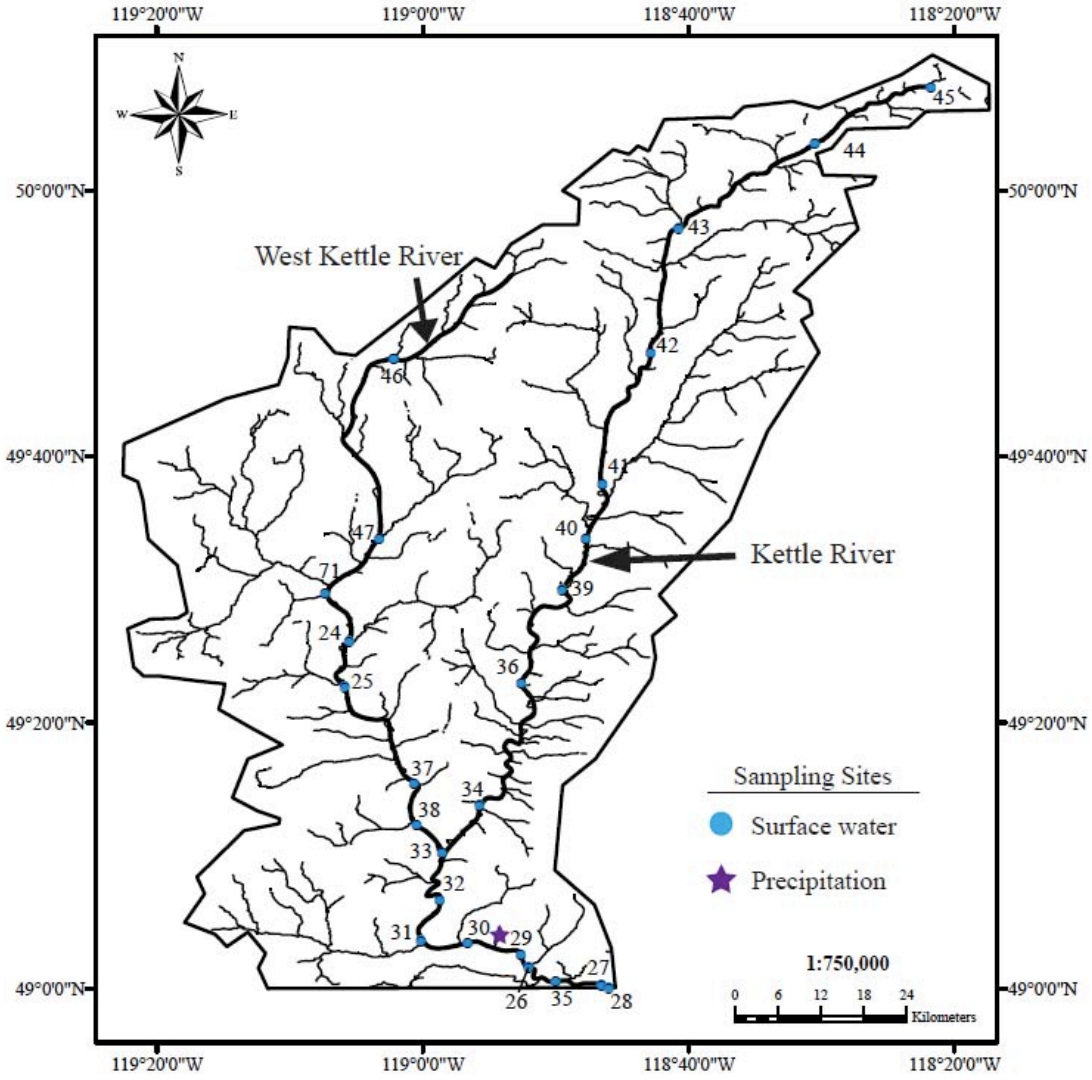

Figure 4-1: Location of surface water and precipitation sampling sites. Numbers corresponding to sites refer to samples collected in June 2010. No samples were collected from site numbers 26, 28 and 35 in October 2009.

Groundwater Samples

Groundwater samples were taken from groundwater wells of residents who volunteered to participate in this project. The locations of groundwater wells were focused in the southern portion of the basin, as shown in Figure 4-2. In October of 2009, one groundwater sample was collected, in June of 2010, 23 groundwater samples were taken and in October of 2010, 24 groundwater samples were collected. The sample

numbers adjacent to the points in Figure 4-2 correspond to sample numbers from June 2010, with the exception of sample #134, which was only obtained in October 2010. The only groundwater sample collected in October of 2009 was from location #62 in Figure 4-2. The sample numbers from each sampling campaign, which correspond to each sampling location are summarized in Appendix A. No information was available regarding the depth of the well and the lithology surrounding the well screen.

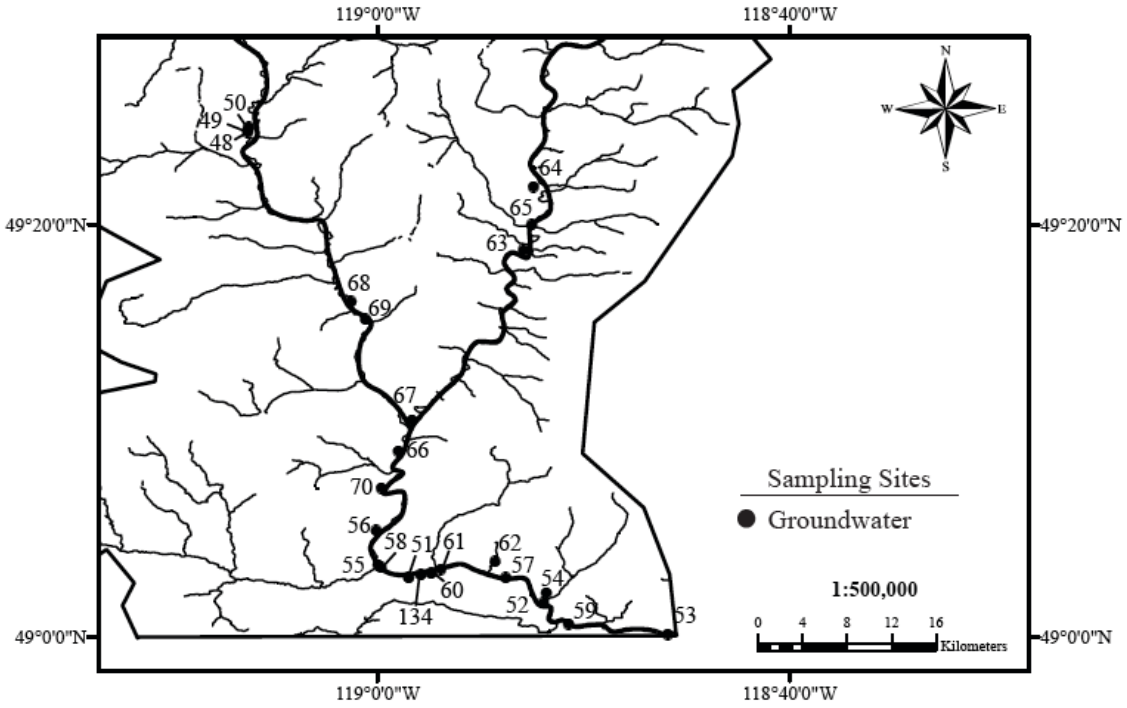

Figure 4-2: Location of groundwater sampling sites in the southern portion of the Kettle River Basin. Numbers corresponding to samples refer to samples collected in June 2010, except #134, which refers to a sample collected in October of 2010, which was not sampled in June 2010.

4.3 Field Methods

Precipitation samples were collected during rain events in June of 2010. Sample bottles were opened during rain events and closed when no precipitation occurred. Surface water samples were collected from the middle of the river, in fast flowing, well mixed sections. Most samples were collected from bridges, using a bucket, which was lowered from the bridge deck into the river. The bucket was rinsed twice with sample water and the sample was collected the third time. In four locations (#26, 28, 35, 39) there were no bridges in close proximity, and so instead, the samples were taken from the side of a fast flowing, well-mixed section of river.

During sample collection, a YSI probe was used to measure temperature, pH, conductivity and dissolved oxygen concentration. For surface water samples, the YSI was lowered into the river until each parameter stabilized. For groundwater samples, the YSI was placed in a bucket while groundwater flowed continuously into the bucket. To ensure the groundwater sample was representative of water in the aquifer, instead of water in the well casing, water was pumped from the well until parameters on the YSI probe stabilized. The reported accuracy of temperature, pH and conductivity is: ± 0.15 °C, ± 0.2 pH units and ± 0.5 % of reading, respectively. The accuracy of dissolved oxygen concentration is the greater of ± 0.2 mg/L or 2 % of reading (YSI, 2011). Parameters measured with the YSI are summarized in Appendix A.

All surface water and groundwater samples were collected for analysis of the following parameters: major anions, major cations, silica and stable isotope abundance ratios of hydrogen ($\delta^{2}H_{H2O}$), oxygen ($\delta^{18}O_{H2O}$), dissolved inorganic carbon ($\delta^{13}C_{DIC}$), nitrate ($\delta^{15}N_{NO3}$ and $\delta^{18}O_{NO3}$) and sulfate ($\delta^{34}S_{SO4}$ and $\delta^{18}O_{SO4}$). Major anions include alkalinity, chloride (Cl^{-}), sulphate (SO_4^{2-}) and nitrate (NO_3^{-}). Major cations include calcium (Ca^{2+}), magnesium (Mg^{2+}), sodium (Na^{+}) and potassium (K^{+}). Although not considered to be a major cation, silica (Si^{4+}) concentrations were also measured for geochemical modelling. All sample water, except an aliquot used to measure alkalinity, was filtered through a 0.45 μm millipore filter. Samples for alkalinity and $\delta^{13}C$ measurements were collected in 125 mL air-tight glass bottles and preserved by

refrigeration. Cation and anion samples were collected in 125 mL plastic high density polyethylene (HDPE) bottles. Cation samples were preserved by addition of HNO_3 to a pH of less than 2. δ^2H and $\delta^{18}O$ samples were collected in 10 mL vacuum-sealed containers. Samples for stable isotope analyses of NO_3^- were collected in 125 mL HDPE bottles and preserved by freezing.

In October of 2009, samples for $\delta^{34}S_{SO4}$ and $\delta^{18}O_{SO4}$ analysis were collected in 125 mL HDPE containers, however, SO_4^{2-} concentrations were insufficient for isotope analysis. To address this problem, in June and October of 2010, a greater volume of sample (1 L) was collected. Samples were preserved by freezing.

Precipitation water was sampled for measurement of anions and cation concentrations, and δ^2H and $\delta^{18}O$ values. There was not enough sample volume to determine the stable isotope abundance ratios of NO_3^- and SO_4^{2-} in precipitation.

4.4 Laboratory Methods

4.4.1 Anions and Cations

All anion and cation concentrations were measured in the Applied Geochemistry Group Laboratory at the University of Calgary. Alkalinity was determined using acid titration analysis, which measures all titratable species including HCO_3^-, CO_3^{2-}, borate, ionized silicic acid, bisulfide and organic acids (Drever, 1997). Borate, ionized silicic acid, bisulfide and organic acids are assumed to be present in insignificant amounts compared to HCO_3^- and CO_3^{2-}, which is valid for most natural waters (Drever, 1997). Standards were titrated before and in between sample titrations. Twenty-four percent of samples were analyzed in duplicate. The average discrepancy between original and duplicate samples was less than 5 %. The alkalinity concentration of precipitation samples was below the working range of the titrator; below ~10 mg/L the titrator is unable to detect an inflection point during titrations.

In titrations, the alkalinity is reported as HCO_3^-, assuming alkalinity was equivalent to HCO_3^-. At the pH range of samples, HCO_3^- is the dominant species of dissolved inorganic carbon, however there are also minor concentrations of CO_3^{2-}. The

geochemical modelling software SOLMINEQ88 was used to determine the concentration of HCO_3^-, given the measured alkalinity and pH values.

The remaining anions (Cl^-, SO_4^{2-} and NO_3^-) were analysed by Ion Chromatography (IC) (Dionex ICS-2000). Three standards were analysed before each sample set, and one standard was analysed after every ten samples, to ensure the instrument was producing accurate results. Duplicate samples were included in each sample set and each sample set was measured twice. The average percent difference between the two runs and between duplicate samples was less than 5 %.

Ca^{2+}, Mg^{2+}, Na^+ and K^+ concentrations were measured using Atomic Absorption Spectrometry (Perkin Elmer AAnalyst 100). Standards and blank samples were run before and during analysis. Each sample was analysed three times and uncertainty in measurements for each sample was less than 5 %. Si^{4+} concentrations were measured using an Inductively Coupled Plasma Optical Emission Spectrometry (ICP-ES) instrument (Varian 725-ES). Three standards and one blank sample were analysed before and after each sample set. In addition, one standard was analysed after every ten samples. Each sample was measured three times and the resulting discrepancy between replicate samples measurements was less than 5 %. When parameters were measured more than once, the average of the all measurements was reported. The reported uncertainty associated with this method is less than 5 %.

The average charge balance of surface water samples was 3.0 % and the average charge balance of groundwater samples was 0.7 %. There are few surface water and groundwater samples that have charge balance values of greater than 5 %. Anion and cation concentrations and resulting charge balance values are tabulated in Appendix A.

4.4.2 Stable Isotope Abundance Analyses

All stable isotope analyses were completed in the Isotope Science Laboratory at the University of Calgary. Results of stable isotope analyses are found in Appendix A. The isotope abundance ratios are expressed in δ notation:

$$\delta_{sample}\ (‰) = [(R)_{sample} - (R)_{standard})/ (R)_{standard}] \times 1000 \quad (4\text{-}1)$$

Values are expressed in units of parts per thousand, or 'per mil' (‰) notation. 'R_{sample}' is the measured ratio of heavy over light isotope, reported relative to international standards ($R_{standard}$) (Appelo and Postma, 2005). Analytical methods for the specific stable isotope ratio measurements used in this study are described below.

$\delta^{18}O_{H2O}$ and $\delta^{2}H_{H2O}$

Abundances ratios of O and H isotopes (^{18}O, ^{16}O, ^{2}H, ^{1}H) were measured using laser spectroscopy. Approximately 750 nL of sample water was injected into a Los Gatos Research 'DLT-100' instrument. The water was vaporized and expanded into the laser cell and measured directly by "Off-Axis Integrated-Cavity Output Spectroscopy". Measurement uncertainty for $\delta^{18}O$ is ± 0.2 ‰ and ± 1.0 ‰ for $\delta^{2}H$. Measured $\delta^{18}O$ and $\delta^{2}H$ values are reported relative to Vienna Standard Mean Ocean Water (VSMOW).

$\delta^{13}C_{DIC}$

Dissolved Inorganic Carbon (DIC) in water was converted to cryogenically purified CO_2 (g) on a glass extraction line, using phosphoric acid. The $^{13}C/^{12}C$ abundance ratios of CO_2 (g) were measured on a VG-903 isotope ratio mass spectrometer. Reported uncertainty of $\delta^{13}C_{DIC}$ is ± 0.2 ‰. Results were reported relative to the Vienna Peedee Belemnite (V-PDB) standard (Isotope Science Lab, 2011).

$\delta^{15}N_{NO3}$ and $\delta^{18}O_{NO3}$

The stable isotope abundance ratios of dissolved NO_3^- (^{15}N, ^{14}N, ^{18}O and ^{16}O) were determined simultaneously using the "denitrifier method" (Sigman et al., 2001; Casciotti et al., 2002). Nitrate (NO_3^-) was reduced to nitrous oxide (N_2O) using denitrifying bacteria. Isotope fractionation occurs during reduction of NO_3^- to N_2O, however if the reaction is complete and all the NO_3^- is converted to N_2O and there are no additional sources of N, the N isotopic composition of N_2O will be the same as that of the initial NO_3^- (Sigman et al., 2001). During the reduction, only one oxygen molecule from the NO_3^- ends up in the N_2O, creating two problems – oxygen isotope fractionation due to loss of oxygen molecules and exchange of oxygen with water during the bacterial reduction reaction. These effects have been quantified and were found to be small (10 and 3 %, respectively) and are accounted for using correction factors (Casciotti et al., 2002) and standards with known $\delta^{18}O_{NO3}$ values.

The denitrifying bacteria were grown in a tryptic soy broth for seven days; after seven days nutrients were exhausted and bacteria were present in sufficient quantities for analysis. The bacteria were then subdivided into individual vials, flushed with inert N_2 and a specific amount of sample NO_3^- was injected. The samples were incubated for ~ 16 hours and then NaOH was added to lyse the bacteria. Samples were then loaded into an autosampler and processed by a PreCon device and HP 6890 gas chromatograph separating N_2O from excess moisture and CO_2, before entering an open split interface that 'leaked' the measurement N_2O gas into the mass spectrometer. The Isotope Science Laboratory (2011) reports an uncertainty of ± 0.5 ‰ for $\delta^{15}N_{NO3}$ and ± 1.0 ‰ for $\delta^{18}O_{NO3}$. Raw $\delta^{15}N_{NO3}$ and $\delta^{18}O_{NO3}$ data were normalized and calibrated against international reference materials and are reported relative to N_2 (air) and VSMOW, respectively.

$\delta^{34}S_{SO4}$ and $\delta^{18}O_{SO4}$

The stable isotope abundance ratios of SO_4^{2-} ($^{34}S/^{32}S$, $^{18}O/^{16}O$) were determined on SO_4^{2-} samples that were converted to pure $BaSO_4$. In order to achieve this, samples were acidified to a pH of less than 4 and passed through anion columns where SO_4^{2-} was exchanged with Cl^-, resulting in retention of SO_4^{2-} on the columns. Beneath each column, 125 mL beakers were placed with 10 mL of barium chloride ($BaCl_2$). The columns were then eluted with 3.0 M potassium chloride (KCl). The elution caused SO_4^{2-} ions to be released from the column and subsequently react with $BaCl_2$ to form a pure $BaSO_4$ precipitate. The $BaSO_4$ was then filtered through a 0.4 μm isopore filter; the precipitate was rinsed with 15-30 mL of DI water to remove any lingering Cl^- from $BaSO_4$ precipitate. In order to determine the $\delta^{34}S$ values, pure $BaSO_4$ (100 to 300 μg) was packed into tin cups, which were loaded in an autosampler and dropped onto a high temperature (1020 °C) quartz tube combustion reactor. A pulse of O_2 gas was injected at the same time as the sample was dropped causing 'flash-combustion'. A helium carrier stream moved the gases produced from flash combustion into a gas chromatograph column where sulfur dioxide (SO_2) was separated from nitrous oxides (NO_x's) and carbon dioxide (CO_2). The SO_2 was then leaked into a mass spectrometer through an open split interface. The Isotope Science Laboratory reports a precision of ± 0.3 ‰ for $\delta^{34}S_{SO4}$ values that were reported relative to Vienna Canyon Diablo Troilite (V-CDT) (Isotope Science Lab, 2011).

The $BaSO_4$ precipitate was also used for determining the $\delta^{18}O$ values of surface water and groundwater SO_4^{2-}. Pure $BaSO_4$ (100 to 300 μg) was packed into silver cups and loaded in an autosampler, which dropped samples into a high temperature (1450 °C) pyrolysis reactor. In this reactor, $BaSO_4$ was converted to CO, which was swept by a carrier gas through a gas chromatograph achieving separation of CO from N_2. CO was then transported through an open split interface into the ion source of a mass spectrometer. The reported uncertainty for $\delta^{18}O_{SO4}$ is ± 0.5 ‰. Results were reported with respect to VSMOW (Isotope Science Lab, 2011) and were normalized with several reference materials.

Chapter Five: Major Ion Chemistry

5.1 Introduction

In this Chapter, major ion chemistry of surface water and groundwater samples from the Kettle River Basin is discussed in terms of temporal and spatial variation. Temporal variation is assessed based on the three sampling events, which were in conducted October 2009, June 2010 and October 2010. Spatial variation in surface water geochemistry is discussed in terms of the three main sections of the rivers: the Kettle and West Kettle Rivers before the confluence and the Kettle River below the confluence. Variation in groundwater geochemistry is also discussed. Surface water and groundwater chemistries are compared to assess the influence of groundwater on surface water chemistry. Major anions include HCO_3^-, SO_4^{2-}, Cl^- and NO_3^-, and major cations include Ca^{2+}, Mg^{2+}, K^+ and Na^+. Discussion of the average, minimum and maximum concentrations of major ions and how these change temporally and spatially provides insight into natural and anthropogenic sources of ions in aquatic systems.

5.2 Total Dissolved Solids

Surface Water

Total Dissolved Solids (TDS) in surface waters decrease as discharge rates increase. Figure 5-1 shows TDS plotted against discharge from hydrometric stations located on the Kettle and West Kettle Rivers and below the confluence of the two rivers. In June, TDS ranges from 19.0 to 114.5 mg/L and in October TDS ranges from 49.7 to 158.7 mg/L. Average TDS in June is 42.9 ± 17.7 mg/L (n=25), while in October, the combined average TDS of 2009 and 2010 is 105.5 ± 29.0 mg/L (n=47). TDS increases with increasing distance downstream for both the Kettle and West Kettle Rivers with the exception of one location near the headwaters of the Kettle River (Figure 5-2). There is also a significant increase in TDS between 65 and 73 km downstream on the West Kettle River. At this location, in June, there is an increase in TDS of 23 % and an increase of 53 % in October (average of 2009 and 2010). These increases correspond to increases in specific ions, which are discussed in Chapter 7.

The confluence of the two rivers is marked by a change in TDS, indicating mixing of waters. Along the Kettle River, TDS gradually increases beyond the confluence, whereas, along the West Kettle River, TDS decreases abruptly (Figure 5-2). As discussed in Chapter 3, the Kettle River contributes 68 % to the flow beyond the confluence while the West Kettle River contributes 32 %. In June, at the last sampling location on the Kettle River before the confluence, TDS is 37.2 mg/L. At the last sampling location on the West Kettle River in June, TDS is 46.5 mg/L. If these values are multiplied by the percentages of flow in each tributary, the calculated estimate of TDS is 40.2 mg/L, whereas the measured value of TDS at the first sampling location after the confluence is 39.8 mg/L. Because the calculated and measured values are very similar, this suggests the cause of the abrupt change in TDS with increasing distance from the headwaters of the West Kettle River, after the confluence, is simply due to mixing of lower TDS waters from the Kettle River with higher TDS waters from the West Kettle River.

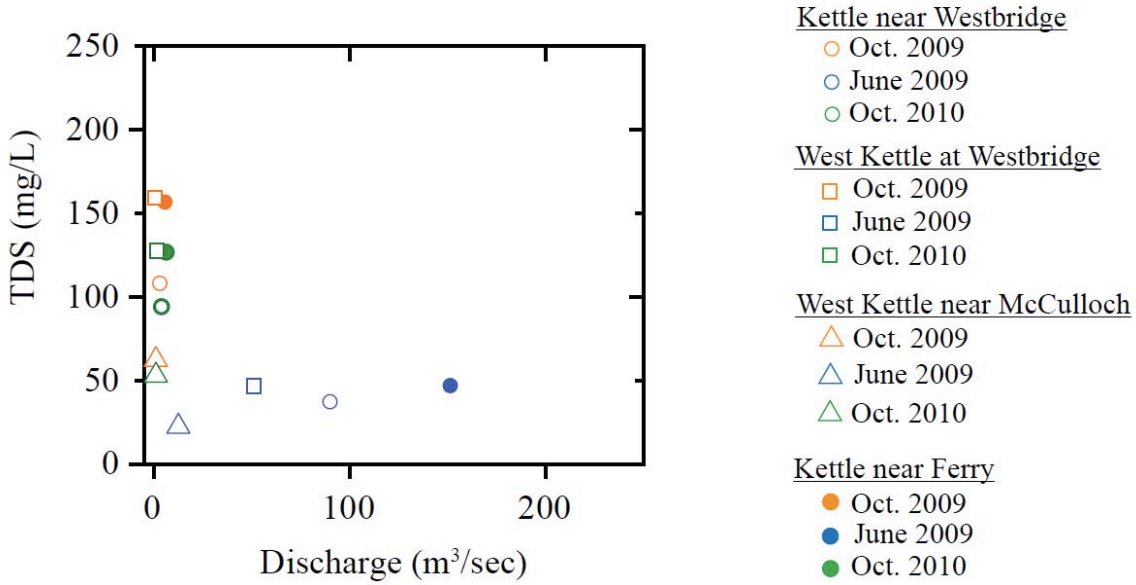

Figure 5-1: TDS versus discharge at four hydrometric stations. Sample locations do not correspond exactly to hydrometric stations so the closest sampling location was used. On the West Kettle River, the McCulloch station was half way between two sampling locations, so the average TDS of these two sampling locations was used.

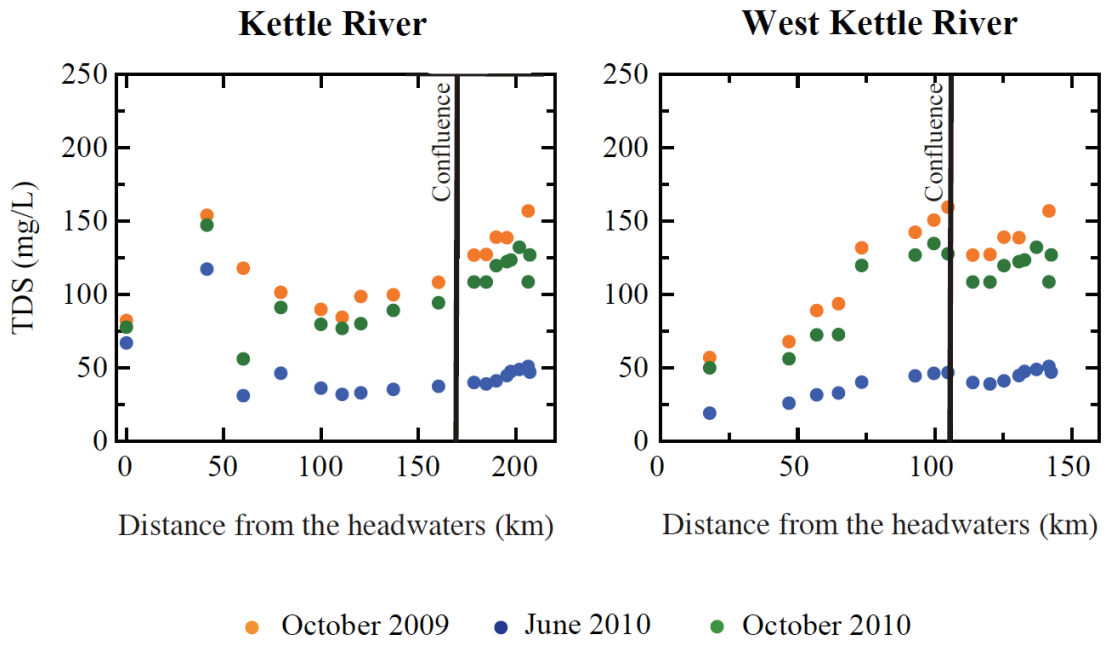

Figure 5-2: TDS versus distance from the headwaters of the Kettle and West Kettle Rivers. The vertical line indicates the confluence of the two rivers.

Groundwater

Groundwater has more time to interact with aquifer materials typically resulting in higher TDS. TDS depends on several factors, such as the rate of groundwater flow, which determines the amount of time water has to interact with aquifer materials, solubility of minerals and the rate of dissolution of minerals (Appelo and Postma, 2005). Groundwater TDS ranges from 145.7 to 571.5 mg/L. Comparison of groundwater samples collected in both June and October of 2010, indicates TDS exhibits little temporal variation – the average TDS in June is 341.8 ± 121.5 mg/L (n=23) and 322.1 ±119.2 mg/L (n=23) in October.

5.3 Major Anions

Precipitation

The anion present in highest concentrations in precipitation is NO_3^-, with lower concentrations of SO_4^{2-} and Cl^-, as summarized in Table 5-1. It was not possible to measure HCO_3^- in precipitation samples as the concentration was below the working range of the titrator.

Table 5-1: Average, standard deviation, minimum and maximum values of major anions in precipitation samples collected in June.

Sampling Event	Statistics	HCO_3^- (mg/L)	SO_4^{2-} (mg/L)	Cl^- (mg/L)	NO_3^- (mg/L)
June n=3	Average	-	0.2 ± 0.1	0.2 ± 0.2	1.4 ± 0.6
	Min	-	0.1	<0.1	0.9
	Max	-	0.3	0.3	2.1

Surface Water

In surface water samples, major anions in order of decreasing average concentration are HCO_3^-, SO_4^{2-}, Cl^- and NO_3^-. All anions have lower average concentrations in June compared to October, similar to TDS, which is due to higher discharge rates in June. Of all anions, HCO_3^- is present in the highest concentrations (up to 104.1 mg/L in October) and NO_3^- occurs in the lowest concentrations. In June, NO_3^- is not detected in any surface water samples and in October of 2009 and 2010, all samples have NO_3^- concentrations less than 0.5 mg/L, except one sample, which has a concentration of 1.7 mg/L. The average, standard deviation, minimum and maximum values of each anion in surface water, in June and October is summarized in Table 5-2.

Table 5-2: Average, standard deviation, minimum and maximum values of major anions in June and October in surface water samples. If concentrations were not detected, this is indicated with 'n.d.'.

Sampling Event	Statistics	HCO_3^- (mg/L)	SO_4^{2-} (mg/L)	Cl^- (mg/L)	NO_3^- (mg/L)
June n=25	Average	25.4 ± 12.9	1.8 ±1.0	0.7 ± 0.3	n.d.
	Min	10.0	0.7	0.1	n.d.
	Max	79.3	5.0	1.2	n.d.
October n=47	Average	67.8 ± 20.0	5.1 ± 2.0	2.1 ± 1.3	0.1 ± 0.3
	Min	27.5	1.3	0.3	n.d.
	Max	104.1	8.3	4.2	1.7

Groundwater

The order of major anions in groundwater samples follows a similar order as in surface water samples, except NO_3^- has a higher average concentration compared to Cl^-. HCO_3^- is present in concentrations of up to 389.9 mg/L in October, whereas NO_3^- is not detected in some samples in June and October. Table 5-3 includes the mean, standard deviation, minimum and maximum concentrations of each anion in June and October. There is much greater variation in the concentrations of anions in groundwater samples. For example, in June, SO_4^{2-} concentrations range from 4.6 to 145.6 mg/L, NO_3^- concentrations range from not detected to 41.3 mg/L and Cl^- concentrations range from 1.5 to 45.1 mg/L. All samples have SO_4^{2-} concentrations less than 40.0 mg/L, except for four samples from two wells, which were both sampled in June and October. These samples have SO_4^{2-} concentrations ranging from 111.2 to 145.6 mg/L. These four samples also have high Na^+ concentrations. The only anion that has concentrations approaching the Maximum Acceptable Concentration (MAC) published in the *Guidelines for Canadian Drinking Water Quality* is NO_3^-, which has a MAC of 45 mg/L (Health Canada, 2010). The Guidelines for Canadian Drinking Water Quality do not have MAC values published for HCO_3^-, Cl^- or SO_4^{2-}, however there is an aesthetic objectives for Cl^- and SO_4^{2-} which are ≤ 250 mg/L and 500 mg/L, respectively. High nitrate concentrations can potentially be due to anthropogenic activities, such as septic systems, synthetic fertilizers, and/or manure (e.g. Kendall et al., 2007). Possible sources of NO_3^- are identified in Chapter 6, using stable isotopes. High concentrations of Cl^- are likely due to

anthropogenic influences, such as road salt application to de-ice highways, as there are no geological sources of Cl^- in the Kettle River Basin. Groundwater samples with high Cl^- concentrations are identified and discussed in Chapter 7.

Table 5-3: Average, standard deviation, minimum and maximum values of major anions in groundwater samples collected in June and October. If concentrations were not detected, this is indicated with 'n.d.'.

Sampling Event	Statistics	HCO_3^- (mg/L)	SO_4^{2-} (mg/L)	Cl^- (mg/L)	NO_3^- (mg/L)
June n=23	Average	189.8 ± 70.0	28.5 ± 33.5	10.7 ±11.8	27.7 ± 8.5
	Min	89.8	4.6	1.5	n.d.
	Max	369.7	145.6	45.1	41.3
October n=25	Average	188.7 ± 65.1	28.4 ± 32.6	11.0 ± 14.1	6.9 ± 5.8
	Min	107.5	4.3	1.1	n.d.
	Max	389.9	139.5	54.7	18.3

5.4 Major Cations

Precipitation

The order of decreasing average concentrations of cations in precipitation samples is Ca^{2+}, Na^+, Mg^{2+} followed by K^+. The highest cation concentration is 1.4 mg/L of Ca^{2+} and K^+ was not detected in some samples. Values are summarized in Table 5-4.

Table 5-4: Average, standard deviation, minimum and maximum values of major cations in precipitation samples collected in June and October. If concentrations were not detected, this is indicated with 'n.d.'.

Sampling Event	Statistics	Ca^{2+} (mg/L)	Mg^{2+} (mg/L)	Na^+ (mg/L)	K^+ (mg/L)
June n=4	Average	1.0 ± 0.3	0.1 ± <0.1	0.3 ± 0.1	0.1 ± <0.1
	Min	0.8	0.1	0.1	n.d.
	Max	1.4	0.2	0.4	0.1

Surface Water

Cations, in order of decreasing average concentration in surface water are Ca^{2+}, Na^+, Mg^{2+} and K^+ in both June and October. Similar to anions, the average concentrations of all cations in surface water samples are higher in October compared to June due to

lower discharge rates in October. The highest cation concentration is 33.5 mg/L of Ca^{2+} in October and the lowest is 0.2 mg/L of K^{+} in June. The average, standard deviation, maximum and minimum values of samples from June and October are summarized in Table 5-5.

Table 5-5: Average, standard deviation, minimum and maximum values of major cations in surface water samples collected in June and October.

Sampling Event	**Statistics**	**Ca^{2+} (mg/L)**	**Mg^{2+} (mg/L)**	**Na^{+} (mg/L)**	**K^{+} (mg/L)**
June n=25	Average	8.1 ± 4.1	0.9 ± 0.2	1.1 ± 0.4	0.4 ± 0.1
	Min	2.8	0.5	0.5	0.2
	Max	24.3	1.3	1.8	0.6
October n=47	Average	18.6 ± 5.8	2.6 ± 0.9	2.9 ± 1.1	0.8 ± 0.2
	Min	7.7	0.7	0.5	0.4
	Max	33.5	3.9	4.2	1.2

Groundwater

Groundwater samples follow the same order of decreasing average concentrations compared to surface waters, which is: Ca^{2+}, Na^{+}, Mg^{2+} and K^{+}. The average concentration of each cation is higher in groundwater compared to surface waters. The highest measured cation concentration is 149.8 mg/L of Na^{+} in October and the lowest is 0.3 mg/L of K^{+} in October. Similar to anions, there is a significant range in concentrations of cations in groundwater. For example, Ca^{2+} varies from 11.7 to 97.0 mg/L and Na^{+} ranges from 2.5 to 149.8 mg/L (Table 5-6). There are only four samples, obtained from two wells sampled in June and October, with Na concentrations greater than 35.0 mg/L. The range in Na^{+} of these four samples is between 109.9 and 149.8 mg/L, similar to the range of SO_4^{2-} concentration in these four groundwater samples. The high Na^{+} and SO_4^{2-} concentrations in these samples is likely due to the geology surrounding the well. The specific mineral sources of these ions are discussed in Chapter 8.

Table 5-6: Average, standard deviation, minimum and maximum values of major cations in groundwater samples collected in June and October.

Sampling Event	Statistics	Ca^{2+} (mg/L)	Mg^{2+} (mg/L)	Na^{+} (mg/L)	K^{+} (mg/L)
June n=23	Average	49.3 ± 20.4	9.2 ± 4.4	21.7 ± 33.3	2.4 ± 1.8
	Min	11.7	2.8	2.5	0.8
	Max	97.0	23.9	137.4	7.9
October n=25	Average	46.8 ± 20.0	9.1 ± 4.9	23.4 ± 36.1	1.9 ± 1.0
	Min	12.0	3.6	3.4	0.3
	Max	87.4	25.1	149.8	5.0

5.5 Combined Anions and Cations

Major anions and cations were plotted on Piper diagrams to investigate spatial variations in surface water chemistry and variations in sample composition between June and October. Piper diagrams consist of two triangular diagrams, one for major cations and one for major anions, which are projected onto a quadrilateral (Drever, 1997).

Precipitation

The normalised cation chemistry of precipitation samples is included on each of the following Piper diagrams (Figures 5-3 to 5-6). The location where precipitation samples plot indicates precipitation has higher Na^{+} + K^{+} proportions compared to most surface water and groundwater samples. The proportion of Ca^{2+} and Mg^{2+} in precipitation is within the range of surface water and groundwater samples. Normalised anion chemistry was not plotted because it was not possible to measure HCO_3^{-}.

Surface Water

Spatial variability in the chemical composition of the three sections of river are shown in the Piper Diagram in Figure 5-3. The Kettle and West Kettle Rivers plot in distinctly different locations suggesting there are different controls on water chemistry in these two rivers. In terms of cations, samples from the Kettle River have higher proportions of Ca^{2+} and lower proportions of Mg^{2+}, Na^{+} and K^{+} compared to samples from the West Kettle River. There is less variation in the relative concentrations of anions

from the different sections of the rivers. Samples from the Kettle River have higher proportions of HCO_3^- and lower proportions of Cl^- compared to the West Kettle River. The proportions of SO_4^{2-} are very similar between the different sections of the river. Beyond the confluence, the water composition appears to be a mixture of compositions from the Kettle and West Kettle Rivers. The cation diagram shows most samples plot along a line, suggesting a possible relationship between Ca^{2+} and Mg^{2+}. Normalised surface water chemistry indicates little variation between June and October (Figure 5-4), indicating differences in TDS between June and October are simply due to dilution.

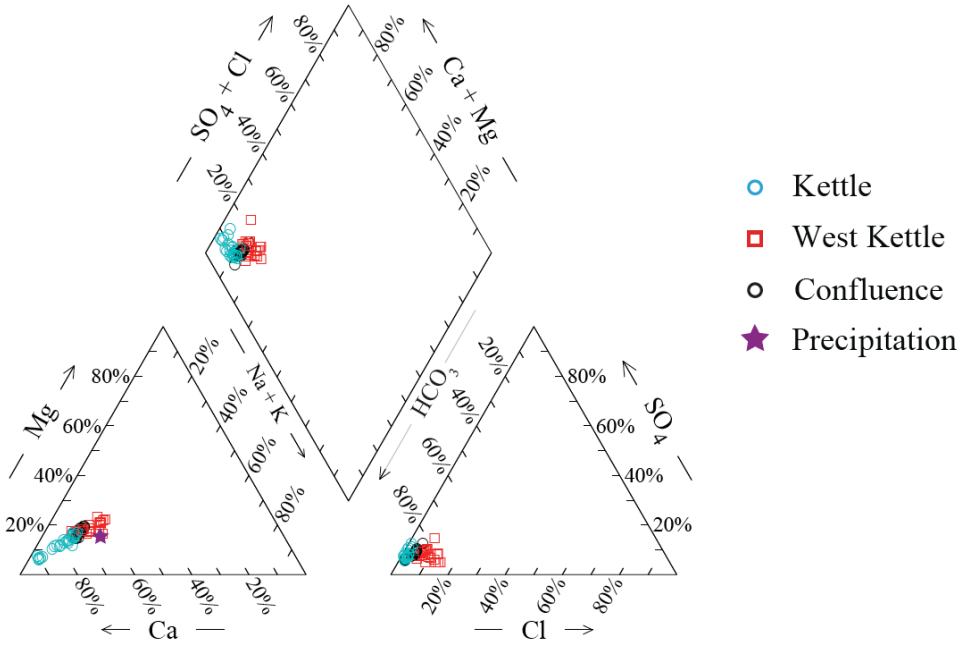

Figure 5-3: Piper diagram of surface water samples from different sections of the river. The normalised cation chemistry of precipitation is also included**.**

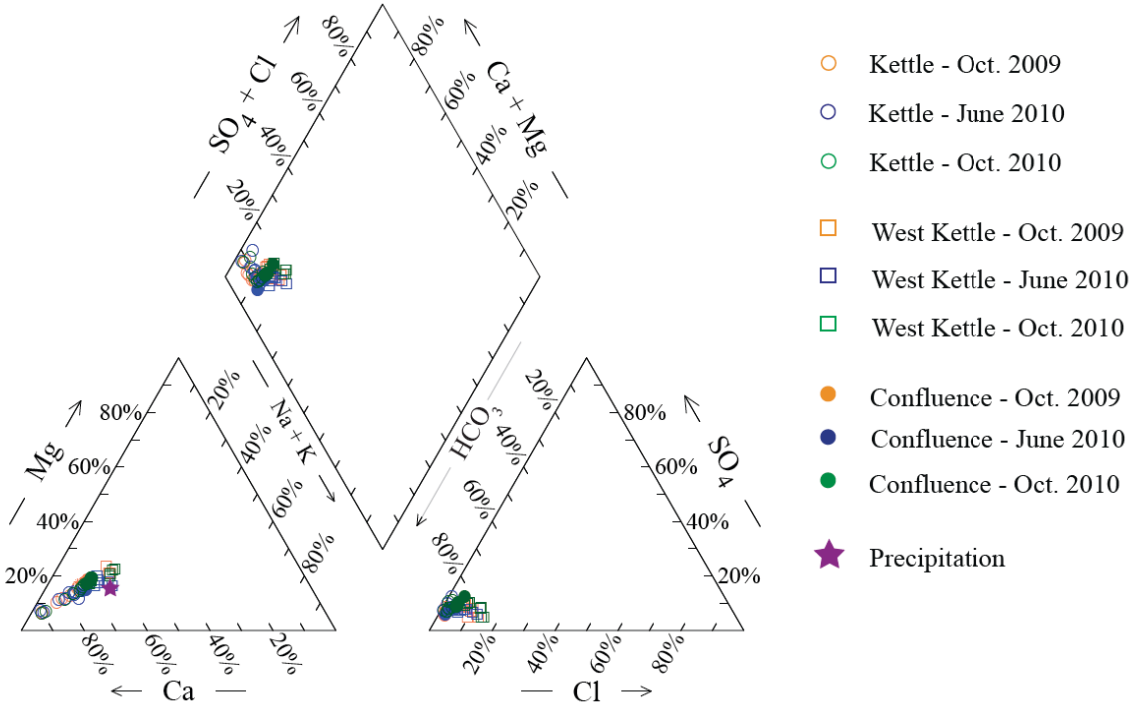

Figure 5-4: Piper diagram of combined influence of temporal and spatial influence on surface waters. The normalised cation chemistry of precipitation is also included.

Groundwater

Groundwater samples plot across a larger area within the cation and anion triangles, compared to surface water samples, because the relative proportions of ions varies more in groundwater samples (Figure 5-5). Weathering of bedrock contributes ions to solution and since the bedrock underlying the Kettle River Basin is not uniform, the reason for greater variability in the proportions of ions in groundwater samples is likely related to geology. The groundwater samples with high SO_4^{2-} and Na^+ concentrations plot distinctly away from the others, which is particularly noticeable on the quadrilateral. The groundwater samples with high Cl^- concentration also plot apart from the majority of samples on the bottom of the anion triangle.

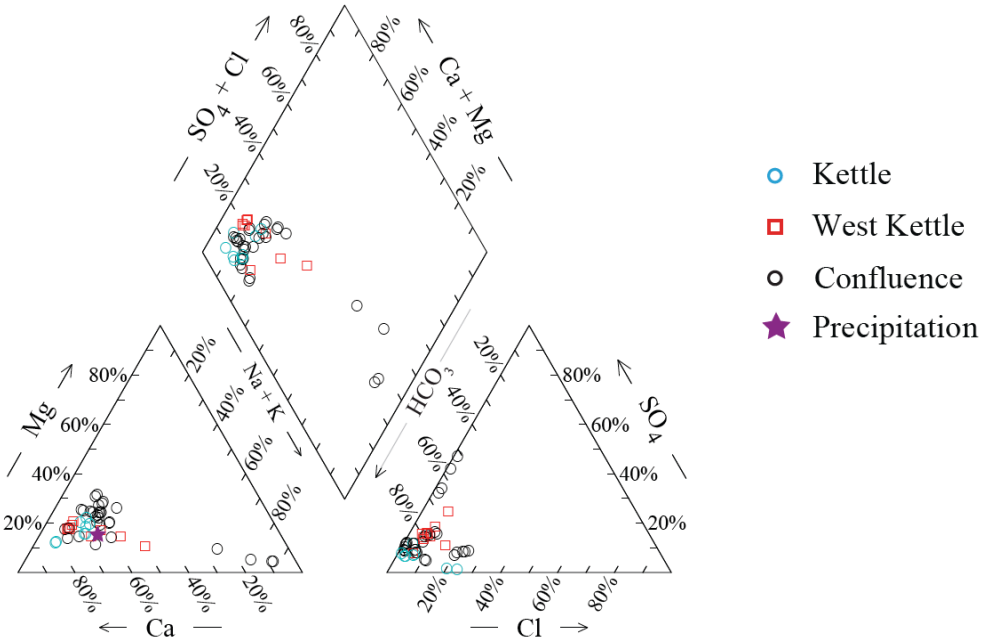

Figure 5-5: Piper diagram of the spatial distribution of groundwater samples. The normalised cation chemistry of precipitation is also included.

Combined Surface Water and Groundwater

Comparison between the groundwater and surface water samples on the Piper diagram suggests a connection between groundwater and surface water samples, as they both plot within the same general area (Figure 5-6). Because the normalised surface water chemistry shows little variation temporally, this suggests that baseflow contributes to riverine flow throughout the year.

Some surface water samples plot outside of the range of groundwater samples in Figure 5-6. These samples have more Ca^{2+} and less Mg^{2+}, Na^{+} and K^{+}. This suggests there may be other factors influencing surface water composition. One possible influence is inputs from precipitation, however as shown in Figure 5-6, the relative proportions of ions in precipitation do not have higher Ca^{2+} and lower Mg^{2+}, Na^{+} and K^{+} compared to groundwater samples. It is also possible that there are more anthropogenic inputs of ions along the West Kettle River and below the confluence, which could potentially change the relative proportions of ions in these sections of the river.

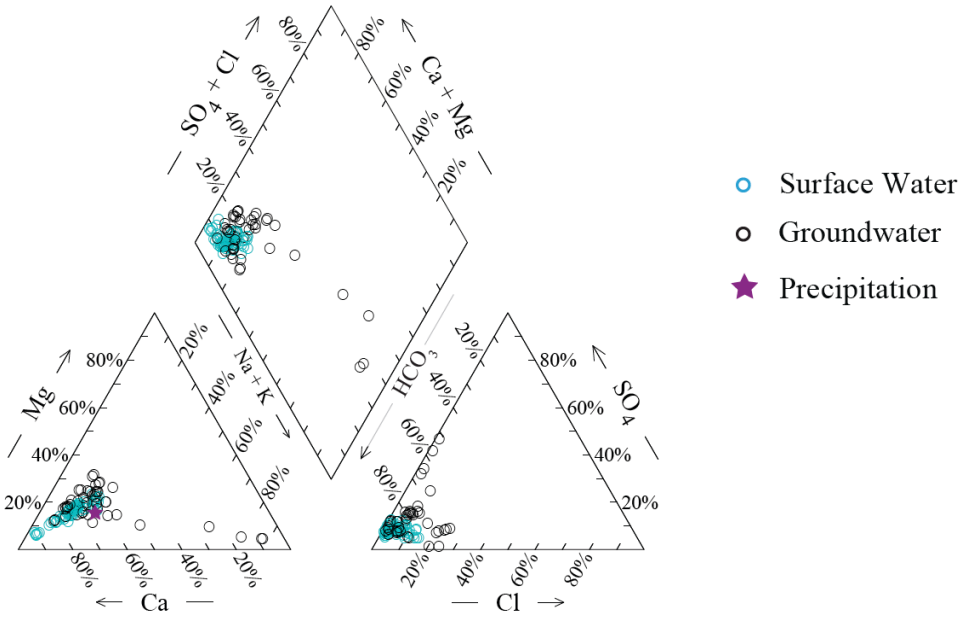

Figure 5-6: Piper diagram of surface water, groundwater and precipitation samples. The normalised cation chemistry of precipitation is also included.

5.6 Conclusion

The relative proportions of ions in surface water differ between the different sections of the river, suggesting there are different inputs or controls on water chemistry in the different sections. Groundwater samples have significantly more compositional variation compared to surface waters, as groundwater samples plot across a greater area in Piper diagrams. There is little variation in the relative proportion of ions from surface water samples collected in June and October, indicating discharge does not affect normalised composition of major ions and baseflow is an important contributor to riverine water throughout the year. Additional inputs from precipitation and anthropogenic activities also appear to be influencing the relative proportions of ions in surface water. The sources of HCO_3^-, NO_3^- and SO_4^{2-} are investigated in Chapter 6 using stable isotopes; inputs from precipitation, anthropogenic activities and bedrock weathering are quantified in Chapter 7.

Chapter Six: Use of Stable Isotopes to Assess the Sources and Processess Influencing Water, Dissolved Inorganic Carbon, Nitrate and Sulfate

6.1 Introduction

Stable isotope abundances can be used to provide information about the source and processes a compound has undergone. Each isotope has a different mass and may therefore participate in chemical, physical and biological reactions at different rates. The preferential reaction of isotopes of different masses during various processes leads to mass-dependent isotope fractionation. Different sources of water, dissolved inorganic carbon, nitrate and sulfate have unique isotopic compositions and so often stable isotopes can aid in source identification. As the elements cycle through various reservoirs, such as the atmosphere, hydrosphere and biosphere, different reactions produce predictable isotopic fractionations. Determining the isotopic composition of water and dissolved solutes can provide insight into processes that may be occurring (Clark and Fritz, 1997; Appelo and Postma, 2005).

Typically the two most abundant isotopes of an element are measured and the ratio of these isotopes is expressed, in relation to that of international standards in the δ notation. The delta (δ) equation for stable isotopes of oxygen, is for example:

$$\delta_{sample}\ (‰) = [(^{18}O/^{16}O)_{sample} - (^{18}O/^{16}O)_{standard})/ (^{18}O/^{16}O)_{standard}\ ] \times 1000 \qquad (6\text{-}1)$$

δ values are expressed in units of parts per thousand, or 'per mil' (‰) (Clark and Fritz, 1997). The standards for isotopic measurements used in this study are summarized in Chapter 4.

Stable isotopes of oxygen (O), hydrogen (H), dissolved inorganic carbon (DIC), nitrate (NO_3^-) and sulfate (SO_4^{2-}) in precipitation, surface water and groundwater samples from the Kettle River Basin are used to assess the sources and processes influencing these compounds.

6.2 Oxygen and Hydrogen

Stable isotopes of O and H can be used to assess the sources of water and processes influencing the different water reservoirs in watersheds. The $\delta^{18}O$ and $\delta^{2}H$ values of precipitation, surface water and groundwater samples in the Kettle River Basin are used to assess the temporal and spatial variations of the sources of water and the influences of weather systems, climate and elevation on processes such as evaporation. Climate variables considered include temperature, precipitation amounts and evaporation rates.

Precipitation

Atmospheric moisture is predominately derived from the ocean. During evaporation of ocean water, equilibrium isotope fractionation occurs causing a depletion of ^{18}O and ^{2}H in water vapour relative to ocean water. The extent of equilibrium isotope fractionation depends on temperature – the cooler the temperature, the greater the fractionation (Craig and Gordon, 1965). In order for equilibrium fractionation to occur, relative humidity must be 100 %. This is attained near the ocean surface and is referred to as the 'boundary layer'. Above the boundary layer, relative humidity decreases and non-equilibrium isotope effects occur. Non-equilibrium isotope effects increase with decreasing humidity (Craig and Gordon, 1965). As atmospheric moisture moves over continents, condensation occurs causing equilibrium isotope fractionation of oxygen and hydrogen isotopes. The heavier isotopes – ^{18}O and ^{2}H, are preferentially 'rained out' leaving the lighter isotopes – ^{16}O and ^{1}H, to accumulate in the remaining vapour. This causes decreasing $\delta^{18}O$ and $\delta^{2}H$ values as more atmospheric moisture is 'rained out' over continents and is referred to as the 'rainout effect' (Clark and Fritz, 1997).

Precipitation in the southern interior of British Columbia is dominantly derived from the west, from weather systems that originate from the Pacific Ocean. In summer months, precipitation can be derived more locally due to convective activity caused by evaporation and transpiration due to high rates of insolation and cool unstable air (Athanasopoulos, 2009; Wassenaar et al., 2011). As weather systems move westward

across British Columbia, successive rainout occurs as systems pass over Coast, Cascade and Intermontane mountains, causing $\delta^{18}O$ and $\delta^{2}H$ values to become increasingly more negative with increasing distance from the coast (Yonge et al., 1989).

$\delta^{18}O$ and $\delta^{2}H$ values of precipitation have been determined on samples collected from around the world and plotted against each other. A linear relationship between $\delta^{18}O$ and $\delta^{2}H$ values in global precipitation was identified in 1961 (Craig, 1961), referred to as the Global Meteoric Water Line (GMWL) which is: $\delta^{2}H = 8 \times \delta^{18}O + 10$. A Canadian Meteoric Water Line (CMWL) of $\delta^{2}H = 7.75 \times \delta^{18}O + 9.83$ has been established based on values from five stations across Canada, where samples were collected for 7 years (Clark and Fritz, 1997). Wassenaar et al. (2011) reported a local meteoric water line for the Okanagan Valley (OMWL) of $\delta^{2}H = 6.6 \times \delta^{18}O - 22.7$, based on 106 precipitation samples collected between April 2006 and June 2010.

Precipitation samples collected in June near Rock Creek, BC, have average $\delta^{18}O$ values of -15.2 ± 1.7 ‰ (n=4) and $\delta^{2}H$ values of -117 ± 13 ‰ (n=4). $\delta^{18}O$ values range from -17.7 to -13.8 ‰ and $\delta^{2}H$ values range from -134 to -103 ‰. The isotope compositions of precipitation samples from the Kettle River Basin in relation to various meteoric water lines are shown in Figure 6-1. Precipitation samples plot either along the OMWL, or between the OMWL and the CMWL. Isotopic compositions of precipitation samples from the Okanagan Basin, collected by Wassenaar et al. (2011) in winter and summer months are also included in Figure 6-1. Wassenaar et al. (2011) defined winter months as November to April and summer months as May through October. Samples from the Kettle River Basin plot in the middle between isotopic compositions of summer and winter samples, near samples collected in June in the Okanagan Basin. As only four precipitation samples were collected in the study area, it is not possible to determine a local meteoric water line for the Kettle River Basin. The Okanagan Valley lies adjacent to the Kettle River Basin, to the west, and receives precipitation from the same Pacific weather systems. Between the West Kettle sub-catchment and the Okanagan Basin, there is one small mountain range and in between the Kettle River sub-catchment and the Okanagan Basin there are two small mountain ranges. It is therefore expected that

precipitation samples from the Kettle River Basin would be only slightly more enriched in ^{16}O and ^{1}H compared to the OMWL, due to rainout.

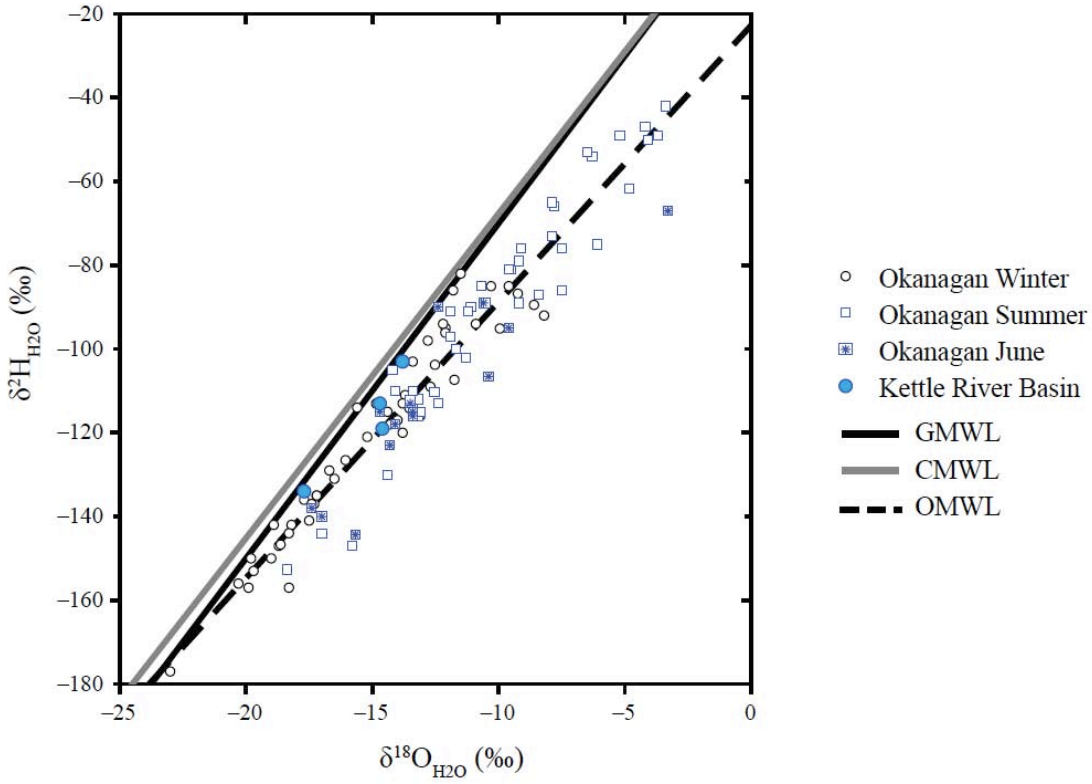

Figure 6-1: $\delta^{18}O_{H2O}$ and $\delta^{2}H_{H2O}$ values of precipitation samples collected in the Kettle River Basin and in the Okanagan by Wassenaar et al. (2011) in relation to Global, Canadian and Okanagan Meteoric Water Lines.

Surface Water

Isotopic compositions of water in surface water bodies such as rivers and lakes often deviate from meteoric water lines due to evaporation, as lighter isotopes are preferentially evaporated, leaving heavy isotopes in the remaining surface water. Both equilibrium and non-equilibrium isotope fractionation occurs during evaporation (Craig and Gordon, 1965). The amount of equilibrium fractionation that occurs is temperature dependent and the amount of non-equilibrium fractionation is primarily dependent on relative humidity (Clark and Fritz, 1997). The relative humidity influences the slope of

the resulting $\delta^{18}O$ and $\delta^{2}H$ linear regression line. Higher amounts of evaporation in surface water samples cause the samples to plot further from the meteoric water line.

The average $\delta^{18}O$ and $\delta^{2}H$ values in surface water samples are -17.0 ± 0.4 ‰ and -129 ± 3 ‰ (n=72), respectively. $\delta^{18}O$ values range from -17.9 to -16.4 ‰ and $\delta^{2}H$ values range from -137 to -125 ‰. Surface water samples plot within a narrow range of values within the range of precipitation samples, between the GMWL and the OMWL (Figure 6-2). Samples plot along a line that deviates from the GMWL indicating slightly elevated $\delta^{18}O$ and $\delta^{2}H$ values trending away from the GMWL, suggesting evaporation has occurred. In terms of temporal variation of evaporation patterns, samples collected in October have higher $\delta^{18}O$ and $\delta^{2}H$ values compared to samples collected in June, indicating that more evaporation has occurred in October (Figure 6-2).

There are three surface water samples that have more negative $\delta^{18}O$ and $\delta^{2}H$ values compared to other surface water samples collected as part of this study (Figure 6-2). These samples were taken from the headwaters of the Kettle River in June 2010, at the highest elevation in the study area. The comparatively low $\delta^{18}O$ and $\delta^{2}H$ values of these samples likely reflect snowmelt contributions as winter precipitation has a more negative isotopic composition due to lower temperature of condensation (Dansgaard, 1964). Additionally, temperatures are typically lower at higher elevations, which causes slightly greater amounts of isotope fractionation during condensation of water vapour; this trend of greater fractionation at higher elevations is referred to as the 'altitude effect' (Clark and Fritz, 1997). The combined influence of seasonal and altitude effects are likely responsible for the negative isotopic composition of these three surface water samples.

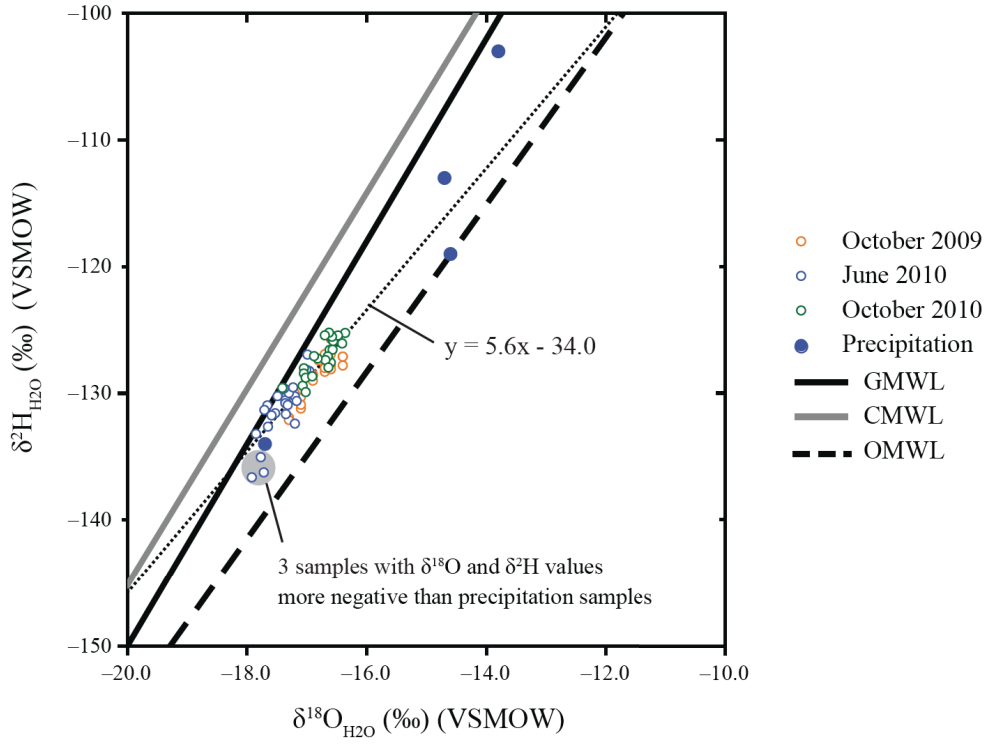

Figure 6-2: Temporal variation in $\delta^{18}O_{H2O}$ and $\delta^{2}H_{H2O}$ values of surface water samples compared to meteoric water lines.

In terms of spatial variation of $\delta^{18}O$ and $\delta^{2}H$ values, surface water samples collected from the West Kettle River are on average slightly more enriched in ^{18}O and ^{2}H compared to samples collected from the Kettle River and plot further from the GMWL (Figure 6-3). This suggests that more evaporation has occurred in the West Kettle River sub-catchment. Alternatively, the reason samples from the Kettle River are slightly more enriched in ^{16}O and ^{1}H could also be due to increased amounts of rainout, as there is a mountain range between the West Kettle River and Kettle River sub-catchments.

Samples from below the confluence of the Kettle and West Kettle Rivers plot within the range of isotopic compositions of the Kettle and West Kettle Rivers, but plot closer to samples from the West Kettle River. As discussed in Chapter 3, the West Kettle River contributes only 32 % to the flow below the confluence, and therefore it would be expected that samples below the confluence plot closer to samples from the Kettle River. Because samples below the confluence plot further from the meteoric water line, this

suggests that surface water below the confluence is subjected to additional evaporation. The corridor between Rock Creek and Midway was previously identified in Chapter 2 to have a warmer climate compared to climate stations further north, supporting the hypothesis that there is further evaporation beyond the confluence of the Kettle and West Kettle Rivers.

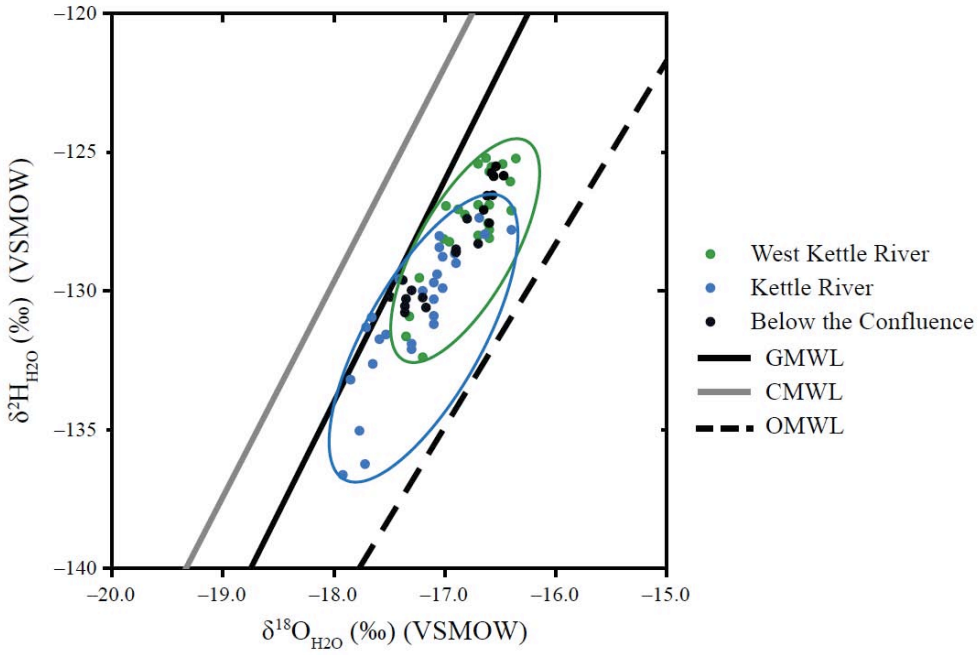

Figure 6-3: Spatial distribution of $\delta^{18}O_{H2O}$ and $\delta^{2}H_{H2O}$ values of surface waters in relation to meteoric water lines. The blue circle indicates the range of samples collected from the Kettle River and the green circle indicates the range of samples collected from the West Kettle River.

$\delta^{18}O$ and $\delta^{2}H$ values are plotted against distance from the headwaters of both the Kettle and West Kettle Rivers (Figure 6-4). Along the Kettle River, the isotopic composition becomes slightly more enriched in ^{18}O and ^{2}H, except for samples collected at the headwaters, while $\delta^{18}O$ and $\delta^{2}H$ values along the West Kettle River show little variation beyond the measurement uncertainty, with increasing distance downstream. After the confluence, there is little change in $\delta^{18}O$ and $\delta^{2}H$ values (Figure 6-4). Reasons for slight variation with distance downstream along the Kettle River, include the effects of

climate and altitude. The southern corridor between Rock Creek and Midway has higher average temperatures resulting in higher rates of evaporation. The southern portions of the watershed are at lower elevations compared to the headwaters. Both of these effects cause preferential incorporation of the heavy isotopes in the remaining surface water, thus explaining the pattern of increasing $\delta^{18}O$ and $\delta^{2}H$ values within increasing distance downstream along the Kettle River.

Surface water samples collected at the headwaters of the Kettle River in October 2009 and 2010, also do not follow the trend of increasing $\delta^{18}O$ and $\delta^{2}H$ values with increasing distance downstream. Instead these samples are enriched in ^{18}O and ^{2}H. At the headwaters of the Kettle River, there is a small lake known as Keefer Lake. Surface water samples were collected immediately below the lake. Throughout summer months, evaporation of lake water can cause enrichment of heavy isotopes in surface waters as ^{16}O and ^{1}H are preferentially removed by evaporation.

Groundwater

Similar to surface water samples, the $\delta^{18}O$ and $\delta^{2}H$ values of groundwater samples plot within the range of precipitation samples and between the GWML and the OMWL (Figure 6-5). The average $\delta^{18}O$ and $\delta^{2}H$ values of groundwater samples are -16.9 ± 0.5 ‰ and -129 ± 5 ‰ (n=48), respectively. $\delta^{18}O$ values range from -18.3 to -15.7 ‰ and $\delta^{2}H$ values range from -143 to -122 ‰. For samples collected in June, the average $\delta^{18}O$ and $\delta^{2}H$ values are -16.8 ± 0.5 ‰ and -130 ± 4 ‰ (n=23), compared to -17.0 ± 0.6 ‰ and -129 ± 5 ‰ (n=25) in October. This indicates that there is no temporal variation in the isotopic composition of groundwater samples since the difference between mean values is within the measurement uncertainty. There are four samples, collected from two wells, sampled in June and October that have more negative $\delta^{18}O$ and $\delta^{2}H$ values (circled in Figure 6-5). These samples have been previously identified as outliers in Chapter 5 due to their high Na^{+} and SO_4^{2-} concentrations. Based on the sampling location and communication with well owners, these wells are likely drilled into bedrock aquifers.

Wassenaar et al. (2011) sampled groundwaters in the Okanagan Valley as well as within the Kettle River Basin – between the western edge of the Kettle River Basin and Bridesville, BC. Groundwater samples were categorized into samples taken from either 'Highland bedrock groundwater' or 'Valley aquifers', as it was observed that groundwater samples taken from bedrock aquifers had more negative $\delta^{18}O$ and $\delta^{2}H$ values compared to samples from the Valley aquifers (Wassenaar et al., 2011), similar to $\delta^{18}O$ and $\delta^{2}H$ values from bedrock samples in this study.

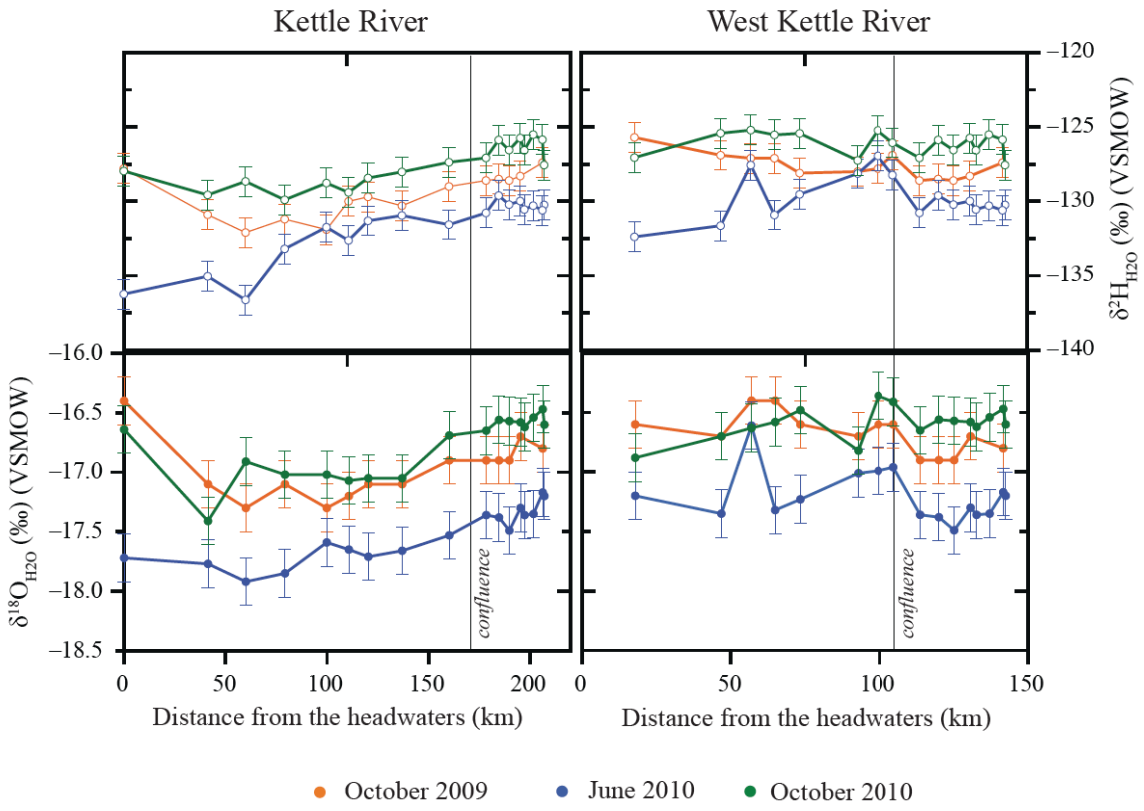

Figure 6-4: $\delta^{18}O_{H2O}$ and $\delta^{2}H_{H2O}$ values of surface water samples with increasing distance from the headwaters of the Kettle and West Kettle Rivers. Error bars indicate the reported measurement uncertainty. The location of the confluence of the two rivers is indicated with a vertical line.

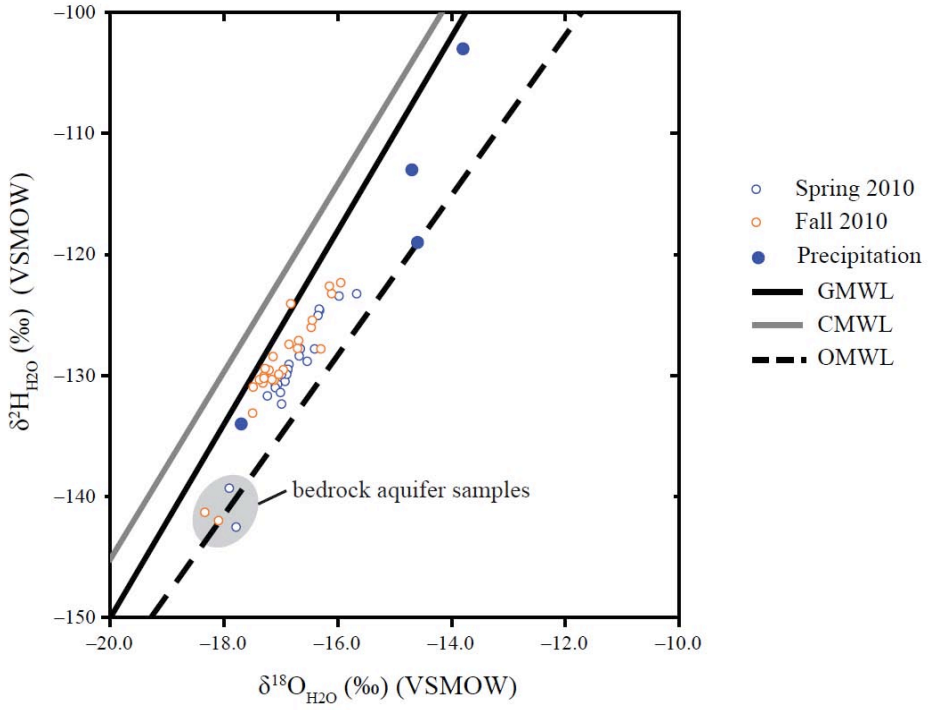

Figure 6-5: Temporal variation of $\delta^{18}O_{H2O}$ and $\delta^{2}H_{H2O}$ in groundwater samples. Circled samples are proposed to be from bedrock aquifers.

Other reasons why groundwater samples from bedrock aquifers have more negative $\delta^{18}O$ and $\delta^{2}H$ values, could be related to the type of recharge, the amount of evaporation or it could be older groundwater representative of a colder climate (Wassenaar et al., 2011). If the bedrock aquifers were primarily recharged by snowmelt, the isotopic signature would be more negative due to colder temperatures during winter months. Alternatively, water recharging bedrock aquifers may undergo limited evaporation, thus maintaining the isotopic signature of precipitation. There is no information available on the evaporation rates in the basin, or on the age of groundwaters in this area, and therefore it is not possible to identify with certainty the processes influencing the isotopic composition of water in bedrock aquifers.

The remainder of groundwater samples are from the unconsolidated aquifers along the valley bottoms. Surface water and groundwater samples have very similar ranges in $\delta^{18}O$ and $\delta^{2}H$ values, as reported above and shown in Figure 6-6, suggesting that surface waters are primarily derived from groundwaters originating from unconsolidated

valley aquifers. As the isotopic compositions of surface water samples fall within the range of those of groundwater samples, it appears that surface water samples do not undergo significantly more evaporation. Because the surface water and groundwater samples both deviate from the GMWL, this suggests that evaporation is occurring during recharge into the uppermost, unconfined aquifers.

In the Okanagan Valley, Wassenaar et al. (2011) identified that valley aquifers were primarily recharged by irrigation waters. In the Kettle River Basin, the land surface above unconsolidated aquifers is often irrigated and surface water used for irrigation could be recharging groundwater. As a consequence, groundwater samples would have $\delta^{18}O$ and $\delta^{2}H$ values similar to those of surface water.

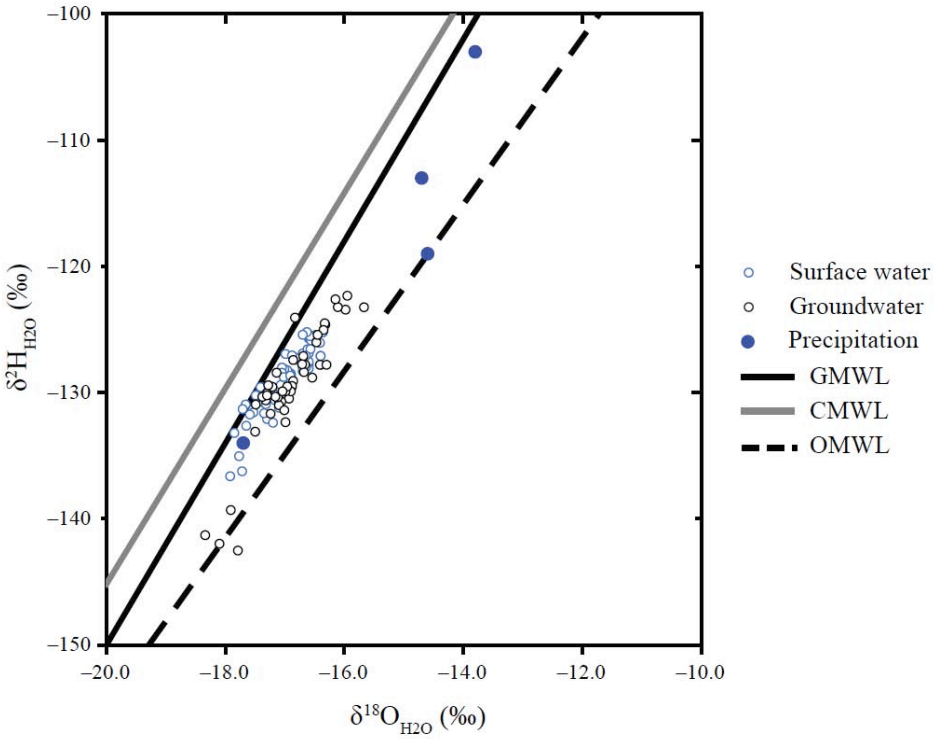

Figure 6-6: $\delta^{18}O_{H2O}$ and $\delta^{2}H_{H2O}$ of precipitation, surface water and groundwater samples in the Kettle River Basin.

6.3 Dissolved Inorganic Carbon

Dissolved Inorganic Carbon (DIC) is the sum of inorganic carbon species in solution – carbonic acid (H_2CO_3), bicarbonate (HCO_3^-) and the carbonate ion (CO_3^{2-}) (Appelo and Postma, 2005). There are several sources of DIC in surface water and groundwater including the atmosphere, biosphere, pedosphere and lithosphere. Sinks of DIC include degasing of CO_2 from surface waters and in-river photosynthesis (Dubois et al., 2010). Each of these sources has a distinct carbon isotopic signature ($\delta^{13}C$), which can be used to determine sources and sinks of DIC (Telmer and Veizer, 1999; Spence and Telmer; Dubois et al., 2010).

Atmospheric $CO_2(g)$ dissolves in water to become $CO_2(aq)$, until equilibrium is reached between the partial pressure of $CO_2(g)$ in the atmosphere and $CO_2(aq)$ in solution (Drever, 1997). Aqueous CO_2 reacts with H_2O to form carbonic acid (H_2CO_3). By common convention, $CO_2(aq)$ and H_2CO_3 are combined and referred to as $H_2CO_3^*$ (Appelo and Postma, 2005). The * denotes the combination of $CO_2(aq)$ and H_2O. $H_2CO_3^*$ is conventionally written, however at 25 °C, $CO_2(aq)$ is ~ 600 times more abundant (Appelo and Postma, 2005). Equation 6-1 is the sum of these reactions. Subsequently, $H_2CO_3^*$ dissociates to produce HCO_3^- and a H proton (H^+) (Equation 6-2). HCO_3^- then dissociates to form CO_3^{2-} and H^+ (Equation 6-3).

$$CO_2(g) + H_2O \rightarrow H_2CO_3^* \ (pKCO_2) \quad (6\text{-}1)$$

$$H_2CO_3^* \rightarrow HCO_3^- + H^+ \ (pK_1) \quad (6\text{-}2)$$

$$HCO_3^- \rightarrow CO_3^{2-} + H^+ \ (pK_2) \quad (6\text{-}3)$$

In addition to atmospheric sources, the soil zone is also a source of $CO_2(g)$ (Clark and Fritz, 1997). Decay and oxidation of organic matter generate $CO_2(g)$ through aerobic respiration. The partial pressure of $CO_2(g)$ in soils has been estimated to be one to two orders of magnitude higher compared to the atmosphere (Appelo and Postma, 2005). As water infiltrates into the subsurface, it equilibrates with the CO_2 generated in the soil zone. The $CO_2(aq)$ reacts to form H_2CO_3 and subsequent dissolution reactions produce

HCO_3^- and CO_3^{2-}. The relative role of Equations 6-1 through 6-3 is dependent on pH. At 25 °C equation 6-1 is the dominant reaction below pH values of 6.3, Equation 6-2 is the dominant dissolution reaction between pH values of 6.3 and 10.3 and above a pH of 10.3, Equation 6-3 is the dominant dissolution reaction.

Lithospheric sources of DIC include dissolution of carbonate minerals. There is no carbonate bedrock present in the Kettle River Basin, however minor calcite has been identified in volcanic lithologies and in veins within intrusive lithologies (Ewert et al., 2008). Formation of secondary calcite occurs from solutions super-saturated in Ca^{2+} and HCO_3^- (Appelo and Postma, 2005). The saturation state is a ratio of the Ion Activity Product (IAP) in a water sample and the solubility product 'K' of activities in equilibrium. The saturation index (SI) is the ratio of IAP and K on a logarithmic scale (Appelo and Postma, 2005). A positive SI value indicates the fluid is super-saturated with respect to a particular mineral and it is possible this mineral may precipitate. Negative SI values indicate the fluid is sub-saturated with respect to a mineral. There are errors associated with saturation indices as values of K are determined experimentally at high temperature. (Bethke, 2008). The program 'The Geochemist's Workbench' was used to determine the saturation state of calcite in surface water and groundwater samples. These values are included in Appendix B. Results indicate that there are no surface water samples with positive SI values for calcite, and 35 % of groundwater samples, corresponding to 14 locations, have positive SI values for calcite. Of these groundwater samples with positive SI values for calcite, the average value is 0.25 ± 0.13, and values range from 0.01 to 0.42. Positive SI values for calcite indicate that it is possible there is calcareous cement in the Kettle River Basin aquifers.

Surface water fed by groundwaters in equilibrium with higher partial pressures of CO_2 (pCO_2) compared to the atmosphere can cause surface waters to degas CO_2, causing a loss of DIC (e.g. Grasby, 1997; Telmer and Veizer, 1999; Dubois et al., 2009). Another potential loss of DIC is in-river photosynthesis (Yang et al., 1996).

Associated with reactions in Equations 6-1 through 6-3 are equilibrium constants (pK), which are dependent on temperature (Clark and Fritz, 1997). Telmer and Veizer

(1999) used regression analysis of published data (temperature and equilibrium constant values) to develop equations for *p*K's for temperatures between 0 and 30 °C. These equations are included in Appendix C. If two parameters from Equations 6-1 to 6-3 are known and *p*K's are determined using temperature, the concentration of remaining species can be determined (Telmer and Veizer, 1999).

The relative abundance of constituents that comprise DIC in surface water and groundwater samples from the Kettle River Basin can be determined using measured HCO_3^- concentrations and measured pH values. On average, in surface water samples (n=72), HCO_3^- constitutes 93.4 ± 4.2 % of DIC, while H_2CO_3 and CO_3^{2-} comprise on average 6.5 ± 4.3 % and 0.18 ± 0.1 %, respectively. In groundwater samples, on average (n=48), the distribution of DIC is as follows: 86.1 ± 9.3 % is HCO_3^-, 13.7 ± 9.4 % is H_2CO_3 and 0.1 ± 0.2 % is CO_3^{2-}. In all surface water and groundwater samples, HCO_3^- is the dominant component of alkalinity. In surface waters samples, HCO_3^- constitutes between 69.1 and 97.9 % of DIC and in groundwater samples, HCO_3^- comprises between 65.1 and 98.0 % of DIC.

Surface Water

In terms of seasonal and spatial variation of DIC in surface water samples, DIC concentrations are higher in all samples collected in October compared to samples collected in June (Figure 6-7). The average DIC concentration of surface water samples collected in October is 2.7 times higher than that of samples collected in June. DIC concentrations range from 0.2 to 1.4 mmol/L in June and from 0.5 to 1.8 mmol/L in October. The average DIC concentration in June is 0.5 ± 0.2 mmol/L (n= 25) and 1.2 ± 0.4 mmol/L (n=47) in October. DIC increases with increasing distance downstream, with the exception of one sampling point near the headwaters of the Kettle River. At this sampling location, TDS was also identified in Chapter 5 to increase in a similar pattern. Possible reasons for higher DIC and TDS could be due to either weathering or anthropogenic inputs and will be discussed in greater detail in Chapter 7.

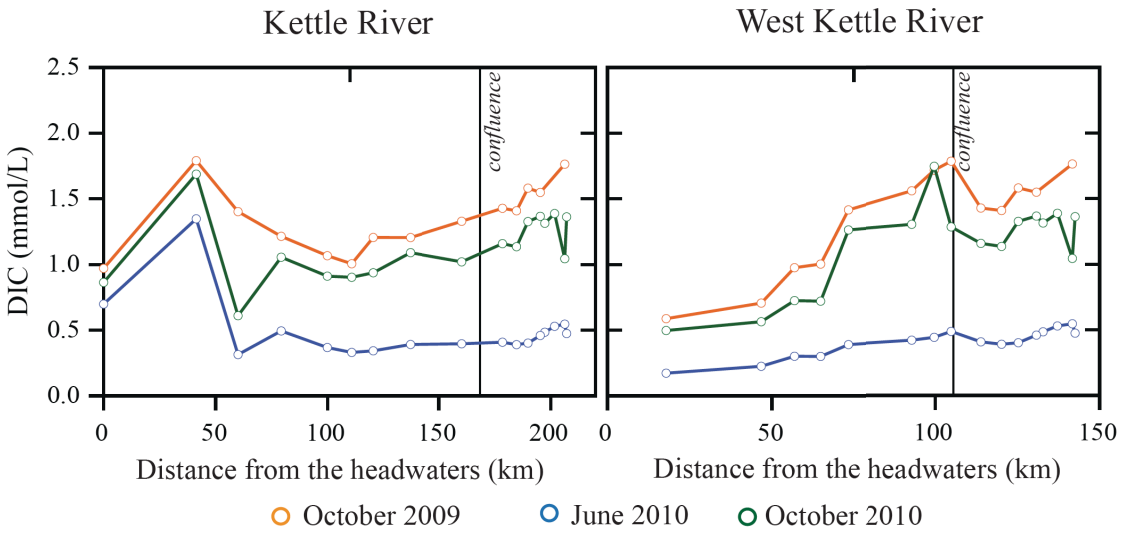

Figure 6-7: DIC concentrations (mmol/L) with distance downstream in the Kettle and West Kettle Rivers. The location of the confluence of these rivers is indicated with a vertical line.

Groundwater

DIC concentrations of groundwater samples were higher than those of surface water samples but exhibited little temporal variation. Groundwater samples obtained in June had an average DIC concentration of 3.6 ± 1.1 mmol/L (n=23) and samples collected in October had an average DIC concentration of 3.7 ± 1.3 mmol/L (n=25). The DIC range for samples collected in June was from 2.0 to 6.8 mmol/L and for samples collected in October, DIC ranged from 2.1 to 7.4 mmol/L.

6.3.1 pCO_2

Recent studies have identified that rivers can degas significant amounts of CO_2 if the pCO_2 values of surface waters are greater than atmospheric pCO_2 (Dubois et al., 2010; Butman and Raymond, 2011). The pCO_2 of the atmosphere is currently 385 ppmv (Keeling et al., 2009). Loss of CO_2 to the atmosphere results in a decrease in DIC concentrations in rivers. The origin of surface waters with high pCO_2, is recharge from groundwaters which obtain high pCO_2 from the soil zone. Using geochemical modeling software SOLMINEQ88, the pCO_2 in equilibrium with surface water and groundwater

samples was determined, based on measured pH, temperature and HCO_3^-. pCO_2 values are included in Appendix B.

Surface Water

The pCO_2 calculated to be in equilibrium with surface water samples exhibit significant variations temporally and spatially. The average pCO_2 of all surface water samples is 846.5 ± 687.4 ppmv (parts per million by volume) (n=72). Surface water samples collected in June have lower pCO_2 values compared to samples collected in October (Figure 6-8). The average pCO_2 of surface water samples collected in June is 461.7 ± 155.8 ppmv (n=25), compared to samples collected in October (1051.3 ± 770.3 ppmv (n=45). Along the length of both the Kettle and West Kettle Rivers, pCO_2 increase up to the confluence of the two rivers. The increase is not gradual – at some sampling locations, there are large increases or decreases in pCO_2, especially in October when baseflow contributes a greater proportion to riverine flow. There is one anomalously high pCO_2 calculated to be in equilibrium with a surface water sample collected from the West Kettle River in October 2010. This could indicate high contributions of CO_2 charged baseflow, or it could reflect an error in recorded pH values during sampling.

Groundwater

The pCO_2 of groundwater samples was higher compared to pCO_2 of surface waters and was also characterized by a greater range in values. The average pCO_2 in groundwater samples is 8181.9 ± 5144.1 ppmv, and values range from 746.8 to 18997.8 ppmv. The pCO_2 of groundwaters in relation to those of surface waters and $\delta^{13}C_{DIC}$ values are discussed below.

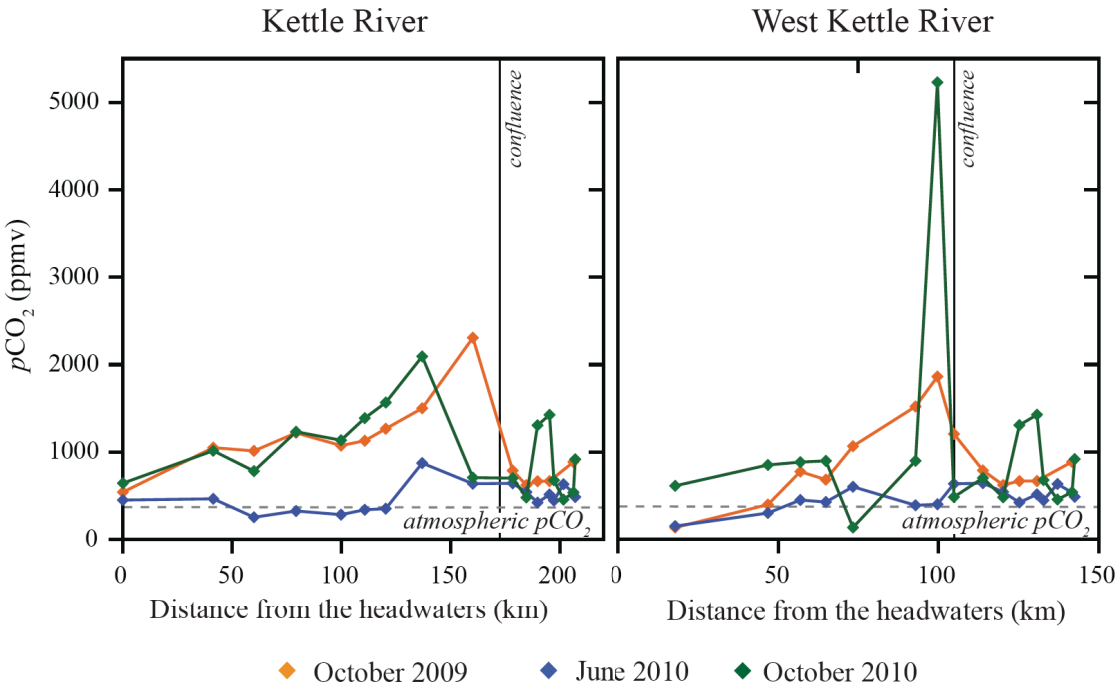

Figure 6-8: pCO_2 (ppmv) versus distance downstream of the Kettle and West Kettle Rivers. The pCO_2 of atmospheric CO_2 and location of the confluence are indicated.

6.3.2 $\delta^{13}C_{DIC}$

The average atmospheric $\delta^{13}C_{CO2}$ value is -8 ‰ (Dubois et al., 2010). Atmospheric $CO_2(g)$ is subsequently isotopically fractionated as it equilibrates with atmospheric moisture (Clark and Fritz, 1997). Isotope fractionation between atmospheric carbon and aqueous carbon is temperature dependent as described in Equation 6-4 (Mook et al., 1974). The enrichment factor (ε) is used to express the isotopic difference between two compounds. Equation 6-4 expresses the carbon isotopic difference between HCO_3^- and $CO_2(g)$.

$$\varepsilon_{[HCO3\text{-}(aq)\ -\ CO2(g)]} = 9.483 \times 10^3/T - 23.89 \qquad (6\text{-}4)$$

The historical average annual temperature from Beaverdell North, Ferry and Osoyoos climate stations within or near the Kettle River Basin is 4.9, 7.0 and 10.1 °C, as discussed in Chapter 2. The average of these temperature values is 7.3 °C. The enrichment

factors between HCO_3^- and CO_2(g) for these temperatures range from 10.2 ‰ at 4.9 °C to 9.6 ‰ at 10.1 °C. The enrichment factors for the average temperature is 9.9 ‰, which is used for further isotope fractionation calculations. According to Equation 6-4, HCO_3^- derived from atmospheric CO_2 has a $\delta^{13}C_{HCO3}$ value of 1.9 ‰ (using a $\delta^{13}C_{CO2}$ value of -8 ‰).

During photosynthesis, C-isotope fractionation in plant foliage occurs during diffusion, dissolution and carboxylation of CO_2 (Clark and Fritz, 1997). For the majority of terrestrial plants, classified as 'C3 plants', the average $\delta^{13}C$ value of soil CO_2(g) produced from decay and oxidation of organic matter and plant remains is -27 ‰ (Clark and Fritz, 1997; Appelo and Postma, 2005; Dubois et al., 2010). According to Equation 6-4, the resulting average $\delta^{13}C$ value of DIC originating from soil CO_2 is -17.1 ‰ at 7 °C which is the average temperature of groundwater samples.

Calcite minerals originating from hydrothermal fluids, which precipitate in fractures or veins of igneous or metamorphic rocks, have a more negative $\delta^{13}C$ value compared to marine carbonates, which have a $\delta^{13}C$ of ~0 ‰ (Dubois et al., 2010). Because calcite forms from a solution supersaturated in HCO_3^- and Ca^{2+}, the $\delta^{13}C$ value of DIC in calcite reflects the $\delta^{13}C$ of the original fluid (Clark and Fritz, 1997). In the Kettle River Basin, carbonate veins have $\delta^{13}C$ values between -7 and -3 ‰ (Nesbitt and Muehlenbachs, 1995). The dominant weathering agent in the Kettle River Basin is H_2CO_3*, originating primarily from pedospheric CO_2, which will be discussed in greater detail in Chapter 8. Therefore, the reaction describing weathering of carbonate veins is:

$$H_2CO_3^* + CaCO_3 <-> Ca^{2+} + 2HCO_3^- \quad (6\text{-}5)$$

The two sources of DIC in this reaction (H_2CO_3* and $CaCO_3$) have distinct $\delta^{13}C$ values. If a 1:1 mixture of sources is assumed (Dubois et al., 2010), the expected range of $\delta^{13}C_{DIC}$ of HCO_3^- originating from dissolution of calcite would be between -12 and -10 ‰. The median of these values is -11 ‰, which will be used for the following discussion.

Sinks of DIC in surface water include degasing of CO_2 into the atmosphere and in-river photosynthesis, both of which cause $\delta^{13}C_{DIC}$ values in the river to increase (Dubois et al., 2010).

Surface Water

Surface water $\delta^{13}C_{DIC}$ values range from -2.3 to -19.9 ‰ (n=72) and the average $\delta^{13}C_{DIC}$ of all surface water samples is -8.4 ± 2.5 ‰. The average $\delta^{13}C_{DIC}$ value of samples collected in June is -8.0 ± 2.6 ‰ (n=25), while samples collected in October have an average $\delta^{13}C_{DIC}$ value of -8.6 ± 2.5 ‰ (n=47), indicating there is statistically no temporal variation. In terms of spatial variation, $\delta^{13}C$ values of DIC vary with distance downstream along both the Kettle and West Kettle Rivers as shown in Figure 6-9. The carbon isotope ratios of all samples, except one sample along the West Kettle, fall between the $\delta^{13}C_{DIC}$ values of DIC expected for dissolution of soil CO_2 and atmospheric CO_2. Because the SI with respect to calcite in surface water samples is negative, dissolution of calcite is assumed to have minimal influence on the $\delta^{13}C$ of surface water samples. Dissolution of calcite could, however, potentially influence DIC in groundwater samples, subsequently influencing the $\delta^{13}C$ of DIC in surface water samples.

Many surface water samples have higher $\delta^{13}C_{DIC}$ values compared to the range of groundwater samples, as shown in Figure 6-9. This suggests that interaction with the atmosphere influences the isotopic composition of DIC of surface waters. A relationship between pCO_2 and $\delta^{13}C_{DIC}$ values has been previously observed in rivers and has been suggested to originate from equilibration with atmospheric CO_2 (Yang et al., 1996; Grasby, 1997). However, it has also been suggested that equilibration with atmospheric CO_2 requires a greater amount of time compared to the residence time of water in rivers, and exchange between atmospheric and riverine CO_2 is unidirectional (Telmer and Veizer, 1999; Butman and Raymond, 2011). During degassing of CO_2, the light isotope (^{12}C) is preferentially incorporated into the gas phase, leaving the heavy isotope (^{13}C) to become relative enriched in surface waters (Dubois et al., 2010; Spence and Telmer, 2005). $\delta^{13}C_{DIC}$ values of surface water samples are higher compared to those of

groundwater samples, suggesting possible exchange between the atmosphere or degassing of CO_2 is occurring in rivers in the Kettle River Basin. However, if atmospheric exchange or degassing were a major process influencing surface waters, it would be expected that $\delta^{13}C_{DIC}$ values of surface water samples collected in June and October would be different, as pCO_2 values in June are much lower compared to values in October. However, the average $\delta^{13}C_{DIC}$ value of surface water samples collected in June compared to that of October samples is only slightly higher (0.6 ‰), suggesting atmospheric equilibration and degassing have a minor influence on $\delta^{13}C_{DIC}$ values of surface water samples.

Alternatively, in-river photosynthesis could also cause higher $\delta^{13}C_{DIC}$ values in surface water compared to groundwater. However if photosynthesis were to influence the $\delta^{13}C_{DIC}$, there should appreciable amounts of biomass in the riverine systems and there would be temporal variation in $\delta^{13}C_{DIC}$ values between samples collected in June and October due to plant growth in the spring/summer months (Telmer and Veizer, 2000; Spence and Telmer, 2005). Spence and Telmer (2005) also suggested that dissolution of atmospheric CO_2 directly into surface water may cause surface water samples to be enriched in ^{13}C. The relative role of atmospheric exchange, in-river photosynthesis and dissolution of atmospheric CO_2 are not known and it is possible a combination of these processes may cause the $\delta^{13}C_{DIC}$ values of surface water samples to be higher compared to those of groundwaters.

Groundwater

The $\delta^{13}C$ values of DIC in groundwater samples range from -10.7 to -16.7 ‰ and the average is -13.7 ± 1.6 ‰ (n=48). There is no temporal variation – the average $\delta^{13}C$ value is -13.5 ± 1.6 ‰ (n=23) for samples collected in June and -13.9 ± 1.6 ‰ (n=25) for samples collected in October. The $\delta^{13}C_{DIC}$ values of groundwater samples plot between the expected $\delta^{13}C_{DIC}$ values for dissolution of soil CO_2 and calcite, suggesting the source of DIC in groundwaters is a mixture of both soil CO_2 and calcite dissolution. Some groundwater samples with higher pCO_2 values approach the $\delta^{13}C_{DIC}$ values of the soil zone (Figure 6-10), suggesting samples with high pCO_2 have greater amounts of DIC from

dissolution of soil CO_2. In Figure 6-10, it appears that groundwater samples with higher $\delta^{13}C_{DIC}$ values also have low pCO_2 suggesting an atmospheric component of DIC in some samples.

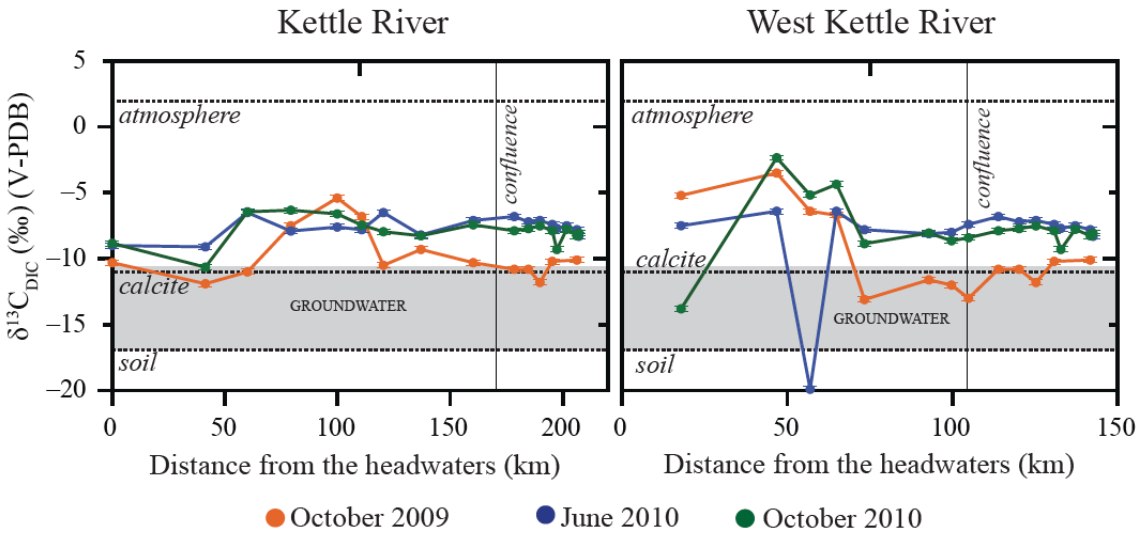

Figure 6-9: $\delta^{13}C_{DIC}$ values of surface water samples versus distance downstream of the Kettle and West Kettle Rivers. Error bars indicate the reported measurement uncertainty.

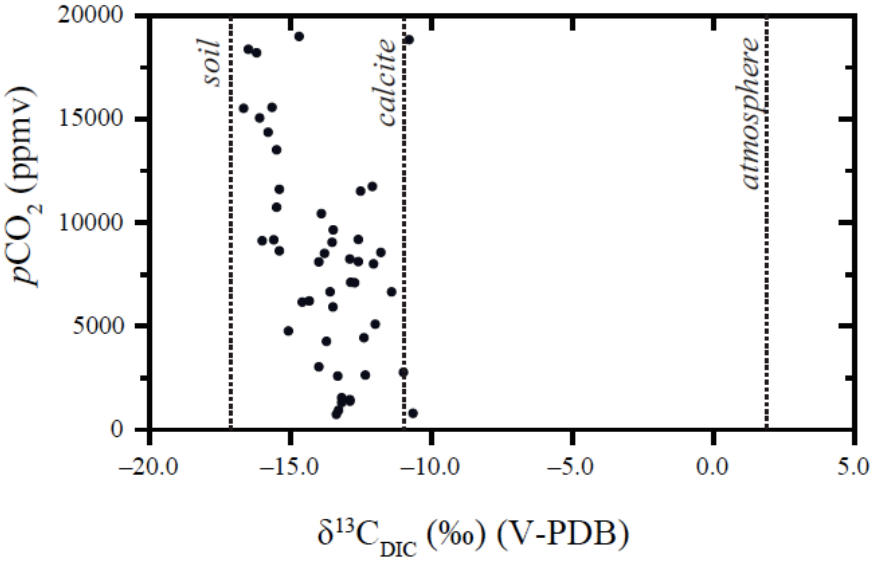

Figure 6-10 pCO_2 versus $\delta^{13}C_{DIC}$ of groundwater samples. Vertical lines indicate the $\delta^{13}C_{DIC}$ values of DIC sources.

6.4 Nitrate

6.4.1 The Nitrogen Cycle

The nitrogen cycle consists of different reservoirs of nitrogen (N), which contain different species that are classified as either biologically unreactive or reactive and inorganic or organic. Inorganic N includes nitrogen gas, and the oxidized species: NO_3^-, nitric acid (HNO_3), nitrous oxides (N_2O) and nitrogen oxides (NO_x) and the reduced species: ammonia (NH_3) and ammonium (NH_4^+) (Galloway et al., 2004). Organic N is bound to carbon forming a wide variety of organic molecules (Socolow, 1999).

Anthropogenic activities have disrupted the distribution of N (Gruber and Galloway, 2008) in these reservoirs in two main ways – production of food and energy. Both food and energy production have specifically increased the amount of biologically reactive N (Galloway et al., 2004). Nitrogen fixation is a naturally occurring process, due to either lightning or by microorganisms, which converts atmospheric N_2 to bioavailable N. Reactive N is often the limiting factor to primary production (Vitousek et al., 1997). To fulfill food requirements of an increasing population in the early 20th century, the Haber-Bosch process was invented, which converts atmospheric N_2 to biologically usable NH_3, which is subsequently applied to crops as fertilizers to enhance crop production (Galloway and Cowling, 2002). Fertilizers such as manures also add biologically usable N to the soils (Kendall et al., 2007). In addition to the application of fertilizers, increased cultivation of rice and legumes, crops that naturally enhance N fixation rates, has also increased the amount of reactive N (Galloway and Cowling, 2002).

During the production of energy, specifically during combustion of fossil fuels, NO_x is released from oxidation of either atmospheric N_2 or fossil N in the fuel (Galloway et al., 2004; Kendall et al., 2007). Canfield et al. (2010) estimated anthropogenic contributions of biologically reactive N "double the terrestrial nitrogen fixation, and (anthropogenic contributions) provide around 45 % of the total fixed nitrogen produced annually on Earth."

Much effort has been made to quantify the fate of anthropogenic reactive N (Vitousek et al., 1997; Galloway and Cowling, 2002; Mayer et al., 2005; Smil, 2002; van

Breemen et al., 2002, Galloway et al., 2004; Galloway et al., 2008; Boyer et al., 2006). Boyer et al. (2006) estimated that less than 25 % of anthropogenic N added to watersheds is discharged through rivers, implying that approximately 75 % is stored in soils and groundwaters, denitrified or volatilized. Fertilizers are considered to be the single largest input of anthropogenic reactive N (Galloway et al., 2004) and N from fossil fuel combustion is thought to be a minor contributor (Mayer et al., 2002). Losses of N to the atmosphere include denitrification and volatilization (Galloway et al., 2004; Beusen et al., 2008). Denitrification is the reduction of NO_3^- to N_2, N_2O or NO gases, whereas volatilization converts ammonium to ammonia gas (Beusen et al., 2008). Anthropogenic perturbations in the N cycle have caused NO_3^- concentrations in aqueous systems to increase (Vitousek et al., 1997).

6.4.2 Sources of Nitrate

There are both natural and anthropogenic sources of NO_3^- in aqueous systems. Natural sources include nitrification of soil organic matter, where NH_4^+ is oxidized to NO_3^-, a process that is mediated by autotrophic bacteria or archaea (Kendall et al., 2007). Atmospheric sources of NO_3^- can be derived from both natural sources such as: lightning, biogenic soil emissions and biogenic biomass burning, and anthropogenic sources including fossil fuel burning from both vehicles and industrial processing facilities and power plants (Kendall et al., 2007). Atmospheric NO_3^- is derived from NO_x, which is oxidized to HNO_3, which subsequently dissociates to NO_3^-. Particulate NO_3 is also a source of atmospheric NO_3^- that is introduced to watersheds through dry deposition and can be either from natural or anthropogenic sources (Kendall et al., 2007). Additional anthropogenic NO_3^- sources include synthetic fertilizers, which originate from N_2 fixation, animal manure, septic systems and waste water treatment plants. Animal manure and septic systems both release organic N and NH_4^+, which is subsequently converted to NO_3^- (Kendall et al., 2007).

NO_3^- in groundwater can be attenuated by denitrification, the reduction of NO_3^- to N_2, N_2O or NO gasses. The reduction reaction is metabolized be either heterotrophic or

chemoautotrophic microorganisms under anoxic conditions – oxygen concentrations of less than 0.5 mg/L (Kendall et al., 2007). Denitrification is considered to be a major process decreasing NO_3^- concentrations in groundwater (Aravena and Robertson, 1998). The amount of denitrification in surface waters is difficult to quantify and there is not a consensus in the scientific community on its role in NO_3^- removal in rivers (Mayer et al., 2002; Seitzinger et al., 2002).

If NO_3^- is present in high concentrations, it can negatively affect both ecosystems and human health. Negative impacts to aquatic ecosystems including rivers, lakes and coastal oceans, are eutrophication, hypoxia and acidification, all of which subsequently lead to a loss of biodiversity (Virousek et al., 1997). High NO_3^- concentrations in drinking water can cause methemoglobinia – a condition that affects the oxygen carrying capacity of blood, specifically in children, gastric cancer and non-Hodgkin's lymphoma (Babiker et al., 2004). From the Guidelines for Canadian Drinking Water Quality, the Maximum Allowable Concentration (MAC) of NO_3^- in Canada is 45 mg/L (Health Canada, 2010).

NO_3^- has been found in increasing concentrations in surface waters and in groundwaters in many different locations (Vitousek et al., 1997; Kendall et al., 2007; Xue et al., 2009). In south central British Columbia, elevated NO_3^- concentrations in groundwater have been documented within 100 km east and west of Midway, BC (Wei et al., 1993; Wei et al., 2010; Athanasopoulos, 2009). To the east, in the Grand Forks area, there are elevated concentrations of NO_3^- in groundwater proposed to be associated with agricultural practices, however the specific source has not been identified (Wei et al., 2010). Similarly, to the west in the agricultural areas surrounding Osoyoos, elevated NO_3^- concentrations have been detected in groundwater and sources are thought to be primarily from inorganic fertilizers associated with agricultural practices (Athanasopoulos, 2009). Groundwater NO_3^- contamination occurs as either a point source, which creates a plume of contamination or as a non-point source, which tends to affect larger portions of aquifers. Point sources include septic systems, waste lagoons and waste storage, whereas non point sources include application of fertilizers and/or manure on agricultural fields (Wassenaar et al., 2006).

The concentration of NO_3^- in surface water and groundwater samples from the Kettle River Basin were discussed in detail in Chapter 5. In surface water samples collected in June, NO_3^- was not detected. In October, NO_3^- concentrations are less than 0.5 mg/L, with the exception of one sample with a concentration of 1.7 mg/L. In groundwater samples, the average concentration in June is 27.7 ± 8.5 mg/L (n=18) and in October is 6.3 ± 5.7 mg/L (n=16). Overall, groundwater NO_3^- concentrations range from not detected to 41.3 mg/L, approaching the MAC.

6.4.3 $\delta^{15}N_{NO3}$ and $\delta^{18}O_{NO3}$

For NO_3^-, a dual isotope approach can be used as this molecule contains the stable isotopes of both N (^{15}N and ^{14}N) and O (^{18}O and ^{16}O). The different sources of NO_3^- often have unique combinations of $\delta^{15}N_{NO3}$ and $\delta^{18}O_{NO3}$ values. Because much research has been completed in this area, the range in values for each NO_3^- source has been well documented (e.g. Mayer, 2005; Kendall et al., 2007). Xue et al. (2009) reported the 10th and 90th percentiles of $\delta^{15}N$ and $\delta^{18}O$ values summarized from many different studies. The $\delta^{15}N$ from synthetic fertilizers ranges from -6 to 6 ‰, $\delta^{15}N_{NO3}$ from atmospheric deposition ranges from -8 to 9 ‰, soil nitrification $\delta^{15}N$ values range from 0 to 8 ‰, $\delta^{15}N$ from NO_3^- in manure ranges from 5 to 25 ‰ and from 4 to 19 ‰ for sewage. Similarly the reported 10th and 90th percentiles of $\delta^{18}O$ for the various sources are: 25 to 75 ‰ for atmospheric NO_3^- deposition, -10 to 15 ‰ for NO_3^- from soil nitrification, 17 to 25 ‰ for NO_3^- from fertilizer (Xue et al., 2009 and references therein). The $\delta^{18}O$ value of NO_3^- in sewage and manure was estimated to be -10 to 15 ‰ from Figure 4 in Mayer (2005).

The range in isotopic compositions of the different sources can be attributed to both the range in N and O isotope ratios of the original material and the fractionation processes, which ultimately produce or attenuate NO_3^-. Fixation from natural or anthropogenic processes, such as the Haber Bosch process, causes minor nitrogen isotope fractionation between -3 to +1 ‰ (Kendall et al., 2007). Mineralization of organic N compounds to ammonium (NH_4^+) is typically accompanied by a minor nitrogen isotope fractionation of ± 1 ‰. Subsequent nitrification of NH_4^+ to NO_3^-, results in nitrogen

isotope fractionation of -38 to -14 ‰ (Kendall et al., 2007). The O isotope fractionation during nitrification is still unresolved, but typically one O in the newly formed NO_3^- is derived from O_2 and the remainder comes from H_2O during the different stages of the oxidation process (Hollocher, 1984). Denitrification causes enrichment of ^{15}N and ^{18}O as NO_3^- concentrations decrease as the light isotopes of N and O are preferentially metabolized by microorganisms and converted to N_2 gas (Mayer, 2005).

Surface Water

Due to low NO_3^- concentrations in surface water, it was only possible to determine $\delta^{15}N$ and $\delta^{18}O$ values for one sample from June and six samples from October of 2010. $\delta^{15}N$ values range from 3.0 to 7.2 ‰ and $\delta^{18}O$ values range from -0.7 to 8.1 ‰. The average $\delta^{15}N$ value is 5.1 ± 1.8 ‰ (n=7) and the average $\delta^{18}O$ value of nitrate is 3.2 ± 3.0 ‰ (n=7).

Groundwater

The overall average $\delta^{15}N$ value of groundwater samples is 7.2 ± 3.9 ‰ (n=38) and the average $\delta^{18}O$ value is -3.7 ± 3.2 ‰ (n=38). The average $\delta^{15}N$ and $\delta^{18}O$ values are 2.0 and 0.2 ‰ higher, respectively, in samples from October compared to samples collected in June. Based on the temporal discrepancy in groundwater samples, measurement uncertainty and the standard deviation, there is no temporal variation in the $\delta^{15}N$ and $\delta^{18}O$ values of groundwater NO_3^-. $\delta^{15}N$ of groundwater NO_3^- collected in June range from 2.5 to 14.7 ‰ and $\delta^{18}O$ values from -7.6 to 3.3 ‰. Samples collected in October range from 3.2 to 18.9 ‰ for $\delta^{15}N$ and -8.7 to 5.5 ‰ for $\delta^{18}O$.

6.4.4 Discussion of Nitrate Sources

When $\delta^{15}N$ and $\delta^{18}O$ values of surface water and groundwater samples are plotted against each other, and compared to the isotopic compositions of different nitrate sources from the literature, NO_3^- in the Kettle River Basin appears to be from soil nitrification,

sewage and/or manure (Figure 6-11). NO_3^- from sewage and animal manure cannot usually be differentiated as the isotopic signatures overlap. Three surface water and seven groundwater samples plot only in the soil nitrification range and ten groundwater samples plot only in the sewage/manure range (Figure 6-11). The remaining four surface water and 21 groundwater samples plot within the range where both sources overlap, indicating either NO_3^- in these samples is derived from soil nitrification or sewage/manure, or it is a mixture of the two sources.

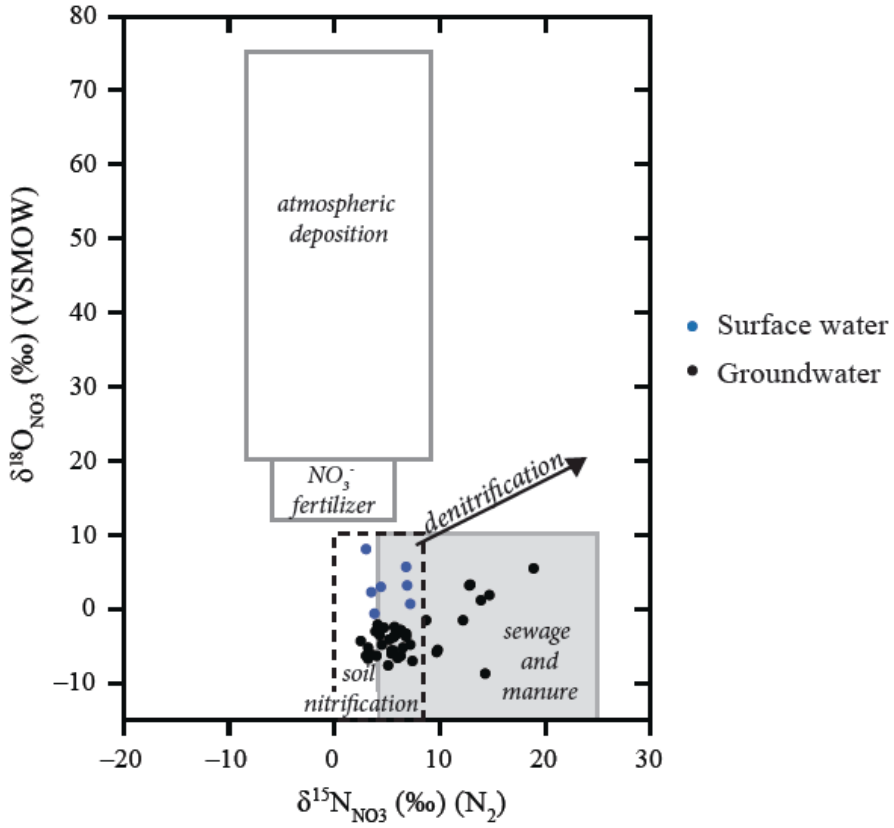

Figure 6-11: $\delta^{15}N_{NO3}$ and $\delta^{18}O_{NO3}$ values of surface water and groundwater samples in relation to ranges of $\delta^{15}N_{NO3}$ and $\delta^{18}O_{NO3}$ values of sources of NO_3^- (after Mayer, 2005; Kendall et al., 2007)

To determine whether the groundwater NO_3^- derived from sewage/manure originates from a point source or a non-point source, the spatial distribution of $\delta^{15}N$ values is investigated. As shown in Figure 6-12, which displays the $\delta^{15}N$ values of groundwater samples collected in June, the anthropogenic NO_3^- contamination, as

indicated by $\delta^{15}N$ values greater than 8.0 ‰, appears to be from point source locations. From wells sampled in June and October, there are six locations that have groundwater $\delta^{15}N$ values greater than 8.0 ‰, five of which are shown in Figure 6-12. The other groundwater well only has $\delta^{15}N$ values greater than 8.0 ‰ in October and therefore is not shown in Figure 6-12.

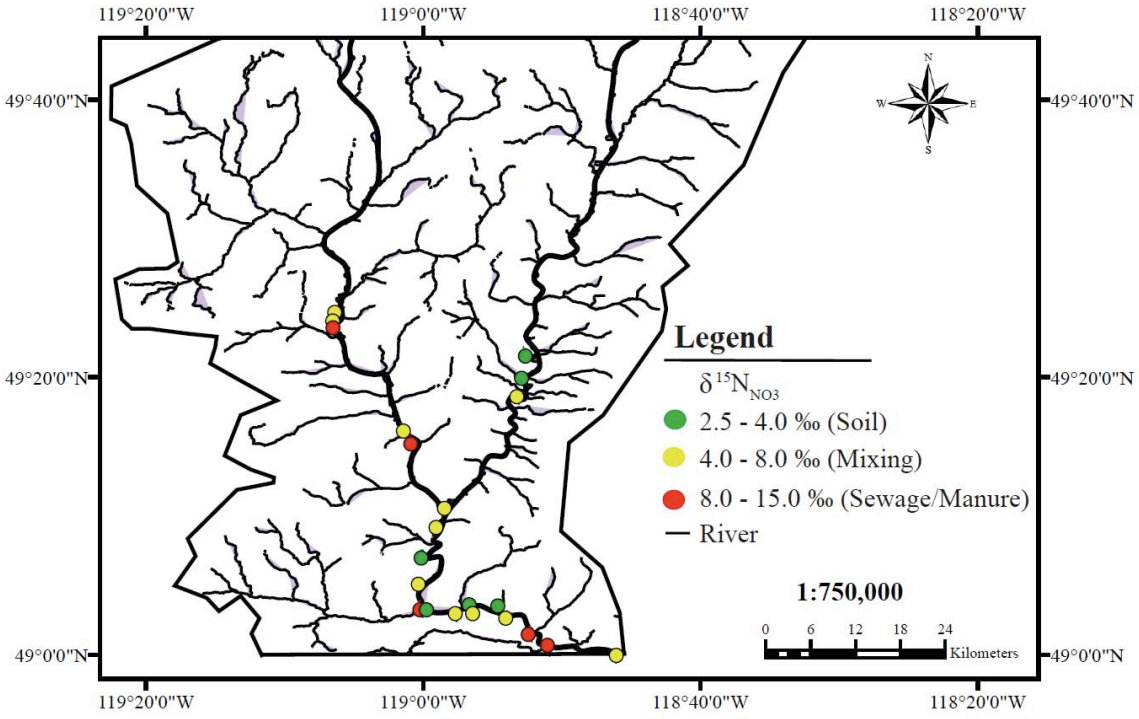

Figure 6-12: Spatial distribution of $\delta^{15}N_{NO3}$ values of groundwater obtained from wells sampled in June 2010.

The source of NO_3^- is of specific interest when concentrations approach or exceed the drinking water standard as NO_3^- concentrations higher than 45 mg/L can adversely affect human health. Combining concentration data and isotopic data can be used to assess mixing between NO_3^- from soil nitrification and sewage/manure, or to indicate whether or not dentrification is an active process attenuating NO_3^- concentrations (Mayer et al., 2002). As indicated with arrows in Figure 6-13, mixing of NO_3^- from nitrification in soils with NO_3^- from sewage/manure causes an increase in both NO_3^- concentrations and

$\delta^{15}N$ values; in contrast, dentrification causes NO_3^- concentrations to decrease and $\delta^{15}N$ values to increase. As shown in Figure 6-13, surface water samples have very low NO_3^- concentrations, which is not likely to be indicative of a denitrification trend. There are three surface water samples (circled in Figure 6-13), which are likely influenced by sewage or manure, as they have higher $\delta^{15}N_{NO3}$ values compared to the other surface water samples. Two of these samples were obtained between Rock Creek and the Canadian – US border, and the other sampling site is located downstream of Beaverdell, BC. Based on the $\delta^{15}N_{NO3}$ values of these three samples and the fact that these sampling sites are located downstream from population centers, a slight anthropogenic NO_3^- influence on surface waters in the Kettle River Basin is hypothesized.

Groundwater samples have higher NO_3^- concentrations in June compared to October. Possible reasons for higher NO_3^- concentrations in June could be related to the fact that recharge during snow melt delivers NO_3^- from soil nitrification or sewage/manure to the groundwater, as it was identified in Chapter 2 that the Kettle River Basin receives high rates of precipitation in June. Some groundwater samples from June appear to follow a mixing trend while some samples collected in October appear to follow a dentrification trend (Figure 6-13). However, overall there does not appear to be a strong correlation consistent with either mixing of NO_3^- from soil nitrification with NO_3^- from sewage/manure, or with dentrification. The $\delta^{15}N_{NO3}$ values and NO_3^- concentrations of samples collected in June and October from the same well are compared to identify possible mixing or denitrification trends in specific locations (Figure 6-14). For most samples, the source of NO_3^- does not change temporally, since the $\delta^{15}N_{NO3}$ values remain constant, as indicated with the horizontal lines in Figure 6-14. There is one groundwater well in which $\delta^{15}N_{NO3}$ values increase and concentrations decrease between June and October suggesting denitrification is an active process. In order for dentrification to proceed, dissolved oxygen concentrations must be less than 0.5 mg/L (Kendall et al., 2007). Dissolved oxygen concentrations of samples collected from this well are greater than 2 mg/L suggesting denitrification in the well is not an active process.

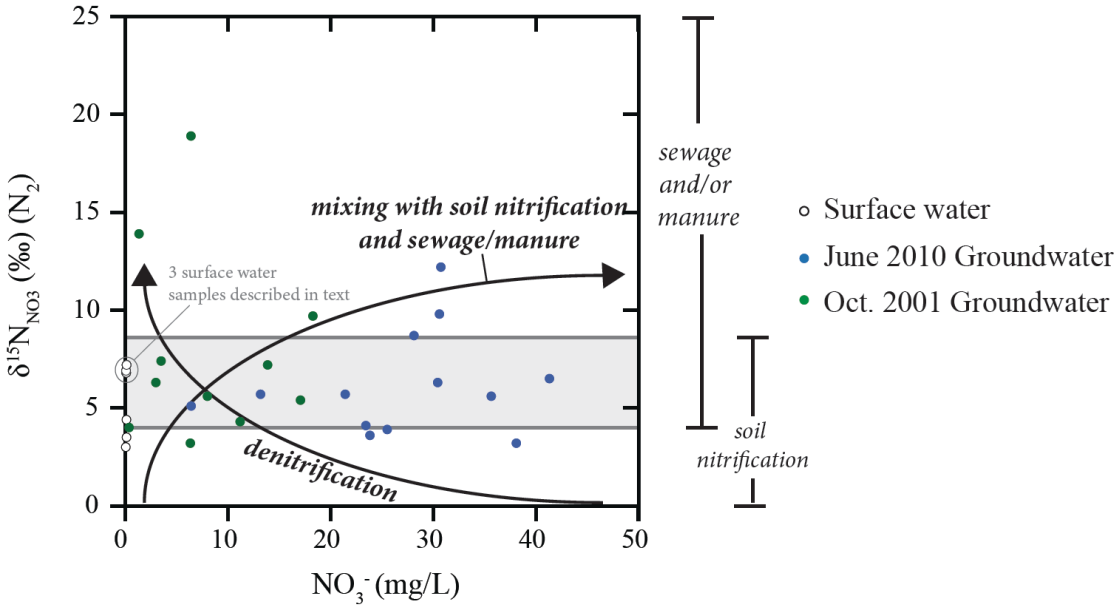

Figure 6-13 $\delta^{15}N_{NO3}$ versus NO_3^- (mg/L) in surface water and groundwater samples in relation to ranges of $\delta^{15}N$ of NO_3^- sources. Arrows indicate the expected trend of mixing and denitrification (after Mayer, 2005).

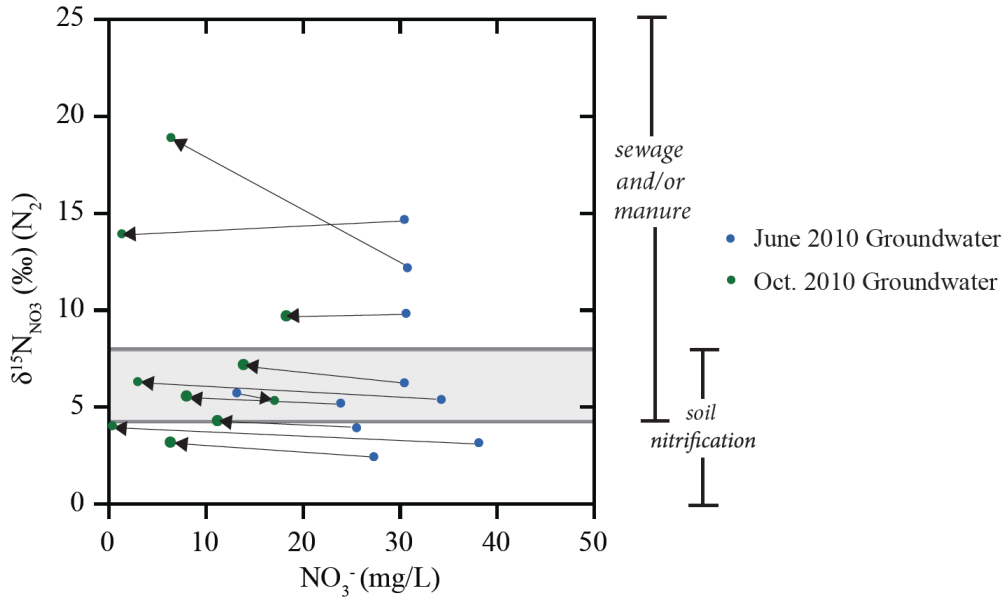

Figure 6-14: $\delta^{15}N_{NO3}$ versus NO_3^- (mg/L) in groundwaters. Lines connect samples collected from the same well in June and October of 2010, respectively.

Based on concentration and stable isotope data for NO_3^-, surface water samples appear to have minimal anthropogenic influence. Of the 25 groundwater wells sampled, six are impacted by NO_3^- from either sewage or manure, while groundwater samples from 15 wells have $\delta^{15}N_{NO3}$ values that plot within both the range of NO_3^- from soil nitrification and sewage/manure. The source of NO_3^- in groundwaters does not change temporally in most wells that were sampled. Based on the spatial distribution of $\delta^{15}N$ values, it appears anthropogenic NO_3^- contamination is limited to a few point sources.

6.5 Sulfate

SO_4^{2-} in aqueous systems can originate from the atmosphere, pedosphere or lithosphere (Mayer, 2005). Anthropogenic activities can contribute SO_4^{2-} from burning of fossil fuels (Clark and Fritz, 1997), soaps and detergents, fertilizers, and compounds added during water treatment (Mayer, 2005). High SO_4^{2-} concentrations can adversely influence ecosystems. Negative impacts include increasing acidity through sulfide oxidation (Clark and Fritz, 1997) and contributing to the hardness of water (Mayer, 2005).

6.5.1 Sulfate concentrations

Surface waters SO_4^{2-} concentrations range from 0.7 to 8.3 mg/L while groundwater SO_4^{2-} concentrations range from 4.3 to 145.6 mg/L. The average SO_4^{2-} concentration of all surface water samples is 4.0 ± 2.3 mg/L (n=72) and the average SO_4^{2-} concentration of groundwater samples is 28.4 ± 32.1 mg/L (n=48). Temporal and spatial variations in SO_4^{2-} concentration are summarized in greater detail in Chapter 5. Figure 6-15 depicts SO_4^{2-} concentrations of surface water with increasing distance downstream.

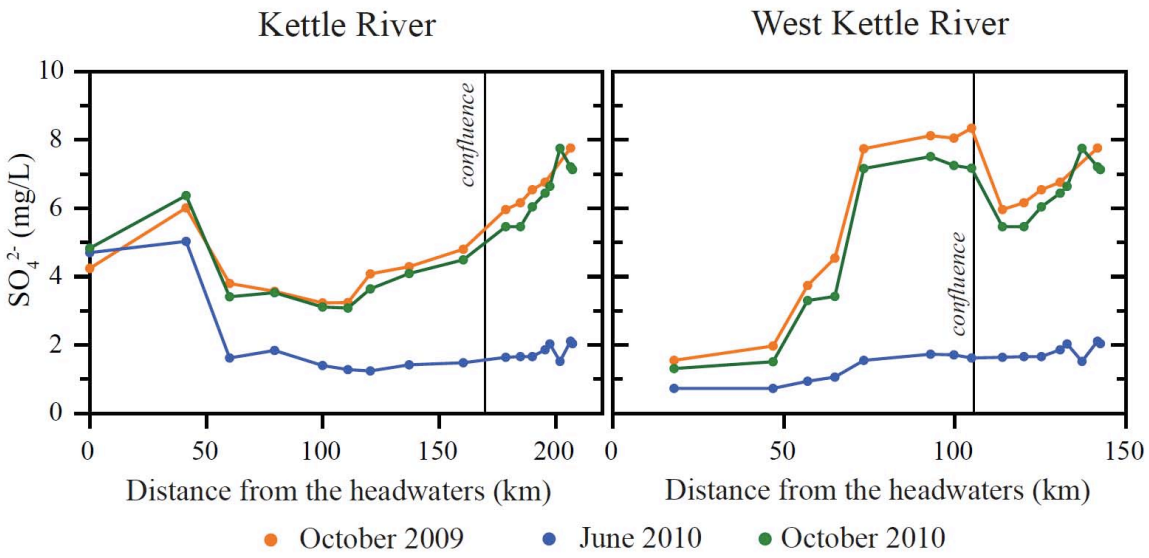

Figure 6-15: SO_4^{2-} (mg/L) concentrations versus distance downstream in the Kettle and West Kettle River tributaries.

6.5.2 $\delta^{34}S_{SO4}$ and $\delta^{18}O_{SO4}$

A dual isotope approach is used to determine the sources of SO_4^{2-}, as different SO_4^{2-} sources often have unique combinations of $\delta^{34}S_{SO4}$ and $\delta^{18}O_{SO4}$ values. The $\delta^{34}S$ and $\delta^{18}O$ values of the various sources of SO_4^{2-} have been extensively studied and documented. Lithospheric sources of SO_4^{2-} include evaporites, mantle and igneous rocks, and sulfide minerals that oxidize to SO_4^{2-}. The $\delta^{34}S$ values of evaporites range from 8 to 35 ‰ and $\delta^{18}O$ values range from 7 to 20 ‰ (Claypool, 1980). Volcanic and magmatic sources of sulfur typically have $\delta^{34}S$ values of 0.0 ± 2.0 ‰. Some heterogeneity has been identified between different igneous varieties (Seal, 2006). For example, the reported average of $\delta^{34}S$ values of sulfide in oceanic island basalts is 1.0 ± 1.9 ‰, while the average of mid-ocean ridge basalts is -0.3 ± 2.3 ‰ and sulfide inclusions in mantle xenoliths have an average $\delta^{34}S$ value of 1.3 ± 3.8 ‰ (Seal, 2006). The $\delta^{34}S_{sulfide}$ values of intrusive igneous varieties have been reported to range from -11.0 to 14.5 ‰, however the reported average of 1.1 ± 6.1 ‰ is still close to zero (Seal, 2006). Oxidation of sulfide minerals releases SO_4^{2-}, a process that produces negligible sulfur isotope fractionation, and therefore aqueous SO_4^{2-} has similar $\delta^{34}S$ values as the reduced sulfide minerals from which it originates (Seal,

2006). During oxidation, four O atoms are incorporated into SO_4^{2-} from H_2O and/or O_2, which causes $\delta^{18}O$ values to be lower than those of atmospheric and evaporite sources of SO_4^{2-} (Mayer, 2005). The $\delta^{34}S$ values of SO_4^{2-} originating from oxidation of sulfide minerals ranges from -30 to 10 ‰ and $\delta^{18}O$ values range from -10 to 0 ‰. The $\delta^{34}S$ values of soil SO_4^{2-} varies between -2 to 10 ‰ and $\delta^{18}O$ values range from 0 to 5 ‰. Atmospheric $\delta^{34}S$ and $\delta^{18}O$ values range from -10 to 20 ‰ and 5 to 15 ‰, respectively (from Figure 1 in Mayer, 2005). $\delta^{34}S$ values of SO_4^{2-} in atmospheric deposition of industrialized countries range from -1 to 6 ‰ (Mayer, 2005).

Surface Water

The average $\delta^{34}S$ values of SO_4^{2-} in surface waters samples is -0.3 ± 3.4 ‰ (n=47). The average of $\delta^{34}S$ values of surface water samples collected in June is -0.8 ± 3.5 ‰ (n=22), while the average of samples collected in October is 0.1 ± 3.4 ‰ (n=25). The difference between average values of $\delta^{34}S$, from samples collected in June and October is 0.9 ‰. Considering the reported measurement uncertainty and standard deviation, there is no temporal variation in $\delta^{34}S$ values. In all surface water samples, $\delta^{34}S$ values of SO_4^{2-} range from -12.1 to 2.5 ‰. The overall average $\delta^{18}O$ value of SO_4^{2-} in surface water samples is 0.0 ± 2.8 ‰ (n=47). Similar to $\delta^{34}S$, $\delta^{18}O$ values of SO_4^{2-} collected in June are slightly more negative compared to those of SO_4^{2-} samples collected in October. The average $\delta^{18}O$ value of SO_4^{2-} in June is -0.6 ± 1.3 ‰ (n=22), while the average in October is 0.5 ± 3.6 ‰ (n=25). The average $\delta^{18}O$ value of surface water SO_4^{2-} samples collected in June is 1.1 ‰ lower compared to values of samples collected in October, which is insignificant based on the reported measurement uncertainty and the standard deviation. $\delta^{18}O$ values in surface water range from -5.0 to 6.3 ‰.

Groundwater

Groundwater samples have an average $\delta^{34}S$ value of SO_4^{2-} of 1.2 ± 2.1 ‰ (n=48). The average $\delta^{18}O$ value of SO_4^{2-} is -4.3 ± 1.9 ‰ (n=48). Similar to surface waters, the average of $\delta^{34}S$ and $\delta^{18}O$ values are more negative in June compared to samples collected

in October. $\delta^{34}S$ values are 0.2 ‰ lower and $\delta^{18}O$ values are 0.8 ‰ more negative. In both cases this is less than or equal to the measurement uncertainty and therefore given the standard deviation, $\delta^{34}S$ and $\delta^{18}O$ values are essentially identical. The range in $\delta^{34}S_{SO4}$ values is -3.4 to 8.0 ‰ and the range in $\delta^{18}O_{SO4}$ values is -7.6 to 0.1 ‰.

6.5.3 Discussion of Sulfate Sources

$\delta^{34}S$ and $\delta^{18}O$ values for surface water and groundwater SO_4^{2-} from the Kettle River Basin are plotted in relation to the ranges of $\delta^{34}S$ and $\delta^{18}O$ of different sources of SO_4^{2-} (Figure 6-16). Figure 6-16 indicates that the sources of surface water SO_4^{2-} are sulfide oxidation, and possibly volcanics, soil and/or atmospheric SO_4^{2-} deposition. Investigation of the variation of $\delta^{34}S$ values of surface water SO_4^{2-} with distance downstream indicates most samples plot within the range of the isotopic composition of SO_4^{2-} in groundwater samples (Figures 6-17).

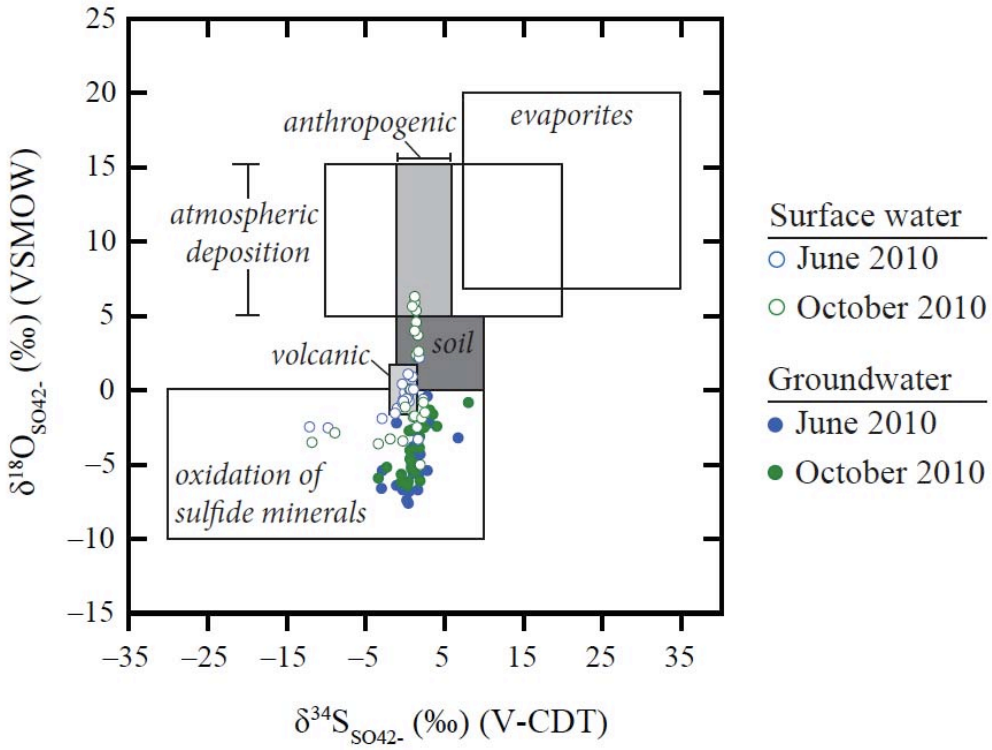

Figure 6-16: $\delta^{34}S_{SO4}$ and $\delta^{18}O_{SO4}$ of surface water and groundwater samples in relation to the ranges of $\delta^{34}S$ and $\delta^{18}O$ values of sources of SO_4^{2-} (after Mayer, 2005).

Surface Water

Sulfate in surface water samples has $\delta^{34}S$ values similar to those typical for volcanics, soil and atmospheric sources suggesting that SO_4^{2-} is possibly a mixture of these sources. Samples collected at the headwaters of the Kettle River have more negative $\delta^{34}S_{SO4}$ values compared to most other samples (Figures 6-17). The geology upstream of these sampling locations is dominated (>60 %) by sedimentary lithologies, whereas the remainder of the Kettle and West Kettle sub-catchments is dominantly (>60 %) underlain by volcanic lithologies. A geological map of the study area is found in Figure 2-7 and the relative abundances of each lithology type are summarized in Table 8-1. The drastic difference in underlying lithologies is a potential reason for the more negative $\delta^{34}S$ values of SO_4^{2-} in samples collected from the headwaters of the Kettle River; sedimentary units contain sulfide minerals that typically have more negative $\delta^{34}S$ values than sulfides in volcanic lithologies, as summarized by Seal (2006). $\delta^{34}S$ values of SO_4^{2-} in surface water samples from the two headwater stations from the Kettle River suggest the source of SO_4^{2-} is oxidation of sulfide minerals.

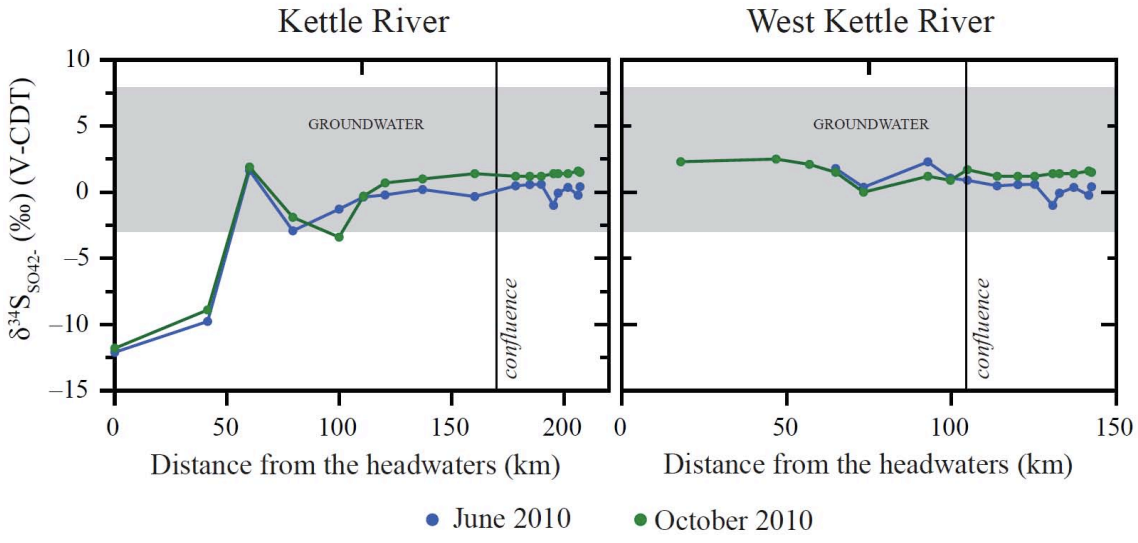

Figure 6-17: $\delta^{34}S_{SO4}$ of surface water samples versus distance downstream of the Kettle and West Kettle Rivers. The range of groundwater $\delta^{34}S_{SO42-}$ values is also indicated.

$\delta^{18}O$ values of SO_4^{2-} in surface water with distance downstream in relation to the ranges of $\delta^{18}O$ of respective SO_4^{2-} sources are shown in Figure 6-18. Prior to the confluence of the Kettle and West Kettle Rivers, $\delta^{18}O$ values of SO_4^{2-} are within the range of SO_4^{2-} from sulfide oxidation, volcanics and soils. Beyond the confluence, a few samples fall within the range of $\delta^{18}O_{SO4}$ values of atmospheric deposition and/or soil SO_4^{2-}. It has been shown that the majority of atmospheric SO_4^{2-}, in industrialized countries, is derived from anthropogenic activities (Benkovitz et al., 1996; Mayer, 2005; Aravena and Mayer, 2010). Weather systems originating in the Pacific Ocean, could transport atmospheric SO_4^{2-} of anthropogenic origin from major population centers on the Pacific Coast, to the Kettle River Basin. Because SO_4^{2-} concentrations increase with increasing distance downstream it is also possible that there are additional sources of SO_4^{2-}, such as ammonium sulfate fertilizers, SO_4^{2-} from soaps and detergents or SO_4^{2-} derived from water treatment processes (Mayer, 2005).

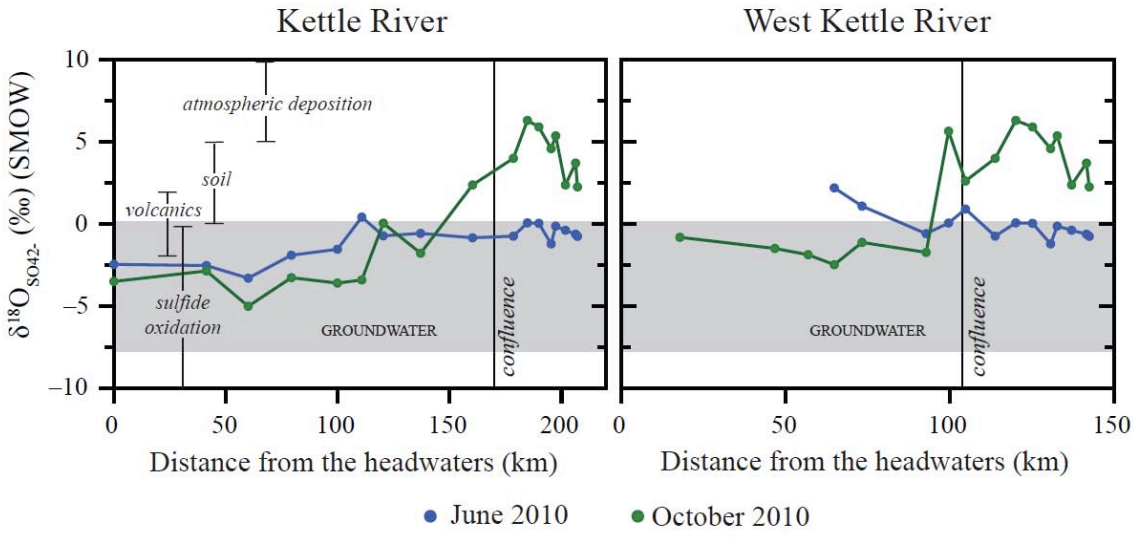

Figure 6-18: $\delta^{18}O_{SO42-}$ of surface water samples versus distance downstream of the Kettle and West Kettle Rivers. The range of groundwater $\delta^{18}O_{SO42-}$ values is also indicated.

Groundwater

Groundwater SO_4^{2-} appears to be predominately derived from sulfide oxidation. The isotopic composition of a few SO_4^{2-} samples are close to the volcanic/magmatic sources range, which overlaps with $\delta^{34}S$ and $\delta^{18}O$ values of sulfate derived from sulfide oxidation, and a few samples plot close to the soil SO_4^{2-} range (Figure 6-16). Therefore it is possible that soil SO_4^{2-} and SO_4^{2-} from volcanic/magmatic sources are also contributing SO_4^{2-} to aquifers.

6.6 Conclusion

$\delta^{18}O$ and $\delta^{2}H$ values of precipitation are consistent with a dominant source of precipitation in the Kettle River Basin from pacific derived weather systems. Water that has entered the basin is subsequently discharged via the Kettle and West Kettle Rivers, or stored in groundwaters. Altitude and climate variations within the basin were correlated to $\delta^{18}O$ and $\delta^{2}H$ values in surface water samples. Evaporation was identified to influence $\delta^{18}O$ and $\delta^{2}H$ values of surface waters and possibly groundwater samples. Irrigation with surface water and subsequent infiltration into aquifers may also influence the isotopic composition of groundwaters.

The source of DIC in surface water and groundwater was investigated using DIC concentration data, saturation indices of calcite, pCO_2 calculated to be in equilibrium with the samples and $\delta^{13}C_{DIC}$ values. Surface water samples have higher $\delta^{13}C$ values compared to those of groundwaters, suggesting that in addition to baseflow contributions to riverine flow, there are other sources of DIC, or active processes influencing the isotopic composition of surface water DIC. Other possible sources of surface water DIC in surface water include dissolution of atmospheric CO_2 and possible processes influencing the isotopic composition of DIC include atmospheric exchange or degassing of CO_2, or in-river photosynthesis. Groundwater DIC originates primarily from pedospheric CO_2 with minor contributions from calcite dissolution and atmospheric derived CO_2.

Interpretation of isotopic results and concentration data suggest that sources of NO_3^- in surface water and groundwater is partially derived from natural sources, but there is also some evidence of anthropogenic influence in a few surface water and many groundwater samples. NO_3^- in surface waters is present in very low concentrations, however groundwater concentrations are significantly elevated and more variable. Spatial variation of both isotopic composition and concentration data of groundwater indicate that NO_3^- originates from either natural sources or anthropogenic point sources and in some cases is a mixture of these two sources. Comparison of $\delta^{15}N_{NO3}$ values and NO_3^- concentration data for samples collected in June and October, from the same well, indicates no change in NO_3^- sources while the concentration of NO_3^- varied.

Based on $\delta^{34}S_{SO4}$ and $\delta^{18}O_{SO4}$ values, SO_4^{2-} in surface water and groundwaters in the Kettle River Basin appears to be derived primarily from natural sources, with minor anthropogenic influences. Surface water SO_4^{2-} concentrations are very low and groundwater SO_4^{2-} concentrations are higher and vary spatially. Upstream of the confluence of the two rivers, $\delta^{34}S_{SO4}$ values in surface water samples fall within the range of groundwaters samples, indicating the importance of baseflow in these rivers. With increasing distance downstream, some surface water samples appear to have SO_4^{2-} contributions from atmospheric deposition that contains SO_4^{2-} of anthropogenic origin, and/or soil SO_4^{2-}. SO_4^{2-} in groundwater samples is predominantly derived from oxidation of sulfide minerals.

DIC, NO_3^- and SO_4^{2-} in the Kettle River Basin originate from the atmosphere, lithosphere, biosphere and pedosphere, with contributions from anthropogenic activities especially in groundwaters. Chemical and isotopic data proved to be a useful tool to identify sources and fluxes of water between reservoirs, and sources and processes affecting dissolved constituents in surface water and groundwaters in the Kettle River Basin.

Chapter Seven: Mass Balance of Major Ions

7.1 Introduction

Weathering of bedrock has been identified as the dominant source of solutes to unpolluted watersheds (Drever, 1997). In order to determine the role of bedrock weathering, other non-weathering components such as atmospheric and biospheric inputs, and inputs from anthropogenic activities must be considered, using a mass balance approach (White and Blum, 1995; Grasby 1997). A mass balance approach considers the flux of materials entering and leaving a system, thus providing insight into processes that may be occurring within the system. This approach has been used in watershed studies to examine the geochemical flux of materials entering or leaving watersheds allowing identification of weathering reactions occurring within the watershed (Garrels and Mackenzie, 1967; Drever, 1997; Bricker et al., 2005). The following mass balance equation incorporates the non-weathering components that may contribute ions to surface water and groundwater (White and Blum, 1995; Grasby, 1997; Bricker et al., 2005):

$$W = SW/GW - At - Bio - IE - An \quad (7\text{-}1)$$

W = Weathering of bedrock
SW/GW = measured value of surface water and groundwater
At = Atmospheric Input
Bio = Biological Input
IE = Ion Exchange
An = Anthropogenic Input

This equation assumes there is no net storage of water within the basin. This assumption is increasingly valid on timescales greater than one year, as there are significant changes in biomass within one year (Drever, 1997). Each component of Equation 7-1 is discussed below.

7.2 Atmospheric Input (At)

The atmospheric component of the mass balance equation includes both wet and dry deposition. Precipitation samples (wet deposition) were collected as part of this project in June of 2010, near Rock Creek. It is assumed that these precipitation samples are representative of the entire basin for the duration of the study. There was no other precipitation chemistry data available in this area of British Columbia (BC).

As discussed in Chapter 2, the geology in the Kettle River Basin is dominated by igneous and metamorphic lithologies (BC Geological Survey, 2005), neither of which contains significant amounts of Cl^-. There are no known evaporite deposits or geological sources of Cl^-. It can therefore be assumed all Cl^- is derived from atmospheric sources (White and Blum, 1995) or anthropogenic sources. Cl^- is considered to be a conservative tracer as it does not participate in exchange reactions and only precipitates out of solution as a salt at very high salinities (Drever, 1997). Evapotranspiration is the only process affecting the concentration of Cl^- in surface waters and groundwaters. Evapotranspiration includes evaporation and transpiration. Subsequently, the term evaporation will be used to describe water loss from evaporation and transpiration. The amount of evaporation can be determined using the evaporation factor:

$$\text{Evaporation Factor} = [Cl^-_{sample}] / [Cl^-_{precipitation}] \quad (7\text{-}2)$$

This evaporation factor can subsequently be applied to other measured major cations and anions in precipitation samples to determine the concentration due to evaporation of precipitation. Subtraction of this 'evaporated precipitation' concentration from the measured concentration allows for determination of the concentration of cations and anions 'corrected' for atmospheric inputs (White and Blum, 1995). Atmospheric inputs include both wet and dry deposition. Dry deposition was not measured in this study. However, assuming wet and dry deposition have the same ratio of anions and cations to Cl^- (White and Blum, 1995), the evaporation factor accounts for wet and dry deposition.

7.2.1 Surface Water

The average evaporation factor of surface waters, calculated from Cl^- concentrations, is 8.8 ± 7.0, the minimum is 0.4 and the maximum is 22.8. A higher evaporation factor indicates more evaporation has occurred. The average and range of evaporation factors varies depending on which section of the river the sample was taken from – the Kettle River, West Kettle River or below the confluence, as summarized in Table 7-1. Of the three sections, the West Kettle River has the highest average evaporation factor and the Kettle River has the lowest. This suggests either there is more evaporation in the West Kettle River compared to the Kettle River or there is an additional source of Cl^- along the West Kettle River. Unfortunately, it was not possible to correlate these evaporation factors with climate data, as there is no available climate data from the Kettle River sub-catchment. However, discussion of stable isotope abundance ratios of water in Chapter 6 also suggests higher evaporation along the West Kettle River compared to the Kettle River. The possibility of an additional source of Cl^- along certain sections of the river will be discussed in greater detail in Section 7.5.

Table 7-1: Average and range in evaporation factors for the Kettle River and West Kettle River rivers, and below the confluence.

Section of River	**Evaporation Factor**		
	Average	**Minimum**	**Maximum**
Kettle River	3.2 ± 1.6 (n = 27)	0.4	6.4
West Kettle River	15.3 ± 7.3 (n = 24)	2.7	22.8
Below the Confluence	8.5 ± 4.3 (n = 21)	2.2	15.6

7.2.2 Groundwater

The average evaporation factor of groundwater samples is 60.2 ± 70.5; the lowest value is 5.8 and the highest is 297.8. A histogram of these values shows the distribution of values indicating that there are several groundwater samples that have much higher evaporation factors compared to the majority of groundwater samples (Figure 7-1). The samples with evaporation factors greater than 100 were obtained from wells at locations very close to highways, indicating that in all likelihood anthropogenic road salt applied to

highways has reached the well screens. Anthropogenic inputs will be considered in greater detail in Section 7.5.

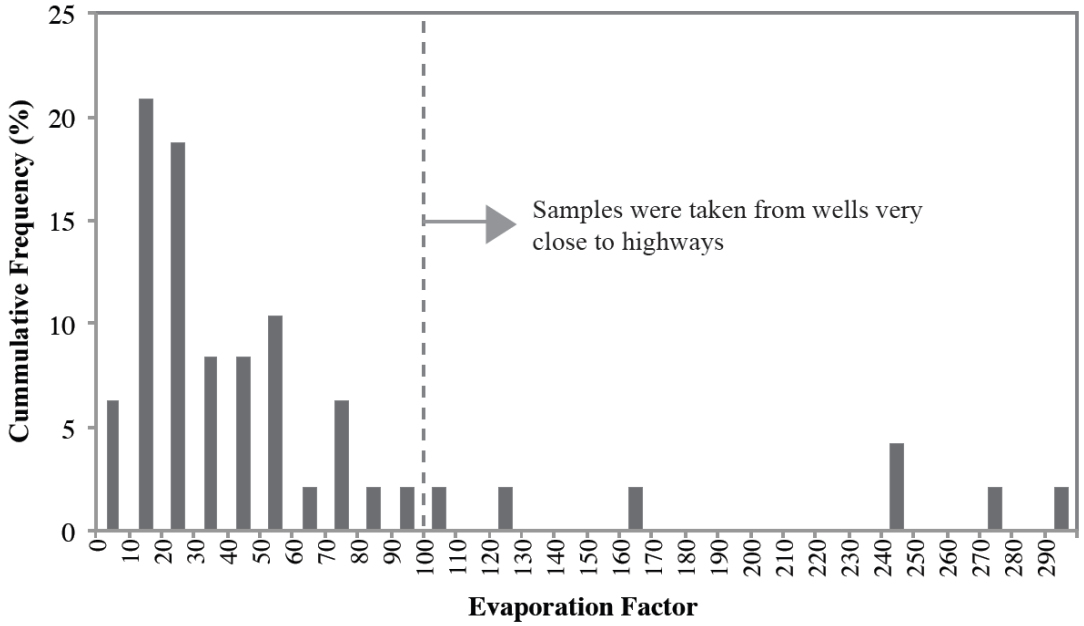

Figure 7-1: Histogram of evaporation factors of groundwater samples.

7.3 Biological (Bio)

The biological component refers to the uptake or release of nutrients from the biomass, which primarily includes plants and microorganisms. Plants take up all the major cations and anions considered in this study, except Na^+, and then eventually decay releasing nutrients back into the watershed (Drever, 1997). Root respiration and decay of organic matter in the soil zone generates CO_2(g) and organic acids, which increase acidity and therefore encourage mineral weathering (Drever, 1994). Weathering agents are discussed in more detail in Chapters 8 and 9. Forested watersheds are considered to be in steady state on long time scales. There are gradual changes in biomass associated with annual growth and more sudden changes associated with logging and forest fires. In the Kettle River Basin, logging is currently active (Dessouki, 2007), however a source for the amount of forest cover removed yearly was not available. There have not been any large fires recorded in the study area (BC Forests and Range, 2011). Because no drastic

changes in the biomass have been reported over the course of this study, for mass balance calculations, it will be assumed, that there is no change in biomass.

7.4 Ion Exchange (IE)

Ion exchange refers to the exchange of ions between solution and solid phases such as clay minerals, organic matter and metal oxy-hydroxide surfaces (Appelo and Postma, 2005). According to Drever (1997), if there is not a significant change in the inputs into the watershed, it can be assumed that ion exchange reactions are in equilibrium with surrounding materials and are in steady state. There are no known changes in atmospheric input parameters and therefore, steady state is assumed. The influence of ion exchange reactions on surface water and groundwater chemistry will be addressed in greater detail in Chapter 8.

7.5 Anthropogenic (An)

Anthropogenic activities, as described in Chapter 2, may be associated with the small towns of Beaverdell, Rock Creek and Midway, as well as dispersed human settlement, irrigated agriculture, ranching, forestry, mineral exploration and the Big White Ski Resort (Dessouki, 2009). Also, in winter months, road salt is applied to Highways 3, 33 and 6. The locations of these highways are shown in Figure 2-8. Each of these anthropogenic activities can add major ions to surface water and groundwater; Table 7-2 summarizes possible anthropogenic sources of major ions. In Chapter 6, using a combination of stable isotopes and concentration data, a few groundwater wells were found to contain NO_3^- derived from ranching/agricultural activities or septic systems. The application of road salt to highways has also been found to add Na^+ and Cl^- to both surface water and groundwater samples. Of all the major ions in Table 7-2, anthropogenic activities in the Kettle River Basin were found to contribute NO_3^-, Cl^- and Na^+ to surface water and groundwater samples.

Table 7-2: Some anthropogenic sources of major ions

Ion	Source
Ca^{2+}	Dust suppressant (Ca_2Cl) (Lawson, pers. comm. 2011)
Mg^{2+}	Dust suppressant (Mg_2Cl) (Lawson, pers. comm. 2011)
Na^{+}	Road salt, septic systems, manure, municipal wastewater treatment facilities, water softeners and some industrial facilities (Appelo and Postma, 2005; Kelly et al., 2010)
K^{+}	Fertilizer (Schindler, 2006), wastewater (Westgate et al., 2000)
Cl^{-}	Road salt, septic systems, manure, municipal wastewater treatment facilities, water softeners and some industrial facilities (Appelo and Postma, 2005; Kelly et al., 2010)
NO_3^{-}	Manure, septic systems, atmospheric deposition, fertilizer (Kendall et al., 2007)
SO_4^{2-}	Atmospheric deposition from fossil fuel combustion, aluminium sulphate (added to drinking water to settle particulate matter), soaps, detergents, fertilizer (Mayer, 2005)

7.5.1 Surface Water

Nitrate

Surface waters in the Kettle River Basin have very low concentrations of NO_3^-. In October of 2009 and 2010, all samples had NO_3^- concentrations less than 0.5 mg/L, except one sample in October 2009, which has a concentration of 1.7 mg/L. In June 2010, NO_3^- concentrations were below the detection limit in all surface water samples. Overall, the NO_3^- concentrations in surface water suggest very limited influence of anthropogenic nitrate. As discussed in Chapter 6, it was only possible to determine $\delta^{15}N_{NO3-}$ and $\delta^{18}O_{NO3}$ values for seven surface water samples due to low concentrations of NO_3^- in the samples. Of these samples, three have $\delta^{15}N$ values less than 4.0 ‰ suggesting the source is soil nitrification and four samples are within the range of both natural and anthropogenic sources. Six of these seven samples are from below the confluence, which is where the highest concentration of anthropogenic activity occurs. However, because the NO_3^- concentrations, with one exception, are all less than 0.5 mg/L, anthropogenic NO_3^- is assumed to have only a minor influence on surface water quality.

Chloride

The primary anthropogenic source of Cl^- to surface waters in the Kettle River Basin is likely road salt because of the close proximity between the river and the road along much of the river. Road salt, typically NaCl, has been applied to highways in British Columbia in winter months since the 1950's (Warrington, 1998) and is applied during winter months to the highways 3, 33 and 6 in the Kettle River Basin (Lawson, pers. comm. 2011). The location of these highways is shown in Figure 2-8. Application lowers the freezing point of water, 'de-icing' roads, or reducing the amount of ice on highways. Rates of application range from 60 – 130 kg/km on a two-lane road, depending on conditions (Warrington, 1998). Much of the West Kettle River parallels Highway 33 and so it is possible that road salt adds Na^+ and Cl^- to this portion of the river, especially during winter months. The Kettle River is primarily paralleled by a gravel road. Because road salt is not used as a de-icer on gravel roads, no influence on water quality along most the Kettle River is expected. Near the headwaters of the Kettle River, the river intersects Highway 6, which could potentially add Na^+ and Cl^- to the Kettle River, as a result of road salt application. When logging is active, $MgCl_2$ is applied to the gravel roads to suppress dust, however this application is sporadic (Lawson, pers. comm. 2011) and is therefore considered to have a negligible influence on water chemistry along the Kettle River. Below the confluence, the river parallels either Highway 33 or Highway 3, which are both highways where road salt is applied during winter months. Cl^- concentrations in surface waters range from 0.1 to 4.2 mg/L. There is 3.4 to 5.4 times more Cl^- in the West Kettle River compared to the Kettle River in June and October 2010, respectively (Table 7-3), which could be due to elevated evaporation, or application of road salt.

Table 7-3: Average Cl^- concentration of surface water samples taken from Kettle River and West Kettle River during the three sampling trips.

Section of River	**Average Cl^- (mg/L)**		
	October 2009	**June 2010**	**October 2010**
Kettle River	0.8 ± 0.3 (n=9)	0.3 ± 0.1 (n=9)	0.7 ± 0.3 (n=9)
West Kettle River	3.8 ± 0.7 (n=8)	1.1 ± 0.2 (n=8)	3.6 ± 0.4 (n=8)
Below the Confluence	2.3 ± 0.4 (n=5)	0.6 ± 0.1 (n=8)	2.1 ± 0.2 (n=8)

Sodium

As road salt was identified as a possible contributor to Cl^- concentrations, Na^+ concentrations are expected to follow similar patterns. Indeed, Na^+ concentrations from the West Kettle River are 1.9 to 2.1 times higher than those of the Kettle River, similar to Cl^- in October and June 2010, respectively (Table 7-4).

Table 7-4: Average Na^+ concentrations of surface water samples taken from Kettle River and West Kettle River during the three sampling trips.

Section of River	Average Na^+ (mg/L)		
	October 2009	June 2010	October 2010
Kettle River	1.6 ± 0.6 (n=9)	0.7 ± 0.2 (n=9)	1.8 ± 0.6 (n=9)
West Kettle River	3.4 ± 0.7 (n=8)	1.5 ± 0.4 (n=8)	3.6 ± 0.7 (n=8)
Below the Confluence	3.5 ± 0.4 (n=5)	1.3 ± 0.1 (n=8)	3.8 ± 0.4 (n=8)

Anthropogenic Influence on Surface Water Samples

In order to differentiate whether higher evaporation factors were due to increased evaporation or addition of road salt, a road salt sample was obtained from a stockpile of salt located between Rock Creek and Midway, BC. The road salt sample was dissolved into deionized water and major anions and cations were measured. As shown in Table 7-5, Na^+ and Cl^- were the most abundant ions. SO_4^{2-} and NO_3^- were 'not detected' (n.d.). The molar ratio of Na^+/Cl^- in precipitation and road salt was determined to be 2.6 and 1.0, respectively. Figure 7-2 shows the distribution of surface water samples relative to precipitation and road salt ratios.

Table 7-5: Major ions in road salt.

Ions	Ca^{2+}	Mg^{2+}	Na^+	K^+	SO_4^{2-}	NO_3^-	Cl^-
mg/L	<0.1	0.1	79.7	0.2	n.d.	n.d.	121.5

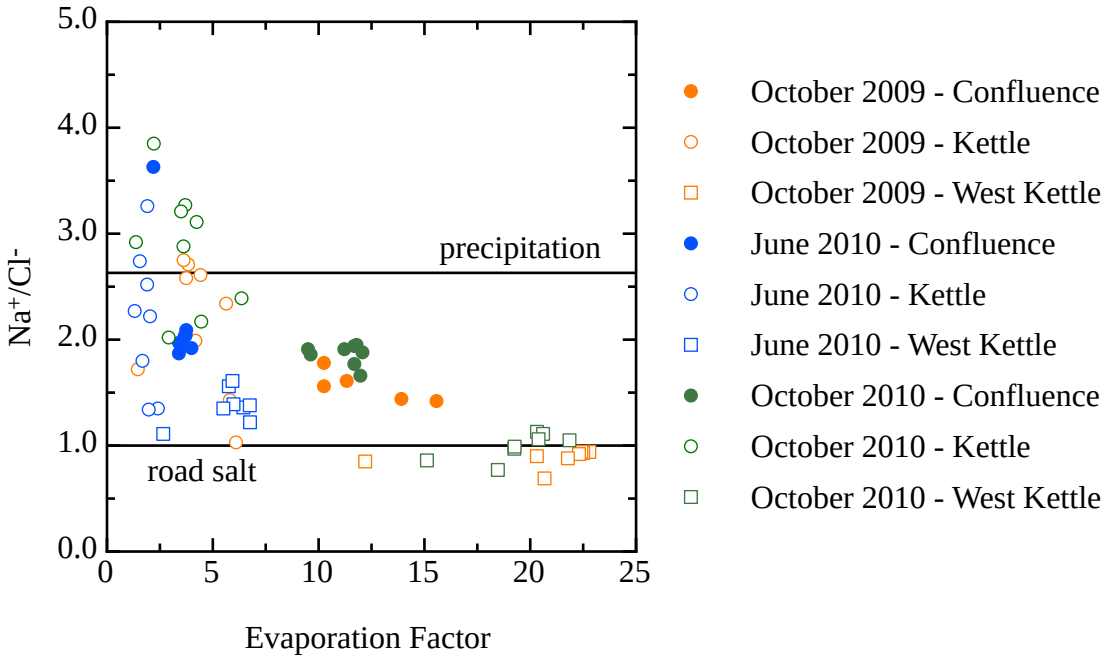

Figure 7-2: Na^+ versus Cl^- from samples collected along different portions of the river during the three sampling trips. The ratio of Na^+/Cl^- in precipitation and road salt is also indicated.

When Na^+ is plotted against Cl^-, there appear to be temporal and spatial correlations. As discussed in Chapter 5, samples collected in June are lower in concentration due to dilution from higher riverine discharge, compared to samples collected in October. As shown in Figure 7-2, samples collected in June have lower concentrations and plot close to the precipitation line. Samples collected in October have higher concentrations and some samples plot between the precipitation line and the road salt line. Samples from the Kettle River plot along or near the precipitation line, whereas samples from the West Kettle River plot in between the precipitation line and the road salt line. This suggests that samples from the West Kettle River contain Na^+ and Cl^- from both precipitation and road salt. Samples from below the confluence plot between samples collected from the Kettle and West Kettle Rivers.

In order to determine if samples approaching the road salt line also have a high evaporation factor, the ratio of Na^+ to Cl^- concentrations were plotted against the evaporation ratio (Figure 7-3). Figure 7-3 reveals that the evaporation factor is correlated

to when and where the sample was collected. Samples collected in October have higher evaporation factors, compared to samples collected in June and samples from the West Kettle River have higher evaporation factors compared to samples from the Kettle River, as summarized in Table 7-1.

As the evaporation factor increases, the ratio of Na^+ to Cl^- trends towards the road salt line, whereas most samples with lower evaporation factors plot closer to the precipitation line (Figure 7-3). There are a few samples with low evaporation factors that plot close to the road salt line. If, as evaporation factors increased, the ratio of Na^+/Cl^- continued to plot near the precipitation line, higher evaporation factors would be simply attributed to increased evaporation. Data presented in Figures 7-2 and 7-3 suggest that samples from the West Kettle River and from below the confluence, with higher evaporation ratios, are likely influenced by road salt due to the proximity to the 'road salt' line. Discussion of $\delta^{18}O$ and $\delta^{2}H$ values in Chapter 6 suggests evaporation is higher along the West Kettle River and below the confluence making it difficult to simply subtract an amount of Na^+ and Cl^- from surface water samples. Instead, a correction factor accounting for Na^+ and Cl^- derived from road salt, will be applied to samples from the West Kettle River and below the confluence, using the chemical composition of road salt.

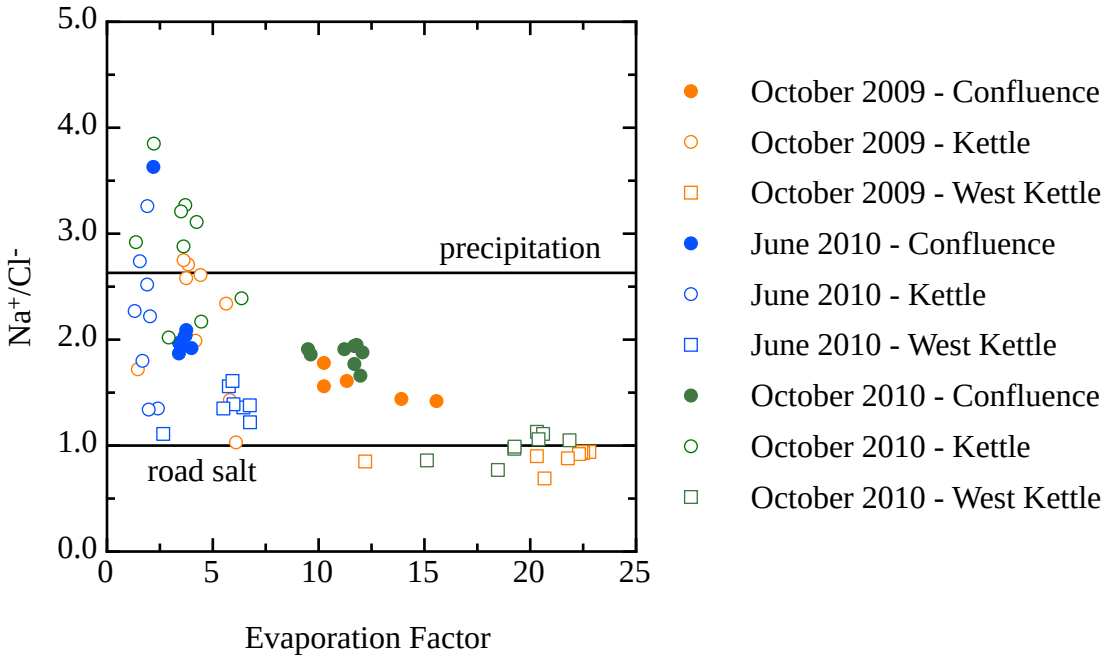

Figure 7-3: Molar ratio of Na^+ to Cl^- versus the evaporation factor of surface water samples collected along different sections of the river and at different times. The ratio of Na^+/Cl^- in precipitation and road salt is also indicated.

The amount of Na^+ and Cl^- from road salt is quantified using the following methodology. The composition of road salt was determined analytically and was found to be composed primarily of Na^+ and Cl^- with less than 0.15 % of concentration derived from Ca^{2+}, Mg^{2+} and K^+ (Table 7-5). Sources of K^+, throughout the entire watershed, can therefore be attributed to non-anthropogenic sources, such as atmospheric input and weathering of bedrock. The Kettle River is assumed to have no exposure to road salt, which is reasonable as much of the road that parallels the Kettle River is gravel and is impassable during winter months. The ratio of Na^+/K^+, along the Kettle River, is therefore assumed to be unaffected by anthropogenic influences. The average ratio of Na^+/K^+ along the Kettle River, for each sampling event was assumed to be the 'pristine' Na^+/K^+ value, meaning unaffected by anthropogenic road salt. This method assumes the affect of geology on water chemistry in the Kettle, West Kettle sub-catchments, and below the confluence is similar. Based on the relative distribution of lithologies summarized in Chapter 8 (Table 8-1), this appears to be a valid assumption. This ratio was then used to

determine the 'pristine' concentration of Na^+ from each sample from the West Kettle River and below the confluence, using the K^+ value from each sample (Equation 7-3). The calculated 'pristine' Na^+ concentration was then subtracted from the measured value of Na^+ to obtain the concentration of Na^+ added due to road salt (Equation 7-4). This value was also subtracted from the measured Cl^- value to obtain the 'pristine' Cl^- concentration (Equation 7-5). All calculations are in units of mmol/L.

$$Na^+/K^+ \text{ of the Kettle River} \times K^+ = \text{'pristine' } Na^+ \quad (7\text{-}3)$$

$$Na^+ \text{ measured} - \text{'pristine' } Na^+ = Na^+ \text{ due to road salt} \quad (7\text{-}4)$$

$$Cl^- \text{ measured} - Na^+ \text{ due to road salt} = \text{'pristine' } Cl^- \quad (7\text{-}5)$$

The Na^+ and Cl^- concentrations from the West Kettle River and from below the confluence were corrected for road salt input using the above approach. Changing the Cl^- concentration affects the estimated evaporation factor and therefore, the atmospheric contributions of each ion were re-calculated.

7.5.2 Groundwater

Nitrate

NO_3^- concentrations of groundwater samples range from 'not detected' to 41.3 mg/L. As discussed in Chapter 6, a few samples with higher NO_3^- concentrations also have elevated $\delta^{15}N_{NO3-}$ values suggesting the influence of sewage and/or manure. The locations of groundwater samples with $\delta^{15}N$ values suggesting the influence of sewage and manure are shown in Figure 6-12. Of the 48 groundwater samples, 21 groundwater samples have nitrate that is derived from soil nitrification or sewage/manure, or it is a mixture of the two sources and ten groundwater samples plot only in the sewage/manure range. Based on the spatial distribution of samples with $\delta^{15}N$ values suggesting anthropogenic influence, it appears that anthropogenic nitrate contamination is confined to a few point sources and is not a widespread problem throughout the Kettle River Basin.

Chloride

Groundwater Cl^- concentrations range from 1.1 to 54.7 mg/L. The concentration of Cl^- will be discussed in context with Na^+ and NO_3^- concentrations, and $\delta^{15}N$ values, to identify which groundwater samples have elevated Cl^- concentrations due to anthropogenic activities.

Sodium

Groundwater Na^+ concentrations range from 2.5 to 149.8 mg/L. Of the 48 groundwater samples collected, 44 have concentrations of less than 35 mg/L. The remaining four samples have Na^+ concentrations greater than 100 mg/L. These samples with high Na^+ concentrations do not have high Cl^- concentrations and have undetectable or low NO_3^- concentrations. This indicates the lack of anthropogenic impact and hence, samples with Na^+ concentrations greater than 100 mg/L are related to natural processes such as bedrock weathering, not anthropogenic activities. Of the 44 samples with Na^+ concentrations of less than 35 mg/L, some have high Cl^- concentrations, suggesting influence from road salt.

Anthropogenic Influence on Groundwater Samples

There are two types of anthropogenic influence on groundwater samples that increase the Cl^- concentration, which are road salt and sewage/manure. Because the focus here is specifically identifying the groundwater samples with anthropogenic chloride, groundwater samples will be classified based on evaporation factors.

Seven groundwater samples, from four wells, within close proximity to the Highway were previously identified to have evaporation factors greater than 100 (Figure 7-1). Of these samples, two have NO_3^- concentrations greater than 30 mg/L, three samples have NO_3^-concentrations less than 30 mg/L and in two samples NO_3^- was not detected. Of these seven samples, four have $\delta^{15}N$ values between 4.0 and 8.0 ‰, two have $\delta^{15}N$ values greater than 8.0 ‰ and in one sample there was insufficient NO_3^- to obtain a $\delta^{15}N$ value. There are three samples with either high NO_3^- concentrations or $\delta^{15}N$ values suggesting

the anthropogenic influence of sewage/manure. The remaining four samples have low NO_3^-concentrations and $\delta^{15}N$ values less than 8.0 ‰ suggesting the anthropogenic influence in these wells is primarily from road salt.

Because there appears to be significant anthropogenic contamination in groundwater samples with evaporation factors greater than 100, the samples with evaporation factors between 70 and 100 are considered next. There are five groundwater samples with evaporation factors ranging between 70 and 100, of which three have NO_3^- concentrations greater than 30 mg/L, while the other two have NO_3^- concentrations less than 30 mg/L. Four of these samples have $\delta^{15}N$ values between 4.0 and 8.0 ‰, while one has a $\delta^{15}N$ value greater than 8.0 ‰. This suggests that four of the five groundwater samples with evaporation factors between 70 and 100 are influenced by sewage/manure and one sample is influenced by road salt.

All of the groundwater samples with evaporation factors greater than 70 have definite anthropogenic influence or either road salt or sewage/manure. From samples with evaporation factors less than 70, some have high NO_3^- concentrations or $\delta^{15}N$ values suggesting anthropogenic influence, however the Cl^- concentration in these samples is low. Of these remaining groundwater samples, there are five with molar concentrations of Na^+ and Cl^- values within 20 % of each other indicating road salt contamination.

In summary, 17 out of 48 groundwater samples collected are influenced by anthropogenic activities. Of these samples, 10 appear to primarily influenced by road salt and seven appear to be influenced by sewage/manure.

7.6 Weathering (W)

In this section, two mass balance scenarios for surface waters will be discussed. One scenario considers only atmospheric inputs (*Scenario I*) and one scenario considers both atmospheric and anthropogenic inputs (*Scenario II*.) Groundwater samples have more compositional diversity, likely related to surrounding variability in geology and 35 % are influenced by anthropogenic activities. Only one scenario that considers atmospheric inputs will be discussed for groundwater samples. However the groundwater

samples that have clear anthropogenic influence will be identified and removed to show the effects of anthropogenic Cl^- on the estimated concentration of cations due to weathering. The effects of the biosphere and ion exchange were discussed, but are assumed to have no net influence on ion concentrations.

In each of the mass balance scenarios for surface waters and groundwaters, the weathering concentrations of major ions, after correction from atmospheric and/or anthropogenic inputs are plotted against Cl^-. HCO_3^- concentrations in precipitation were below the detection limit and it was not possible to calculate the concentration due to weathering. NO_3^- is not derived from weathering of bedrock, as discussed in Chapter 6. If bedrock weathering did not contribute any ions to the solution, concentrations would plot at zero. Ions with concentrations greater than zero, indicate contributions from bedrock weathering. Ion exchange reactions can exchange ions between solution and clay minerals acting as a source or sink of ions, increasing or decreasing ion concentrations. For example, if two Na^+ ions replace one Mg^{2+} ion on an exchange site, Na^+ concentrations would decrease and Mg^{2+} concentrations would increase in solution. In this example, if the amount of Na^+ removed from solution due to ion exchange, was greater than that produced from weathering of bedrock, it is possible for this sample to have a weathering concentrations less than zero. In the above example, both weathering of bedrock and ion exchange are considered to be active, however it is not possible to determine the relative role of each of these influences. Specific ion exchange reactions occurring with the Kettle River Basin and their influence on solution chemistry will be considered in greater detail in Chapter 8.

7.6.1 Surface Water

Surface Water - Scenario I

After taking into consideration inputs from the atmosphere, the remaining concentrations are assumed to be from weathering of bedrock. Discussion of ion concentrations due to weathering of bedrock will be subsequently referred to as 'weathering contributions'. Comparison of ions in Figure 7-4 indicates that major ion weathering contributions are correlated to location. Samples from the West Kettle River have higher concentrations of Cl^-, compared to the Kettle River. As mentioned previously, this may be attributed to greater amounts of evaporation or road salt. If road salt were a major contributor of Na^+ and Cl^-, removing a portion of these ions would result in a smaller range in Cl^- concentrations. Lower Cl^- concentrations would result in a smaller evaporation factor, resulting in a smaller contribution from the atmosphere. Therefore, when the evaporation of precipitation is subtracted from the measured value, a higher contribution due to weathering would result. The samples would move in the approximate direction shown by the arrow in Figure 7-4 (for Ca^{2+} versus Cl^-) if some of the Cl^- was subtracted to account for road salt. The influence of road salt is addressed in greater detail in *Scenario II*.

Samples from below the confluence appear to be a mixture of water from the Kettle and West Kettle Rivers, plotting in between samples from the Kettle and West Kettle River. As expected, samples collected in June have lower weathering contributions compared to October. In most samples, Ca^{2+}, Mg^{2+} and SO_4^{2-} concentrations are greater than zero, indicating weathering of bedrock is the source of these ions. K^+ and Na^+ plot close to zero, indicating weathering of bedrock does not add significant concentrations of these ions, or ion exchange reactions may be a controlling factor. The weathering contributions of ions from the samples collected from the West Kettle River are less than zero in many samples, which may be due to the addition of road salt, as discussed previously.

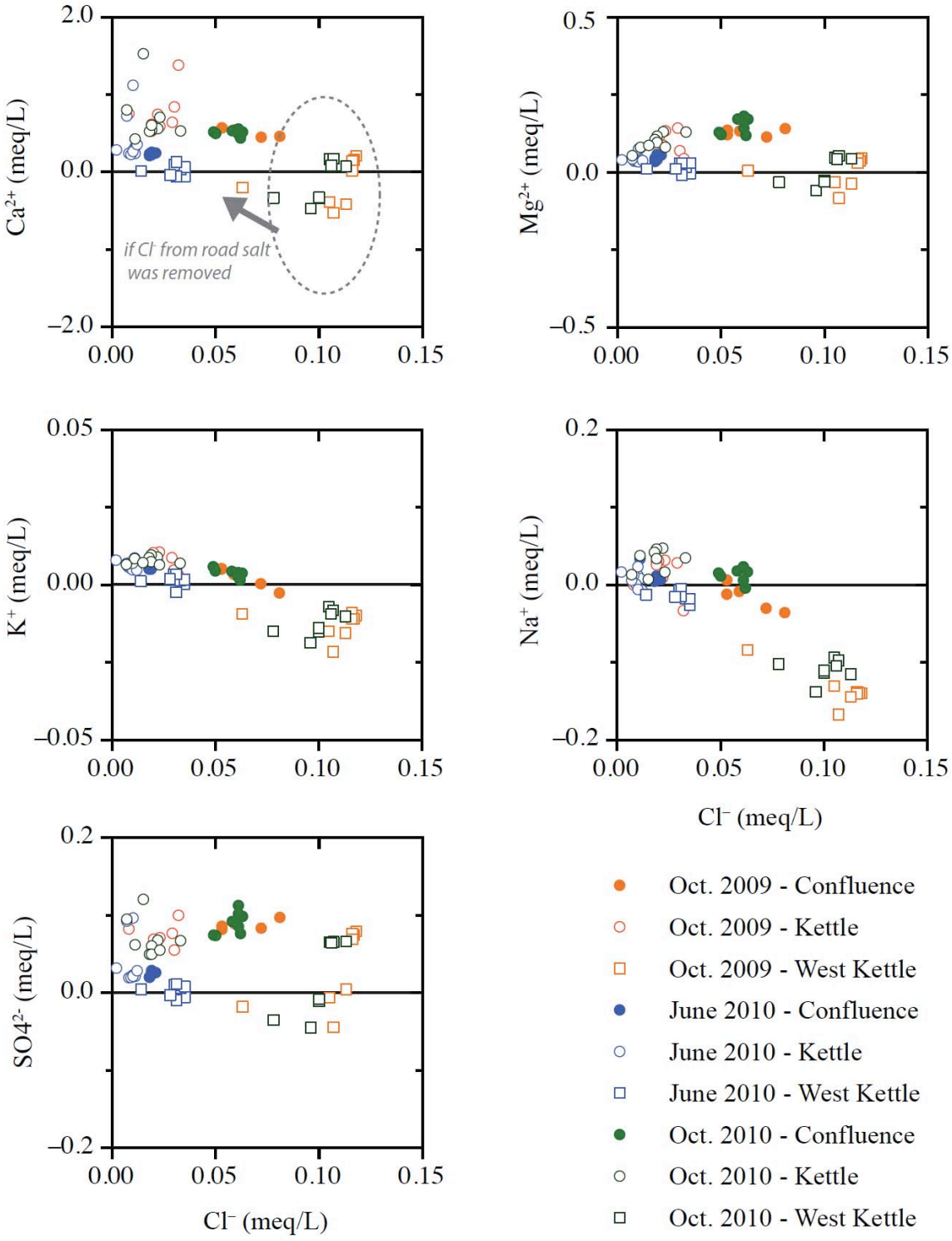

Figure 7-4: Weathering contribution of major ions, corrected for atmospheric input versus Cl^- for surface water samples from the Kettle and West Kettle Rivers and below the confluence, for samples taken in October 2009, June 2010 and October 2010.

In general, the weathering contributions of ions increases with increasing distance downstream. Along the Kettle River, the weathering contribution of most samples is greater than zero (Figure 7-5), however along the West Kettle River, many samples have ion contributions below zero (Figure 7-6). Specifically, the weathering contribution of K^+ and Na^+ are less than zero, suggesting that either ion exchange is an important control on these ions, or this section of the river is influenced by road salt. As discussed previously, the addition of road salt causes an underestimation of the weathering component of ions.

At a few specific locations in each tributary, there are abrupt increases in weathering contribution (Figures 7-5 and 7-6). These increases occur in samples from both June and October, which negates the possibility that these changes can be attributed to temporal variations. On the Kettle River, downstream of Highway 6 (the second sampling point from the headwaters), contributions of Ca^{2+} and SO_4^{2-} increase abruptly (Figure 7-5). Ion contributions along the West Kettle River, corrected for atmospheric inputs, are close to zero or less than zero, up to ~73 kilometres downstream (Figure 7-6). At this point, the weathering proportion of Ca^{2+}, Mg^{2+} and SO_4^{2-} increases abruptly. Because these cations can be derived from weathering of bedrock, this suggests contributions are dependent on the area upstream of these sampling points. Ca^{2+} and SO_4^{2-} contributions in relation to upstream area for sampling locations along the West Kettle River (Figure 7-7) suggest that weathering contributions are proportional to upstream area. Increases in Mg^{2+} followed a similar pattern, however the change in contributions with increasing upstream area was much smaller. There are many other factors that also influence ion contributions, such as ion exchange, temperature and concentrations of weathering agents, which will be investigated in greater detail in Chapters 8 and 9.

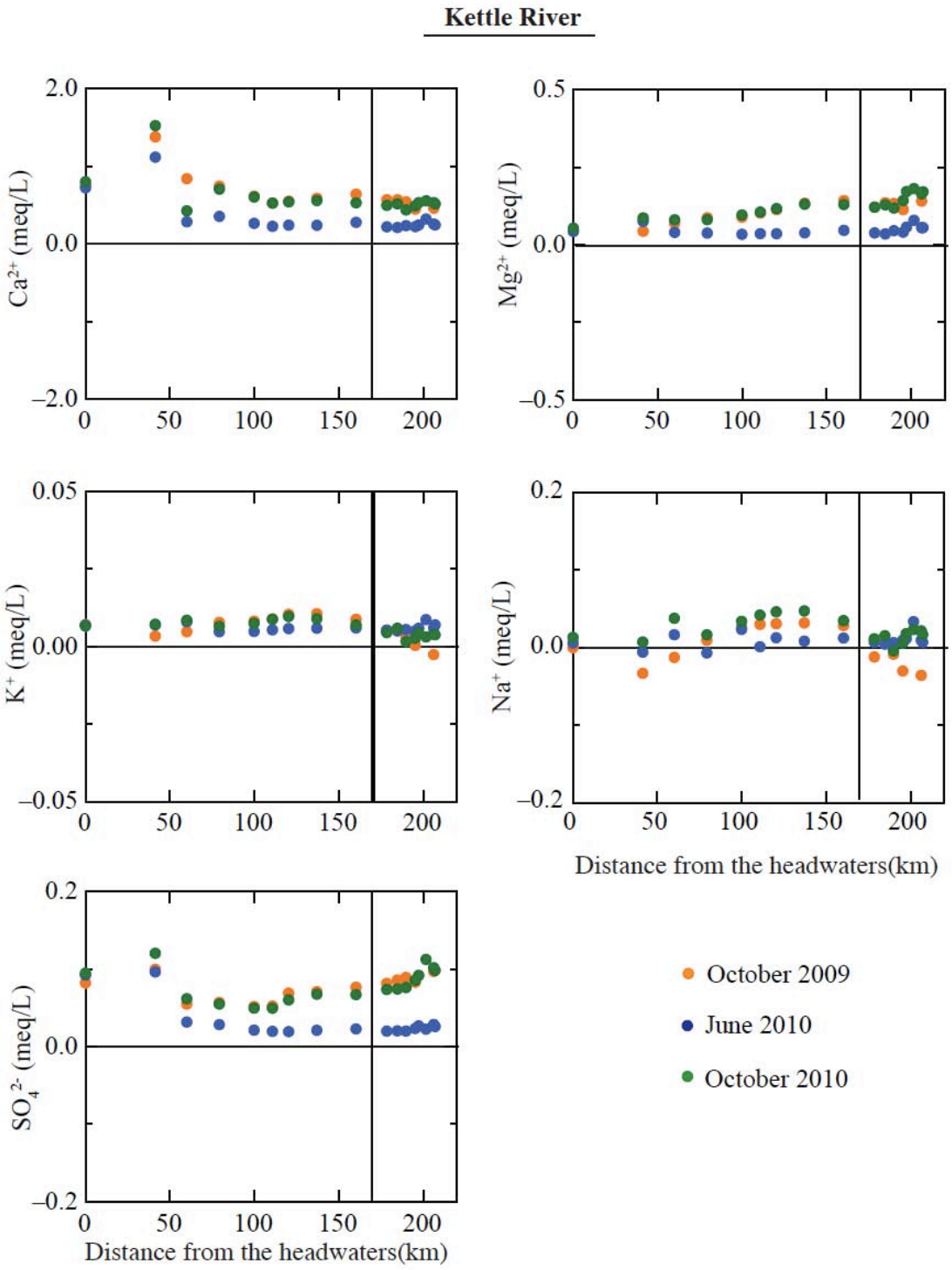

Figure 7-5: Weathering contribution of major ions in surface water, corrected for atmospheric inputs, versus distance from the headwaters of the Kettle River. The confluence of the two rivers is indicated with a vertical line.

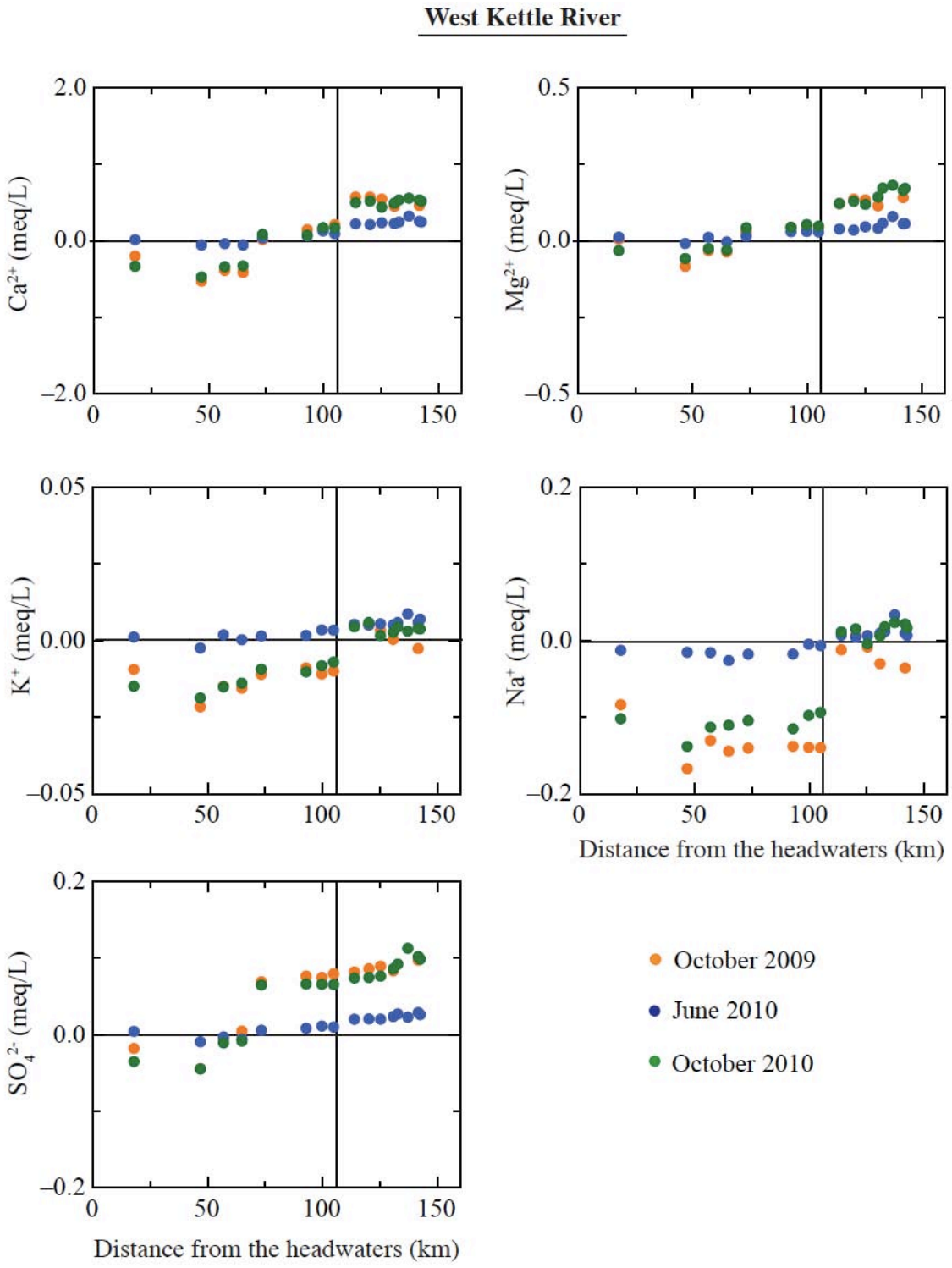

Figure 7-6: Weathering contribution of major ions in surface water, corrected for atmospheric inputs, versus distance from the headwaters of the West Kettle River. Vertical line indicates the confluence of the two rivers.

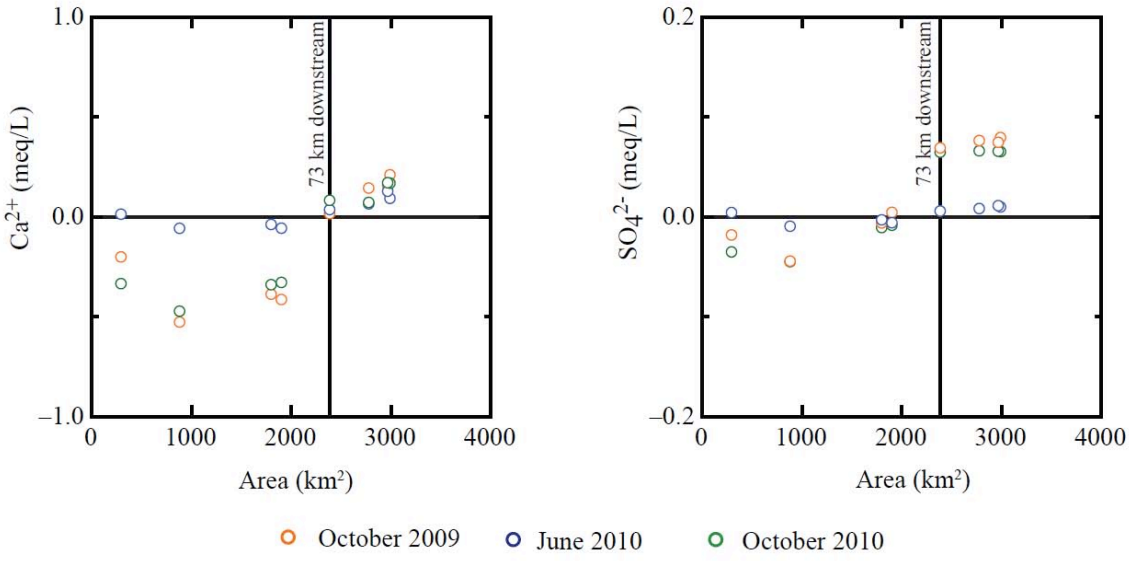

Figure 7-7: Weathering contribution of Ca^{2+} and SO_4^{2-} versus area upstream along the West Kettle River. The vertical line indicates the sampling point that corresponds to 73 km downstream – the sampling location where there is a drastic increase in TDS.

Surface Water – Scenario II:

In addition to considering inputs from atmospheric input, the anthropogenic influence of road salt is considered in *Scenario II*. Using the method outlined in Section 7.5.1, a correction factor was applied to Na^+ and Cl^- concentrations requiring recalculation of the atmospheric input of the mass balance. Using the calculated 'pristine' Cl^- value, the evaporation factor and expected concentrations due to evaporation were re-calculated and subtracted from the measured concentration, using the same procedure as was used in *Scenario I*. The resulting value was the weathering contribution, taking into consideration atmospheric and road salt influences. In the case of Na^+, the expected concentration due to evaporation was subtracted from the 'pristine' value, instead of the measured value.

Similar to figures in *Scenario I*, Figure 7-8 shows the weathering component of major ions plotted against 'pristine' Cl^-. Samples from the West Kettle River and from below the confluence move in the expected direction as indicated by the arrow in Figure 7-4. As a result of considerations of *Scenario II,* there are fewer samples with contributions less than zero and more points with contributions greater than zero. This

suggests that if the influence of road salt is removed, samples from the West Kettle River and below the confluence have weathering contributions suggesting greater amounts of bedrock weathering and that ion exchange of Na^+ and K^+ is less important.

In *Scenario I*, samples from below the confluence plotted between samples from the Kettle and West Kettle Rivers (Figure 7-4). In *Scenario II*, samples from below the confluence still plot between the two rivers on the x-axis (Figure 7-8), indicating that water from below the confluence is a mixture of waters with lower Cl^- concentrations from the Kettle River with waters of higher Cl^- concentration from the West Kettle River. However on the y-axis, samples from the below the confluence, plot higher than samples from the Kettle and West Kettle Rivers (Figure 7-8). This suggests that in addition to being a mixture of both sources, there is additional weathering of bedrock contributing solutes to river water. The area below the confluence accounts for 15 % of the watershed and so it is possible that additional weathering could be accounting for the higher weathering contributions of ions.

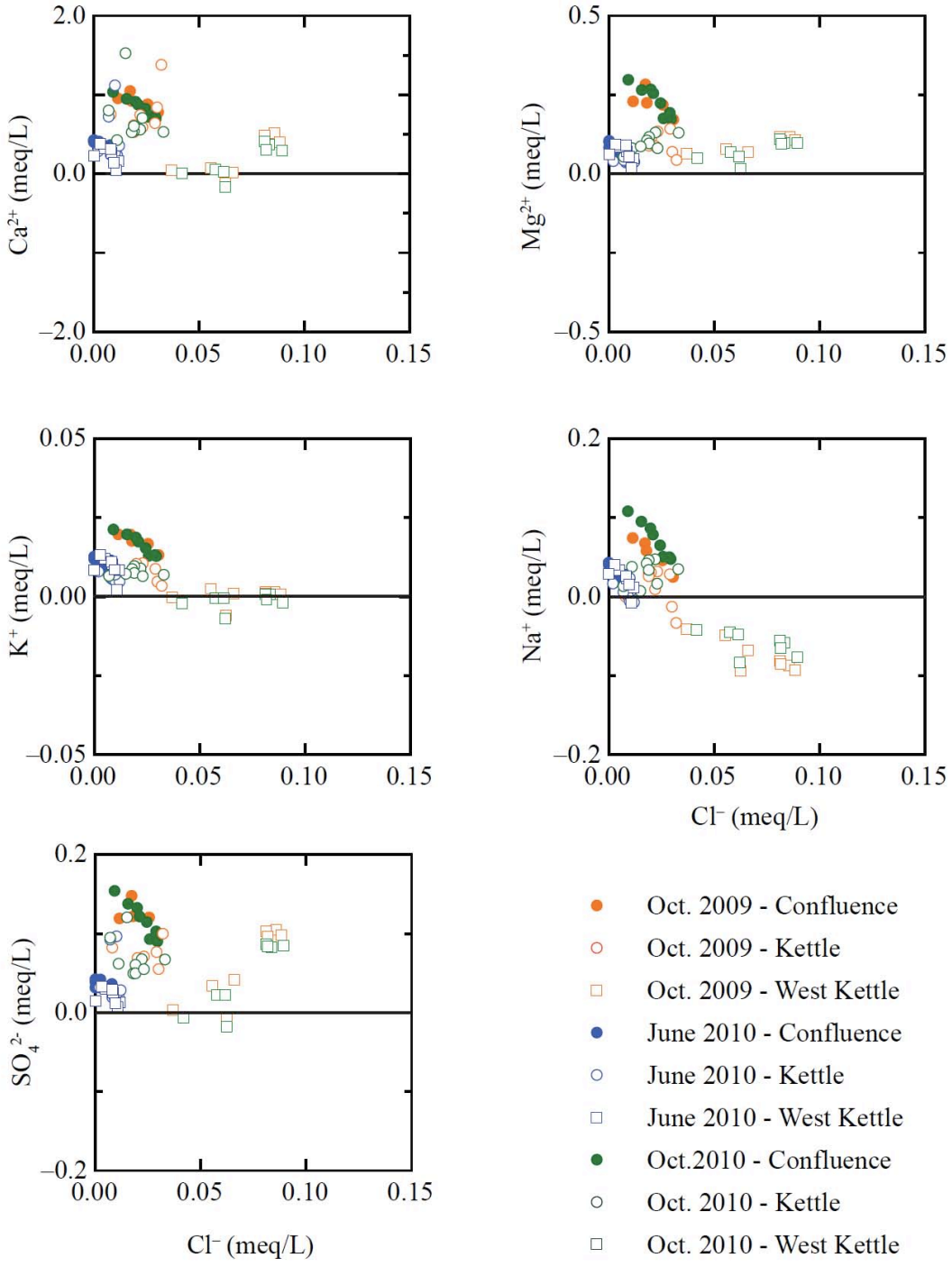

Figure 7-8: Weathering contribution of major ions corrected for atmospheric and anthropogenic road salt inputs versus Cl^- for surface water samples from the Kettle and West Kettle Rivers and below the confluence, from samples taken in October 2009, June 2010 and October 2010.

7.6.2 Groundwater

Groundwater samples have weathering contributions of Ca^{2+}, Mg^{2+} and SO_4^{2-} greater than zero and weathering contributions of Na^+ and K^+ close to zero (Figure 7-9). Samples collected in June and October overlap on Figure 7-9, indicating that weathering contributions do not change temporally. The weathering contributions also do not appear to be spatially correlated. There are four samples obtained from two wells sampled in June and October, which have significantly higher Na^+ and SO_4^{2-} weathering contributions. These samples have Na^+ contributions near 5 meq/L in Figure 7-9. Additionally, there is another well with consistently high contributions of Ca^{2+} and Mg^{2+}. Due to the diverse geology in this area, these outliers with high contributions of particular ions are likely influenced by bedrock composition. In Chapter 6, samples from two of these wells were identified to have $\delta^{18}O$ and δ^2H values lower than all other water samples and it was concluded these samples are from bedrock aquifers. Based on high contributions of Mg^{2+} and Ca^{2+} derived from weathering of bedrock, three samples collected from the third well are also likely from a bedrock aquifer. Weathering reactions that produce each of these cations are discussed in Chapter 8.

Based on the location groundwater samples plotted in Figure 7-9, there appears to be an inverse relationship between the weathering contributions of major anions and Cl^-, when Cl^- concentrations are greater than ~0.37 meq/L, which is equivalent to an evaporation factor of 70. A vertical line in the Ca^{2+} vs Cl^- plot in Figure 7-9 indicates where a Cl^- concentration of 0.37 meq/L lies. The samples with anthropogenic Cl^- were identified in Section 7.5.2. The samples with the highest Cl^- concentration are circled in Figure 7-9 and the arrow points in the direction the samples would trend if anthropogenic Cl^- were removed. If anthropogenic Cl^- were removed, contributions of cations in samples would increase, indicating higher contributions due to weathering.

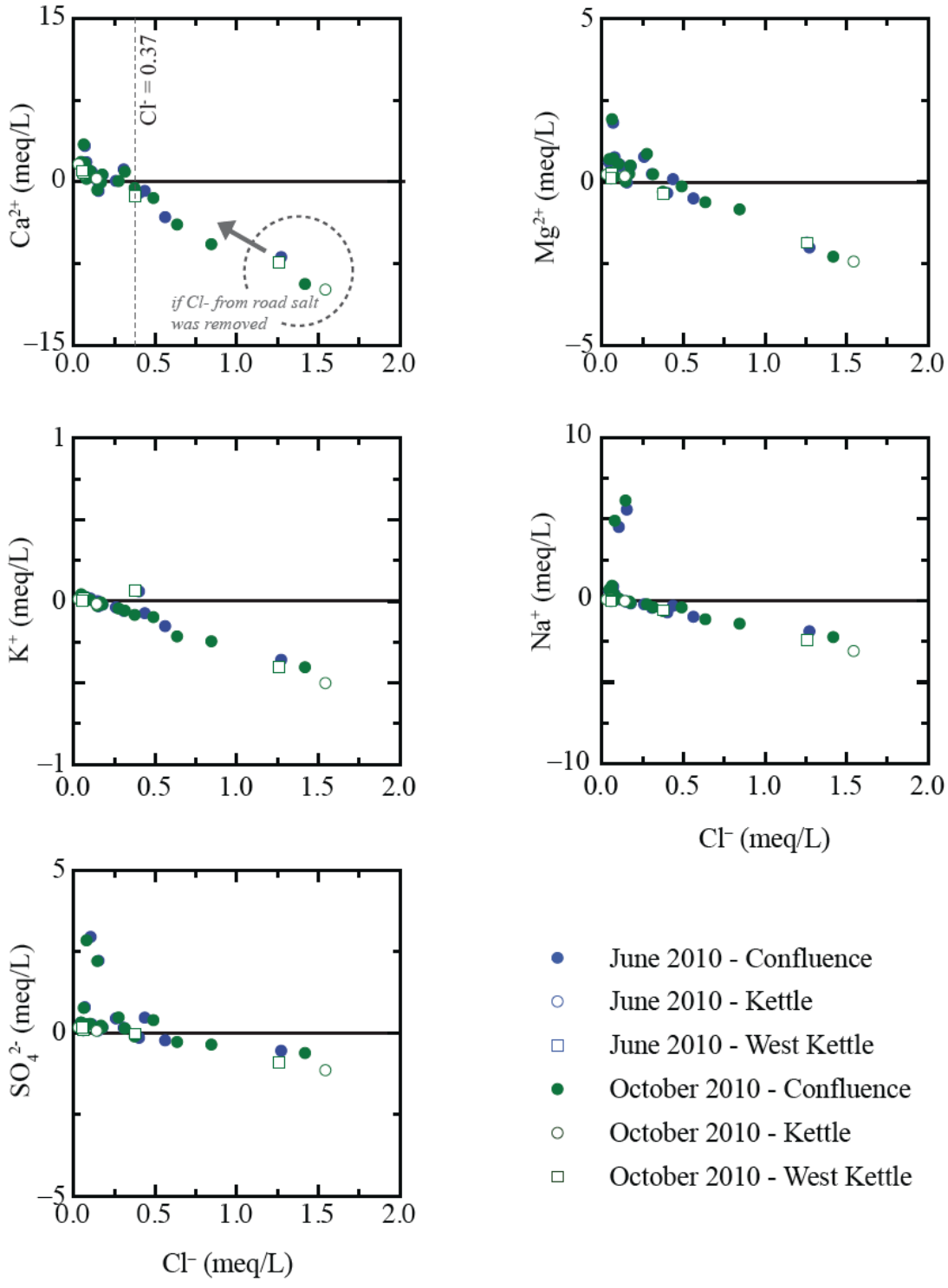

Figure 7-9: Weathering contribution of major ions corrected for atmospheric inputs versus Cl^- for groundwater samples collected in June and October 2010 from each section of the river.

It is difficult to remove the anthropogenic Cl^- from groundwater samples because the bedrock geology is diverse and therefore groundwater samples may not have a uniform Na/K ratio, which was used to correct for anthropogenic Cl^- in surface waters. Instead of applying a correction factor, groundwater samples with evaporation factors greater than 70 - samples previously identified to have anthropogenic Cl^- concentrations from either road salt or septic systems, were simply removed (Figure 7-10). These samples correlate to those in Figure 7-9 with Cl^- concentrations greater than 0.37 meq/L. As discussed in Section 7.5.2, there are five samples with evaporation factors less than 70, with clear evidence suggesting anthropogenic Cl^- contamination. Instead of discarding these samples, they are distinctly labelled in Figure 7-10. Figure 7-10 is essentially Figure 7-9 with a much smaller range along the x-axis. The five samples with clear anthropogenic influence do not plot apart from other samples, however, these samples do plot near the upper end of Cl^- values. If the concentration of anthropogenic Cl^- was removed from these samples, they would move up and to the left, which would indicate higher cation contributions due to weathering. In mass balance calculations, the addition of anthropogenic Cl^- causes the contributions of cations due to bedrock weathering to be underestimated.

In Figure 7-10, the distribution of positive cation contributions is shown in greater detail. In most groundwater samples the weathering contributions of Ca^{2+}, Mg^{2+} and SO_4^{2-} are greater than zero. Most samples have Na^+ and K^+ weathering contributions slightly greater than zero or close to zero. There are a few samples with K^+ contributions less than zero, some of which have clear anthropogenic influence.

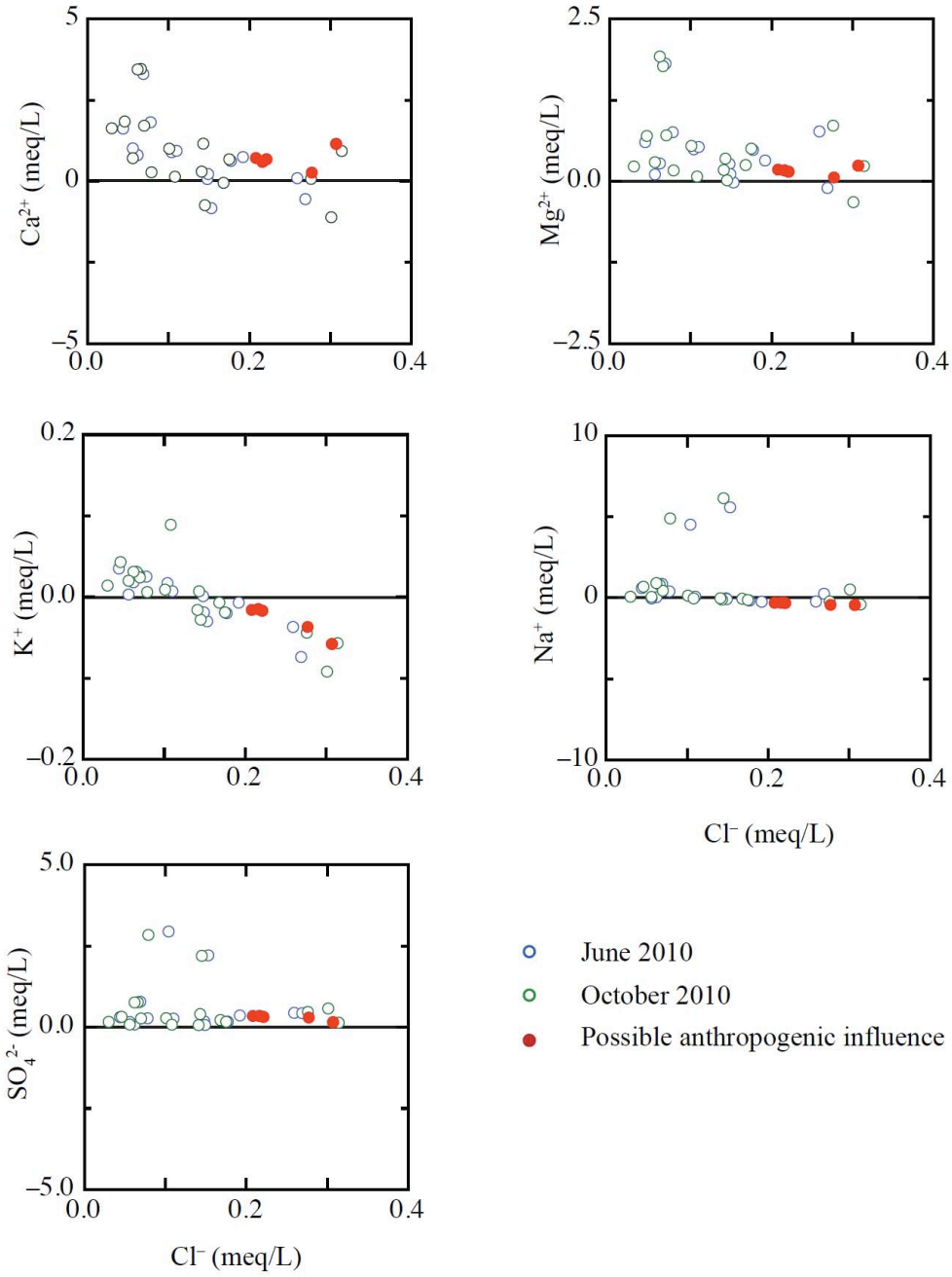

Figure 7-10: Weathering contribution of major cations corrected for atmospheric input versus Cl^-. Samples were collected in June and October 2010. Groundwater samples with Cl^- concentrations greater than 0.37 meq/L were removed as these samples showed clear anthropogenic input of Cl^-. Groundwater samples with concentrations less than Cl^- concentrations of 0.37 meq/L, which also have signs of anthropogenic input are indicated with red dots.

7.7 Conclusion

A mass balance approach was used, considering inputs from the atmosphere, anthropogenic activities and weathering of bedrock. For surface water samples, two mass balance scenarios were discussed. *Scenario I* accounted for atmospheric inputs and *Scenario II* accounted for atmospheric and anthropogenic road salt inputs. Results from *Scenario I* indicated weathering contributions of Ca^{2+}, Mg^{2+} and SO_4^{2-} greater than zero, suggesting these ions are derived from weathering of bedrock, and Na^+ and K^+ contributions are close to zero, suggesting ion exchange is occurring or that weathering of bedrock does not contribute these ions to solution. Results from *Scenario II* indicated higher weathering contributions of all ions implying when the influence of road salt is considered, mass balance calculations result in a higher estimate of bedrock weathering.

For groundwater samples, mass balance calculations only accounted for atmospheric inputs, as it was not possible to remove anthropogenic Cl^- due to variable water-rock interactions reactions occurring in aquifers. Results were similar to surface waters, indicating bedrock weathering is a likely source for Ca^{2+}, Mg^{2+} and SO_4^{2-}, and Na^+ and K^+ contributions are influenced by ion exchange or that bedrock weathering does not contribute high amounts of these ions. The presence of anthropogenic Cl^- in groundwater samples causes mass balance calculations to underestimate the contributions of cations attributable to bedrock weathering. Overall, sources of Ca^{2+}, Mg^{2+}, Na^+, K^+ and SO_4^{2-} in the Kettle River Basin were found to be from the atmosphere, anthropogenic activities and weathering of bedrock. The specific minerals involved in silicate weathering will be investigated in more detail in Chapter 8, by identifying weathering agents, weathering reactions and using thermodynamic modelling.

Chapter Eight: Silicate Weathering Reactions

8.1 Introduction

In Chapter 7, weathering of bedrock was identified as a source of ions in surface water and groundwater. The specific reactions responsible for producing these ions are of interest as some reactions consume $CO_2(g)$. In order to identify these reactions, possible weathering agents and the composition of bedrock are examined. Geochemical modeling is used to predict stability relationships between primary and secondary minerals, calculate which water samples are supersaturated with respect to particular minerals and aid in identification of possible ion-exchange relationships.

8.2 Weathering Agents

Weathering agents are acids that increase the acidity of the water thereby promoting mineral weathering. Weathering agents include carbonic acid (H_2CO_3), sulphuric acid (H_2SO_4) and organic acids (Lerman and Wu, 2006). Organic acid analyses indicated that such acids were not present in detectable amounts. Therefore, the only weathering agents considered will be H_2CO_3 and H_2SO_4.

8.2.1 Carbonic acid

Carbonic acid originates from $CO_2(g)$ in the atmosphere, which dissolves in water to become $CO_2(aq)$, which subsequently reacts with H_2O, as discussed in Chapter 6. The sum of these reactions is Equation 8-1, where the * denotes the combination of $CO_2(aq)$ and H_2O. $H_2CO_3^*$ is written by convention, however, at 25 °C, $CO_2(aq)$ is ~ 600 times more abundant (Appelo and Postma, 2005).

$$CO_2(g) + H_2O = H_2CO_3^* \quad (8\text{-}1)$$

In addition to infiltrating precipitation that introduces CO_2 into the subsurface, root respiration and decay of organic matter also generate $CO_2(g)$. The partial pressure of $CO_2(g)$ in soils is often one to two orders of magnitude higher compared to that of the

atmosphere (Appelo and Postma, 2005). Higher CO_2 concentrations cause acidity to increase, which enhances mineral weathering (Beaulieu et al., 2010). Silicate weathering enhanced by H_2CO_3 [$CO_2(g) + H_2O$] releases HCO_3^- and other ions (Equation 8-2). Equation 8-2 also indicates that $CO_2(g)$ is a reactant in this equation indicating it is consumed during weathering.

$$CaSiO_3 + 2CO_2 + 3H_2O = H_4SiO_4 + 2HCO_3^- + Ca^{2+} \quad (8\text{-}2)$$

8.2.2 Sulfuric Acid

Oxidation of sulfide minerals, of which pyrite (FeS_2) is the most common (Seal et al., 2000), leads to the production of sulfuric acid (H_2SO_4) that can subsequently dissolve other minerals (e.g. $CaSiO_3$), which results in release of SO_4^{2-} and other ions (Equations 8-3 and 8-4) (Spence and Telmer, 2005). Pyrite has been identified in intrusive lithologies in the Kettle River Basin (Ewert et al., 2008). Using stable isotopes, the primary source of SO_4^{2-} in most samples was identified to be oxidation of sulfide minerals, as discussed in Chapter 6.

$$FeS_2 + O_2 + H_2O = Fe_2O_3 + H_2SO_4 \quad (8\text{-}3)$$

$$H_2SO_4 + CaSiO_3 + H_2O = SO_4^{2-} + Ca^{2+} + H_4SiO_4 \quad (8\text{-}4)$$

8.2.3 Role of weathering agents

The relative importance of the two weathering agents is of interest as weathering with H_2CO_3 consumes $CO_2(g)$, while weathering with H_2SO_4 does not. Assuming Equations 8-2 and 8-4 represent silicate weathering reactions within the basin, the relative proportions of the products – HCO_3^- and SO_4^{2-} (in mmol/L), can provide an indication of the dominant weathering agents. In surface waters, HCO_3^- and SO_4^{2-} comprise on average 90.4 % and 6.6 %, respectively, of the anions. The remaining 2.9 % of anions are Cl^- (5.0 %) and NO_3^- (0.1 %). In groundwaters, on average, 79.2 % of anions are HCO_3^-, 10.6 % are SO_4^{2-}, 4.5 % are Cl^- and 7.9 % are NO_3^-. Based on these values, carbonic acid is considered to be the dominant weathering agent. During weathering of sulfide minerals,

which releases SO_4^{2-}, other cations are also released as described in Equation 8-4. The specific cation released is dependent on the mineral being weathered. Considering the abundance of SO_4^{2-}, it will be assumed the cations derived from weathering with H_2SO_4 contribute minimally to TDS, compared to cations originating from weathering due to H_2CO_3.

8.3 Weathering of Silicate Bedrock

Weathering of bedrock has been identified as a source of ions to surface water and groundwater. Bedrock varies in both composition and sensitivity to chemical weathering (Meybeck, 2005). As discussed in Chapter 2, the Kettle River Basin is underlain by dominantly igneous and metamorphic bedrock. Table 8-1 indicates the relative abundance of main lithology types – sedimentary, igneous (volcanic, intrusive, ultramafic) and metamorphic, upstream of each surface water sampling location. Values in this table were calculated using ArcGIS mapping software and data from the BC Geological Survey (2005). There is some compositional variation within volcanic, intrusive and metamorphic lithologies identified in Figure 2-7 and summarized in more detail in Appendix D. For volcanic, intrusive and metamorphic lithologies, the most spatially abundant varieties of each lithology were used – basalt was the most abundant of the volcanic rocks and granite was the most abundant of the intrusive rocks. Typical minerals present in basalt and granite are summarized in Table 8-2 and the average chemical composition of typical basalts is summarized in Table 8-3. Metamorphic rocks had equal amounts of greenstone/greenschist and 'undivided metamorphic rocks' from the Shuswap Assemblage. Limited information was available on the undivided metamorphic rocks and so the greenstone/greenschist composition was used to represent the metamorphic lithology. The protolith of greenstones/greenschists are mafic igneous rocks; therefore, the mineralogy used for the metamorphic lithology was basalt plus chlorite, actinolite, epidote and albite (Winter, 2001).

Table 8-1: Relative abundance of lithology upstream of each sampling point and distances from headwaters. Below the confluence, the distance downstream is measured from the West Kettle River. A digital geology map was obtained from the BC Geological Survey (2005) and relative abundance of each area was calculated using ArcGIS.

		% Lithology					
River	**Location**	**Distance (km)**	**Sedimentary**	**Volcanics**	**Intrusives**	**Ultramafics**	**Metamorphic**
Kettle River	Keef	0.0	79.0	21.0	-	-	-
	Hwy 6	41.3	67.2	15.7	17.0	-	-
	Bruer	60.0	17.1	11.9	62.2	-	8.8
	KRCross	79.3	10.4	8.9	66.6	-	14.1
	Goat	99.9	7.2	8.0	55.4	-	29.4
	Grano	110.8	4.8	13.6	58.2	-	23.3
	Dear	120.4	4.4	15.1	59.0	-	21.5
	Lost	137.0	4.2	16.9	57.3	-	21.6
	Fiva	160.2	3.6	17.9	58.2	-	20.2
West Kettle River	Big White	17.8	-	10.9	43.1	-	46.0
	Trap	46.8	-	11.2	60.7	-	28.1
	Carmi	56.9	0.2	9.0	75.3	-	15.5
	Beaverdell	64.9	0.2	8.7	76.2	-	15.0
	Tuzo	73.3	0.1	7.9	74.1	-	17.8
	Rhone N	92.8	0.1	7.7	76.8	-	15.3
	Rhone S	99.7	0.2	8.4	76.8	-	14.6
	Westbridge	104.8	0.2	9.0	76.3	-	14.5
Below the confluence	KVCamp	113.9	2.2	15.0	65.3	-	17.5
	Pub	120.2	2.1	15.0	64.9	-	17.9
	KVB	125.3	2.7	15.2	61.9	-	20.1
	Ingram	130.8	2.9	15.5	61.6	0.1	20.0
	Bugeaud	132.8	2.9	15.6	61.5	0.1	19.9
	Bick	137.1	3.2	16.9	60.2	0.1	19.7
	Midway	141.7	3.2	17.3	59.9	0.1	19.6
	Border	142.5	3.2	17.4	59.9	0.1	19.5

Table 8-2: Typical minerals present in each lithology. Major and minor constituents are from Klein (2002) and chemical formulas are from Appelo and Postma (2005).

Minerals	Basalt	Granite
Major	enstatite (pyroxene) – $MgSiO_3$ diopside (pyroxene) –$MgCaSi_2O_6$ anorthite - $CaAl_2Si_2O_8$	quartz – (SiO_2) K-feldspar - $KAlSi_3O_8$ albite – $NaAlSi_3O_8$ muscovite - $KAl_2(AlSi_3)O_{10}$
Minor	olivine – Mg_2SiO_4	amphiboles – $Na_2(Mg_3Al_2)Si_8O_{22}(OH)_2$ biotite – $K(Mg_2Fe)(AlSiO_3)O_{10}(OH)_2$

Table 8-3: Average chemical composition of basalt and granite (Klein, 2002).

	Weight %	
Oxides	**Basalt**	**Granite**
SiO_2	48.36	72.08
Al_2O_3	16.84	13.86
CaO	11.07	1.33
MgO	8.06	0.52
FeO	7.92	1.67
K_2O	0.56	5.46
Fe_2O_3	2.55	0.86
Na_2O	2.26	3.08
TiO_2	1.32	0.37
H_2O	0.64	0.53
P_2O_5	0.24	0.18
MnO	0.18	0.06
	100	100

The resistance of each of these minerals to chemical weathering depends on thermodynamic instability; the more unstable minerals will weather more easily (Appelo and Postma, 2005). The order of decreasing resistance to weathering is: quartz >> K-feldspar, micas >> albite > anorthite, amphiboles > pyroxenes > olivine > dolomite > calcite >> pyrite (Stallard, 1995; Meybeck, 2005; Appelo and Postma, 2005). Combining mineralogy and weathering resistance of minerals suggests that basalt is more easily weathered than granite. This has been previously suggested by Dessert et al. (2003) and basalt has been estimated, using numerical modelling, to be eight times more susceptible to chemical weathering compared to granite (Dupré et al., 2003). Basalt combined with

metamorphic rocks, which have a basalt protolith, underlie ~40 % of the Kettle River Basin, while granite bedrock underlies the remaining ~ 60 % of the Kettle River Basin.

Advance and recession of glaciers in this area have led to erosion of bedrock and deposition of unconsolidated materials at the bottom of river valleys, adjacent to and underlying the present day position of the Kettle and West Kettle Rivers. The depth to bedrock has been estimated to range from 150 to 250 meters in central portions of the valley, and from 0 to 35 meters along the perimeter (Wei et al., 2010). The general composition of the bedrock is known, however the composition of unconsolidated aquifer materials is not known. The composition of unconsolidated aquifer materials will therefore be assumed to be composed of similar mineralogy as the underlying bedrock. As discussed in previous Chapters, the majority of wells are drilled into unconsolidated valley aquifer materials. Based on major ion chemistry and stable isotope abundance ratios of hydrogen and oxygen, it has been suggested that only three wells are completed in bedrock aquifers.

Major ions derived from chemical weathering of bedrock in surface waters and groundwaters were determined in Chapter 7 and are Ca^{2+}, Mg^{2+}, Na^{+}, K^{+}, and SO_4^{2-}, HCO_3^{-} is also a major anion present in both surface water and groundwater samples, as discussed previously. It was not possible to determine the weathering component of HCO_3^{-} as it was not possible to measure the concentration of HCO_3^{-} in precipitation water. Combining mineralogy, resistance to weathering and the average composition of basalt and granite, suggests that weathering of basalt is the dominant source of Ca^{2+} and Mg^{2+} and weathering of granite is the main source of Na^{+} and K^{+}. The primary mineral sources of Ca^{2+} are anorthite and pyroxene. The main primary minerals which weather to form Mg^{2+}, Na^{+} and K^{+} are pyroxenes, albite and K-feldspar, respectively.

Aluminum (Al) containing silicate minerals are very insoluble. Therefore primary silicate minerals weather to form secondary minerals – commonly clay minerals, which conserve Al in the solid phase (Appelo and Postma, 2005). Clay minerals are fine grained, typically less than 2 μm, crystalline, hydrous silicates (Drever, 1997). Clay minerals generally consist of tetrahedral and octahedral coordination layers. In the tetrahedral

layers, Si^{4+} is surrounded by oxygen and in the octahedral layers Al^{3+} is surrounded by hydroxyls (Appelo and Postma, 2005). Within the scope of this project, it was not possible to identify clay minerals within the Kettle River Basin and previous studies in the area have not identified specific clay minerals. Therefore, it will be assumed common clays are present – which include kaolinite, smectite (beidellite), chlorite and illite (Appelo and Postma, 2005). In order to determine potential weathering reactions, stability diagrams were created using geochemical modelling software.

8.4 Geochemical Modeling

The geochemical modeling software used was SOLMINEQ88 and 'The Geochemist's Workbench' (GWB). 'SOLMINEQ88' was used to determine inorganic carbon species and GWB was used to determine species activities, saturation indices and create stability diagrams. It was not possible to determine the saturation indices of aluminosilicate minerals because the concentration of aluminum was not measured, as it is a difficult parameter to analyze (Appelo and Postma, 2005). In order to determine which aluminosilicate minerals may be stable, stability diagrams, which conserve aluminum, were created using GWB.

8.4.1 Stability Diagrams

Stability diagrams were created using a thermodynamic database within GWB. The calculated species activities were plotted on phase diagrams which allowed for identification of stable minerals involved in water-rock weathering reactions and possible equilibrium reactions controlling water chemistry (Abercrombie, 1989). All stability diagrams were calculated for temperatures of 5 °C, as this is the average temperature of surface water and groundwater samples, and pressures of 1 bar. Figures 8-1 a.) through d.) show log activity ratios $Ca^{2+}/(H^+)^2$, $Mg^{2+}/(H^+)^2$, Na^+/H^+ and K^+/H^+ plotted against log activity of $SiO_2(aq)$, with the activities of surface water and groundwater samples overlain. Log activity ratios of surface water and groundwater samples, in relation to stability

boundaries of clay minerals, indicate which clay mineral is most likely to form as a result of weathering of a particular primary silicate mineral.

All stability diagrams contain primary minerals, except the Mg^{2+} stability diagram (Figure 8-1b.). As summarized in Table 8-2, pyroxenes, the primary mineral sources of Mg^{2+} do not contain aluminum. Aluminum lacking minerals weather congruently, and therefore do not form clay minerals (Faure, 1998). There are aluminum bearing Mg^{2+} primary minerals, however these minerals contain also other cations (e.g. biotite, amphiboles) (Faure, 1998).

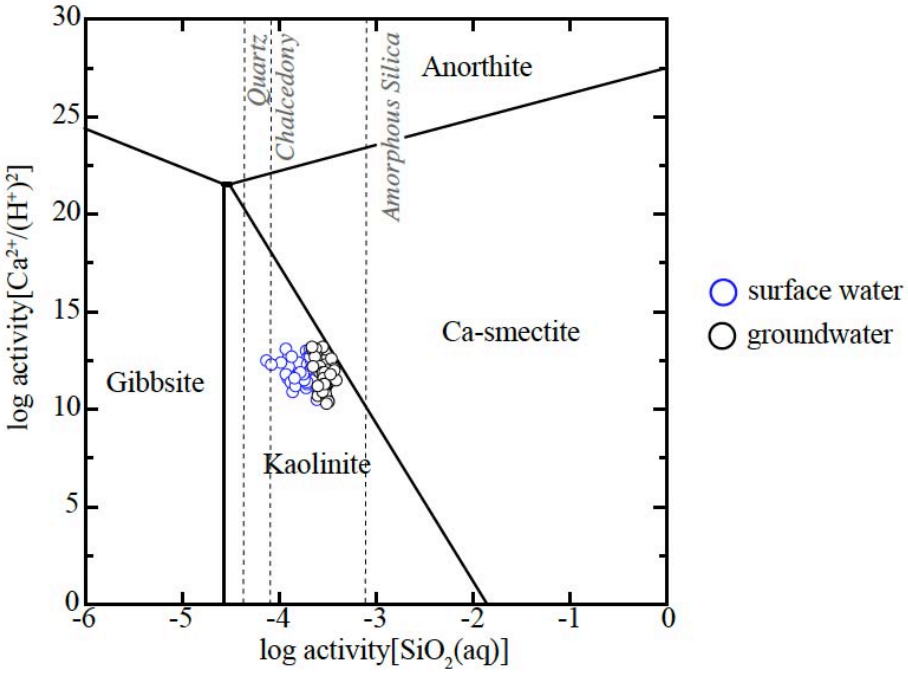

Figure 8-1a.): Log activity of $Ca^{2+}/(H^+)^2$ vs. log activity of $SiO_2(aq)$ at 5 °C and 1 bar. The primary mineral is anorthite.

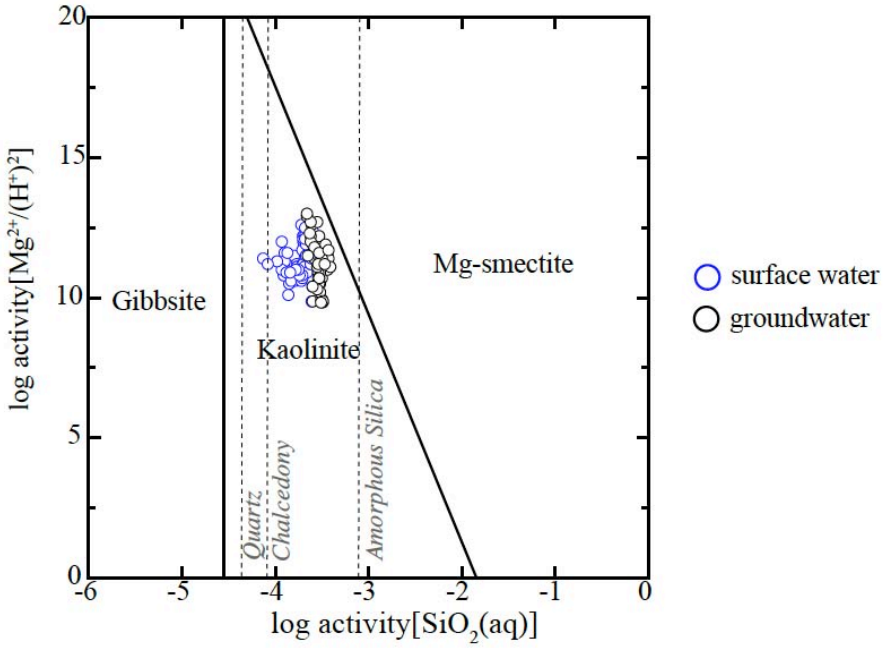

Figure 8-1b.): Log activity of $Mg^{2+}/(H^+)^2$ vs. log activity of $SiO_2(aq)$ at 5 °C and 1 bar. The primary minerals which weather to form Mg^{2+} do not contain aluminum and therefore are not included in this Figure.

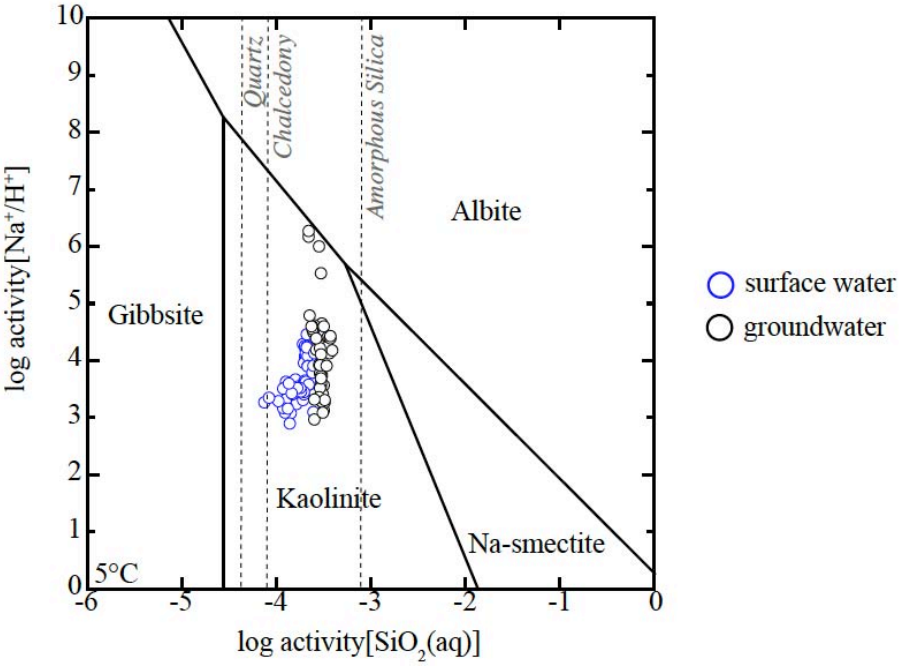

Figure 8-1c.): Log activity of Na^+/H^+ vs. log activity of $SiO_2(aq)$ at 5 °C and 1 bar. The primary silicate is albite.

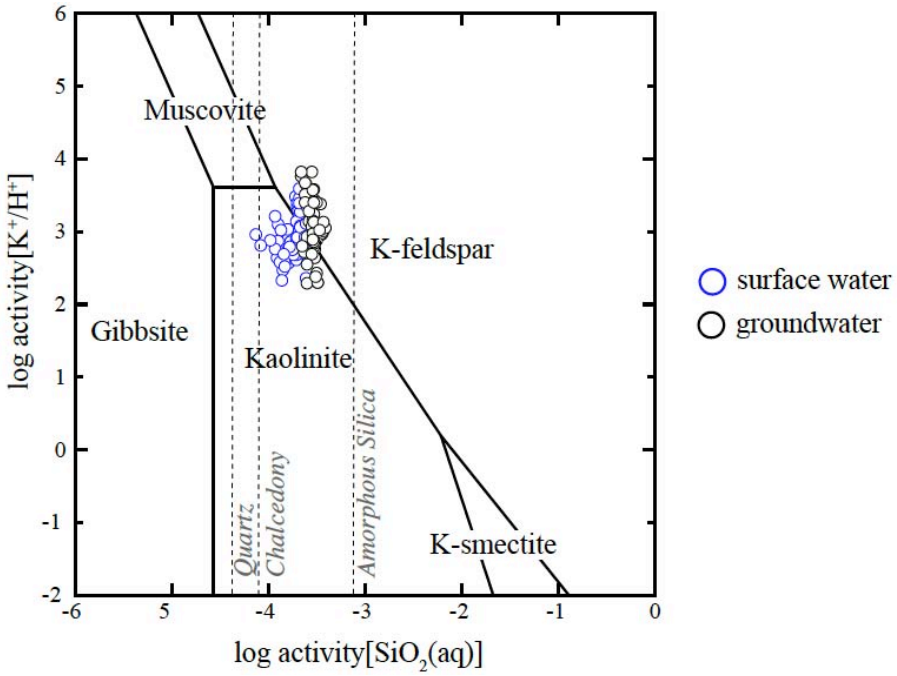

Figure 8-1d.) Log activity of K^+/H^+ vs. log activity of $SiO_2(aq)$ at 5 °C and 1 bar. The primary silicate minerals are muscovite and K-feldspar.

In stability diagrams in Figure 8-1 a.) through d.), ion activity ratios of surface water and groundwater samples plot across several orders of magnitude. The reason for variation in ion activities ratios could be related to either the activities of cations or H^+. As discussed in Chapter 5, the average pH of groundwater samples is 7.4 ± 0.4, whereas the average pH of surface water samples is 7.8 ± 0.3. These values indicate that groundwater samples have slightly higher H^+ concentrations and therefore slightly higher H^+ activities, compared to surface waters, which would result in a lower ion ratio. Therefore, in order for groundwater samples to fall within a similar range as surface waters, groundwater samples must have higher cation activities. As discussed in more detail in Chapter 5, the concentrations of major cations in groundwaters, and therefore cation activities are higher compared to those of surface waters. A few groundwater samples have anomalously high ion activity ratios (Figure 8-1c.); possible reasons for this will be discussed in more detail in Section 8.4.3.

Groundwater samples have consistently higher SiO_2 activities compared to surface water. Groundwater samples with higher SiO_2 activities are closer to being in equilibrium with Ca- and Mg-smectite. This observation between SiO_2 activities and Ca- and Mg-smectite will be discussed in relation to silicate dissolution reactions below and in relation to saturation indices of quartz and polymorphs of quartz in Section 8.4.2.

Surface water and groundwater samples plot primarily within the kaolinite stability field in the above stability diagrams. Based on Figures 8-1a.) to d.), likely silicate dissolution reactions are suggested below, revealing possible sources of Ca^{2+}, Mg^{2+}, Na^+ and K^+ (Equations 8-5 to 8-9). As shown in Table 8-3, 8.1 % of the chemical composition of basalt is MgO, indicating minerals within basalt must contribute Mg^{2+}. Possible sources of Mg^{2+} include pyroxenes, of which there are many varieties – only some of which contain aluminum and can potentially weather to form clay minerals. The weathering reactions for two common pyroxenes are shown below in Equations 8-6 and 8-7. Each of these weathering reactions consumes CO_2, may form secondary clay minerals and silicic acid (H_4SiO_4), and produces cations and HCO_3^-. The latter is the dominant component of alkalinity at the pH range of surface waters and groundwaters.

Ca^{2+}:

$$CaAl_2Si_2O_8 + 2CO_2 + 3H_2O \rightarrow Al_2Si_2O_5(OH)_4 + 2HCO_3^- + Ca^+ \quad (8\text{-}5)$$

Anorthite *Kaolinite*

Mg^{2+}:

$$MgSiO_3 + 2CO_2 + 3H_2O \rightarrow H_4SiO_4 + 2HCO_3^- + Mg^{2+} \quad (8\text{-}6)$$

Enstatite (Pyroxene)

Ca^{2+} and Mg^{2+}:

$$MgCaSi_2O_6 + 4CO_2 + 6H_2O \rightarrow 2H_4SiO_4 + 4HCO_3^- + Mg^{2+} + Ca^{2+} \quad (8\text{-}7)$$

Diopside (Pyroxene)

Na^+:

$$2NaAlSi_3O_8 + 2CO_2 + 11H_2O \rightarrow Al_2Si_2O_5(OH)_4 + 4H_4SiO_4 + 2HCO_3^- + 2Na^+ \quad (8\text{-}8)$$

Albite *Kaolinite*

K^+:

$$2KAlSi_3O_8 + 2CO_2 + 11H_2O \rightarrow Al_2Si_2O_5(OH)_4 + 4H_4SiO_4 + 2HCO_3^- + 2K^+ \quad (8\text{-}9)$$

K-feldspar *Kaolinite*

In Figure 8-1 a.) and b.) groundwater samples with higher ion activity ratios and SiO_2 activities plotted within or near the smectite stability field. Equations 8-5 through 8-7 indicate Ca^{2+}, Mg^{2+} and SiO_2 (written as H_4SiO_4) are released during weathering, causing the solution composition to plot closer to the smectite stability field. If it can be assumed that activity ratios are proportional to primary weathering of silicate minerals, this suggests these samples with prolonged water rock interactions, trend towards the smectite stability field. As discussed earlier in Section 8.3, Ca^{2+} and Mg^{2+} are dominantly derived from basaltic minerals. Hence interaction between water and basalt produces waters within or trending towards the smectite stability field. This observation that smectite can be formed if the solution gains sufficient Ca^{2+}, Mg^{2+} and SiO_2 was first reported by Garrels and Mackenzie (1967). As the solution reaches the equilibrium boundary between kaolinite and smectite, the reaction is:

$$1.17\ Al_2Si_2O_5(OH)_4 + 0.17\ Ca^{2+} + 1.33\ H_4SiO_4 = Ca_{0.165}Al_{2.33}Si_{3.67}O_{10}(OH)_2 + 0.33\ H^+ + 3.83\ H_2O \quad (8\text{-}10)$$

Kaolinite *Ca-Smectite*

The chemical formulas of smectite varieties were obtained from GWB. Beyond this boundary, within the smectite stability field, kaolinite will no longer be present in the system. Anorthite will then react directly to Ca-smectite (Equation 8-11). In the case of the reactions in Equations 8-6 and 8-7, which do not directly produce secondary clay minerals, the H_4SiO_4 produced can be consumed in the reaction between kaolinite and Ca-smectite (Drever, 1997).

$$1.17\ CaAl_2Si_2O_8 + 1.33\ H_4SiO_4 + 2CO_2 = Ca_{0.165}Al_{2.33}Si_{3.67}O_{10}(OH)_2 + 2HCO_3^- + Ca^+ + 0.66\ H_2O \quad (8\text{-}11)$$

Anorthite *Ca-Smectite*

The silicate weathering reactions in Equations 8-6 to 8-9 produce H_4SiO_4 whereas Equations 8-10 and 8-11 that involve Ca-smectite consume H_4SiO_4. The consumption of SiO_2 (written as H_4SiO_4) in Equations 8-10 and 8-11 suggests that as the solution trends towards equilibrium with smectite, SiO_2 concentrations will begin to decrease instead of continuing to increase. Ca^{2+} is consumed during the reaction between kaolinite and smectite, and released during the reaction between anorthite and Ca-smectite. It is not possible to predict the direction in which the solution will evolve, based simply on Equations 8-10 and 8-11, as weathering reactions described in Equations 8-5 to 8-9 also release and consume SiO_2 and various cations. However, the consumption of SiO_2 associated with the Ca-smectite does suggest the solution composition will move upwards along the equilibrium boundary between kaolinite and Ca-smectite, toward the anorthite stability field in Figure 8-1a.).

The stability boundaries between smectites and primary and secondary minerals, in Figures 8-1a.) through d.), are calculated assuming the activity of smectite is equal to one, indicating it is a solid pure phase (Anderson, 1996). However, in geochemical modelling, smectite can be modelled as an ideally mixed, solid solution of Ca, Mg, K and Na components (Abercrombie, 1989; Grasby, 1997). Because oxidation of pyrite has been identified in the Kettle River basin, indicating Fe is present, smectites will be modelled as a solid solution of Ca, Mg, K, Na and Fe components. As determination of the chemical composition of smectite was not within the realm of this project, the chemical compositions of smectites in freshwater environments were obtained from several sources (Nadeau and Bain, 1986; Robert and Goffe, 1992; Christidis and Dunham, 1997; Christidis, 2001 and Wolters et al., 2009). Smectite compositions in these studies were determined using either electron microprobe or x-ray fluorescence and were reported as weight % oxide. Reported oxide values were used to determine the mole fractions of Ca, Mg, Na, K and Fe. The average, minimum and maximum mole proportions are summarized in Table 8-4. The chemical formulas of each smectite component, using the average molar proportion from Table 8-4 are $Ca_{0.101}Al_{2.33}Si_{3.67}O_{10}(OH)_2$, $Mg_{0.555}Al_{2.33}Si_{3.67}O_{10}(OH)_2$, $Na_{0.269}Al_{2.33}Si_{3.67}O_{10}(OH)_2$ and $K_{0.075}Al_{2.33}Si_{3.67}O_{10}(OH)_2$. The

chemical compositions of smectites obtained from the literature are tabulated in Appendix E. The molar proportions are then assumed to be equal to the activity of each smectite component (Anderson, 1996); for example: the average mole fraction of Ca is 0.101, which is assumed to be equal to the activity of Ca-smectite.

Table 8-4: Average ± standard deviation (SD), maximum and minimum values of cation mole fractions in smectite, from Nadeau and Bain (1986), Robert and Goffe (1992), Christidis and Dunham (1997), Christidis (2001) and Wolters et al. (2009).

Cation	**Ca**	**Mg**	**Na**	**K**
Average ± SD	0.101 ± 0.157	0.555 ± 0.192	0.269 ± 0.226	0.075 ± 0.013
Maximum	0.573	0.963	0.680	0.314
Minimum	0.001	0.183	0.001	0.002

The maximum and minimum activities for Ca-, Mg-, K- and Na-smectite were used to re-calculate the location of stability boundaries between smectites and primary and secondary silicate minerals. Figures 8-2a.) to d.) show re-calculated stability boundaries using maximum and minimum activity values. The location of stability boundaries shifts either left or right, however the slope remains unaffected. An example calculation for the equilibrium line shift between albite and Na-smectite from Figure 8-2c.) is included in Appendix C.

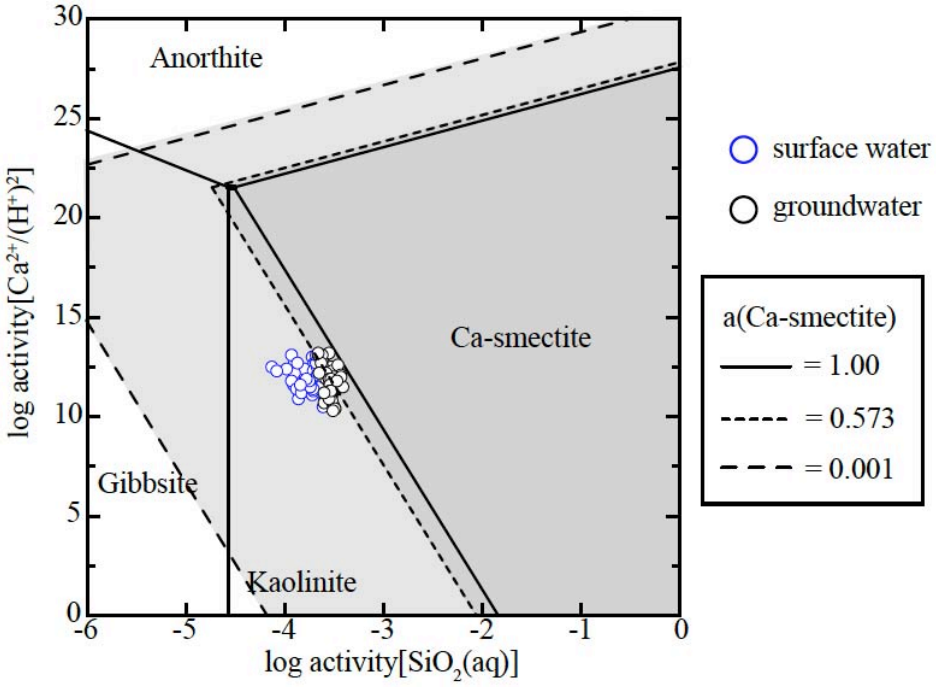

Figure 8-2a.): Log activity of $Ca^{2+}/(H^+)^2$ vs. log activity of $SiO_2(aq)$ at 5 °C and 1 bar with the activity of Ca-smectite equal to 1, 0.573 (maximum value) and 0.001 (minimum value).

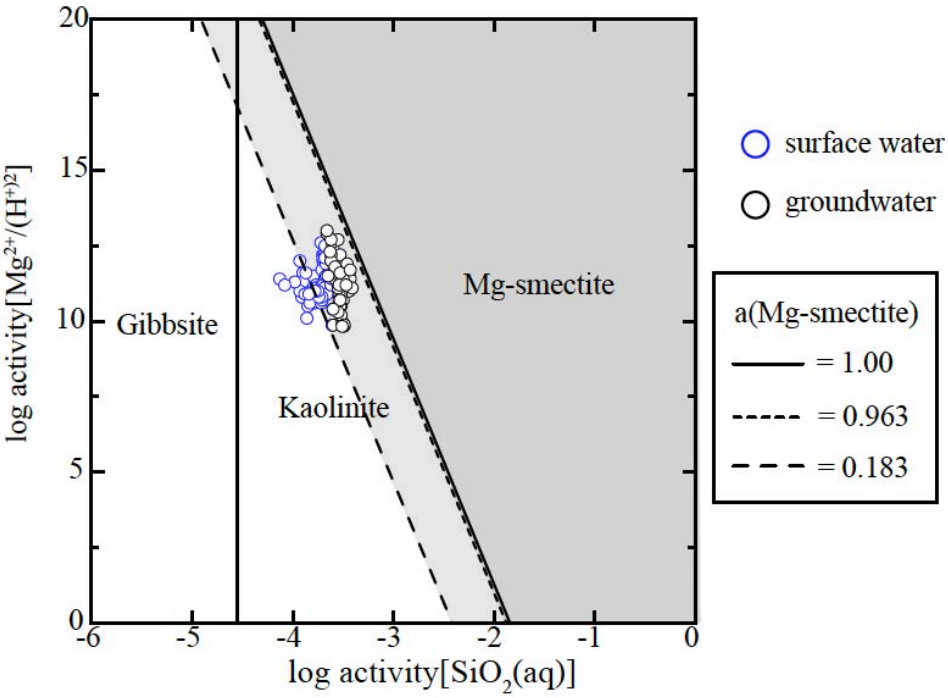

Figure 8-2b.): Log activity of $Mg^{2+}/(H^+)^2$ vs. log activity of $SiO_2(aq)$ at 5 °C and 1 bar with the activity of Ca-smectite equal to 1, 0.963 (maximum value) and 0.183 (minimum value).

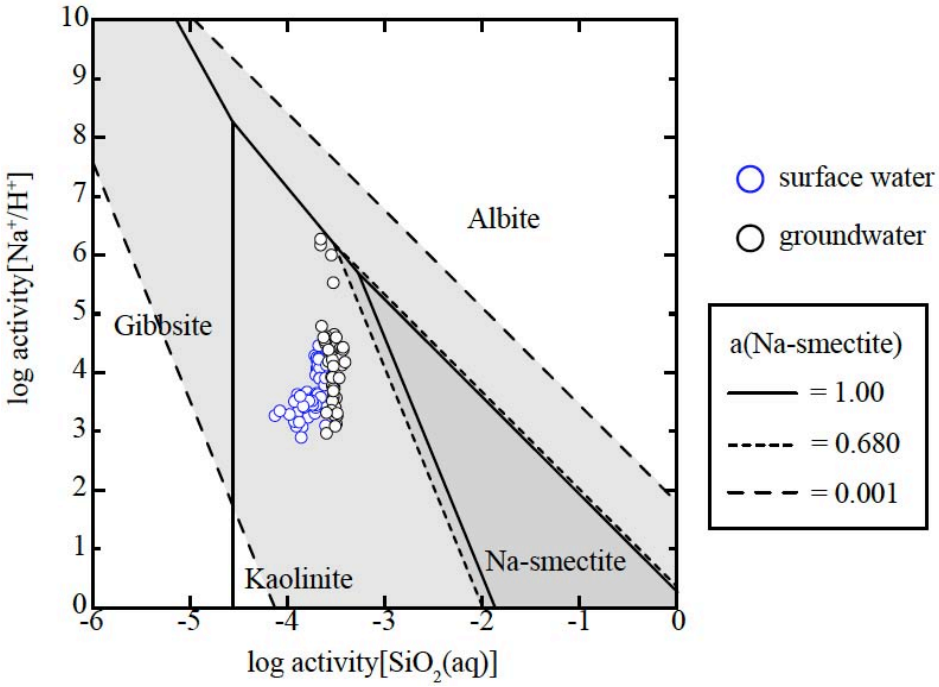

Figure 8-2c.): Log activity of Na^+/H^+ vs. log activity of $SiO_2(aq)$ at 5 °C and 1 bar with the activity of Na-smectite = 1, 0.680 (maximum value) and 0.001 (minimum value).

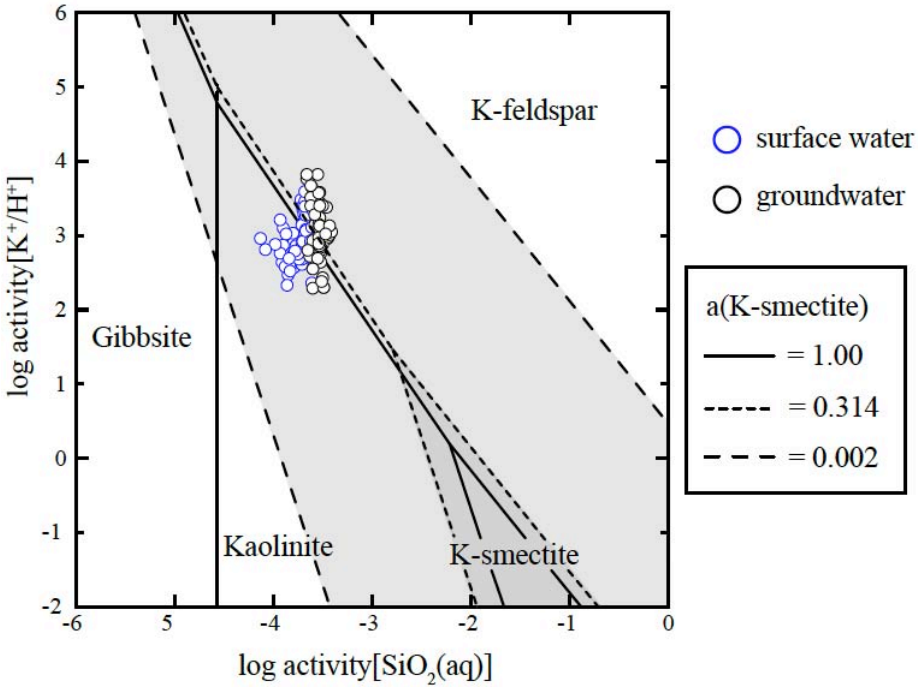

Figure 8-2d.) Log activity of K^+/H^+ vs. log activity of $SiO_2(aq)$ at 5 °C and 1 bar with the activity of K-smectite equal to 1, 0.314 (maximum value) and 0.002 (minimum value).

As shown in Figures 8-2a.) through d.), when the activity of each smectite component is considered, it is possible surface water and groundwater samples plot along or near the equilibrium boundary between kaolinite and each smectite variety, or within the stability field of each smectite. In general, surface water and groundwater samples more strongly parallel the equilibrium lines between kaolinite and Mg- and Ca-smectite, compared to Na- and K-smectite. In Figures 8-2a.) through d.) surface water and groundwater samples do not plot along the same line, which suggests there is variation in activities of smectite components within the Kettle River basin. For example in Figure 8-2a.), the maximum activity of Ca-smectite appears to represent the majority of groundwater samples, however there are a few groundwater samples which plot on either side of the equilibrium line indicating slightly higher or lower Ca-smectite activities. Surface water samples all plot on the left side of the maximum Ca-smectite equilibrium line, suggesting the activity of Ca-smectites in equilibrium with surface water is lower compared to groundwaters or that surface waters samples are not in equilibrium with smectite. Overall, if samples plot parallel to an equilibrium boundary line, there is potentially a reaction relationship between minerals and the co-existing water.

8.4.2 Saturation Indices

Activities of ions in solution can be used to identify weathering reactions as well as to determine the state of mineral saturation. The saturation index (SI) is the ratio of Ion Activity Product and the solubility product 'K' on a logarithmic scale (Appelo and Postma, 2005), as discussed in Chapter 6. SI values of surface water and groundwater samples, with respect to various minerals, are summarized in Appendix B.

Quartz and polymorphs of quartz – tridymite and chalcedony, have positive SI values in all surface water and groundwater samples. Cristobalite, another polymorph of quartz, also has positive SI values in most samples. The positive SI of quartz and polymorphs of quartz results from weathering of primary silicate minerals, which release SiO_2 (written as H_4SiO_4) (Equations 8-6 to 8-9). Weathering of silicate minerals, such as feldspars and pyroxenes occurs at a relatively fast rate in comparison to quartz, a mineral

that is very resistant to weathering (Appelo and Postma, 2005). Quartz precipitation at low temperatures occurs very slowly, causing quartz and polymorphs of quartz to be supersaturated (Bjørlykke and Egeberg, 1993). Solutions supersaturated with quartz have been found to persist to 60 °C (Abercrombie et al., 1994 and references therein). Because groundwater samples collected in the Kettle River Basin all had temperatures of less than 10 °C, it is unlikely quartz precipitation is occurring.

Solutions oversaturated with quartz have been found to encourage metastable precipitation of silica rich phases such as smectite (Abercrombie et al., 1994). The stability boundaries of quartz at 5 °C is indicated with vertical lines in Figures 8-1a.) through d.). Samples approaching equilibrium with Ca- and Mg-smectite are the most super-saturated with respect to quartz, which supports the suggestion that metastable precipitation of smectite occurs in solutions oversaturated with respect to quartz.

GWB calculated a positive saturation index (SI) for a few non-silicate minerals, suggesting the possibility of other water-rock reactions, complimenting chemical weathering of primary silicates. Calcite and dolomite have positive SI values, up to 0.42 for calcite and 1.3 for dolomite, in 33 % and 50 % of groundwater samples, respectively, suggesting the possible presence of calcareous or dolomitic cements. There were no surface water samples with positive SI values for calcite or dolomite. Because precipitation of dolomite in modern environments is rare and the SI value of dolomite produced by GWB may be unrealistically high, as the stability at low temperatures is not known (Bethke, 2008), it will be assumed that dolomite is not present. As discussed in Chapter 6, a positive SI value with respect to calcite indicates that it is possible that there is calcareous cement in Kettle River Basin aquifers.

Because not all groundwater samples are in equilibrium with calcite, this suggests there is variability in water rock interactions, which could be attributed to the mineralogical composition of the aquifer or bedrock, or the amount of time waters have had to interact with subsurface materials. The samples with positive calcite SI values correspond to 14 locations, most of which have groundwater with positive SI values for calcite in both June and October. These samples are all located below the confluence, with

one exception along the West Kettle River. Below the confluence, bedrock geology is dominated by basalt with minor chert and ultramafics as shown in Figure 2-4, whereas along the West Kettle and Kettle Rivers, granitic intrusives are the dominant bedrock type. This suggests lithology is the dominant control on calcite SI values. Weathering of basalts typically produces more basic waters (Winter, 2001); the average pH of the samples corresponding to the 14 locations discussed above are indeed higher (7.7 ± 0.3) compared to the average pH of groundwater samples with negative SI values with respect to calcite in other groundwater samples (7.1 ± 0.4). As discussed in Chapter 6, the relative distribution of DIC is pH dependent. HCO_3^- concentrations will be greatest at a pH of around 8.3 (Appelo and Postma, 2005). Therefore basic waters produced from weathering of basalt will have higher concentrations of HCO_3^- compared to more acidic waters produced from weathering of granite. Indeed samples from the 14 locations have an average HCO_3^- concentration of 229.6 ± 72.4 mg/L, compared to 192.8 ± 71.4 mg/L, which is the average of all groundwater samples. As formation of secondary calcite consumes Ca^{2+} and HCO_3^- and releases $CO_2(g)$ as shown in Equation 8-12, more basic waters with higher HCO_3^- concentrations would be favoured for formation of secondary calcite.

$$Ca^{2+} + HCO_3^- \leftrightarrow CO_2(g) + H_2O + CaCO_3 \quad (8\text{-}12)$$

8.4.3 Ion Exchange

Clay minerals, produced through weathering of primary silicate minerals, can participate in ion exchange reactions with ions in solution. In the tetrahedral layer of clay minerals, Si^{4+} can be replaced by Al^{3+} and in the octahedral layer Al^{3+} can be replaced by many ions including: Fe^{2+}, Mg^{2+}, Zn^{2+}. Substitution results in an overall negative charge on the clay mineral, which is neutralized by adsorption of cations (Faure, 1998). There are many types of clays, with different combinations of tetrahedral and octahedral layers and therefore variable Cation Exchange Capacity (CEC). CEC of soil or sediment is expressed in units of meq/kg. Common clay minerals kaolinite, smectite, chlorite and illite have a

CEC of 30-150, 800-1200, 100-400, and 200-500 meq/kg, respectively (Appelo and Postma, 2005). The CEC is also dependent on pH and the type of ion occupying the exchange site (Drever, 1997). Based on the range of CEC of common clay minerals, smectites have the highest CEC and are thought to control major cation ratios between clay minerals and solution (Bluth and Kump, 1994; Grasby, 1997).

To identify ion exchange relationships between clay minerals and ions in solution, GWB was used to create simple stability diagrams and surface water and groundwater samples were overlain (Figures 8-3 through 8-8). As discussed previously, GWB calculates the stability diagrams assuming the activity of each smectite variety is equal to 1. Using the average activities of Ca-, Mg-, Na- and K-smectite from Table 8-4, the equilibrium lines between smectite and primary and secondary minerals that parallel surface water and groundwater samples, were re-calculated and are included on Figures 8-3 through 8-8.

When ion activity ratios of major cations are plotted against each other on stability diagrams, linear relationships are observed. Previously, plots of $Ca^{2+}/(H^+)^2$ and $Mg^{2+}/(H^+)^2$ vs. $SiO_2(aq)$ indicated samples are in equilibrium or are close to equilibrium with Ca- and Mg-smectite stability fields (Figure's 8-1 a.) and b.)), respectively. A plot of log activity $Mg^{2+}/(H^+)^2$ versus $Ca^{2+}/(H^+)^2$ (Figure 8-3), indicates samples plot along the equilibrium line between Ca-smectite and Mg-smectite determined with average smectite activities from the literature. This suggests ion exchange between Ca- and Mg-smectite (Equation 8-13) likely influences concentrations of Ca^{2+} and Mg^{2+} in surface waters and groundwaters.

$$0.17Mg^{2+} + \underset{\textit{Ca-smectite}}{Ca_{0.17}Al_{2.33}Si_{3.67}O_{10}(OH)_2} \leftrightarrow \underset{\textit{Mg-smectite}}{Mg_{0.17}Al_{2.33}Si_{3.67}O_{10}(OH)_2} + 0.17\ Ca^{2+} \qquad (8\text{-}13)$$

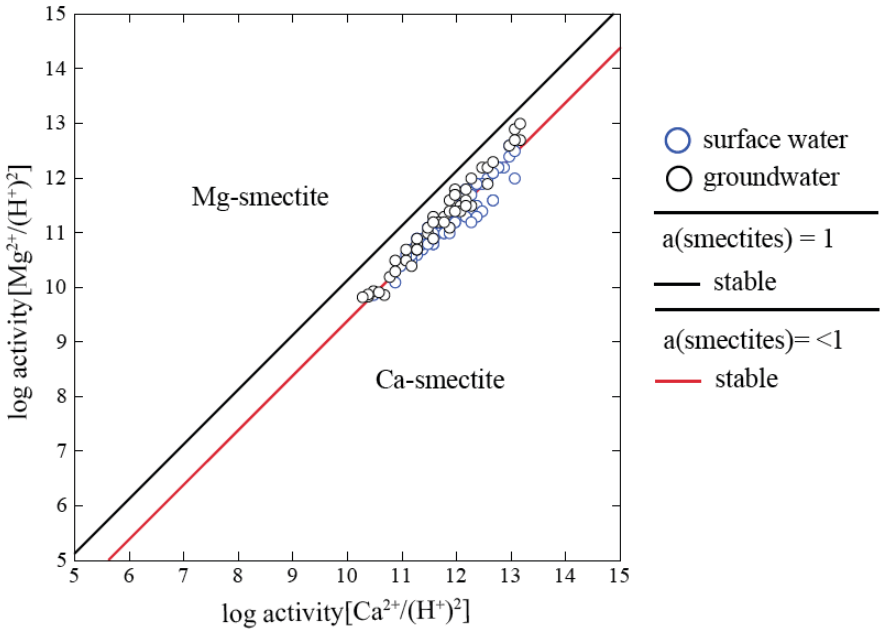

Figure 8-3: Log activity of $Mg^{2+}/(H^+)^2$ versus $Ca^{2+}/(H^+)^2$ at 5 °C, 1 bar and a log activity of $SiO_2(aq)$ equal to -3.7, which is the average of surface water and groundwater samples. The a(smectite) = 1 refers to the default setting in GWB. Values of a(smectite) <1 were re-calculated based on average values from the literature summarized in Table 8-4.

On the log activity diagram of Na^+/H^+ vs K^+/H^+, most samples plot parallel to the stable or metastable equilibrium line between Na- and K-smectite, similar to observations made by McFarland (1997) and Grasby et al. (1999) (Figure 8-4). This suggests an ion exchange relationship between Na- and K-smectite (Equation 8-14). A few groundwater samples plot along the boundary between K-feldspar and Na-smectite (Equation 8-15). The equilibrium line re-calculated with average Na- and K-smectite activities moved in the opposite direction from surface water and groundwater samples, indicating the activities of K- and Na-smectite in the Kettle River Basin, are different than average activities calculated from the literature. The average Na-smectite activity is greater than the average K-smectite activity. In order for the equilibrium line to move towards Kettle River Basin samples, the activity of K-smectite must be greater than that of Na-smectite.

$$0.33\ K^+ + Na_{0.33}Al_{2.33}Si_{3.67}O_{10}(OH) \leftrightarrow 0.33\ Na^+ + K_{0.33}Al_{2.33}Si_{3.67}O_{10}(OH)_2 \quad (8\text{-}14)$$

Na-smectite *K-smectite*

$$0.33\ Na^{+} + 2CO_2 + 2H_2O + 2.33\ KAlSi_3O_8 = \underset{\textit{K-feldspar}}{} \quad (8\text{-}15)$$

$$Na_{0.33}Al_{2.33}Si_{3.67}O_{10}(OH)_2 + 2.33\ K^{+} + 3.33SiO_2 + 2HCO_3^{-}$$

Na-smectite

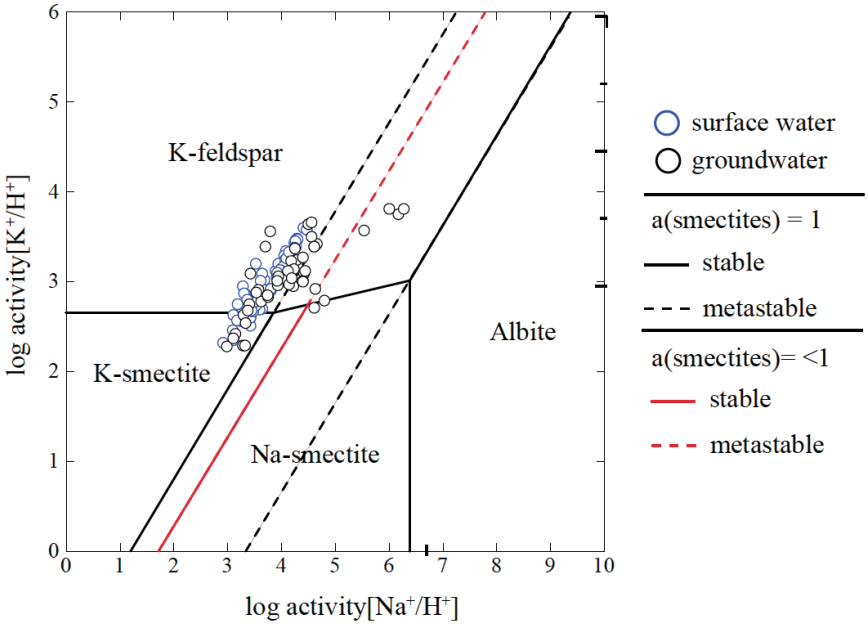

Figure 8-4: Log activity of K^{+}/H^{+} versus Na^{+}/H^{+} at 5 °C, 1 bar and a log activity of SiO_2(aq) equal to -3.7, which is the average of surface water and groundwater samples. The a(smectite) = 1 refers to the default setting in GWB. Values of a(smectite) <1 were re-calculated based on average values from the literature summarized in Table 8-4.

Linear relationships are also observed on log activity diagrams of Na^{+}/H^{+} and K^{+}/H^{+} plotted against $Mg^{2+}/(H^{+})^2$ and $Ca^{2+}/(H^{+})^2$ (Figures 8-5 through 8-8). The linear distribution of samples in these figures, parallels the equilibrium between Na- and K-smectite. In the case of K^{+}/H^{+} versus $Mg^{2+}/(H^{+})^2$ and $Ca^{2+}/(H^{+})^2$, samples also parallel the metastable line between smectites, within the K-feldspar stability field (Figures 8-7 and 8-8). Because the linear relationship exhibited on each of these diagrams parallels the stable and/or metastable equilibrium line between smectites, ion exchange relationships between each of these cations likely influence water composition of both surface water and groundwater. On log activity diagrams of Na^{+}/H^{+} versus $Mg^{2+}/(H^{+})^2$ and $Ca^{2+}/(H^{+})^2$, (Figures 8-5 and 8-6) surface water and groundwater samples are linearly distributed,

however, these linear relationships do not parallel equilibrium boundaries between Na- and Mg-smectite and Na- and Ca-smectite, suggesting that it is unlikely ion exchange is occurring between these smectites.

In order for the equilibrium line to coincide with samples in Figure 8-5, the activity of Ca-smectite must be greater than that of Na-smectite. In Figures 8-6 and 8-7, in order for the equilibrium line to coincide with sample locations, the difference between the activities of Mg- and Na-smectite, and Ca- and K-smectite, must be much greater than the difference between the average smectite compositions. The average Mg- and K-smectite activities compositions shown in Figure 8-8 are close to coinciding with surface water and groundwater samples, however the difference between Mg- and K-smectite activities must be slightly greater. Average activities of smectites increase in the following order: K < Ca < Na < Mg. For equilibrium lines to coincide with data from the Kettle River basin, smectite activites must be in the order: Na < K < Ca <Mg.

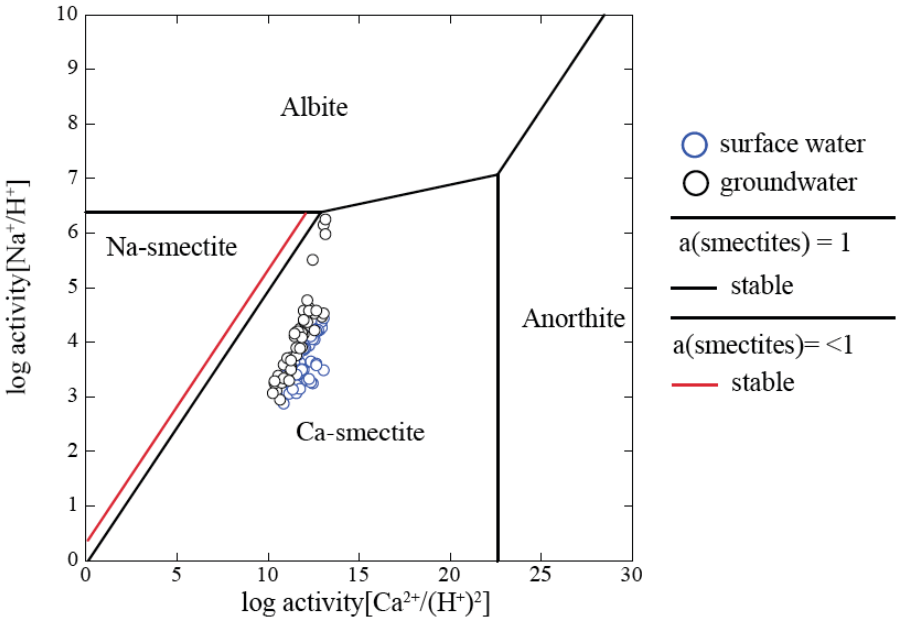

Figure 8-5: Log activity of Na^+/H^+ versus $Ca^{2+}/(H^+)^2$ at 5 °C, 1 bar and a log activity of $SiO_2(aq)$ equal to -3.7, which is the average of surface water and groundwater samples. The a(smectite) = 1 refers to the default setting in GWB. Values of a(smectite) <1 were re-calculated based on average values from the literature summarized in Table 8-4.

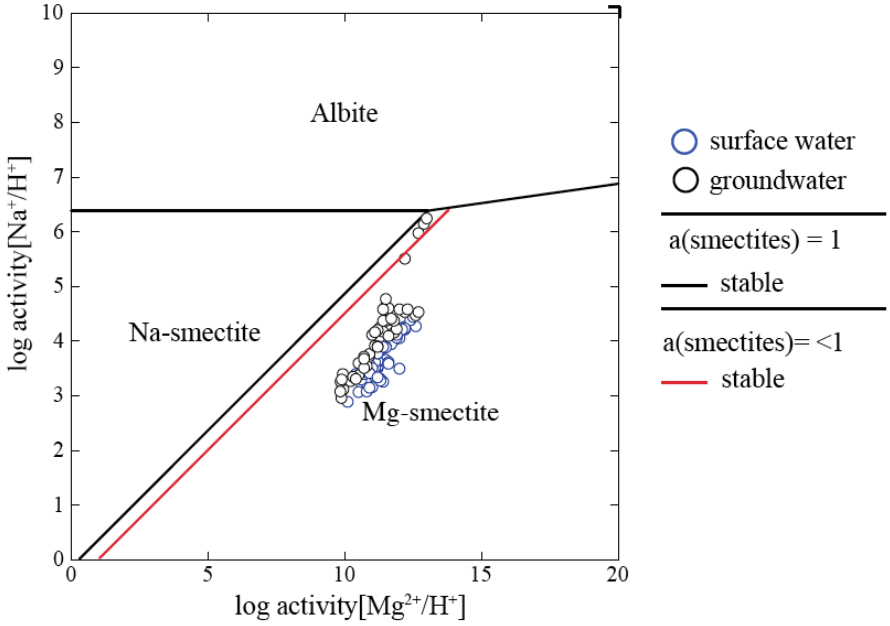

Figure 8-6: Log activity of Na^+/H^+ versus $Mg^{2+}/(H^+)^2$ at 5 °C, 1 bar and a log activity of SiO_2(aq) equal to -3.7, which is the average of surface water and groundwater samples. The a(smectite) = 1 refers to the default setting in GWB. Values of a(smectite) <1 were re-calculated based on average values from the literature summarized in Table 8-4.

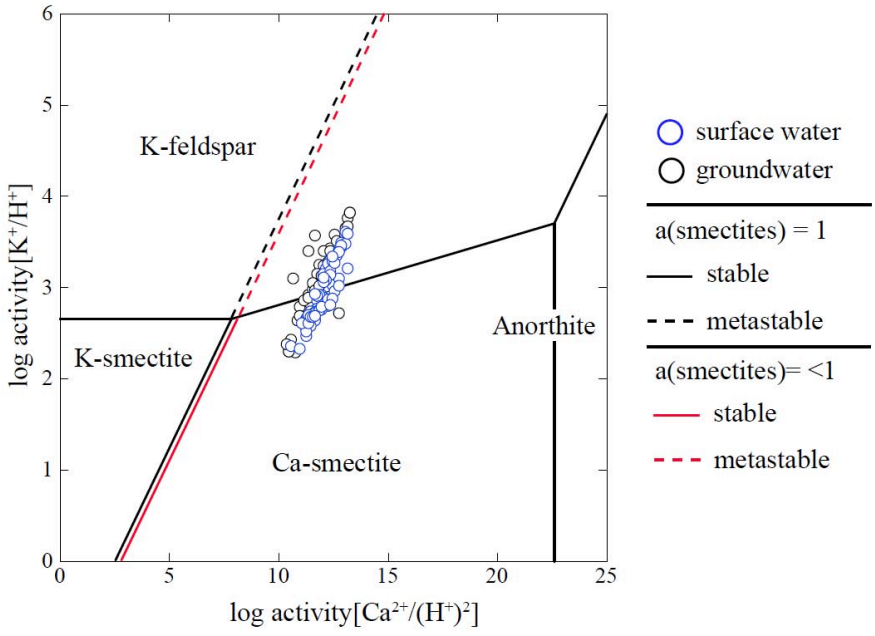

Figure 8-7: Log activity of K^+/H^+ versus $Ca^{2+}/(H^+)^2$ at 5 °C, 1 bar and a log activity of SiO_2(aq) equal to -3.7, which is the average of surface water and groundwater samples. The a(smectite) = 1 refers to the default setting in GWB. Values of a(smectite) <1 were re-calculated based on average values from the literature summarized in Table 8-4.

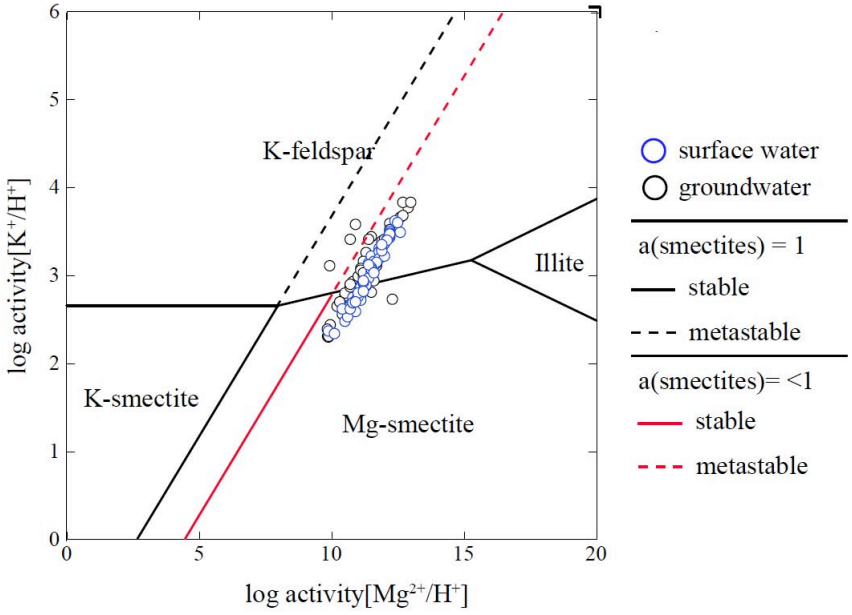

Figure 8-8: Log activity of K^+/H^+ versus $Mg^{2+}/(H^+)^2$ at 5 °C, 1 bar and a log activity of $SiO_2(aq)$ equal to -3.7, which is the average of surface water and groundwater samples. The a(smectite) = 1 refers to the default setting in GWB. Values of a(smectite) <1 were re-calculated based on average values from the literature summarized in Table 8-4.

Surface Water

In all of the above phase diagrams, surface water samples plot along a line that is slightly offset from groundwater samples. This suggests water sources, other than groundwater, are influencing the composition of surface water, such as precipitation. If this were the case, it would be expected the influence of precipitation water would be more pronounced in June, during the freshet. Indeed, samples from June have lower average ion activity ratios compared to those obtained in October, however samples collected in June plot along the same line as samples from October. This indicates that ion exchange reactions influence surface water compositions regardless of variable precipitation inputs throughout the year. Consistent differences between surface water and groundwater activity ratios, may be attributable to subtle variation in the chemical composition of smectites interacting with surface water and groundwater compositions.

Groundwater

There are a few groundwater samples in Figures 8-4 through 8-8, that plot away from the majority of samples. In Figure 8-4, four groundwater samples, which correspond to two wells sampled in June and October, previously identified to originate from bedrock aquifers have higher ion activity ratios compared to other samples. These four samples plot within the K-feldspar stability field close to the metastable equilibrium line between K-feldspar and Na-smectite. Also along this metastable equilibrium line, are two groundwater samples collected in October of 2010. Equation 8-15 represents this reaction between K-feldspar and Na-smectite. Because these equations involve both primary and secondary minerals, this suggests prolonged interaction between groundwater and aquifer materials. If the equilibrium lines between smectite and primary minerals were re-drawn with the activities of smectite components in the Kettle River Basin, it is possible, the location of equilibrium lines would shift slightly and these outliers may no longer lie on boundaries between primary minerals and smectite. Flow in crystalline bedrock aquifers is mostly along joints, fractures and faults and has limited connectivity with surface waters (Wei et al., 2010). Therefore these groundwater samples likely have little influence on surface water chemistry, however they do highlight some of the less common silicate weathering reactions occurring within the basin. It is assumed the remainder of groundwater samples were collected from wells completed in unconsolidated sand and gravel valley aquifers.

8.5 Silicate Weathering Reactions and CO_2 consumption

There are several different types of reactions associated with weathering of silicate bedrock. The main source of ions into solution due to weathering is through direct weathering of primary minerals to secondary clay minerals as described in Equations 8-5 through 8-9, 8-11 and 8-15. Each of these reactions consumes $CO_2(g)$. In addition to simple weathering reactions, geochemical modelling indicates some groundwater samples have positive SI values for calcite, suggesting precipitation of secondary calcite may be occurring, resulting in consumption of Ca^{2+} and HCO_3^- and release of $CO_2(g)$ as outlined

in Equation 8-12. Ion exchange appears to be an important control on water composition, however these reactions do not produce or consume CO_2. Overall, the major reactions that consume CO_2(g) are direct weathering of primary minerals to form secondary minerals. Using reactions identified in this Chapter, the amount of CO_2(g) consumed during weathering of silicate minerals will be estimated in Chapter 9.

8.6 Conclusion

Combining carbonic acid as the dominant weathering agent and silicate bedrock allows for identification of probable weathering reactions between primary and secondary minerals using simple phase diagrams. Weathering of basalt is identified as the dominant source of Mg^{2+} and Ca^{2+}, whereas weathering of granite is identified to be the source of Na^{+} and K^{+}. On ion activity vs SiO_2 activity diagrams, samples plot primarily within the kaolinite stability field, however once the activities of smectite components are considered, it appears likely that samples may also fall along the equilibrium line between kaolinite and smectite or within the smectite stability field. On all ion activity diagrams, linear relationships are observed. On most figures, linear relationships parallel the stable or metastable equilibrium line between smectites, suggesting that ion exchange is a dominant process influencing surface water and groundwater compositions. Comparing the location of the linear distribution of sample points and the average activity of smectite components, indicates that in the Kettle River basin, the order of smectite activities increases as follows: Na < K < Ca < Mg, compared to the order of average smectite components from the literature which is: K < Ca < Na < Mg. Weathering of basalt produces more basic waters, compared to weathering of granite, which preferentially allows calcite formation and may also influence the relative abundance of smectite components. Consistent differences between surface water and groundwater activity ratios, may be attributable to subtle variation in the chemical composition of smectites, or other factors such as influences of precipitation. The dominant reactions consuming CO_2 and releasing ions were weathering reactions between primary and secondary minerals.

CO_2 sequestration during silicate weathering, storage in groundwaters and subsequent transport out of the basin through surface water will be discussed in Chapter 9.

Chapter Nine: Chemical Weathering and CO_2 consumption

9.1 Introduction

Many studies have focused on understanding the intricacies related to consumption of atmospheric CO_2(g) during chemical weathering of silicate minerals (e.g. Walker et al., 1981; Berner et al., 1983; Gaillardet et al., 1999; Millot et al., 2003; Dupre et al., 2003; Spence and Telmer, 2005; Lerman and Wu, 2006; Beaulieu et al., 2011). This relationship is complicated by factors including climate (e.g. Walker et al., 1981), vegetation and soils (Drever, 1994), lithology (e.g. Bluth and Kump, 1994; Dessert et al., 2003) and physical erosion (e.g. Millot et al., 2002; West et al., 2005). The CO_2 consumed during silicate weathering, produces HCO_3^-, which is subsequently stored in aquifers. The timescale at which HCO_3^- and therefore, CO_2 is stored in aquifers, is also dependent on intrinsic characteristics of the aquifer, such as porosity, grain size and permeability, as well as characteristics of the groundwater flow regime (Freeze and Cherry, 1979). The amount of CO_2 stored in groundwaters is dependent on the amount of CO_2 available to react with aquifer materials and the mineralogical composition of aquifer materials. In order to investigate the relationship between chemical weathering and CO_2 consumption, geochemical modeling is used to determine the partial pressure of CO_2 (pCO_2) in equilibrium with groundwater samples and the amount of CO_2 required to reach the pCO_2 in equilibrium with groundwater samples. This allows for a quantitative estimation of the amount of CO_2 consumed and stored in aquifers associated with chemical weathering of silicate minerals. In order to assess the influence of climatic and lithologic factors on silicate weathering, a watershed in a temperate climate – the Kettle River Basin, is compared with a watershed in a tropical climate – the Paraná Basin in Brazil. Within these two watersheds, there are variations in the mineralogical composition of aquifers, which will allow for the influence of lithology to be assessed. The timescale of CO_2 storage in aquifers in both basins and the export of HCO_3^- out of the Kettle River Basin to the ocean is also addressed.

9.2 Factors Influencing Weathering Rates

9.2.1 Climate

Atmospheric $CO_2(g)$ is a greenhouse gas, which absorbs and emits radiation, resulting in a greenhouse effect on earth's climate (Walker, 1981). Atmospheric climate models suggest that CO_2 concentrations are linked to warmer temperatures, changing precipitation patterns and increased runoff (Labat et al., 2004; Gislason et al., 2009). Increased runoff leads to higher rates of chemical weathering, as $CO_2(g)$ in the atmosphere is in equilibrium with $CO_2(aq)$, which subsequently reacts with H_2O, forming H_2CO_3 – which increases acidity and encourages chemical weathering. Chemical weathering of silicate minerals consumes $CO_2(g)$ and produces HCO_3^-, which is eventually transported by rivers to the ocean and forms carbonate minerals (e.g. Berner et al., 1983; Bluth and Kump, 1994). The connection between $CO_2(g)$ concentrations in the atmosphere and silicate weathering was first proposed by Siever (1968). Walker et al. (1981) suggested the weathering rate is dependent on surface temperature and the hydrologic cycle. This feedback system is thought to moderate climate on the earth's surface (e.g. Gislason et al., 2009). On timescales greater than one million years, consumption of CO_2 through weathering is balanced by volcanism and metamorphism (e.g. Berner et al., 1983).

Since the late 18th century, the onset of the industrial revolution, anthropogenic activities, including burning of fossil fuels and changes in land use, have resulted in steadily increasing $CO_2(g)$ concentrations in the atmosphere (Sabine et al., 2004). This increase in CO_2 concentration in the atmosphere led Gislason et al. (2009) to address the validity of the feedback system proposed by Siever (1968) on shorter timescales. Gislason et al. (2009) found over the past 44 years statistically significant correlations between weathering rates and temperature exist, suggesting a link between these two variables exists on shorter timescales. Of the amount of $CO_2(g)$ emitted by anthropogenic sources, only about half has remained in the atmosphere (Takahashi, 2004). The missing CO_2 is thought to have been taken up by either the ocean or by the terrestrial biosphere, however the relative role of these sinks is still debated (Sabine et al., 2004). It is possible that

chemical weathering of silicate minerals and subsequent storage as HCO_3^- in aquifers may be another sink of CO_2 on shorter timescales.

9.2.2 Vegetation/Soil

In the soil zone, root respiration and decay of organic matter generate CO_2(g) and organic acids which cause increased acidity, encouraging mineral weathering (Drever, 1994). The partial pressure of CO_2 in soils is estimated to be one to two orders of magnitude higher compared to the atmosphere (Appelo and Postma, 2005). The amount of root respiration is dependent on the type and density of vegetation, which varies seasonally. Increased atmospheric CO_2 concentrations lead to increased biological activity, which results in higher CO_2 concentrations in the soil (Andrews and Schlesinger, 2001). Increases in temperatures also enhance biological activity (Beaulieu et al., 2010), however water and soil conditions must also be suitable for biological activity (Appelo and Postma, 2005). The development of soil profiles varies depending on many factors such as climate and physical weathering rates and the correlation between soil thickness and chemical weathering is not well understood (Drever, 1997).

9.2.3 Lithology

Silicate minerals weather to form secondary minerals - reactions that consume CO_2 and release ions in solution, as discussed in Chapter 8. Ions in solution may then participate in ion exchange and mineral precipitation reactions. The weathering rate depends on the weathering agent, type of bedrock and on specific minerals resistance to weathering. In general more mafic lithologies, such as basalt are less resistant to weathering compared to felsic lithologies such as granite, as discussed in Chapter 8.

9.2.4 Physical Erosion

Physical erosion is the mechanical breakdown of material and is usually determined using the measured amount of suspended sediment and the runoff rate measured in rivers. If erosion rates are higher, there is an excess of material available for

chemical weathering, whereas in the case of lower erosion rates there is less material available (West et al., 2005). The role of physical weathering, specifically the role of relief, in chemical weathering has been debated (Drever, 1997). Millot et al. (2002) identified a strong correlation between chemical and physical weathering in small and large catchments, for both basaltic and plutonic watersheds.

9.2.5 Connection between factors

Chemical weathering of silicate minerals and consumption of CO_2 is dependent on the amount of CO_2 available to act as a weathering agent which is dependent on the amount of infiltrating precipitation and properties of vegetation and soils. The concentration of CO_2 in the atmosphere has been proposed to influence climate, and therefore the rate of infiltration of precipitation, soil CO_2 concentrations, as well as physical erosion rates. The amount of chemical weathering is also dependent on the susceptibility to weathering of specific minerals. The interconnectedness of the factors influencing chemical weathering have made it difficult to differentiate the individual effect of each factor (e.g. Millot et al., 2002; Amiotte Suchet et al., 2002; Spence and Telmer, 2005; West et al., 2005). The influence of climatic and lithologic factors on silicate weathering rates will be investigated in this Chapter by comparing characteristics of the Kettle River Basin and the Paraná Basin in Brazil .

9.3 Comparison of the Kettle River and the Paraná Basin

To investigate the role of climate, soil CO_2 and lithology on weathering rates groundwater samples from the Kettle River Basin are compared with groundwater samples from the northern part of Guarani Aquifer System (GAS), located in southeast Brazil (Figure 9-1). Groundwater samples were taken from an area of 500,000 km^2, within the greater GAS (Gastmans et al., 2010a), which covers an area of about 1,090,000 km^2 of the South American countries Brazil, Argentina, Paraguay and Uruguay. The GAS supplies drinking water to an estimated 90 million people (Gastmans et al., 2010b). The unconfined portion of the aquifer covers an area of 85,000 km^2, while the remainder of

the aquifer is confined by basalts from the Serra Geral Formation (Gastmans et al., 2010a).

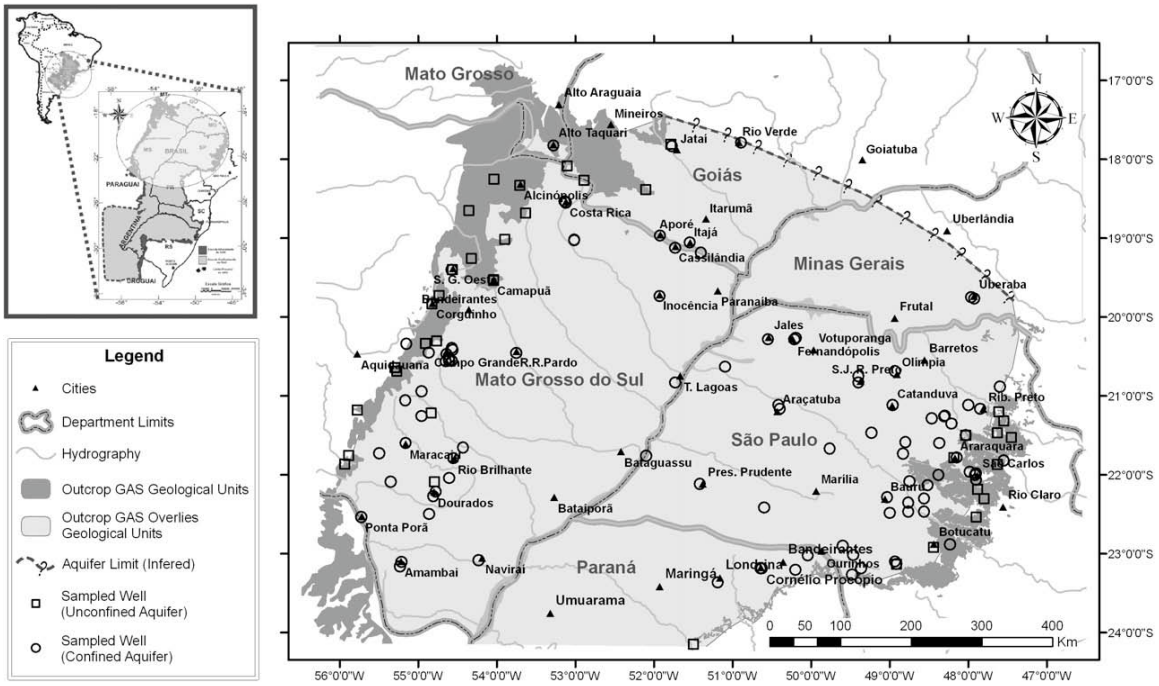

Figure 9-1: Location of the GAS in Brazil (from Gastmans et al., 2010a).

9.3.1 Climate

Temperature and precipitation data for the Kettle River Basin were summarized in Chapter 2. At different climate stations located throughout the basin (Figure 2-2), historical average temperatures range from 4.9 °C to 10.1 °C and historical average annual precipitation (which includes rainfall and snowfall) ranges from 318 to 482 mm. The historical normal amount of snow recorded at different locations in the basin (Figure 2-2) varies between 106 and 440 mm (snow-water equivalent). The average temperature of groundwater samples in the Kettle River Basin is 7 °C.

The study area of the GAS in Brazil occupies a very large area of South America. For the purposes of this study, an excerpt on the climate of the area is taken from Gastmans et al. (2010b): "The climate of the study area is a pluviometric regime marked by the occurrence of two well defined seasons: the rainy summer and the dry winter. The

summer extends from October to March, and the winter from September to April. The annual rainfall is approximately 1,700 mm, with the highest rainfall from November to January. Mean annual temperature is 22 °C, reaching 40 °C (on selected days) during the summer." The average temperature of groundwater samples from the GAS is 27 °C.

9.3.2 pCO_2

The dominant weathering agent identified in Chapter 8 is $H_2CO_3^*$, of which the dominant component is $CO_2(aq)$. The * denotes the combination of $CO_2(aq)$ and H_2O. Using geochemical modeling software SOLMINEQ88, the pCO_2 in equilibrium with groundwater samples in both the Kettle River Basin and in the GAS in Brazil was determined, given pH, temperature and HCO_3^-. $H_2CO_3^*$ and pCO_2 are related to each other by a temperature dependent equilibrium constant (K_{CO2}), known as Henry's law constant (Equation 9-1) (Drever, 1997).

$$H_2CO_3^* = K_{CO2} \times pCO_2 \qquad (9\text{-}1)$$

In the Kettle River Basin, the average pCO_2 in equilibrium with groundwater samples is $10^{-2.09} \pm 10^{-2.29}$ atm (n=48), and values range from $10^{-3.13}$ and $10^{-1.72}$ atm; the spatial distribution of these values is shown in Figure 9-2. There appears to be some spatial correlation in the pCO_2. For example, between Rock Creek and the Canadian – US border, the log[pCO_2] values in equilibrium with groundwater samples are less than $10^{-2.50}$ atm, and north of Rock Creek and pCO_2 increases to values between $10^{-2.50}$ and $10^{-2.00}$ atm between Rock Creek and Midway, as shown in Figure 9-2.

The average pCO_2 in equilibrium with groundwater samples from the GAS in Brazil is $10^{-1.83} \pm 10^{-1.70}$ atm (n=77), and values range from $10^{-3.70}$ to $10^{-1.08}$ atm. The available groundwater data from Brazil is from three types of aquifers – the basaltic aquifer of the Serra Geral formation (Hutcheon, pers. comm. 2011) and the unconfined and confined sandstone aquifers of the GAS (Gastmans et al., 2010a). Groundwater data

from Brazil is included in Appendix E. Of these three aquifers, groundwater samples from the unconfined aquifer have the highest average pCO_2, while samples from the confined aquifer have the lowest average pCO_2 (Table 9-1). The highest and lowest calculated pCO_2 values were formed in the basaltic aquifer. The unconfined aquifer also has high pCO_2 values.

Comparison between pCO_2 values in equilibrium with groundwater samples from the Kettle River Basin and the GAS in Brazil, indicate that groundwater samples in Brazil have a greater range in pCO_2 values. The average pCO_2 value of all groundwater samples from Brazil is 79.5 % higher compared to that for groundwater samples from the Kettle River Basin.

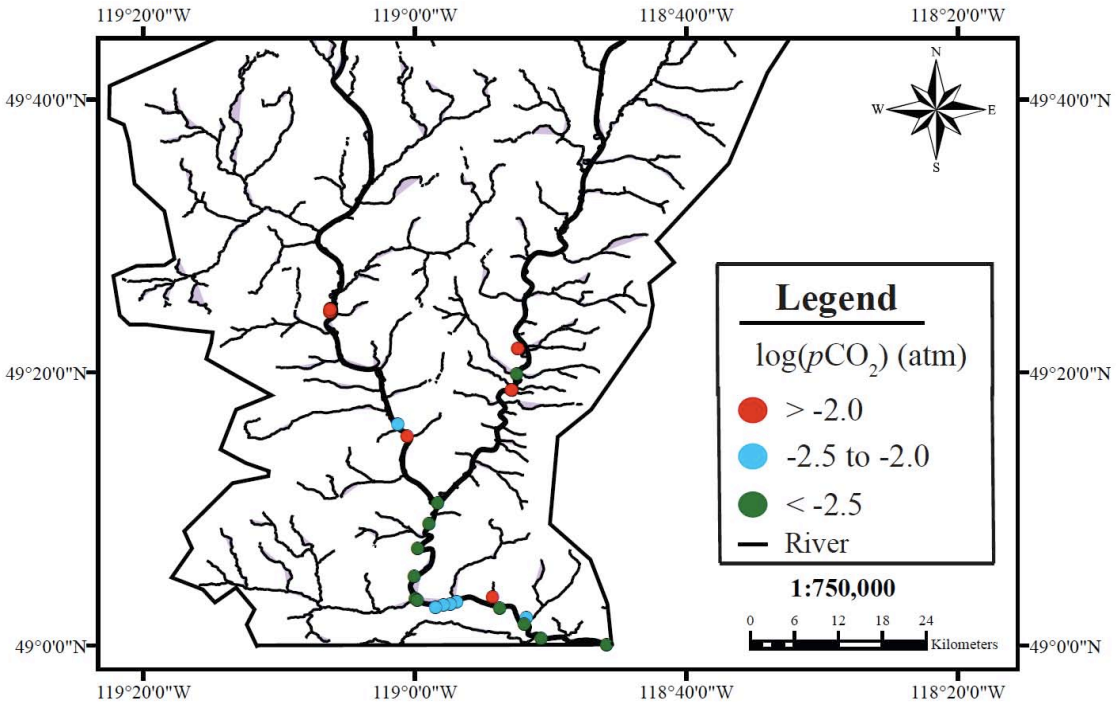

Figure 9-2: Spatial distribution of pCO_2 values in equilibrium with groundwater samples in the Kettle River Basin. Map was created with ArcGIS with data from the BC Geological Survey (2005).

Table 9-1: Average, maximum and minimum pCO_2 (atm) values from three types of aquifers in Brazil.

	pCO_2 (atm)			
Source	**Average**	**St. Dev.**	**Maximum**	**Minimum**
Unconfined GAS (n=38)	$10^{-1.73}$	$10^{-1.68}$	$10^{-1.09}$	$10^{-3.32}$
Confined GAS (n=16)	$10^{-2.19}$	$10^{-2.18}$	$10^{-1.65}$	$10^{-3.27}$
Basaltic Aquifer (n=23)	$10^{-1.84}$	$10^{-1.63}$	$10^{-1.08}$	$10^{-3.70}$

9.3.3 Lithology

In Chapter 2, the geology of the Kettle River Basin was identified to be composed primarily of igneous and metamorphic bedrock – as shown in Figure 2-7. The relative abundance of main lithology types is indicated in Table 8-1. Mass balance calculations in Chapter 7 revealed bedrock weathering contributes ions to surface water and groundwater and in Chapter 8 the specific mineralogical sources of ions and likely reactions between primary and secondary minerals were identified. Ion exchange reactions were identified between most major cations in solution and secondary clay minerals.

In South America, the GAS is located within the Paraná Sedimentary Basin, which is comprised of a volcano-sedimentary sequence up to 8000 meters thick. The unconfined and confined aquifers of the GAS consist of sandstones from the Triassic Piramobiòa and Jurassic-Neo-Cretaceous Botucatu Formations, which have a combined average thickness of 268 meters (Sracek and Hirata, 2002). The GAS is primarily composed of quartz-feldspar sandstones, with significant variations in the percentages of minerals. Pore-lining cements have been recognized - composed of early hematite +/- illite, quartz and feldspar overgrowth, and opal and chalcedony in the deepest portions of the basin. Pore-filling cements composed of calcite and dolomite are also present, primarily at depths greater than 250 meters. Reported porosities range from 0.1 to greater than 0.35 (Gastmans et al., 2010a,b; Sracek and Hirata, 2002). Basalts of the Serra Geral Formation, which overlie parts of the GAS, have a thickness of up to 1200 meters (Gastmans et al., 2010a) and are

composed of plagioclaise, augite, accessory magenetite, olivine, apatite and devitrified glass (Lastoria et al., 2006). Reported porosities of the Serra Geral basalts range from 0.01 to 0.05 (Sracek and Hirata, 2002).

Groundwater samples from both the Kettle River and Paraná Basins were sampled from aquifers dominated by silicate minerals. The specific mineralogy of aquifer materials in either location is not known, however the mineralogy in the Kettle River basin was estimated in Chapter 8 and weathering reactions for major minerals were identified (Equations 8-5 through 8-9). It will be assumed that these weathering reactions between primary and secondary minerals are also representative of weathering reactions in the Paraná Basin. This assumption is supported by the choice of primary minerals used in Ca- and K-stability diagrams in Gastmans et al. (2010a), which were the same as primary minerals used in stability diagrams in Chapter 8.

9.3.4 Ion Exchange

In order to determine whether groundwater samples in the Paraná Basin participate in ion exchange reactions, as groundwater samples from the Kettle River Basin, ion activity ratios of groundwater samples from Brazil (Gastmans et al., 2010a; Hutcheon, pers. comm. 2011) are plotted on diagrams, similar to those created in Chapter 8. Stability diagrams were created using geochemical modeling program, 'The Geochemist's Workbench' (GWB). The equilibrium lines for groundwater samples from the Paraná Basin are modeled at 27 °C, which is the average temperature of groundwater samples. Figures 9-3 through 9-8 show the ion activity diagrams with groundwater samples from the Kettle River and Paraná Basins.

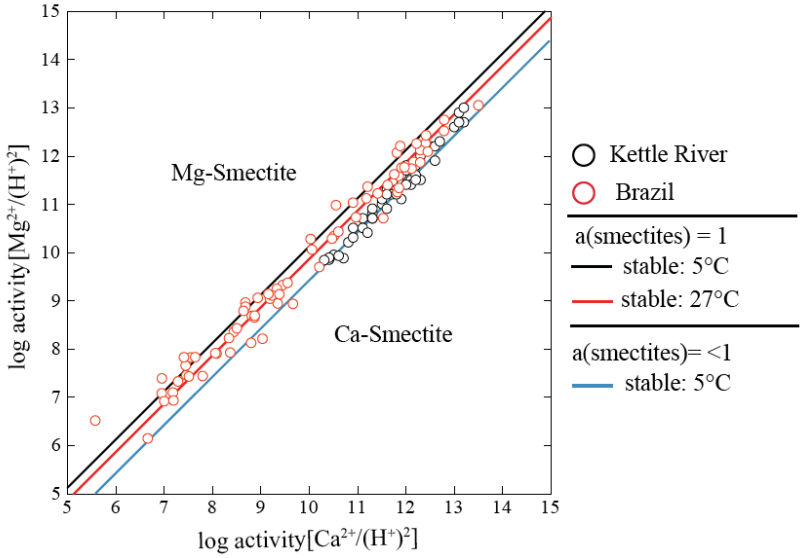

Figure 9-3: Log activity of $Mg^{2+}/(H^+)^2$ versus $Ca^{2+}/(H^+)^2$ at 5 °C , 1 bar and a log activity of SiO_2 value of -3.53 for the Kettle River. Samples from Brazil were modeled for 27 °C, 1 bar and a log activity of SiO_2(aq) equal to -3.12. The a(smectite) equal to 1 refers to the default setting in GWB. Values of a(smectite) <1 were re-calculated based on average values from the literature summarized in Table 8-4; the average value of Ca- and Mg-smectite used are 0.101 and 0.555, respectively.

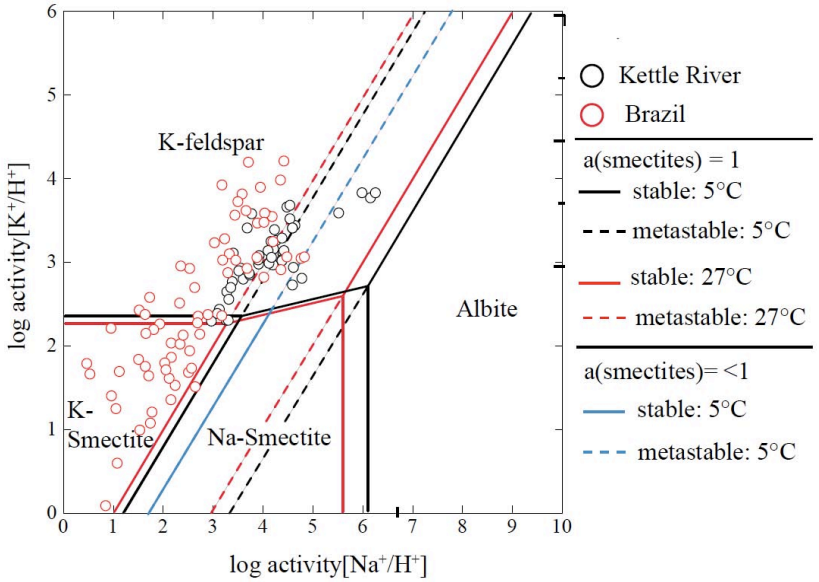

Figure 9-4: Log activity of K^+/H^+ versus Na^+/H^+ at 5 °C, 1 bar and a log activity of SiO_2 value of -3.53 for the Kettle River. Samples from Brazil were modeled for 27 °C, 1 bar and a log activity of SiO_2(aq) equal to -3.12. The a(smectite) equal to 1 refers to the default setting in GWB. Values of a(smectite) <1 were re-calculated based on average values from the literature summarized in Table 8-4; the average value of K- and Na-smectite used are 0.075 and 0.269, respectively.

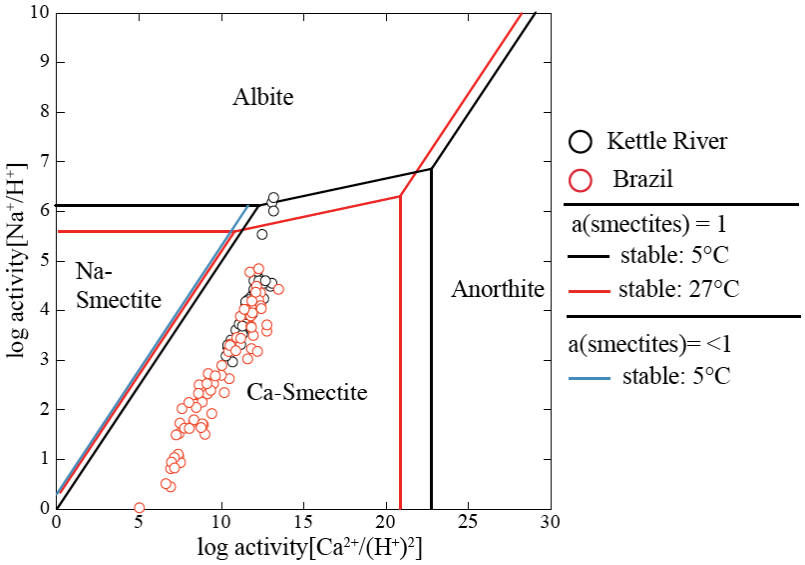

Figure 9-5: Log activity of Na^+/H^+ versus $Ca^{2+}/(H^+)^2$ at 5 °C, 1 bar and a log activity of SiO_2 value of -3.53 for the Kettle River. Samples from Brazil were modeled for 27 °C, 1 bar and a log activity of SiO_2(aq) equal to -3.12. The a(smectite) equal to 1 refers to the default setting in GWB. Values of a(smectite) <1 were re-calculated based on average values from the literature summarized in Table 8-4; the average value of Na- and Ca-smectite used are 0.269 and 0.101, respectively.

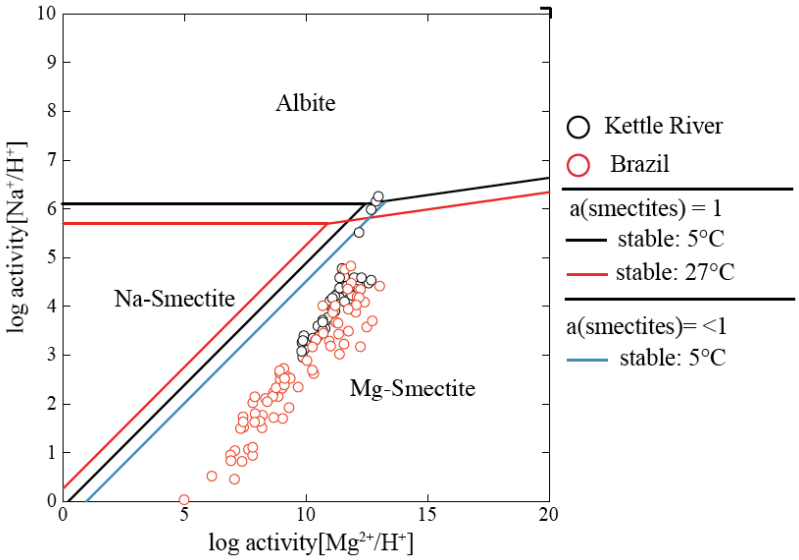

Figure 9-6: Log activity of Na^+/H^+ versus $Mg^{2+}/(H^+)^2$ at 5 °C, 1 bar and a log activity of SiO_2 value of -3.53 for the Kettle River. Samples from Brazil were modeled for 27 °C, 1 bar and a log activity of SiO_2(aq) equal to -3.12. The a(smectite) equal to 1 refers to the default setting in GWB. Values of a(smectite) <1 were re-calculated based on average values from the literature summarized in Table 8-4; the average value of Na- and Mg-smectite used are 0.269 and 0.555, respectively.

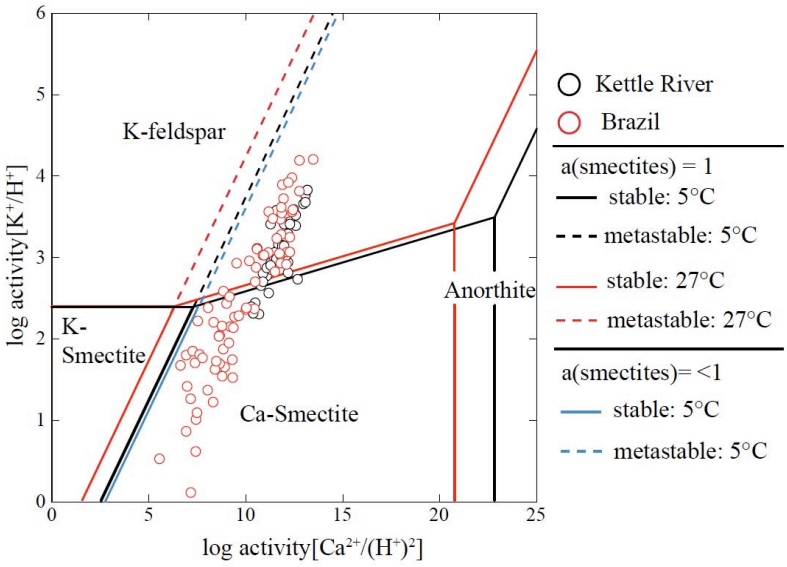

Figure 9-7: Log activity of K^+/H^+ versus $Ca^{2+}/(H^+)^2$ at 5 °C, 1 bar and a log activity of SiO_2 value of -3.53 for the Kettle River. Samples from Brazil were modeled for 27 °C, 1 bar and a log activity of SiO_2(aq) equal to -3.12. The a(smectite) equal to 1 refers to the default setting in GWB. Values of a(smectite) <1 were re-calculated based on average values from the literature summarized in Table 8-4; the average value of K- and Ca-smectite used are 0.075 and 0.101, respectively.

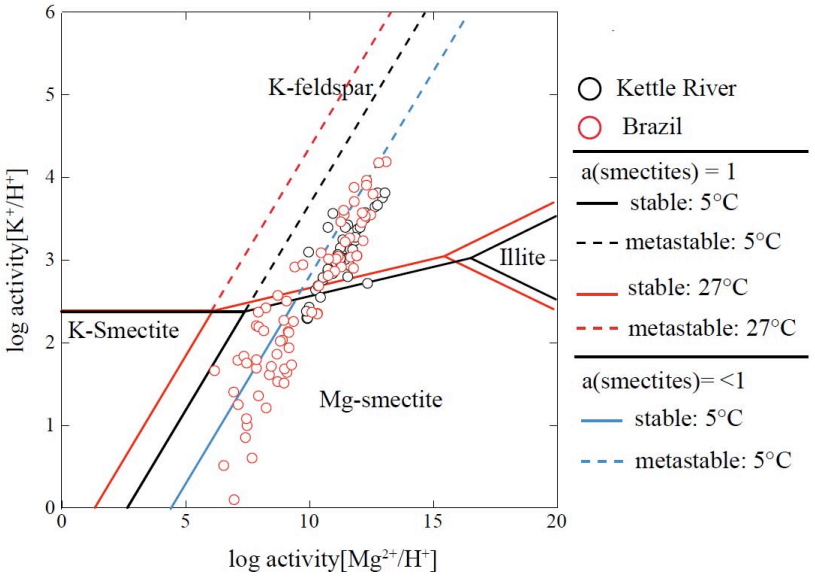

Figure 9-8: Log activity of K^+/H^+ versus $Mg^{2+}/(H^+)^2$ at 5 °C, 1 bar and a log activity of SiO_2 value of -3.53 for the Kettle River. Samples from Brazil were modeled for 27 °C, 1 bar and a log activity of SiO_2(aq) equal to -3.12. The a(smectite) equal to 1 refers to the default setting in GWB. Values of a(smectite) <1 were re-calculated based on average values from the literature summarized in Table 8-4; the average value of K- and Mg-smectite used are 0.075 and 0.555, respectively.

The ion activity ratios calculated from groundwater samples from the Paraná Basin plot along lines parallel to groundwater samples from the Kettle River valley indicating groundwater samples participate in similar ion exchange reactions (Figures 9-3 through 9-8). There is more scatter on the ion activity diagrams associated with groundwater samples from the Paraná Basin, suggesting there is more variation in the activities of Ca-, Mg-, Na-, and K-smectite components. It is assumed based on the bedrock geology in the Paraná Basin, that weathering reactions between primary and secondary minerals in Brazil are similar to the previously identified reactions in the Kettle River.

9.4 Geochemical Modeling

As mentioned previously, CO_2(g) in groundwater is derived from infiltrating precipitation and root respiration and decay of organic matter, and the amount of root respiration is dependent on the type and density of vegetation. The amount of CO_2(g) in equilibrium with groundwater samples, determined above is considered to be a 'snap shot' of the amount of pCO_2 in equilibrium with groundwater samples. Therefore, the pCO_2 values calculated above do not represent how much pCO_2 was originally in the groundwater samples as it is not known how much CO_2 is derived from root respiration and decay and how much CO_2 has been consumed during weathering. However, if a few assumptions are made regarding climate and lithology, the amount of CO_2 consumed during weathering can be estimated using geochemical modeling.

9.4.1 Conceptual Model

Using the REACT program within GWB, rainwater was reacted with common silicate minerals, likely found in aquifers in the Kettle River and Paraná Basins. The amount of CO_2(g) required to reach the pCO_2 in equilibrium with groundwater samples was calculated. The basis, or the starting composition of the solution in the model, is shown in Table 9-2, which was measured from rainwater samples in the Kettle River Basin. It was not possible to measure HCO_3^- in precipitation samples as the concentration

was below the detection limit. Instead HCO_3^- was calculated using measured pH and the equilibrium reaction $K_2 = [H^+][CO_3^{2-}]/[HCO_3^-]$, assuming the concentration of CO_3^{2-} is insignificant at a pH of 4.7. The equilibrium constant was calculated at 5 °C using equations developed by Telmer and Veizer (1999), which are included in Appendix C. The model also required that SiO_2 and Al^{3+} were present in the basis and so these species were added in very small concentrations (1x 10^{-6} mg/L).

Table 9-2: Composition of precipitation used as the basis for the REACT model. A very small concentration of Fe^{2+} (1 x 10^{-6} mg/L) was required in order for reaction with minerals containing Fe.

Ions	**Ca^{2+}**	**Mg^{2+}**	**Na^+**	**K^+**	**HCO_3^-**	**SO_4^{2-}**	**NO_3^-**	**Cl^-**	**pH**
mg/L	0.96	0.14	0.31	0.07	0.12	0.20	1.37	0.18	4.7

Taking aquifer mineralogy, porosity and groundwater temperature into consideration, the amount of CO_2 consumed in both the Kettle River and Paraná Basins can be estimated. Aquifer mineralogy of the Kettle River Basin was estimated based on description of the geology (BC Geological Survey, 2005; Dostal et al., 2006; Hinchey and Carr, 2006). Mineralogy of aquifers in the Paraná Basin was taken from previous studies. Porosity values were also obtained from previous studies (Sracek and Hirata, 2002; Lastoria et al., 2006). The % volume of each mineral was multiplied by the density to determine the mass of each mineral. The resulting mass was then multiplied by porosity to determine the mass of each mineral added as a reactant in the model. The unit of mass used is grams (g), which when considered over a volume of a cubic centimeter (cm^3), yielded density values within the range of sand and gravel, or bedrock aquifers.

9.4.2 Kettle River Basin

The mineralogy of quaternary sand and gravel aquifers in the Kettle River Basin was estimated based on mineralogy of underlying extrusive and intrusive igneous lithologies within the basin, as these are the dominant lithologies underlying the Kettle River Basin (Figure 2-7). There are several varieties of volcanic and intrusive rocks, which

have different ages and compositions. The relative proportion of these varieties are summarized in Appendix D. The volcanic units, present in highest abundance, are from basalts from the Penticton Group (BC Geological Survey, 2005; Dostal et al., 2006), and intrusive rocks present in the highest abundance are granite and syenite rocks of the Ladybird leucogranite suite (Hinchey and Carr, 2006), part of the Okanagan Batholith (BC Geological Survey, 2005). The mineralogy of basalts from the Penticton Group was obtained from Dostal et al. (2006) and the mineralogy of granites and syenites from the Ladybird Suite was estimated from (Hinchey and Carr, 2006). These two compositions, summarized in Table 9-3, were used as reactants for two scenarios in the React model. In a numerical groundwater model of the Grand Forks aquifer, Allen et al. (2004) used a porosity value of 0.2. Because this project area is located close to the Grand Forks aquifer and has likely undergone similar glacial fluvial history, a porosity value of 0.20 was also assumed for this model. The % volume, density, resulting mass and mass considering porosity are found in Table 9-3. The two scenarios were modelled at 7 °C, which is the average temperature of groundwater samples in the basin.

Table 9-3: Modal composition of lithologies in the Kettle River Basin, used as 'Reactants' in the GWB model. Small proportions (<5 %) of Fe-Ti oxides and apatite were also described in both basalts and leucogranties, however were not included in the model.

Reactants	% volume	Density (g/cm^3)	Mass (g)	Mass (g) considering porosity
Scenario I – Penticton Group basalts				
Anorthite	13.8	2.76	0.38	0.31
Albite	27.8	2.62	0.73	0.58
K-feldspar	11.6	2.56	0.30	0.24
Analcime	16.0	2.27	0.36	0.29
Diopside	26.6	3.23	0.86	0.69
Phlogopite (Biotite)	3.7	2.79	0.10	0.08
Annite (Biotite)	0.5	3.31	0.01	0.01
Total	100.0		2.74	2.19
Scenario II – Ladybird Leucogranitic Suite				
Quartz	29.7	2.65	0.79	0.63
Anorthite	23.9	2.76	0.66	0.53
Albite	6.8	2.62	0.18	0.14
K-feldspar	29.7	2.56	0.76	0.61
Phlogopite (Biotite)	5	2.79	0.14	0.11
Annite (Biotite)	5	3.31	0.17	0.13
Total	100.0		2.69	2.15

The amount of CO_2 reacted/consumed was found to be related to the pCO_2 values in equilibrium with groundwater samples – a greater amount of CO_2 is required to reach a higher pCO_2 value (Figure 9-9). The basaltic scenario required more CO_2 in order to reach a given pCO_2 value compared to granitic scenarios. Basalt contains a higher percentage of mafic minerals which are more easily weathered compared to felsic minerals, for example – quartz, which is the mineral most resistant to weathering. As discussed in Chapter 8, studies have estimated that basalt is eight times more susceptible to weathering than granite. This indicates, a material more susceptible to weathering also consumes more weathering agent – in this case the weathering agent is CO_2.

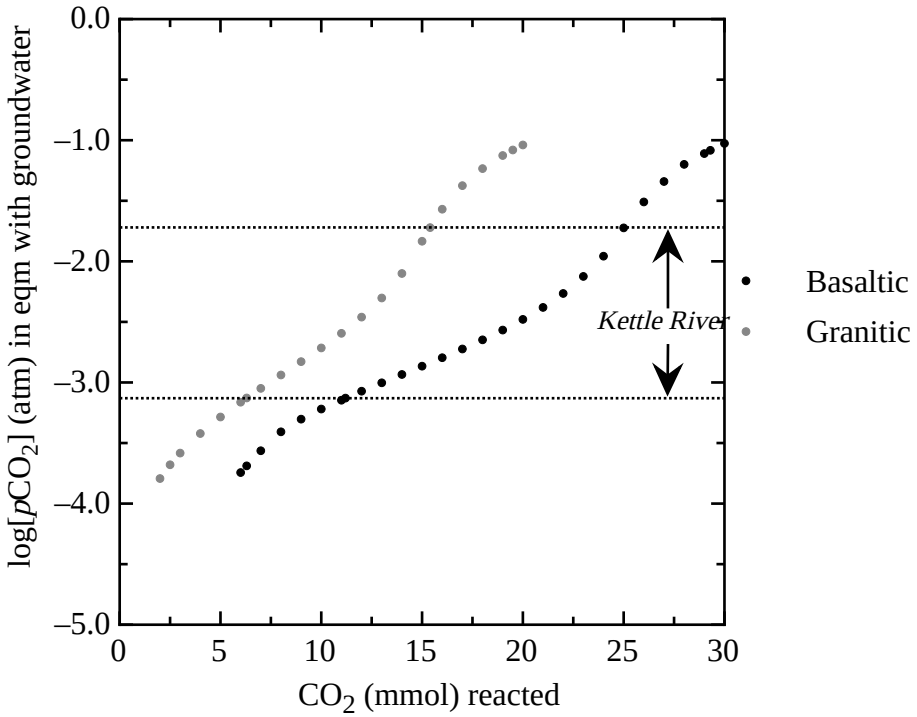

Figure 9-9: Amount of CO_2 reacted versus log[pCO_2] (atm) in equilibrium with groundwater samples at 7 °C. The range of pCO_2 values in equilibrium with groundwater samples from the Kettle River Basin is also shown.

9.4.3 Paraná Basin, Brazil

The mineralogy of the Piramobiòa and Botucatu Formations that comprise the GAS were obtained from Sracek and Hirata (2002). Lastoria et al. (2006) estimated the mineralogy of the Serra Geral Formation. Sracek and Hirata (2002) also estimated the porosities of both aquifers with ranges of the GAS from 0.10 to 0.15 and for the Serra Geral from 0.01 to 0.05. There are other porosity estimates for the GAS, which range up to 0.35, however the consensus in the literature is a value between 0.10 and 0.15 is representative of most of the formation (Sracek and Hirata, 2002; Gastmans et al., 2010a,b). Based on these values, for the REACT model, a porosity of 0.13 was used for the GAS and a value of 0.05 was used for the Serra Geral aquifer. The mineralogy and mass of minerals reacted considering porosity of both GAS and Serra Geral aquifers are summarized in Table 9-4. The two aquifers in Brazil were modeled at 27 °C, which is the average temperature of groundwater samples.

Table 9-4: Minerals used as the reactants in the REACT model for GAS and Serra Geral aquifers. The mass was determined using the same methodology as in Table 9-3.

	GAS		Serra Geral	
Reactants	**% volume**	**Mass (g) considering porosity**	**% volume**	**Mass (g) considering porosity**
Quartz	90.0	2.09	-	-
Amorphous Silica	-	-	12.0	0.24
Anorthite	3.0	0.07	30.0	0.79
Albite	3.0	0.07	10.0	0.25
K-feldspar	3.0	0.07	5.0	0.12
Enstatite	0.5	0.01	17.0	0.52
Diopside	0.5	0.01	16.0	0.50
Forsterite	-	-	5.0	0.15
Fayalite	-	-	5.0	0.21
Total	100.0	2.32	100.0	2.41

As shown in Figure 9-10, the Serra Geral aquifer consumes a much higher amount of CO_2 reacted per cm^3 compared to the GAS. The two aquifers differ in both mineralogy and porosity. Mineralogical variations were discussed in Section 9.4.2 and it is apparent that a higher % volume of mafic materials consumes more CO_2 during weathering. The Serra Geral aquifer contains a higher % of mafic minerals compared to the GAS. There is an order of magnitude difference in porosity between the two aquifers, which may also influence the amount of CO_2 reacted as porosity constrains the area of water-rock interaction. The influence of porosity is addressed in the following section.

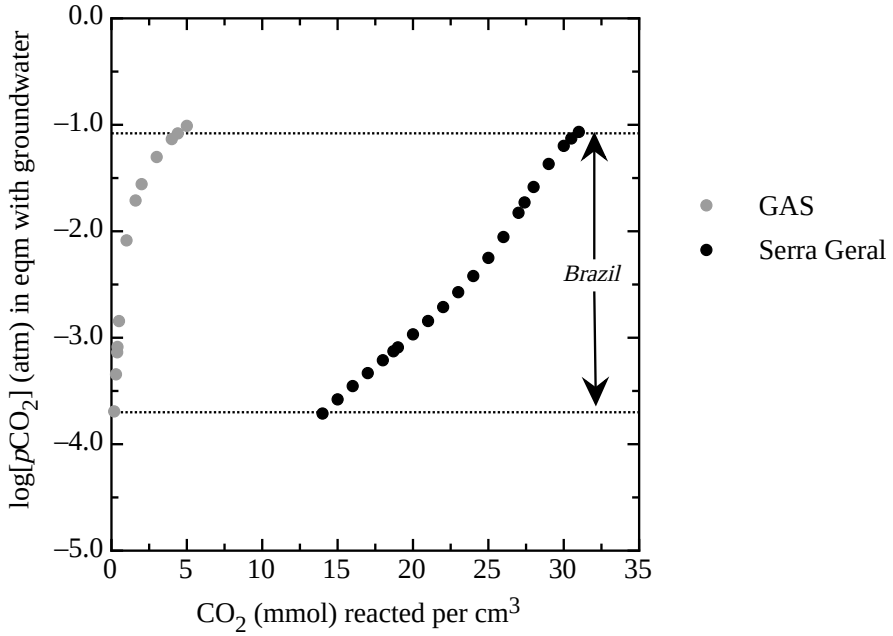

Figure 9-10: Amount of CO_2 reacted versus log[pCO_2] (atm) in equilibrium with groundwater samples from Brazil at 27 °C. The range of pCO_2 values in equilibrium with groundwater samples from aquifers in Brazil is also shown.

9.4.4 Influence of Porosity

The aquifer porosity constrains the physical area for water-rock interactions to occur. In order to assess how porosity influences the amount of CO_2 reacted, different porosity scenarios were considered, keeping the mineralogy and temperature constant. The basaltic aquifer composition summarized in Table 9-3 was used, at a temperature of 7 °C. As shown in Figure 9-11, the scenario with the lowest porosity consumes the most CO_2. The amount of CO_2 consumed to reach pCO_2 values less than ~ $10^{-3.0}$, does not seem to be influenced by porosity. At high pCO_2, the influence of porosity is greater. Aquifer materials with lower porosity have less surface area available for water rock interactions, however there is a greater volume of material available to react. Because the actual surface area of aquifer materials is not considered in this model, it is possible that this modeling scenario is not representative of how changes in porosity influence the amount of CO_2 consumed.

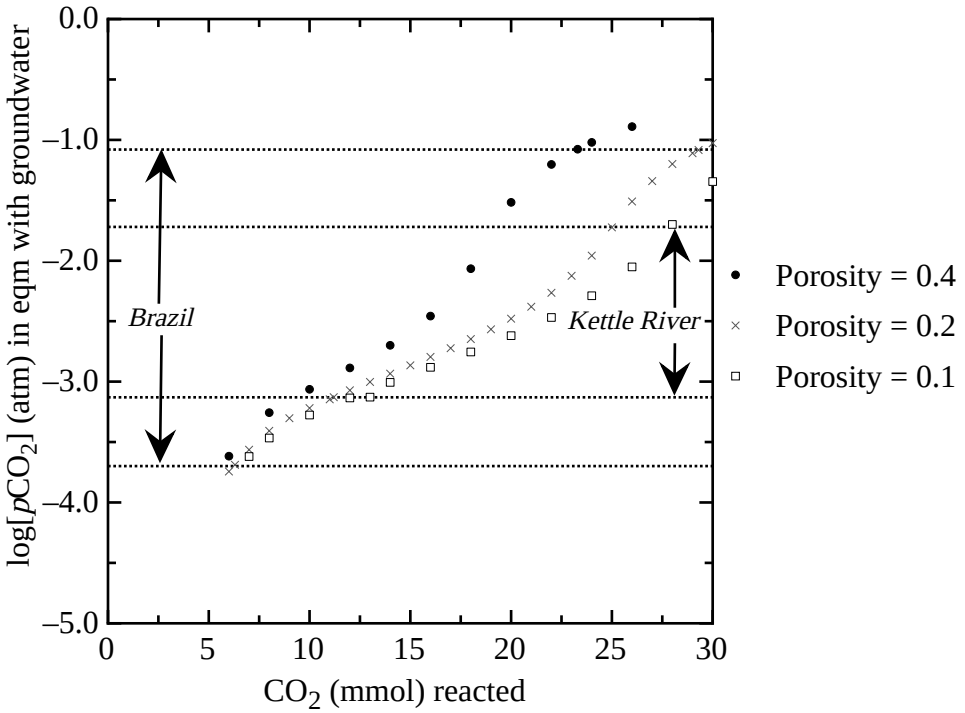

Figure 9-11: Amount of CO_2 reacted versus log[pCO_2] (atm) in equilibrium with groundwater samples at 7 °C, with different porosities. The range of pCO_2 values in equilibrium with groundwater samples from the Kettle River and Paraná Basins are also shown. The volcanic mineralogy from Scenario I summarized in Table 9-3 was used.

9.4.5 Influence of Temperature

The effect of temperature is considered using the average temperatures of groundwater samples from the Kettle River and Paraná Basins – 7 °C and 27 °C, respectively. For both scenarios, mineralogy and porosity were held constant - the mineralogy of the basaltic aquifer summarized in Table 9-3 was used. Results indicate that lower temperatures require more CO_2 to reach pCO_2 in equilibrium with groundwater samples. This effect diminishes as pCO_2 values decrease. For pCO_2 values less than ~$10^{-3.1}$, the opposite trend is observed, indicating more CO_2 is consumed at higher temperatures.

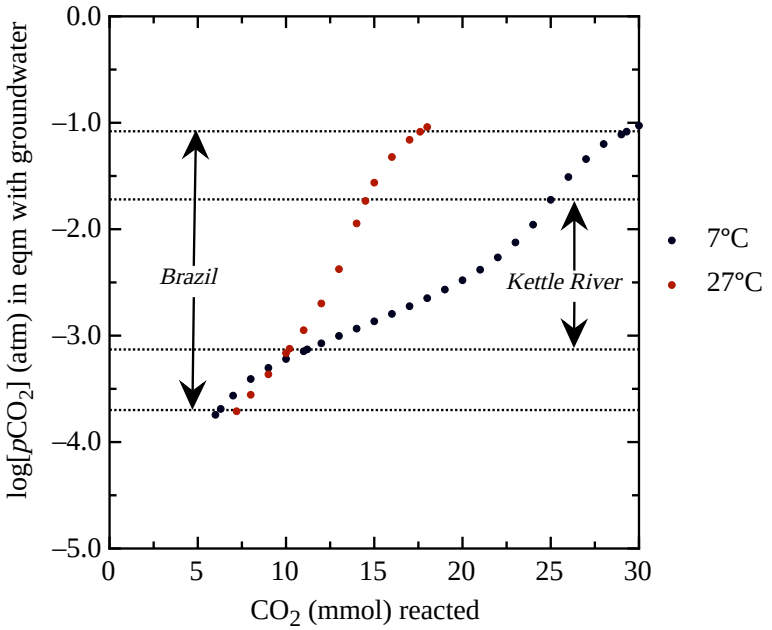

Figure 9-12: Amount of CO_2(g) reacted versus log[pCO_2] (atm) in equilibrium with groundwater samples at 7 °C and 27 °C, the average temperatures of groundwater samples from the Kettle River and Paraná Basins. The volcanic mineralogy from Scenario I summarized in Table 9-3 and a porosity value of 0.20 was used.

9.4.6 Summary of Modeling Scenarios

The amount of CO_2 reacted or consumed was approximated for the aquifers in both the Kettle River and Paraná Basins, and was found to be dependent on both mineralogy and temperature. In general, aquifers with greater proportions of mafic minerals consume more CO_2 due as more CO_2 is consumed during weathering of mafic minerals. The scenario with the lowest porosity consumed the most CO_2, suggesting more CO_2 is consumed when there is a greater volume of materials available to react in the model, however it is also possible that this modeling scenario may not be representative of the influence of porosity on CO_2 consumption. Lower temperatures were found to consume more CO_2 compared to warmer temperatures, except when pCO_2 values were lower than $10^{-3.0}$. Geochemical modeling provided insight into the factors which influence the amount of CO_2 consumed during weathering. The modeled estimate of the amount of CO_2 consumed to reach pCO_2 values in equilibrium with groundwater samples from the

Kettle River and Paraná Basins will now be used to estimate how much CO_2 is consumed by silicate weathering on a basin scale.

9.5 Basin Scale CO_2 Sequestration Associated with Silicate Weathering

Using results from the REACT modeling scenarios, the amount of CO_2 sequestered on a basin scale in both the Kettle River and Paraná Basins can be estimated. In order to compare the consumption between the two climates, the amount must be calculated per volume, as the two basins have different spatial extents. The total amount of CO_2 consumed in each area will also be estimated.

In the Kettle River Basin, a total of 31.4 km^2 of sand and gravel aquifers have been mapped by the Ministry of Environment (MOE), surrounding the communities of Beaverdell, Westbridge, Rock Creek and Midway (BC Ministry of Environment, 2007). There are likely many more aquifers, however they have not been mapped. Allen et al. (2004) reported the average depth to bedrock is ~105 meters in the Grand Forks Aquifer, based on available well logs. As there is limited information available on the depth to bedrock in the Kettle River Basin, an average depth of 105 meters is used as an estimate of aquifer thickness. Using the maximum and minimum pCO_2 in equilibrium with groundwater samples from the Kettle River Basin, the maximum and minimum amount of CO_2 reacted per m^3 in both the basaltic and plutonic aquifer scenarios is calculated. Based on the area of mapped aquifer and average depth to bedrock, the estimated volume of aquifers is 3.3 km^3, equivalent to 3.3×10^9 m^3. The amount of CO_2 required to reach the maximum and minimum pCO_2 values ranges between 2.8×10^5 to 6.8×10^5 g/m^3, as summarized in Table 9-5. Based on these minimum and maximum values for both scenarios, the estimated total amount of CO_2 consumed in mapped aquifers in the Kettle River Basin, ranges between 9.1×10^{14} to 3.6×10^{15} g.

Table 9-5: Amount of CO_2 consumed per m^3 for volcanic and plutonic scenarios, to reach the maximum and minimum pCO_2 values in equilibrium with groundwater samples in the Kettle River Basin.

Scenarios		**pCO_2 (atm)**	**CO_2 consumed in g/m^3**
Scenario I - Basaltic	Minimum	$10^{-3.13}$	4.9×10^5
	Maximum	$10^{-1.72}$	1.1×10^6
Scenario II - Plutonic	Minimum	$10^{-3.13}$	2.8×10^5
	Maximum	$10^{-1.72}$	6.8×10^5

The groundwater samples from the Paraná Basin were obtained from an area of ~500 000 km^2 within the GAS. In the hydrostratigraphic section of the Paraná Basin, the Serra Geral Basalts overlie the GAS for the majority of this area. The spatial distribution of confined and unconfined GAS is depicted in Figure 9-1. The GAS outcrops, and is therefore unconfined for approximately 85 000 km^2. The Serra Geral Formation has an estimated thickness of up to 1200 m (Gastmans et al., 2010a). Sracek and Hirata (2002) described this unit as a regional aquitard, with only the upper 200 meters being an unconfined aquifer. Therefore for the calculations in this section, a depth of 200 meters is used for the Serra Geral aquifer. The average thickness of Botucatu and Piramobiòa Formations were reported to be 138 m and 130 meters, respectively (Sracek and Hirata, 2002). The total thickness of materials where the Serra Geral acts as confining layer is estimated at 468 meters, which is the sum of the average thicknesses of the GAS Formations and the thickness of unconfined Serra Geral basalts. Where the GAS is unconfined, the estimated thickness is 268 meters. The total volume of unconfined Serra Geral basalts is 8.3×10^{13} m^3 and the total volume of confined and unconfined GAS aquifer is 1.3×10^{14} m^3 for a total of 2.2×10^{14} m^3. The maximum and minimum amounts of CO_2 consumed over the total volume ranges from 7.9×10^3 to 1.4×10^6 g/m^3 as summarized in Table 9-6. The estimated total amount of CO_2 consumed in this 500,000 km^2 area of the Paraná Basin ranges between is 5.2×10^{19} to 1.4×10^{20} g.

Table 9-6: Amount of CO_2 consumed per m^3 for Serra Geral and GAS aquifers, to reach the maximum and minimum pCO_2 values in equilibrium with groundwater samples.

Scenarios		**pCO_2 (atm)**	**CO_2 consumed in g/m^3**
Serra Geral	Minimum	$10^{-3.70}$	6.2×10^5
	Maximum	$10^{-1.08}$	1.4×10^6
GAS	Minimum	$10^{-3.70}$	7.9×10^3
	Maximum	$10^{-1.08}$	1.9×10^5

Because of the difference in size of the two basins, the total amount of CO_2 consumed in the Paraná Basin is much greater than that consumed in the Kettle River Basin. However the amount of CO_2 consumed per unit volume in the Kettle River Basin falls within the range of the amount consumed in the Paraná Basin. The amount of CO_2 that has reacted to reach pCO_2 values has been estimated in both basins, however the rate at which CO_2 is consumed has yet to be considered. The amount of CO_2 that reacts per unit time is dependent on how much water enters the system, the rate at which water moves through the system, as well as previously discussed factors such as the amount of weathering agent and the composition of aquifer materials. The flux of water through the aquifer is dependent on intrinsic characteristics of the soil zone and aquifers, specifically, hydraulic conductivity. Quantification of physical variables such as recharge and evapotranspiration and more detailed estimates of hydraulic conductivity and aquifer thicknesses were not within the scope of this project and therefore a quantitative comparison of the rates of CO_2 consumption between the Kettle River and Paraná Basin is not possible.

During silicate weathering CO_2 is consumed and HCO_3^- is produced and therefore the concentration of HCO_3^- in groundwaters can be used to quantify the amount of CO_2 stored in groundwaters in the Kettle River and Paraná Basins. The average HCO_3^- concentration is 193.3 mg/L in the Kettle River Basin, 74.5 mg/L in the GAS and 67.6 mg/L in the Serra Geral aquifer. Given aquifer volumes and porosities of aquifers in each basin, there is ~ 2.1×10^9 moles of HCO_3^- and therefore CO_2, stored in the Kettle River Basin and 2.4×10^{13} moles stored in the Paraná Basin. These values are equivalent to 2.5×10^{-5} gigatons (Gt), equal to a billion tons, of carbon stored in the Kettle River Basin and

0.29 Gt stored in the Paraná Basin. The major global carbon reservoirs estimated by Falkowki et al. (2000) are: > 75,000,000 Gt in the lithosphere (sedimentary carbonates and kerogens), 68,400 Gt in the oceans, 4,130 Gt in fossil fuels, 2000 Gt in the terrestrial biosphere, 1-2 Gt in the aquatic biosphere and 720 Gt in the atmosphere. There is limited information available on the amount of carbon stored in aquifers globally. In the 500,000 km^2 area of the GAS considered here, 0.29 Gt of stored carbon have been estimated. This suggests that the total amount of carbon stored in aquifers globally is likely a major carbon reservoir that has so far received little attention in discussions of the global C cycle.

9.6 Export of CO_2 from Continents to the Ocean

The CO_2 sequestered in aquifers has a finite residence time, as groundwater eventually recharges surface waters. The range in residence times of groundwater ranges from 14 days to 10,000 years (Freeze and Cherry, 1979). In groundwater the HCO_3^- produced during consumption of CO_2 during silicate weathering, eventually discharges into surface waters, where it is transported to the ocean and forms carbonate minerals. As discussed in Chapter 6, the source of HCO_3^- in the Kettle River Basin is ultimately derived from the atmosphere, either through direct infiltration of precipitation water or through uptake and subsequent release of CO_2 in the biosphere and pedosphere. In silicate dominated watersheds, HCO_3^- can almost entirely be from silicate weathering (Meybeck, 2005). Other sources of HCO_3^- include dissolution of primary and secondary calcite. Calcite precipitates were found to be present only in minor amounts within the Kettle River Basin, and therefore it is assumed that the majority of HCO_3^- is sourced from silicate weathering. Therefore the measured amount of HCO_3^- in surface waters can be used to indicate the flux of carbon moving from terrestrial systems to the ocean.

In the Kettle River Basin, a surface water sample was taken along the Canada – US border, which represents the drainage from the entire basin considered in this study. The concentration of HCO_3^- ranges from 27.2 to 79.2 mg/L in June and October, respectively. Proximal to this sampling location is the Ferry hydrometric station, which recorded a

discharge rate of 159.1 and 6.6 m^3/s in June and October, respectively, when the samples were collected. Based on these values, the estimated flux of HCO_3^- leaving the basin ranges from 2.7 x 10^8 to 2.2 x 10^9 moles/year, which is equivalent to the amount of CO_2 consumed per year in the basin. This estimate could be refined if samples were collected every day and correlated to daily discharge. Ludwig et al. (1998) summarized the HCO_3^- flux of major world rivers, which included the Columbia River Basin. The reported flux of HCO_3^- from the Columbia River was 2.48 x 10^{11} moles/year. The area of the Kettle River Basin considered in this project, estimated using ArcGIS, occupies approximately 1.1 % of the Columbia River Basin. The estimated flux of HCO_3^- from the Kettle River is 0.1 to 0.9 % of the flux from the entire Columbia River Basin. The upper end of this estimate (0.9 %) approaches the percentage of area the Kettle River Basin occupies (1.1 %), suggesting the flux of HCO_3^- in the Kettle is approximately proportional to the area. One possible reason the estimated flux from the Kettle River is not exactly proportional to its area could be because the entire Columbia River Basin does not have the same lithological proportions as the Kettle River basin. Lithological proportions of the Columbia River Basin were reported in Amiotte-Suchet et al. (2003).

As mentioned previously, of the carbon released into the atmosphere from burning of fossil fuels, only about half has remained in the atmosphere (Takahashi, 2004). Chemical weathering of silicate minerals was suggested to be a possible sink of CO_2. In order to assess whether this is a possibility, the magnitude of annual fluxes of carbon released from burning of fossil fuels are compared with the fluxes of HCO_3^- from the Kettle River and Columbia River Basins. Anthropogenic burning of fossil fuels has been estimated to release 6.5 to 7 Gt of carbon annually to the atmosphere (Pascala and Socolow, 2004). Ludwig et al. (1998) estimated that 0.625 Gt of carbon of atmospheric or pedospheric origin, is exported annually from continents to the ocean. Of this exported carbon, originating from the atmosphere/pedosphere, 37 % was reported to be exported as HCO_3^-. Of the global annual flux of carbon as HCO_3^- to the oceans, the Kettle River Basin exports 0.0002 to 0.0023 % of HCO_3^- that originated in the atmosphere. Comparison between estimates of carbon fluxes from anthropogenic burning of fossil

fuels and silicate weathering indicates that the carbon flux associated with silicate weathering is likely consuming a small portion of the anthropogenic carbon emitted into the atmospheric annually.

9.7 Conclusion

Chemical weathering of silicate minerals is governed complicated by various factors such as climate, vegetation, lithology and physical erosion. Geochemical modeling allowed for a quantitative estimation of the amount of CO_2 consumed to reach the pCO_2 in equilibrium with groundwater samples in both the Kettle River and the Paraná Basins, as well as quantitative estimates of the influence of lithology, porosity and temperature. More mafic minerals were found to be more susceptible to weathering and therefore consume more CO_2 compared to felsic minerals, indicating basaltic basins likely consume more CO_2 compared to basins underlain by more felsic plutonic rocks. Weathering at lower temperatures consumed more CO_2 compared to higher temperatures suggesting more CO_2 is consumed in climates with lower annual temperatures. Within the scope of this project it was not possible to compare the rate at which CO_2 is consumed in the two different climates of the Kettle River and the Paraná Basins. Considering the average HCO_3^- concentration and the volume and porosity of aquifers, the mass of carbon stored in both the Kettle River and the Paraná Basins was estimated and compared to other major carbon reservoirs, suggesting aquifers may store significant amounts of CO_2, which may not be completely considered in global carbon reservoir estimates. HCO_3^- concentrations in surface water samples in the Kettle River Basin allowed for a quantitative estimate of the annual amount of HCO_3^- exported from the basin, which also allowed for an estimate of the annual amount of CO_2 consumed in the basin by silicate weathering. Compared to the global flux of HCO_3^- from land to the oceans, the Kettle River Basin exported a very small amount, however when the aerial extent of the basin is considered and compared to the Columbia River Basin, this amount is proportional to the size of the Kettle River Basin. Comparison of reported estimates of carbon fluxes of anthropogenic fossil fuel burning to the atmosphere, and riverine fluxes of carbon

originating from the atmosphere/pedosphere to the oceans, suggests silicate weathering is likely consuming a small portion of the anthropogenic carbon emitted annually.

Chapter Ten: Conclusions

The sources and processes influencing water and major anions and cations dissolved in water in the Kettle River basin were investigated using major ion concentrations, stable isotope data and geochemical modeling. Various sources were identified to contribute ions to solution, including: the atmosphere, biosphere, pedosphere, lithosphere and anthropogenic activities. A mass balance approach was used to quantify the proportion of ions derived from weathering of silicate bedrock. Weathering of primary silicate minerals to secondary clay minerals, and ion exchange reactions between clay minerals and solution were investigated using geochemical modelling. The amount of CO_2 consumed to reach pCO_2 values in groundwater samples from the Kettle River and Paraná Basins was calculated in order to investigate the influence of lithology and temperature. Carbon storage in aquifers in the Kettle River Basin and Paraná Basin was compared to global carbon reservoirs, and the flux of carbon exported from the Kettle River Basin was compared to global carbon fluxes.

10.1 Sources and Processes Influencing Water

$\delta^{18}O$ and $\delta^{2}H$ values of precipitation indicate that the dominant sources of precipitation in the Kettle River Basin are weather systems that originate from the Pacific Ocean. Water that enters the basin is subsequently discharged via Kettle and West Kettle Rivers or stored in groundwaters. Comparison between historical average climate, hydrometric and hydrogeologic data with data from 2009 and 2010, indicated that discharge rates and groundwater levels were lower than average. The observed decreases may be due to climatic conditions or anthropogenic surface water and groundwater use, however there was not sufficient climate or anthropogenic water use data available to determine the reason for the decline. $\delta^{18}O$ and $\delta^{2}H$ values of surface water samples deviate from meteoric water lines suggesting evaporation has occurred. Groundwater $\delta^{18}O$ and $\delta^{2}H$ values are within the same range as those of surface water samples suggesting evaporation is occurring during recharge into the uppermost unconfined aquifers.

10.2 Sources and Processes Influencing Solutes

Combining lines of evidence from major ion and stable isotope geochemistry, and geochemical modelling suggests that surface waters are strongly influenced by geochemical compositions of groundwater, but also by atmospheric inputs and anthropogenic activities. The relative proportions of major ions of most surface water samples fell within the range of groundwater samples; a few surface water samples had higher relative proportions of Ca^{2+}, presumably due to ion exchange reactions. Anthropogenic road salt was identified to contribute Na^{+} and Cl^{-} to the West Kettle River and the Kettle River below the confluence. $\delta^{13}C_{DIC}$ values of surface water samples are higher than those of groundwaters, suggesting dissolution of atmospheric CO_2 may contribute DIC to surface waters. Alternatively, processes such as equilibrium with atmospheric CO_2, degassing of CO_2 from the river to the atmosphere, or in-river photosynthesis may also be occurring. The source of NO_3^- in surface water, using a combination of $\delta^{15}N_{NO3}$ and $\delta^{18}O_{NO3}$ values and NO_3^- concentration data, was found to primarily originate from soil nitrification with additional influence from anthropogenic activities downstream from population centers. $\delta^{34}S_{SO4}$ and $\delta^{18}O_{SO4}$ values of most surface water samples were similar to those of groundwater samples, suggesting that the dominant source of SO_4^{2-} is oxidation of sulfide minerals. With increasing distance downstream, surface water $\delta^{18}O_{SO4}$ values increase suggesting additional sources of SO_4^{2-}. The highest $\delta^{18}O_{SO4}$ values fall within the range of atmospheric deposition. Because the majority of atmospheric SO_4^{2-} in industrialized countries originates from anthropogenic activities (Benkovitz et al., 1996; Aravena and Mayer, 2010), a portion of surface water SO_4^{2-} is likely of anthropogenic origin.

Sources of major ions in groundwater samples primarily originate from the lithosphere (bedrock). In contrast, the source of the dominant weathering agent (H_2CO_3) originates primarily from CO_2 in the biosphere/pedosphere and to a lesser degree from the atmosphere. $\delta^{13}C_{DIC}$ values of groundwater samples indicate the dominant source of DIC is from pedospheric CO_2, with minor contributions from calcite dissolution and the

atmosphere. Groundwater $\delta^{15}N_{NO3}$ and $\delta^{18}O_{NO3}$ values indicate that there are a few point sources of anthropogenic NO_3^-, originating from either manure or septic systems, but most groundwater NO_3^- is derived from soil nitrification. $\delta^{34}S_{SO4}$ and $\delta^{18}O_{SO4}$ values of groundwater samples indicate the primary source of SO_4^{2-} is oxidation of sulfide minerals.

Weathering of silicate bedrock and associated CO_2 consumption was identified to contribute Ca^{2+}, Mg^{2+}, Na^+, K^+, SO_4^{2-} and HCO_3^- to solutions. Increased concentrations of Cl^- in surface water and groundwater samples, from anthropogenic activity, caused mass balance calculations to underestimate the role of bedrock weathering. The source of Ca^{2+} and Mg^{2+} was identified to be primarily from weathering of minerals in basalt and the source of Na^+ and K^+ was predominantly from weathering of minerals associated with intrusive volcanic lithologies. Weathering of basalt produces more basic waters, compared to weathering of granite, which encourages formation of secondary calcite.

10.3 Ion Exchange Reactions

The use of simple phase diagrams allowed for identification of probable weathering reactions between primary and secondary minerals. Surface water and groundwater samples were found to be in equilibrium with kaolinite and smectite, once the activities of smectite were considered. Linear relationships were observed, which parallel the stable or metastable equilibrium line on ion activity diagrams, between most smectite varieties suggesting that ion exchange influences surface water and groundwater compositions. The order of smectite activities in the Kettle River basin was found to increases in the following order: Na < K < Ca < Mg. Consistent differences between surface water and groundwater activity ratios, may be attributable to subtle variation in the chemical composition of smectites, or the influence of atmospheric inputs.

10.4 CO_2 Consumption, Storage and Export from Watersheds

CO_2 originating from the atmosphere and the biosphere/pedosphere is consumed during silicate weathering. The amount of CO_2 consumed to reach the pCO_2 in equilibrium with groundwater samples was quantified using geochemical modelling. Comparison between groundwater samples from the Kettle River Basin and the Paraná Basin in Brazil, allowed the effects of lithology and temperature to be considered. Modeling results indicated that the amount of CO_2 consumed to reach pCO_2 in equilibrium with groundwater samples, was greater for mafic minerals compared to felsic minerals, and watersheds with lower average groundwater temperatures consume greater amounts of CO_2 compared to watersheds with higher average temperatures.

HCO_3^- produced during silicate weathering is stored in groundwaters. Using measured HCO_3^- concentrations in groundwater samples and the volume and porosity of aquifers, the mass of carbon stored in the Kettle River and the Paraná Basins were estimated and compared to major global carbon reservoirs. It was concluded that globally, aquifers store a significant amount of CO_2, which may not be completely considered in global carbon reservoir estimates. Rivers export carbon from the continents to the ocean. The annual flux of HCO_3^- exported out of the Kettle River Basin, is small compared to global estimates, but proportional to the area of the Kettle River Basin. The estimated global annual flux of carbon from rivers is much smaller compared to that from anthropogenic fossil fuel burning (Ludwig et al., 1998; Pascala and Socolow, 2004) suggesting that it is possible that silicate weathering consumes a portion of the missing CO_2 released from anthropogenic fossil fuel burning.

10.5 Future Work

Sample collection and analysis, conducted during this project resulted in creation of a chemical and isotopic database, which could be used for future studies in the area. In many places throughout this thesis lack of data prevented more detailed assessments and conclusions. Climate data in the Kettle River Basin could provide further insight into why surface water discharge rates and groundwater levels were lower than average in 2009 and 2010. Mineralogy of bedrock geology, alluvial aquifers and clay minerals would allow for more detailed discussion of active chemical weathering reactions between primary and secondary minerals, and between secondary clay minerals and solutions.

The flux of carbon in and out of watersheds is of recent interest due to anthropogenic influences on the carbon cycle (Butman and Raymond, 2011; Moosdorf et al., 2011). Future research in the Kettle River Basin could focus on quantifying carbon consumption, storage and export in greater detail. Silicate weathering was found to consume CO_2, however the silicate weathering rates were not determined. The amount of carbon stored in aquifers globally could be quantified in greater detail to assess how carbon stored in aquifers compares to major global carbon reservoirs. Export of carbon, discussed in this project, included degasing of CO_2 to the atmosphere, and transport of HCO_3^- in rivers. The rate of CO_2 evasion in the Kettle River Basin could be estimated using flux equations, similar to those described by Dubois et al. (2010). As described by Ludwig et al. (1998), carbon is also exported out of watersheds in the form of dissolved organic carbon and particulate carbon, and hence carbon export from the Kettle River Basin could be assessed in more detail through a more comprehensive sampling and analytical program.

References

Abercrombie, H.J. 1989. *Water-rock interaction during diagenesis and thermal recovery, Cold Lake, Alberta*. Ph.D. Thesis. Department of Geology and Geophysics. University of Calgary, Alberta.

Abercrombie, H.J., Hutcheon, I.E., Bloch, J.D and P. de Caritat. 1994. Silica activity and the smectite-illite reaction. *Geology*. 22: 539-542.

Agriculture and Agri-Food Canada. 2011. Soil Landscapes of Canada. http://res.agr.ca/cansis/nsdb/slc/intro.html [accessed 23 Aug 2011].

Agricultural Land Commission. 2002. About the Agricultural Land Reserve. http://www.alc.gov.bc.ca/alr/alr_main.htm [accessed 25 March 2011].

Agricultural Land Commission. 2011. Agricultural Land Reserve Polygons.

Allen, D.M., Mackie, D.C. and M. Wei. 2004. Groundwater and climate change: a sensitivity analysis for the Grand Forks aquifer, southern British Columbia, Canada. *Hydrogeology Journal* 12: 270-290.

Amiotte Suchet, P., Probst, J. and Ludwig, W. 2003. Worldwide distribution of continental rock lithology: Implications for the atmospheric/soil CO_2 uptake by continental weathering and alkalinity river transport to the oceans. *Global Biogeochemical Cycles* 17(2): 1038-1051.

Anderson, G.M. 1996. *Thermodynamics of Natural Systems*. John Wiley & Sons, Inc., New York, NY.

Andrews, J.A. and W.H. Schlesinger. 2001. Soil CO_2 dynamics, acidification, and chemical weathering in a temperate forest with experimental CO_2 enrichment. *Global Biogeochemical Cycles* 15(1): 149-162.

Appelo, C. A.J. and D. Postma. 2005. *Geochemistry, Groundwater and Pollution*, 2nd ed. A. A. Balkema Publishers, Amsterdam.

Aravena, R. and W.D. Robertson. 1998. Use of Multiple Isotope Tracers to Evaluate Denitrification in Groundwater: Study of Nitrate from a Large Septic System Plume. *Groundwater* 36 (6):975-982.

Aravena, R. and B. Mayer. 2010. Isotopes and Processes in the Nitrogen and Sulfur Cycles, Chapter 7. In *Environmental Isotopes in Biodegradation and Bioremediation* (Aelion, C.M., Höhener, P., Hunkeler, D., Aravena, R. eds). CRC Press. 203-246.

Association of Mineral Exploration British Columbia. 2009. Uranium Exploration, Mining and Development. http://www.amebc.ca/policy/land-access-and-use/uranium-exploration.aspx [accessed 20 September 2010].

Athanasopoulos, P. 2009. *Using Stable Isotopes to Develop A Regional Hydrogeological Model and Characterize Nitrate Sources in Groundwater.* M.Sc. Thesis. Department of Geological Sciences, University of Saskatchewan, Saskatoon, Saskatchewan.

Babiker, I.S., Mohamed, M.A.A., Terao, H., Kat, K. and K. Ohta. 2004. Assessment of groundwater contamination by nitrate leaching from intensive vegetable cultivation using geographical information system. *Environment International* 29(6): 1009-1017.

BC Forests and Range. 2011. Wildfire Management Branch, Wildfire History – Large Fires. http://bcwildfire.ca/History/LargeFires.htm [accessed 15 June 2011].

BC Geological Survey (2005). Digital Geology Maps. http://www.empr.gov.bc.ca/Mining/Geoscience/PublicationsCatalogue/DigitalGeologyMaps/Pages/default.aspx [accessed 15 Feb 2011].

BC Government. 2010. Water Licenses Report. http://a100.gov.bc.ca/pub/wtrwhse/water_licences.input [accessed 2 August 2010].

BC Ministry of Energy and Mines. 2011. Minfile Mineral Inventory. http://minfile.gov.bc.ca/ [accessed 8 July 2011].

BC Ministry of Environment. 1977. Kootenay Air and Water Quality Study Phase 1 – Water Quality in Region 9 The Kettle River Basin. www.env.gov.bc.ca/wat/wq/kootenay/kootenayI9.pdf [accessed 16 September 2010].

BC Ministry of Environment. 2003. Ground Water Wells. https://apps.gob.bc.ca/pub/geometadata/metadataDetail.do?recordUID=3845&recordSet=ISO19115 [accessed 12 May 2011].

BC Ministry of Environment. 2007. Groundwater Aquifers. https://apps.gov.bc.ca/pub/geometadata/metadataDetail.do?recordUID=3841&recordSet=ISO19115 [accessed 12 May 2011].

BC Ministry of Environment. 2010. Observation Well Network. http://www.env.gov.bc.ca/wsd/data_searches/wells/index.html [accessed 5 December 2010].

BC Ministry of Environment. 2011. Soils – Soil Landscapes of BC. http://www.env.gov.bc.ca/soils/landscape/index.html [accessed 23 August 2011].

BC Ministry of Forests, Lands and Natural Resources Operations. 2011. River Forecast Centre. http://bcrfc.env.gov.bc.ca/about/ [accessed 21 October 2011].

BC Parks. 2011. Conservation – British Columbia Heritage Rivers Program. http://www.env.gov.bc.ca/bcparks/heritage_rivers_program/bc_rivers/kettle_river.html [accessed 23 August 2011].

BC Stats. 2006. British Columbia Municipal Census Populations, 1921-2006. http://www.bcstats.gov.bc.ca/data/pop/pop/mun/mun1921_2006.asp [accessed September 16, 2010].

Beaulieu, E., Goddéris, Y., Labat, D., Roelandt, C., Oliva, P. and B. Guerrero. 2010. Impact of atmospheric CO_2 levels on continental silicate weathering. *Geochem. Geophys. Geosyst.* 11(7): 1-18.

Beaulieu, E., Goddéris, Y., Labat, D., Roelandt, C, Calmels, D. and J. Gaillardet. 2011. Modeling of Water-rock interaction in the Mackenzie Basin: competition between sulphuric and carbonic acids. *Chemical Geology* 289: 114-123.

Benkovitz, C.M., Schotlz, M.T., Pacyna, J., Tarrason, L., Dignon, J., Voldner, E.C., Spiro, P.A., Logan, J.A. and T.E., Graedel. 1996. Global gridded inventories of anthropogenic emissions of sulfur and nitrogen. *Journal of Geophysical Research* 101 (D22): 29,239-29,253.

Berardinucci, J. and K. Ronneseth. 2002. *Guide to Using the BC Aquifer Classification Maps For the Protection and Management of Groundwater*. http://www.env.gov.bc.ca/wsd/plan_protect_sustain/groundwater/aquifers/index.html [accessed 25 November 2010].

Berner, R.A., Lasaga, A.C. and R.M. Garrels. 1983. The Carbonate-Silicate Geochemical Cycle and its Effect on Atmospheric Carbon Dioxide over the Past 100 Million Years. *American Journal of Science* 283: 641-683.

Bethke, C.M. 2008. *Geochemical and Biogeochemical Reaction Modelling*, 2nd Ed. Cambridge University Press, Cambridge, UK.

Beusen, A.H.W., Bouwman, A.F., Heuberger, P.S.C., van Drecht, G. and K.W. van der Hoek. 2008. Bottom-up uncertainty estimates of global ammonia emissions from global agricultural production systems. *Atmospheric Environment* 42 (24): 6067-6077.

Bjørlykke, K. and P.K. Egeberg. 1993. Quartz cementation in sedimentary basins. *The American Association of Petroleum Geologists Bulletin* 77(9): 1538-1548.

Bluth, G.J.S. and L.R. Kump. 1994. Lithological and climatologic controls of river chemistry. *Geochimica et Cosmochimica Acta* 58(10): 2341-2359.

Boyer, E.W., Howarth, R.W., Galloway, J., Dentener, F.J., Green, P.A. and C.J. Vörösmarty. 2006. Riverine nitrogen export from the continents to the coasts. Global *Biogeochemical Cycles* 20: 1-9.

Bricker, O. P., Jones, B. F. and C.J. Bowser. 2005. Mass-balance approach to Interpreting Weathering Reactions. In *Watershed Systems in Surface and Groundwater, Weathering and Soils* (Drever J.I. ed) Vol. 5 *Treatise on Geochemistry* (Holland H.D. and Turekian K.K. eds) Elseiver-Pergamon. Oxford. 119-132.

Butman, D. and P.A. Raymond. 2011. Significant efflux of carbon dioxide from stream and rivers in the United States. *Nature Geoscience* 4: 837-842.

BWP Consulting. 2003. *Canada – British Columbia Water Quality Monitoring Agreement, Water Quality Assessment of the Kettle River at Midway (1972 – 2000).* Prepared for Environment Canada and BC Ministry of Environment. http://www.llbc.leg.bc.ca/public/pubdocs/bcdocs/403935/kettle_river_midway.pdf [accessed 27 November 2009].

Canada Post. 2010. Householder Counts and Maps. https://www.canadapost.ca/cpc2/addrm/hh/current/details/tdBCrV0H-e.asp#1A0 [accessed September 16, 2010].

Canfield, D.E. Glazer, A.N. and P.G. Falkowski. 2010. The Evolution and Future of Earth's Nitrogen Cycle. *Science* 330: 192-196.

Casciotti, K.L., Sigman, D.M., Hastings, M.G., Böhlke, J.K. and A. Hiklert. 2002. Measurment of the Oxygen Isotopic Composition of Nitrate in Seawater and Freshwater Using the Denitrifier Method. *Analytical Chemistry* 74: 4905-4912.

Christidis, G.E. 2001. Formation and growth of smectites in bentonites: A case study from Kimolos Island, Aegean, Greece. *Clays and Clay Minerals* 49 (3): 204-215.

Christidis, G. and A.C. Dunham. 1997. Compositional variations in smectites. Part II: alteration of acidic precursors, a case study from Milos Island, Greece. *Clay Minerals* 32: 253-270.

Christopher, P.A. 2005. *Technical Report on Blizzard Uranium Deposit Beaverdell Area, British Columbia, Canada* for Santoy Resources Ltd. www.santoy.ca/i/pdf/BLizzardAug05.pdf [accessed 17 September 2011].

Clague, J.J. and T.S. James. 2002. History and isostatic effects of the last ice sheet in southern British Columbia. *Quaternary Science Reviews* 21: 71-87.

Clark, I. and P. Fritz. 1997. *Environmental Isotopes in Hydrogeology*. CRC Press.

Claypool, G.E., Hoser, W.T., Kaplan, I.R., Sakai, H and I. Zak. 1980. The age curves of sulphur and oxygen isotopes in marine sulphate and their mutual interpretation. *Chemical Geology* 28: 199-260.

Craig, H. 1961. Isotopic variations in meteoric waters. *Science* 133: 1702-1703.

Craig, H. and L.I. Gordon. 1965. Deuterium and oxygen 18 variations in the ocean and the marine atmosphere. In: *Stable Isotopes in Oceanographic Studies and Paleo-Temperatures* (Tongiorgi, E. eds). Laboratorio Di Geologia Nucleare, Pisa. 9-130

Dansgaard, W. 1964. Stable isotopes in precipitation. *Tellus* 16 (4): 436-468.

Dessert, C., Dupré, B., Gaillardet, J., François, L.M. and C.J. Allègre. 2003. Basalt weathering laws and the impact of basalt weathering on the global carbon cycle. *Chemical Geology* 202: 257-273.

Dessouki, T.C.E. 2009. *Canada – British Columbia Water Quality Monitoring Agreement: Water Quality Assessment of the Kettle River at Midway and Carson (1990 – 2007)*. Prepared for the Ministry of Environment. www.env.gov.bc.ca/wat/wq/quality/kettle_midway/kettle-midway07.pdf [accessed 27 November 2009].

Dostal, J., Breitsprecher, K., Church, B.N., Thorkelson, D. and T.S. Hamilton. 2003. Eocene melting of Precambrian lithospheric mantle: Analcime-bearing volcanic rocks from the Challis-Kamloops belt of south central British Columbia. *Journal of Volcanology and Geothermal Research* 126: 303-326.

Drever, J.I. 1994. The effect of land plants on weathering rates of silicate minerals. *Geochimica et Cosmochimica Acta* 58(10): 2325-2332.

Drever J.I. 1997. *The Geochemistry of Natural Waters*, 3rd ed. Prentice Hall Inc. Upper Saddle River, N.J.

Dubois, K.D., Lee, D. and J. Veizer. 2010. Isotopic constraints on alkalinity, dissolved organic carbon, and atmospheric carbon dioxide fluxes in the Mississippi River. *Journal of Geophysical Research* 115: 1-11.

Dupré, B., Dessert, C., Oliva, P., Goddéris, Y., Viers, J., François, L., Millot, R. and J. Gaillardet. 2003. Rivers, chemical weathering and Earth's climate. *Surface Geosciences* 335: 1141-1160.

Environment Canada. 2003. Kettle River at Midway, Federal-Provincial Monitoring Station. http://waterquality.ec.gc.ca/waterqualityweb/stationOverview.aspx?stationId=BC08NN0011 [accessed 22 November 2009].

Environment Canada. 2010a. Canada-British Columbia Water Quality Monitoring Agreement. http://ncrweb.ncr.ec.gc.ca/eaudouce-freshwater/default.asp?lang=En&n=7BE713BE-1 [accessed 2 October 2010].

Environment Canada. 2010b. Archived Hydrometric Data. Water Survey of Canada. http://www.wsc.ec.gc.ca/applications/H2O/index-eng.cfm [accessed 20 August 2010].

Environment Canada. 2010c. Real-time Hydrometric data. http://www.wateroffice.ec.gc.ca/index_e.html [accessed 24 August 2010].

Environment Canada. 2011a. Canadian Climate Normals or Averages 1971-2000. http://www.climate.weatheroffice.gc.ca/climate_normals/index_e.html [accessed 23 August 2011].

Environment Canada. 2011b. Daily Data: Canada's National Climate Archive. http://www.climate.weatheroffice.gc.ca/climateData/dailydata_e.html?StationID=1041&Month=8&Day=22&Year=2011&timeframe=2 [accessed 23 August 2011].

Environment Canada and BC Ministry of Environment. 2007. *Canada – British Columbia Water Quality Agreement, Annual Report 2006 – 2007.* http://www.waterquality.ec.gc.ca/web/Environment~Canada/Water~Quality~Web/assets/PDFs/Reports/ANNUAL%20REPORT%2006-07%20-%20Final.doc [accessed 27 November 2009].

Environment Canada, BC Ministry of Environment and Yukon Department of Environment. 2007. *British Columbia and Yukon Territory Water Quality Report (2001 – 2004): An application of the Canadian Water Quality Index.* http://www.env.gov.bc.ca/wat/wq/wq_sediment.html#data [accessed 6 February 2010].

Ewert, W., Puritch, E., Armstrong, T. and A. Yassa. 2008. *Technical Report and Resource Estimate on the Carmi Molybdenum Deposit, Kettle River Property Greenwood Mining Division, British Columbia* for Hi Ho Silver Resources Inc. P& E Mining Consultants Inc. www.cnq.ca/Storage/1211/108887_Carmi_Technical _Report.pdf [accessed 8 July 2011].

Falkowski, P. Scholes, R.J., Boyle, E., Canadell, J., Canfield, D., Elser, J., Gruber, N., Hibbard, K., Högber, P., Linder, S., Mackenzie, F.T., Moore, B., Pederson, T., Rosenthan, Y., Seitzinger, S., Smetacek, V. and W. Steffen. 2000. The Global Carbon Cycle: A Test of Our Knowledge of Earth as a System. *Science* 290: 291-296.

Faure, G. 1998. *Principles and Applications of Geochemistry*, 2nd ed. Prentice-Hall, Inc., Upper Saddle River, NJ.

Freeze, R.A. and J.A. Cherry. 1979. Groundwater. Prentice-Hall, Inc. Englewood Cliffs, N.J.

Gabrielse, H. and C.J. Yorath. 1991. Chapter 1: Introduction. In: *Geology of the Cordilleran Orogen in Canada* (Gabrielse, H. and Yorath, C.J., eds.). Geological Survey of Canada, Ottawa, 3-11.

Gaillardet, J., Dupré, B., Louvat, P. and C.J. Allègre. 1999. Global silicate weathering and CO_2 consumption rates deduced from the chemistry of large rivers. *Chemical Geology* 159: 3-30.

Galloway, J.N. and E.B. Cowling. 2002. Reactive Nitrogen and The World: 200 Years of Change. *A Journal of the Human Environment* 31: 64-71.

Galloway, J.N., Dentener, F.J., Capone, D.G., Boyer, E.W., Howarth, R.W., Seitzinger, S.P. Asner, G.P., Cleveland, C.C., Green, P.A., Holland, E.A., Karl, D.M., Michaels, A.F., Porter, J.H., Townsend, A.R. and C.J.Vörösmarty. 2004. Nitrogen cycles, past, present, and future. *Biogeochemistry* 70: 153-226.

Galloway, J.N., Townsend, A.R., Erisman, J.W., Bekunda, M., Cai, Z., Freney, J.R., Martinelli, L.A., Seitzinger, S.P. and M.A., Sutton. 2008. Transformations of the Nitrogen Cycle: Recent Trends, Questions, and Potential Solutions. *Science* 320: 889-892.

Garrels, R.M., and F.T. Mackenzie. 1967. Origin of the chemical compositions of some springs and lakes. In *Equilibrium Concepts in Natural Systems* (Stumm, W. ed) *Advances in Chemistry Series 67*. American Chemical Society. Washington, D.C. 222-242.

Gastmans, D., Chang, H.K. and I. Hutcheon. 2010a. Groundwater geochemical evolution in the northern portion of the Guarani Aquifer System (Brazil) and its relationship to diagenetic features. *Applied Geochemistry* 25: 16-33.

Gastmans, D., Chang, H.K. and I. Hutcheon. 2010b. Stable isotopes (^{2}H, ^{18}O and ^{13}C) in groundwaters from the northwestern portion of the Guarani Aquifer System (Brazil). *Hydrogeology Journal* 18: 1497-1513.

Gislason, S.R., Oelkers, E.H., Eiriksdotter, E.S., Kardjilov, M.I., Gisladottir, G., Sigfusson, B., Snorrason, A., Elefsen, S., Hardardottir, J., Torssander, P. and N. Oskarsson. 2009. Direct evidence of the feedback between climate and weathering. *Earth and Planetary Science Letters* 277: 213-222.

Grasby, S.E. 1997. *Controls on the Chemistry of the Bow River, Southern Alberta, Canada*. Ph.D. thesis, Department of Geology and Geophysics. University of Calgary, Alberta.

Grasby, S.E., Hutcheon, I., McFarland, L. 1999. Surface-water-groundwater interaction and the influence of ion exchange reactions on river chemistry. *Geology* 27(3): 223-226.

Gruber, N. and N. Galloway. 2008. An Earth-system perspective of the global nitrogen cycle. *Nature* 451: 293-296.

Health Canada. 2010. Guidelines for Canadian Drinking Water Quality – Summary Table. Environmental and Workplace Health. http://www.hc-sc.gc.ca/ewh-semt/pubs/water-eau/2010-sum_guide-res_recom/index-eng.php [accessed 10 November 2011].

Hi Ho Silver Resources Inc. 2011. Hi Ho Silver Resources Inc. – Carmi, BC. http://www.hihoresources.com/?page_id=61 [accessed 8 July 2011].

Hinchey, A.M. and S.D. Carr. 2006. The S-type Ladybird leucogranite suite of southeastern British Columbia: Geochemical and isotopic evidence for a genetic link with migmatite formation in the North American basement gneisses of the Monashee complex. *Lithos* 90: 223-248.

Hollocher, T.C. 1984. Source of the Oxygen Atoms of Nitrate in the Oxidation of Nitrite by *Nitrobacter agili* and evidence against a P-O-N Anhydride Mechanism in Oxidative Phosphoylation. *Archvies of Biochemistry and Biophysics* 233(2): 721-727.

Intigold Mines Ltd. 2011. Beaverdell Property. http://intigold.com/beaverdell-property/ [accessed 9 July 2011].

Isotope Science Lab. 2011. Instrumental Techniques used in the ISL. http://www.ucalgary.ca/uofcisl/node/5 (accessed 30 November 2011).

Keeling, R.F., S.C Piper, A.F. Bollenbacher and J.S. Walker. 2009. Atmospheric CO_2 records from sites in the SIO air sampling network. In Trends: A Compendium of Data on Global Change. Carbon Dioxide Information Analysis Center, Oak Ridge National Laboratory, U.S. Department of Energy, Oak Ridge, T.N. http://cdiac.ornl.gov/trends/co2/sio-mlo.html [accessed 22 November 2011].

Kelly, W.R., Panno, S.V., Hackley, K.C., Hwang, H. H., Martinsek, A.T. and M. Markus. 2010. Using chloride and other ions to trace sewage and road salt in the Illinois Waterway. *Applied Geochemistry* 25 (5): 661-6.

Kendall, C., Elliott, E.M., and S. D. Wankel. 2007. Tracing anthropogenic inputs of nitrogen to ecosystems, Chapter 12. *In Stable Isotopes in Ecology and Environmental Science*, 2nd edition (Michener R.H. and Lajtha K. eds) Blackwell Publishing. 375-449.

Kinross Gold Corporation. 2009. Operation: Kettle River-Buckhorn USA. http://www.kinross.com/operations/operation-kettle-river-buckhorn-usa.aspx [accessed 7 July 2011].

Klein, C. 2002. *The 22nd Edition of the Manual of Mineral Science*. John Wiley & Sons, Inc., New York, NY.

Labat, D., Goddéris,Y., Probst, J.L. and J.L. Guyot. 2004. Evidence for global runoff increase related to climate warming. Advances in Water Resources 27(6): 631-642.

Lastoria, G., Sinelli, O., Kiang, C.H., Hutcheon, I., Filho, A.C.R. and D. Gastmans. 2006. Hydrogeology of the Serra Geral Formation, Paraná Sedimentary Basin in Mato Grosso Do Sul State, Brazil. *Águas Subterrâneas* 20 (1): 139-150.

Lerman, A. and L. Wu. 2006. CO_2 and sulphuric acid control of weathering and river water composition. *Journal of Geochemical Exploration* 88: 427-430.

Ludwig, W., Amiotte-Suchet, P., Munhoven, G. and J. Probst. 1998. Atmospheric CO_2 consumption by continental erosion: present-day controls and implications for the last glacial maximum. *Global and Planetary Change* 16-17: 107-120.

Mayer, B., Boyer, E.W., Goodale, C., Jaworski, N.A., van Breemen, N., Howarth, R.W., Seitzinger, S., Billen, G., Lajtha, K., Nadelhoffer, K., van Dam, D., Hetling, L.J., Nosal, M. and K. Paustian. 2002. Sources of nitrate in rivers draining sixteen watersheds in northeastern U.S.: Isotopic constraints. *Biogeochemistry* 57/58: 171-197.

Mayer, B. 2005. Assessing Sources and Transformations of Sulfate and Nitrate in the Hydrosphere Using Isotope Techniques, Chapter 6. In *Isotopes in the Water Cycle* (Aggarwal, P.K., Gat, J.R. and Froehlich, K.F.O eds) Springer. Netherlands.

McFarland, L.M. 1997. *Using the Chemical and Isotopic Characteristics of Drinking Water to Determine Sources of Potable Water and Subsurface Geological Controls on Water Chemistry, Stoney Indian Reserve, Morley, AB.* M.Sc. Thesis, Department of Geology and Geophysics. University of Calgary, Alberta.

Meybeck, M. 2005. Global Occurrence of Major Elements in Rivers. In *Watershed Systems in Surface and Groundwater, Weathering and Soils* (Drever J.I. ed) Vol. 5 *Treatise on Geochemistry* (Holland H.D. and Turekian K.K. eds) Elsevier-Pergamon. Oxford. 207-223.

Millot, R., Gaillardet, J., Dupré, B. and C.J. Allègre. 2002. The global control of silicate weathering rates and the coupling with physical erosion: new insights from rivers of the Canadian Shield. *Earth and Planetary Science Letters* 196: 83-98.

Millot, R., Gaillardet, J., Dupré, B. and C.J. Allègre. 2003. Northern latitude chemical weathering rates: Clues from the Mackenzie River Basin, Canada. *Geochimica et Cosmochimica Acta* 67(7): 1305-1329.

Monger, J.W.H., Price, R.A. and D.J. Tempelman-Kluit. 1982. Tectonic accretion and the origin of the two major metamorphic and plutonic welts in the Canadian Cordillera. *Geology* 10(2): 70-75.

Mook, W.G., Bommerson, J.C. and W.H. Staverman. 1974. Carbon isotope fractionation between dissolved bicarbonate and gaseous carbon dioxide. *Earth and Planetary Science Letters 22*: 169-174.

Moosdorf, N., Hartman, J., Lauerwald, R., Hagedorn, B. and S. Kempe. 2011. Atmospheric CO_2 consumption by chemical weathering in North America. *Geochimica et Cosmochimica Acta* 75: 7829-7854.

Nadeau, P.H. and D.C.Bain. 1986. Composition of some smectites and diagentic illitic clays and implications for their origin. *Clays and Clay Minerals* 34(4): 455-464.

Nesbitt, B.E. and K. Muehlenbachs. 1995. Geochemistry of syntectonic, crustal fluid regimes along the Lithoprobe Southern Canadian Cordillera Transect. *Canadian Journal of Earth Science* 32: 1699-1719.

Outdoor Recreation Council of BC. 2011. The Endangered Rivers List. http://www.orcbc.ca/pro_endangered.htm [accessed 12 December 2011].

Parrish, R.R., Carr, S.D. and D.L. Parkinson. 1988. Eocene Extensional Tectonics and Geochronology of the Southern Omineca Belt, British Columbia and Washington. *Tectonics* 7(2): 181-212.

Pascala S. and R. Socolow. 2004. Stabilization Wedges: Solving the Climate Problem for the Next 50 Years with Current Technologies. *Science* 305: 968-971.

Pommen Water Quality Consulting. 2003. *Water Quality Assessment of Myers Creek at the International Boundary (1998-2002*). Canada-British Columbia Water Quality

Monitoring Agreement. www.env.gov.bc.ca/wat/wq/quality/myers/myers_creek.pdf [accessed 2 October 2010].

Pope & Talbot. 2008. Our Company History. http://www.poptal.com/about/history.htm [accessed 24 August 2011].

Price, R.A. and J.W.H. Monger. 2000. *A transect of the southern Canadian Cordillera from Calgary to Vancouver*. Geological Association of Canada, Cordilleran Section, Vancouver, BC.

Regional District of Kootenay Boundary. 2011. Kettle River Watershed Committee. http://rdkb.com/HotTopics/KettleRiverWatershedCommittee.aspx [accessed 12 December 2011].

Robert, C. and B. Goffe. 1992. Zeolitization of basalts in subaqueous freshwater settings: Field observations and experimental study. *Geochimica et Cosmochimica Acta* 57: 3597-3612.

Rocchini, R. J., J. C. Arber, J. J. Feddes, L. A. Gregory, and L. W. Pommen. 1977. *Kootenay Air and Water Quality Study Phase I. Water Quality in Region 9, The Kettle River Basin.* Water Investigations Branch, Ministry of Environment. http://www.env.gov.bc.ca/wat/wq/wq_sediment.html#kootenay [accessed 27 November 2009].

Sabine, C.L., Feely, R.A., Gruber, N., Key, R.M., Lee, K., Bullister, J.L., Wanninkhof, R., Wong, C.S., Wallace, D.W.R., Tilbrook, B., Millero, F.J., Peng, T., Kozyr, A., Ono, T. and A.F. Rios. 2004. The Oceanic Sink for Anthropogenic CO_2. *Science* 305: 367-371.

Seal, II, R.R., Alpers, C.N. and R.O. Rye. 2000. Stable Isotope Systematics of Sulfate Minerals. *Reviews in Mineralogy and Geochemistry* 40(1): 541-602.

Seal, R.R. 2006. Sulfur Isotope Geochemistry of Sulfide Minerals. *Reviews in Mineralogy and Geochemistry* 61: 633-677.

Schindler, D.W., Dillon, P.J. and H. Schreier. 2006. A review of anthropogenic sources of nitrogen and their effects on Canadian aquatic ecosystems. *Biogeochemistry* 79: 25-44.

Seitzinger, S.P., Styles, R.V., Boyer, E.W., Alexander, R.B., Billen, G., Howarth, R.W., Mayer, B. and N. van Breemen. 2002. Nitrogen Retention in rivers: model development and application to watersheds in northeastern U.S.A. *Biogeochemistry* 57/58: 199-237.

Siever, R. 1968. Sedimentological consequences of a steady-state ocean atmosphere. *Sedimentology* 11: 5-29.

Sigman, D.M., Cascoitti, K.L., Andreani, M., Barford, C., Galanter, C. and J.K. Böhlke. 2001. A Bacterial Method for Nitrogen Isotopic Analysis of Nitrate in Seawater and Freshwater. *Analytical Chemistry* 74: 4905-4912.

Sprout, P.N. and C.C. Kelly. 1964. *Soil Survey of the Kettle River Valley in the Boundary District of British Columbia – Report No. 9 of the British Columbia Soil Survey*. BC Department of Agriculture, Kelowna, BC and Research Branch, Canada Department of Agriculture. http://sis.agr.gc.ca/cansis/publications/bc/bc9/intro.html [accessed 7 July 2011].

Smil, V. 2002. Nitrogen and Food Production: Protein for Human Diets. *A Journal of the Human Environment* 31: 126-131.

Socolow, R.H. 1999. Nitrogen management and the future of food: Lessons from the management of energy and carbon. *Proceedings of the National Academy of Sciences of the United States of America* 96: 6001-6008.

Spence, J. and K. Telmer. 2005. The role of sulphur in chemical weathering and atmospheric CO_2 fluxes: Evidence from major ions, $\delta^{13}C_{DIC}$, and $\delta^{34}S_{SO4}$ in rivers in the Canadian Cordillera. *Geochimica et Cosmochimica Acta* 69: 5441-5458.

Sracek, O. and R. Hirata. 2002. Geochemical and stable isotopic evolution of the Guarani Aquifer System in the state of São Paulo, Brazil. *Hydrogeology Journal* 10: 643-655.

Stallard, R.F. 1995. Tectonic, Environmental and Human Aspects of Weathering and Erosion: A Global Review using a Steady-State Perspective. *Annu. Rev. Earth Planet. Sci.* 23: 11-39.

St. Elias Mines. 2011. St. Elias Mines - Beaverdell Project, Canada. http://www.steliasmines.com/canada3.htm [accessed 7 July 2011].
Takahashi, T. 2004. The Fate of Industrial Carbon Dioxide. *Science* 305: 352-353.

Telmer, K. and J. Veizer. 1999. Carbon fluxes, pCO_2 and substrate weathering in a large northern river basin: carbon isotope perspectives. *Chemical Geology* 159: 61-86.

United States Geologic Survey (USGS). 2010. USGS Real-Time Data for USGS 12401500 Kettle River Near Ferry, WA. http://waterdata.usgs.gov/nwis/uv?12401500 [accessed 20 August 2010].

United States Geological Survey. 2011. USGS 12401500 Kettle River near Ferry, WA. http://waterdata.usgs.gov/nwis/nwisman/?site_no=12401500&agency_cd=USGS [accessed 23 August 2011].

van Breemen, N., Boyer, E.W., Goodale, C.L., Jawarski, N.A., Paustian, K., Seitzinger, S.P., Lajtha, K., Mayer, B., van Dam, D., Howarth, R.W., Nadelhoffer, K.J., Eve, M. and G. Billen. 2002. Where did all the nitrogen go? Fate of nitrogen inputs to large watersheds in the northeastern U.S.A. *Biogeochemistry* 57/58: 267-293.

Village of Midway, BC, 2009. Midway Emergency Plan. www.midwaybc.ca [accessed 8 July 2011].

Virginia Energy Resources Inc. 2011. Blizzard Uranium Deposit, British Columbia. http://www.santoy.ca/s/Blizzard.asp [accessed 7 July 2011].

Vitousek, P.M., Aber, J.D., Howarth, R.W., Likens, G.E., Matson, P.A., Schindler, D.W., Schlesinger, W.H. and D.G. Tilman. 1997. Human Alteration of the Global Nitrogen Cycle: Sources and Consequences. *Ecological Applications* 7(3): 737-750.

Walker, J.C.G., Hays, P.B. and J.F. Kastings. 1981. A negative feedback mechanism for the long term stabilization of earth's surface temperature. *Journal of Geophysical Research* 86(10): 9776-9782.

Warrington, P.D. 1998. *Road Salt and Winter Maintenance for British Columbia Municipalities*, Ministry of Environment. http://www.env.gov.bc.ca/wsd/data_searches/wrbc/index.html [accessed 16 June 2011].

Wassenaar, L.I., Hendry, M.J. and N. Harrington. 2006. Decadal Geochemical and Isotopic Trends for Nitrate in a Transboundary Aquifer and Implications for Agricultural Beneficial Management Practices. *Environmental Science and Technology:* 40: 4626-4632.

Wassenaar, L.I., Athanasopoulos, P., Hendry, M.J. 2011. Isotope hydrology of precipitation, surface and ground waters in the Okanagan Valley, British Columbia, Canada. *Journal of Hydrology* 411: 37-48.

Webber, T. N. and L. W. Pommen. 1996. *State of Water Quality of the Kettle River at Midway (1980-1994)*. Water Quality Branch, BC Environment. http://www.env.gov.bc.ca/wat/wq/quality/wqbcm/wqbcm.html [accessed 22 November 2009].

Wei, M., Kohut, A.P., Kalyn, D. and F. Chwojka. 1993. Occurrence of nitrate in groundwater, Grand Forks, British Columbia. *Quaternary International* 20: 39-49.

Wei, M., D. M. Allen, V. Carmichael, and K. Ronneseth. 2010. *State of Understanding of the Hydrogeology of the Grand Forks Aquifer.* Ministry of Environment, Simon Fraser University. http://www.env.gov.bc.ca/wsd/plan_protect_sustain/groundwater/library/aquifers/gf_report_feb_5-10.pdf [accessed 1 September 2010].

West, J., Galy, A. and Bickle, M. 2005. Tectonic and climatic controls on silicate weathering. *Earth and Planetary Science Letters* 235: 211-228.

Westgate, E.J., Kroeger, K.D., Pabich, W.J. and I.Valiela. 2000. Fate of Anthropogenic Nitrogen in a Nearshore Cape Cod Aquifer. *Ecology, Biogeochemistry, and Population Biology* 199: 221-223.

White, A. and A. Blum. 1995. Effects of climate on chemical weathering in watersheds. *Geochimica et Cosmochimica Acta*. 59(9): 1729-1747.

Whitehead, P.G., Wilby, R.L., Battarbee, R.W., Kernan, M. and A.J. Wade. 2009. A review of the potential impacts of climate change on surface water quality. *Hydrological Science Journal* 54(1): 101-123.

Winter, J.D. 2001. *An introduction to igneous and metamorphic petrology.* Prentice-Hall Inc., Upper Saddle River, NJ.

Wolters, F., Lagaly, G., Kah, G., Nueesch, R. and K Emmerich. 2009. A comprehensive characterization of dioctahedral smectites. *Clays and Clay Minerals* 57 (1): 115-33.

Xue, D., Botte, J., De Baets, B., Accoe, F., Nestler, A., Talyer, P., van Cleemput, O., Berglund, M. and P. Boeckx. 2009. Present limitations and future prospects of stable isotopes methods for nitrate source identification in surface- and groundwater. *Water Research* 43: 1159-1170.

Yang, C., Telmer, K. and J.Veizer. 1996. Chemical dynamics of the "St.Lawrence" riverine system: δD_{H2O}, $\delta^{18}O_{H2O}$, $\delta^{13}C_{DIC}$, $\delta^{34}S_{sulfate}$, and dissolved $^{87}Sr/^{86}Sr$. *Geochimica et Cosmochimica Acta* 60: 851-866.

Yonge, C., Goldenberg, L. and H.R. Krouse. 1989. An isotope study of water bodies along a traverse of southwestern Canada. *Journal of Hydrology* 106: 245-255.

YSI Inc. 2011. YSI 600XLM Specifications. http://www.ysi.com/productsdetail.php?600XL-and-600XLM-7 [accessed 6 December 2011].

APPENDIX A:

Table A-1: Surface water sample identification, location and distance from the headwaters of Kettle and West Kettle Rivers. The distance from the headwaters, below the confluence is shown from the headwaters of the Kettle River.

Section	Name	Sample ID			Location		Distance from headwaters (km)
		Oct. 2009	June 2010	Oct. 2010	N	W	
Below the Confluence	BORDER	-	28	100	49.000 °	-118.767 °	207
	MIDWAY	1	27	101	49.004 °	-118.776 °	206
	BICK	-	35	109	49.008 °	-118.833 °	202
	BUGEAUD	-	26	108	49.027 °	-118.867 °	197
	INGRAM	2	29	107	49.043 °	-118.877 °	195
	KVB	3	30	106	49.057 °	-118.944 °	190
	PUB	4	31	105	49.060 °	-119.002 °	185
	KVCAMP	5	32	104	49.110 °	-118.979 °	178
Kettle River	FIVA	7	34	102	49.230 °	-118.928 °	160
	LOST	8	36	117	49.382 °	-118.876 °	137
	DEAR	9	39	118	49.500 °	-118.825 °	120
	GRANO	10	40	119	49.564 °	-118.795 °	111
	GOAT	11	41	120	49.632 °	-118.775 °	100
	KRCROSS	12	42	121	49.797 °	-118.714 °	79
	BRUER	13	43	122	49.953 °	-118.679 °	60
	HWY6	14	44	123	50.059 °	-118.508 °	41
	KEEF	15	45	124	50.130 °	-118.363 °	0
West Kettle River	WESTBRG	6	33	103	49.170 °	-118.975 °	105
	RHONE S	16	38	110	49.205 °	-119.008 °	100
	RHONE N	17	37	116	49.256 °	-119.011 °	93
	TUZO	18	25	115	49.378 °	-119.097 °	73
	BEAVERDELL	19	24	114	49.435 °	-119.092 °	65
	CARMI	20	71	113	49.789 °	-119.036 °	57
	TRAP	21	47	112	49.564 °	-119.055 °	47
	BW	22	46	111	49.495 °	-119.122 °	18

Table A-2a: Surface water samples from October 2009: Field Measurements

		Field Measurements			
Section	**ID**	**pH**	**Temp. (°C)**	**Cond. (µS/cm)**	**DO (mg/L)**
Below the Confluence	1	8.0	2.77	156	12.6
	2	8.1	2.77	144	12.8
	3	8.1	2.75	142	12.6
	4	8.1	2.79	136	12.7
	5	8.0	2.81	134	12.4
Kettle River	7	7.5	2.82	115	11.7
	8	7.6	2.18	99	12.4
	9	7.7	2.55	93	12.0
	10	7.7	1.77	86	12.6
	11	7.7	1.37	92	12.7
	12	7.7	1.93	106	12.1
	13	7.9	1.09	122	12.5
	14	8.0	2.29	169	11.7
	15	8.0	0.81	84	11.3
West Kettle River	6	7.9	3.01	172	11.8
	16	7.7	0.86	205	13.0
	17	7.7	1.47	197	13.0
	18	7.9	0.49	185	13.1
	19	7.9	-0.98	127	13.8
	20	7.8	-0.84	116	14.1
	21	8.0	-0.93	88	13.7
	22	8.4	-0.95	-	13.3

Table A-2b: Surface water samples from June 2010: Field Measurements

Section	Field Measurements				
	ID	**pH**	**Temp. (°C)**	**Cond. (µS/cm)**	**DO (mg/L)**
Below the Confluence	28	7.7	6.88	54	11.1
	27	7.7	6.84	60	11.1
	35	7.7	7.96	49	11.2
	26	7.8	6.70	58	11.1
	29	7.7	6.91	51	11.3
	30	7.7	7.15	50	11.2
	31	7.6	7.15	60	11.3
	32	7.5	6.25	43	11.5
Kettle River	34	7.5	6.42	37	11.6
	36	7.4	5.69	36	11.6
	39	7.7	5.40	31	11.6
	40	7.7	5.09	32	11.6
	41	7.9	5.17	35	11.6
	42	7.9	5.36	48	11.3
	43	7.8	5.14	31	11.4
	44	8.2	6.54	113	10.9
	45	7.9	10.00	78	10.7
West Kettle River	33	7.6	6.92	46	11.6
	38	7.8	9.07	48	10.7
	37	7.8	8.54	46	10.8
	25	7.5	6.10	50	10.6
	24	7.6	5.82	39	10.7
	71	7.6	7.43	31	10.9
	47	7.6	5.18	24	11.5
	46	7.8	4.29	17	11.3

Table A-2c: Surface water samples from October 2010: Field Measurements

Section		Field Measurements			
	ID	pH	Temp. (°C)	Cond. (µS/cm)	DO (mg/L)
Below the Confluence	100	7.9	4.50	144	12.4
	101	8.0	4.56	145	12.6
	109	8.2	4.21	142	13.9
	108	8.0	3.61	134	13.9
	107	7.7	1.56	135	13.4
	106	8.3	5.08	131	13.2
	105	8.1	5.25	126	12.9
	104	8.0	4.77	124	12.9
Kettle River	102	7.9	4.34	104	12.7
	117	7.4	-0.30	101	13.6
	118	7.5	0.22	93	13.3
	119	7.5	-0.51	88	13.8
	120	7.6	-0.75	95	13.8
	121	7.7	-0.51	110	13.5
	122	7.6	-0.57	67	13.1
	123	8.0	0.82	174	12.6
	124	7.9	3.87	90	11.2
West Kettle River	103	8.2	3.07	151	13.8
	110	7.2	-1.43	149	14.8
	116	7.9	1.51	141	13.2
	115	7.7	0.46	133	13.5
	114	7.6	-1.89	86	14.2
	113	7.6	-2.25	84	14.3
	112	7.5	-2.93	62	14.5
	111	7.6	-3.26	53	18.8

Table A-3a: Surface water samples from October 2009: Major Anions, Cations and Silica . CB = Charge Balance

		Anions (mg/L)				Cations (mg/L)					
Section	**ID**	**HCO_3^-**	**NO_3^-**	**Cl^-**	**SO_4^{2-}**	**Ca^{2+}**	**Mg^{2+}**	**Na^+**	**K^+**	**Si^{4+}**	**CB (%)**
Below the Confluence	1	103	1.70	2.9	7.8	24	3.9	4.1	1.01	5.7	-6.1
	2	91	-	2.6	6.8	22	3.3	3.7	1.00	5.6	-3.7
	3	93	0.087	2.1	6.5	22	3.2	3.4	0.94	5.7	-5.9
	4	82	0.011	1.88	6.2	21	3.1	3.4	0.93	5.7	-1.6
	5	83	0.023	1.88	6.0	21	2.9	2.9	0.94	5.7	-3.0
Kettle River	7	72	0.29	1.03	4.8	18.3	2.5	2.4	0.75	5.4	-2.8
	8	68	-	0.81	4.3	16.0	2.3	2.1	0.73	5.4	-5.3
	9	68	0.051	0.70	4.1	14.7	1.92	1.91	0.68	5.3	-10.5
	10	57	-	0.67	3.2	14.0	1.76	1.83	0.61	5.0	-3.8
	11	61	0.022	0.69	3.2	15.9	1.61	1.77	0.59	4.7	-2.8
	12	69	-	0.77	3.6	18.9	1.65	1.53	0.60	4.5	-2.7
	13	81	0.087	1.07	3.8	22	1.66	1.53	0.60	4.4	-3.6
	14	104	0.084	1.12	6.0	34	1.39	1.15	0.57	3.6	-0.3
	15	57	0.016	0.27	4.2	16.5	0.74	0.46	0.38	2.1	-5.6
West Kettle River	6	104	0.407	4.2	8.3	26	3.8	3.9	1.23	6.9	-4.9
	16	97	-	4.1	8.1	25	3.6	3.9	1.17	7.0	-3.9
	17	89	-	4.1	8.1	24	3.7	3.9	1.24	7.0	-0.5
	18	81	0.044	4.1	7.7	22	3.5	3.8	1.16	6.9	-1.4
	19	58	0.086	4.0	4.5	12.6	2.6	3.5	0.94	6.6	-6.2
	20	56	0.024	3.7	3.7	11.7	2.5	3.4	0.86	6.4	-6.9
	21	41	0.022	3.8	1.97	9.3	1.90	2.6	0.62	5.8	-4.4
	22	34	-	2.2	1.55	7.7	1.78	1.90	0.50	5.4	-2.2

Table A-3b: Surface water samples from June 2010: Major Anions, Cations and Silica. CB = Charge Balance

		Anions (mg/L)				Cations (mg/L)					
Section	**ID**	**HCO_3^-**	**NO_3^-**	**Cl^-**	**SO_4^{2-}**	**Ca^{2+}**	**Mg^{2+}**	**Na^+**	**K^+**	**Si^{4+}**	**CB (%)**
Below the Confluence	28	27	-	0.73	2.0	8.7	1.24	1.41	0.56	4.8	9.3
	27	31	-	0.67	2.1	8.6	1.19	1.37	0.49	4.8	2.0
	35	30	-	0.40	1.52	8.5	1.27	1.46	0.49	4.7	6.1
	26	28	-	0.69	2.0	8.5	1.22	1.44	0.50	4.8	7.1
	29	26	-	0.68	1.86	8.0	1.02	1.39	0.47	4.7	6.6
	30	23	-	0.64	1.66	8.1	1.05	1.25	0.46	4.7	12.8
	31	22	-	0.62	1.66	7.5	0.90	1.17	0.44	4.6	10.7
	32	23	-	0.63	1.64	7.7	0.95	1.23	0.45	4.5	10.8
Kettle River	34	22	-	0.35	1.48	7.4	0.83	0.88	0.37	3.9	9.5
	36	21	-	0.37	1.42	6.8	0.75	0.83	0.38	3.8	7.7
	39	19.6	-	0.29	1.24	6.3	0.65	0.78	0.34	3.5	7.4
	40	18.9	-	0.31	1.28	6.1	0.67	0.55	0.33	3.5	6.6
	41	21	-	0.35	1.40	7.1	0.68	1.14	0.33	3.5	9.5
	42	29	-	0.44	1.84	9.4	0.80	0.60	0.36	3.6	4.4
	43	18.2	-	0.08	1.62	6.1	0.55	0.52	0.34	3.3	6.9
	44	79	-	0.36	5.0	24	1.19	0.49	0.42	3.4	-2.5
	45	41	-	0.24	4.7	16	0.71	0.55	0.36	2.9	6.2
West Kettle River	33	28	-	1.06	1.62	7.4	1.16	1.65	0.54	5.5	3.2
	38	26	-	1.09	1.71	8.3	1.20	1.75	0.56	5.7	10.6
	37	24	-	1.24	1.73	7.8	1.31	1.71	0.55	5.5	10.9
	25	22	-	1.18	1.55	6.9	1.09	1.61	0.52	5.5	10.2
	24	16.8	-	1.24	1.06	5.3	0.91	1.52	0.49	5.3	11.6
	71	16.9	-	1.01	0.94	4.5	0.91	1.37	0.47	5.4	6.6
	47	12.7	-	1.10	0.73	4.6	0.73	1.53	0.33	4.2	17.8
	46	10.0	-	0.49	0.73	2.8	0.52	0.54	0.24	3.7	5.0

Table A-3c: Surface water samples from October 2010: Major Anions, Cations and Silica. CB = Charge Balance

		Anions (mg/L)				Cations (mg/L)					
Section	**ID**	**HCO_3^-**	**NO_3^-**	**Cl^-**	**SO_4^{2-}**	**Ca^{2+}**	**Mg^{2+}**	**Na^+**	**K^+**	**Si^{4+}**	**CB (%)**
Below the Confluence	100	79	0.043	2.2	7.1	22	3.8	4.2	1.00	5.8	3.4
	101	61	0.078	2.1	7.2	22	3.6	4.2	0.98	5.7	13.8
	109	81	0.075	2.2	7.8	22	3.9	4.2	0.96	5.9	2.8
	108	75	0.097	2.1	6.6	21	3.7	3.9	0.97	5.9	4.8
	107	77	0.115	2.1	6.4	21	3.4	3.8	0.94	6.0	1.8
	106	76	0.063	2.2	6.0	20	3.1	3.7	0.91	6.0	0.5
	105	67	0.026	1.75	5.5	19.5	2.9	3.3	0.91	5.9	4.7
	104	68	0.050	1.77	5.5	19.2	2.8	3.3	0.86	6.0	3.2
Kettle River	102	59	0.029	1.17	4.5	16.7	2.5	2.8	0.72	5.6	3.6
	117	58	-	0.78	4.1	15.3	2.2	2.4	0.65	5.5	0.5
	118	51	-	0.68	3.6	14.4	1.94	2.2	0.64	5.4	3.5
	119	49	0.138	0.64	3.1	13.9	1.78	2.1	0.59	5.1	3.0
	120	51	-	0.66	3.1	15.6	1.68	1.91	0.55	5.0	5.2
	121	59	-	0.82	3.5	18.4	1.61	1.78	0.57	4.7	3.6
	122	34	-	0.41	3.4	10.7	1.29	1.57	0.49	4.0	6.0
	123	98	-	0.54	6.4	33	1.46	1.08	0.49	3.8	2.6
	124	50	-	0.25	4.8	17.4	0.84	0.74	0.36	2.4	2.5
West Kettle River	103	75	-	3.7	7.2	23	3.4	4.2	1.17	7.2	4.9
	110	84	0.033	3.8	7.2	23	3.5	4.2	1.14	7.0	0.9
	116	75	-	4.0	7.5	22	3.6	4.2	1.15	7.1	4.0
	115	71	0.108	3.7	7.2	21	3.4	4.0	1.08	6.9	3.9
	114	40	-	3.5	3.4	11.9	2.3	3.5	0.83	6.8	7.6
	113	40	0.038	3.5	3.3	11.7	2.4	3.4	0.78	6.7	6.8
	112	32	-	3.4	1.51	8.3	1.90	2.6	0.58	6.1	3.9
	111	28	-	2.8	1.31	7.8	1.74	2.4	0.49	5.7	7.7

Table A-4a: Surface water samples from October 2009: Stable Isotope Abundance Ratios

		Stable Isotope Abundance Ratios (‰)						
Section	**ID**	**$\delta^{18}O_{water}$**	**$\delta^{2}H_{water}$**	**$\delta^{15}N_{nitrate}$**	**$\delta^{18}O_{nitrate}$**	**$\delta^{13}C_{DIC}$**	**$\delta^{34}S_{BaSO4}$**	**$\delta^{18}O_{BaSO4}$**
Below the Confluence	1	-16.8	-127	-	-	-10.1	-	-
	2	-16.7	-128	-	-	-10.2	-	-
	3	-16.9	-129	-	-	-11.8	-	-
	4	-16.9	-128	-	-	-10.8	-	-
	5	-16.9	-129	-	-	-10.8	-	-
Kettle River	7	-16.9	-129	-	-	-10.3	-	-
	8	-17.1	-130	-	-	-9.3	-	-
	9	-17.1	-130	-	-	-10.5	-	-
	10	-17.2	-130	-	-	-6.8	-	-
	11	-17.3	-132	-	-	-5.4	-	-
	12	-17.1	-131	-	-	-7.5	-	-
	13	-17.3	-132	-	-	-11.0	-	-
	14	-17.1	-131	-	-	-11.9	-	-
	15	-16.4	-128	-	-	-10.3	-	-
West Kettle River	6	-16.6	-127	-	-	-13.0	-	-
	16	-16.6	-128	-	-	-12.0	-	-
	17	-16.7	-128	-	-	-11.6	-	-
	18	-16.6	-128	-	-	-13.1	-	-
	19	-16.4	-127	-	-	-6.7	-	-
	20	-16.4	-127	-	-	-6.4	-	-
	21	-16.7	-127	-	-	-3.5	-	-
	22	-16.6	-126	-	-	-5.2	-	-

Table A-4b: Surface water samples from June 2010: Stable Isotope Abundance Ratios

		Stable Isotope Abundance Ratios (‰)						
Section	**ID**	**$\delta^{18}O_{water}$**	**$\delta^{2}H_{water}$**	**$\delta^{15}N_{nitrate}$**	**$\delta^{18}O_{nitrate}$**	**$\delta^{13}C_{DIC}$**	**$\delta^{34}S_{BaSO4}$**	**$\delta^{18}O_{BaSO4}$**
Below the Confluence	28	-17.2	-130	-	-	-8.3	0.4	-0.8
	27	-17.2	-131	-	-	-7.8	-0.2	-0.6
	35	-17.4	-130	-	-	-7.5	0.4	-0.4
	26	-17.4	-131	-	-	-7.7	-0.1	-0.1
	29	-17.3	-130	-	-	-7.4	-1.0	-1.2
	30	-17.5	-130	-	-	-7.1	0.6	0.0
	31	-17.4	-130	-	-	-7.2	0.6	0.1
	32	-17.4	-131	3.8	-0.6	-6.8	0.5	-0.7
Kettle River	34	-17.5	-132	-	-	-7.1	-0.3	-0.8
	36	-17.7	-131	-	-	-8.2	0.2	-0.6
	39	-17.7	-131	-	-	-6.5	-0.2	-0.7
	40	-17.7	-133	-	-	-7.8	-0.4	0.4
	41	-17.6	-132	-	-	-7.6	-1.3	-1.5
	42	-17.9	-133	-	-	-7.9	-2.9	-1.9
	43	-17.9	-137	-	-	-6.5	1.6	-3.3
	44	-17.8	-135	-	-	-9.1	-9.8	-2.5
	45	-17.7	-136	-	-	-9.0	-12.1	-2.5
West Kettle River	33	-17.0	-128	-	-	-7.4	0.9	0.9
	38	-17.0	-127	-	-	-8.0	1.1	0.1
	37	-17.0	-128	-	-	-8.1	2.3	-0.6
	25	-17.2	-130	-	-	-7.8	0.4	1.1
	24	-17.3	-131	-	-	-6.4	1.8	2.2
	71	-16.6	-128	-	-	-19.9	-	-
	47	-17.4	-132	-	-	-6.4	-	-
	46	-17.2	-132	-	-	-7.5	-	-

Table A-4c: Surface water samples from October 2010: Stable Isotope Abundance Ratios

		Stable Isotope Abundance Ratios (‰)						
Section	**ID**	**$\delta^{18}O_{water}$**	**$\delta^{2}H_{water}$**	**$\delta^{15}N_{nitrate}$**	**$\delta^{18}O_{nitrate}$**	**$\delta^{13}C_{DIC}$**	**$\delta^{34}S_{BaSO4}$**	**$\delta^{18}O_{BaSO4}$**
Below the Confluence	100	-16.6	-128	3.0	8.1	-8.1	1.5	2.3
	101	-16.5	-126	6.8	5.7	-8.3	1.6	3.7
	109	-16.5	-126	-	-	-7.8	1.4	2.4
	108	-16.6	-127	4.4	3.0	-9.3	1.4	5.4
	107	-16.6	-126	3.5	2.3	-7.9	1.4	4.6
	106	-16.6	-127	6.9	3.2	-7.5	1.2	5.9
	105	-16.6	-126	-	-	-7.7	1.2	6.3
	104	-16.7	-127	-	-	-7.9	1.2	4.0
Kettle River	102	-16.7	-127	-	-	-7.4	1.4	2.4
	117	-17.1	-128	-	-	-8.3	1.0	-1.8
	118	-17.1	-128	-	-	-8.0	0.7	0.1
	119	-17.1	-129	-	-	-7.4	-0.3	-3.4
	120	-17.0	-129	-	-	-6.6	-3.4	-3.6
	121	-17.0	-130	-	-	-6.3	-1.9	-3.3
	122	-16.9	-129	-	-	-6.4	1.9	-5.0
	123	-17.4	-130	-	-	-10.6	-8.9	-2.9
	124	-16.6	-128	-	-	-8.8	-11.8	-3.5
West Kettle River	103	-16.4	-126	-	-	-8.4	1.7	2.6
	110	-16.4	-125	-	-	-8.6	0.9	5.7
	116	-16.8	-127	-	-	-8.1	1.2	-1.7
	115	-16.5	-125	7.2	0.7	-8.9	0.0	-1.1
	114	-16.6	-126	-	-	-4.4	1.5	-2.5
	113	-16.6	-125	-	-	-5.2	2.1	-1.9
	112	-16.7	-125	-	-	-2.3	2.5	-1.5
	111	-16.9	-127	-	-	-13.8	2.3	-0.8

Table A-5: Groundwater sample identification and location.

Sub-catchment	Name	Sample ID			Location	
		Oct. 2009	June 2010	Oct. 2010	N	W
Below the Confluence	BOLT	-	53	130	49.002 °	-118.765 °
	BICK	-	59	143	49.011 °	-118.845 °
	BUGEAUD	-	52	141	49.028 °	-118.866 °
	NICHOL	-	54	142	49.035 °	-118.863 °
	BARTELING	-	57	138	49.047 °	-118.896 °
	HUTCHEON	23	62	144	49.061 °	-118.905 °
	HOWES	-	60	136	49.055 °	-118.949 °
	K ERICKSON	-	-	134	49.050 °	-118.965 °
	F&C ERICSON	-	61	137	49.052 °	-118.957 °
	EATON	-	51	135	49.048 °	-118.975 °
	DENNILL	-	58	133	49.056 °	-118.998 °
	FUNNEL	-	55	132	49.058 °	-119.000 °
	SHANE	-	56	140	49.086 °	-119.001 °
	SMITH	-	70	150	49.120 °	-118.998 °
	GILL	-	66	139	49.150 °	-118.983 °
Kettle River	EVANS	-	67	131	49.175 °	-118.972 °
	DENNIS	-	63	152	49.313 °	-118.882 °
	NELSON	-	65	153	49.333 °	-118.876 °
	DELAIRE	-	64	151	49.364 °	-118.874 °
West Kettle River	THORDARSON	-	69	149	49.257 °	-119.010 °
	MOAT	-	68	145	49.271 °	-119.021 °
	CHAMPAGNE #1	-	48	146	49.408 °	-119.105 °
	CHAMPAGNE #2	-	49	147	49.411 °	-119.105 °
	CHAMPAGNE #3	-	50	148	49.412 °	-119.104 °

Table A-6a: Groundwater samples from June 2010: Field Measurements

		Field Measurements			
Sub-catchment	**ID**	**pH**	**Temp(°C)**	**Cond. (µS/cm)**	**DO (mg/L)**
Below the Confluence	53	7.4	7.73	523	3.3
	59	7.2	6.87	282	1.0
	52	7.3	7.57	374	1.40
	54	8.4	9.65	729	1.1
	57	7.5	5.39	376	4.4
	62	7.4	6.90	571	9.0
	60	8.1	6.16	315	3.9
	61	7.9	9.33	293	3.2
	51	7.9	10.02	825	5.0
	58	7.1	5.38	231	5.0
	55	7.5	6.91	657	9.0
	56	7.6	8.05	469	2.5
	70	7.7	5.76	472	11.3
	66	7.3	6.87	311	6.6
Kettle River	67	7.5	6.98	529	6.0
	63	6.9	5.29	181	3.5
	65	7.0	6.30	165	9.8
	64	6.8	8.60	215	3.2
West Kettle River	69	6.8	6.94	321	10.6
	68	7.7	9.63	287	2.0
	48	7.1	6.35	444	2.4
	49	7.0	4.92	402	6.0
	50	7.2	6.45	404	8.5

Table A-6b: Groundwater samples from October 2009 and 2010: Field Measurements

		Field Measurements			
Sub-catchment	**ID**	**pH**	**Temp. (°C)**	**Cond. (µS/cm)**	**DO (mg/L)**
Below the Confluence	23	7.3	9.39	739	9.6
	130	7.3	6.81	453	7.3
	143	7.4	5.94	242	2.9
	141	7.3	8.50	328	7.3
	142	8.5	8.49	621	1.5
	138	7.6	5.00	336	6.9
	144	7.5	9.98	566	9.6
	136	8.1	5.37	306	7.2
	134	7.7	7.25	374	6.5
	137	7.9	6.92	294	5.6
	135	8.3	8.77	587	6.1
	133	7.2	4.80	235	7.9
	132	7.5	6.51	592	8.1
	140	7.5	8.32	399	4.3
	150	7.3	7.34	443	8.0
	139	7.4	7.18	339	10.0
Kettle River	131	7.5	5.98	590	4.9
	152	6.8	3.95	200	8.0
	153	7.2	3.80	230	11.4
	151	6.8	5.92	233	7.6
West Kettle River	149	7.3	8.28	192	6.3
	145	7.7	6.67	304	4.3
	146	7.1	4.55	327	5.6
	147	6.9	5.00	322	8.3
	148	7.0	5.10	309	8.6

Table A-7a: Groundwater samples from June 2010: Major Anions, Cations and Silica. CB = Charge Balance

		Anions (mg/L)				Cations (mg/L)					
Sub-catchment	**ID**	**HCO_3^-**	**NO_3^-**	**Cl^-**	**SO_4^{2-}**	**Ca^{2+}**	**Mg^{2+}**	**Na^+**	**K^+**	**Si^{4+}**	**CB (%)**
Below the Confluence	53	229	34	15.5	39	64	12.9	19.0	3.1	8.1	-3.5
	59	154	30	3.9	17.0	39	9.4	8.4	1.79	8.4	-5.1
	52	185	34	1.54	16.6	41	8.5	16.5	1.98	10.2	-6.2
	54	291		5.4	112	11.7	3.9	137	0.91	6.3	-2.5
	57	211	24	2.8	16.2	51	11.3	13.9	2.1	7.4	-1.5
	62	370		2.4	40	79	24	23.9	1.99	9.7	0.3
	60	176	27	6.3	15.0	45	10.7	6.7	1.64	6.9	-4.6
	61	119	41	19.9	10.5	39	9.1	11.2	1.73	6.8	-2.5
	51	250	6.4	3.7	146	37	8.8	110	2.1	8.2	0.6
	58	117	24	5.3	14.3	29	7.3	8.2	2.1	8.3	-5.6
	55	229	31	45	23	97	10.2	33.7	3.4	8.6	9.4
	56	203	36	9.2	31	50	16.4	10.5	2.1	8.3	-5.1
	70	263	26	10.9	19.3	80	11.3	8.4	1.94	9.7	-0.9
	66	181	30	14.2	8.21	54	6.7	7.6	7.9	8.0	-3.4
Kettle River	67	296		45	4.6	84	11.6	21	1.50	10.3	-0.9
	63	108	23	2.2	6.4	28	5.0	4.5	1.53	9.0	-7.1
	65	90		1.99	9.8	31	2.8	2.5	0.90	7.1	4.6
	64	131	38	5.3	9.0	32	5.4	7.2	1.32	9.2	-12.8
West Kettle River	69	113	31	13.4	13.2	44	5.8	9.3	7.8	8.6	4.4
	68	158		9.5	31	39	6.0	22	0.77	7.1	-1.2
	48	166	28	9.8	25	57	8.3	6.8	2.3	9.0	-1.4
	49	176	13.2	7.4	25	53	7.9	5.5	2.2	8.4	-3.1
	50	152	21	6.8	25	51	9.1	6.1	2.4	8.2	0.9

Table A-7b: Groundwater samples from October 2009 and 2010: Major Anions, Cations and Silica. CB = Charge Balance

		Anions (mg/L)				Cations (mg/L)					
Sub-catchment	**ID**	**HCO_3^-**	**NO_3^-**	**Cl^-**	**SO_4^{2-}**	**Ca^{2+}**	**Mg^{2+}**	**Na^+**	**K^+**	**Si^{4+}**	**CB (%)**
Below the Confluence	23	390	0.060	2.4	39	82	23	22	2.1	10.0	-1.7
	130	228	3.0	17.3	37	61	11.6	20.0	2.9	8.1	-1.0
	143	155	1.33	3.6	17.2	39	9.4	9.2	1.73	8.2	2.2
	141	206	-	1.63	17.1	45	9.7	18.5	2.3	10.9	2.1
	142	263	-	5.1	111	12.0	4.1	150	0.90	6.3	5.0
	138	204	8.0	2.5	15.6	47	10.5	14.3	1.90	7.3	0.5
	144	369	-	2.2	39	81	25	24.6	2.1	10.3	2.0
	136	171	6.3	6.2	14.8	46	10.9	7.5	1.67	6.9	2.4
	134	158	3.5	30	15.2	42	12.7	18.5	1.98	6.8	2.2
	137	139	1.98	22	10.9	39	9.7	12.0	0.27	6.6	1.4
	135	195	-	2.8	140	20	4.2	117	1.31	8.1	2.4
	133	109	-	6.0	17.0	30	7.6	8.9	2.0	8.2	5.5
	132	238	18.3	50	25	74	10.7	34	3.6	8.8	0.5
	140	226	-	9.8	33	53	17.9	11.5	2.0	8.2	-0.1
	150	252	11.2	11.1	18.7	77	11.4	9.6	2.1	9.6	2.3
	139	181	13.9	13.3	9.0	58	6.5	8.1	1.90	8.0	1.1
Kettle River	131	293	-	55	4.3	87	12.3	22	1.56	10.5	-0.3
	152	108	5.1	1.99	6.2	25	5.1	4.7	1.56	8.7	-3.3
	153	134	0.33	1.07	9.1	38	3.6	3.4	0.97	7.1	-0.8
	151	132	0.36	5.0	8.5	32	6.0	7.9	1.32	9.0	-0.4
West Kettle River	149	109	6.4	3.8	7.9	23	3.8	5.7	5.0	8.2	-8.5
	145	133	-	10.7	39	34	4.3	30	0.52	6.4	0.8
	146	179	6.2	7.9	24	55	7.8	6.0	2.4	8.1	-0.8
	147	158	17.1	7.7	25	52	7.9	6.1	2.4	8.5	-0.3
	148	159	4.3	5.1	25	50	8.1	6.2	2.3	7.9	2.3

Table A-8a: Groundwater samples from June 2010: Stable Isotope Abundance Ratios

		Stable Isotope Abundance Ratios (‰)						
Sub-catchment	**ID**	**$\delta^{18}O_{water}$**	**$\delta^{2}H_{water}$**	**$\delta^{15}N_{nitrate}$**	**$\delta^{18}O_{nitrate}$**	**$\delta^{13}C_{DIC}$**	**$\delta^{34}S_{BaSO4}$**	**$\delta^{18}O_{BaSO4}$**
Below the Confluence	53	-17.0	-132	5.4	-6.0	-12.9	1.2	-4.8
	59	-16.9	-130	14.7	1.9	-13.8	0.9	-4.3
	52	-16.7	-128	12.9	3.3	-12.6	-1.1	-2.2
	54	-17.8	-143	-	-	-13.3	-2.9	-5.4
	57	-17.2	-132	5.2	-4.1	-13.6	0.9	-2.7
	62	-16.5	-129	4.5	-4.8	-12.1	3.1	-2.2
	60	-16.9	-130	2.5	-4.3	-12.9	0.5	-6.8
	61	-16.9	-129	6.5	-5.2	-12.9	1.0	-5.6
	51	-17.9	-139	5.1	-7.6	-11.0	1.0	-3.8
	58	-16.3	-125	3.6	-6.2	-11.8	1.5	-3.8
	55	-17.1	-131	9.8	-5.5	-13.5	1.7	-5.7
	56	-17.1	-131	5.6	-5.6	-12.0	-0.3	-6.7
	70	-15.7	-123	3.9	-3.0	-12.4	2.8	-0.4
	66	-16.7	-128	6.3	-6.3	-14.0	1.9	-4.3
Kettle River	67	-16.4	-128	6.0	-3.3	-15.4	2.8	-5.4
	63	-16.0	-123	4.1	-2.1	-15.5	1.5	-4.4
	65	-16.3	-125	3.0	-6.3	-12.6	-3.0	-6.6
	64	-16.9	-129	3.2	-6.7	-10.8	1.6	-6.7
West Kettle River	69	-16.4	-125	12.2	-1.5	-16.1	1.7	-2.9
	68	-17.1	-131	4.7	-2.5	-14.0	6.7	-3.2
	48	-17.0	-131	8.7	-1.5	-15.5	-1.1	-6.4
	49	-16.9	-130	5.7	-2.4	-15.8	0.4	-7.6
	50	-17.0	-130	5.7	-3.6	-15.6	0.2	-7.4

Table A-8b: Groundwater samples from October 2009 and 2010: Stable Isotope Abundance Ratios

		Stable Isotope Abundance Ratios (‰)						
Sub-catchment	**ID**	**$\delta^{18}O_{water}$**	**$\delta^{2}H_{water}$**	**$\delta^{15}N_{nitrate}$**	**$\delta^{18}O_{nitrate}$**	**$\delta^{13}C_{DIC}$**	**$\delta^{34}S_{BaSO4}$**	**$\delta^{18}O_{BaSO4}$**
Below the Confluence	23	-16.3	-128	-	-	-16.5	3.8	-2.0
	130	-17.0	-130	6.3	-2.8	-13.5	1.2	-5.5
	143	-17.3	-130	13.9	1.2	-14.3	0.6	-4.0
	141	-16.7	-127	12.8	3.2	-13.5	0.4	0.1
	142	-18.1	-142	-	-	-13.4	-3.4	-5.9
	138	-17.5	-131	5.6	-3.8	-13.7	0.6	-4.6
	144	-16.7	-128	-	-	-12.5	3.5	-1.6
	136	-17.2	-130	3.2	-5.2	-13.2	0.8	-5.1
	134	-17.3	-131	7.4	-7.0	-12.3	0.8	-4.9
	137	-17.1	-130	-	-	-13.2	0.8	-5.3
	135	-18.3	-141	14.3	-8.7	-10.7	2.4	-2.5
	133	-16.8	-124	6.0	-6.6	-11.4	0.9	-2.6
	132	-17.3	-129	9.7	-5.8	-12.7	1.6	-3.4
	140	-17.2	-130	6.8	-3.7	-12.9	-0.5	-5.7
	150	-16.1	-123	4.3	-3.5	-13.9	3.1	-1.3
	139	-17.1	-128	7.2	-4.8	-14.6	1.8	-3.9
Kettle River	131	-16.5	-126	6.8	-3.3	-16.0	4.0	-2.4
	152	-16.0	-122	-	-	-16.7	1.8	-3.1
	153	-16.2	-123	-	-	-12.1	-2.3	-5.2
	151	-16.9	-127	4.0	-6.3	-14.7	1.9	-6.1
West Kettle River	149	-16.5	-125	18.9	5.5	-15.1	0.5	-2.7
	145	-17.5	-133	-	-	-13.3	8.0	-0.8
	146	-17.4	-130	-	-	-15.4	-0.5	-6.2
	147	-17.3	-130	5.4	-5.6	-16.2	0.4	-6.1
	148	-17.0	-130	-	-	-15.7	0.3	-6.4

Table A-9: Precipitation data: Location, pH and Stable Isotope Abundance Ratios

		Location			Stable Isotopes	
ID	**Date Sampled**	**N**	**W**	**pH**	**$\delta^{18}O_{water}$**	**$\delta^{2}H_{water}$**
72	June 8-9-2010	49.061 °	-118.905 °	4.7	-17.7	-134.1
73	June 8-9-2010	49.061 °	-118.905 °	-	-14.6	-119.3
74	June 16-17-2010	49.061 °	-118.905 °	-	-13.8	-102.9
75	June 18-2010	49.061 °	-118.905 °	-	-14.7	-113.3

Table A-10: Precipitation data: Major Anions and Cations. CB = Charge Balance

	Anions (mg/L)				Cations (mg/L)					
ID	**HCO_3^-**	**NO_3^-**	**Cl^-**	**SO_4^{2-}**	**Ca^{2+}**	**Mg^{2+}**	**Na^+**	**K^+**	**Si^{4+}**	**CB (%)**
72	-	1.13	0.31	0.173	0.92	0.152	0.121	0.087	-	-
73	-	2.1	0.23	0.34	0.79	0.144	0.41	-	-	-
74	-	0.92	0.0127	0.079	0.75	0.187	0.39	-	-	-
75	-	-	-	-	1.38	0.081	0.34	0.055	-	-

APPENDIX B:

Table B-1a: Surface water samples from October 2009: Geochemical Modeling Results

Sub-catchment	ID	Saturation Indices [log(Q/K)]							
		Quartz	**Chalcedony**	**Cristobalite**	**Tridymite**	**Chrysotile**	**Calcite**	**Dolomite**	***p*CO₂ (ppmv)**
Below the Confluence	1	0.743	0.450	0.139	0.555	-5.585	-0.136	-0.076	885.7
	2	0.736	0.443	0.132	0.547	-5.367	-0.146	-0.130	666.7
	3	0.739	0.446	0.136	0.551	-5.353	-0.138	-0.119	665.8
	4	0.740	0.447	0.136	0.551	-5.506	-0.215	-0.279	621.3
	5	0.739	0.446	0.135	0.551	-6.178	-0.312	-0.500	787.9
Kettle River	7	0.718	0.425	0.115	0.530	-9.562	-0.992	-1.857	2307.4
	8	0.729	0.436	0.124	0.541	-8.843	-0.908	-1.688	1500.1
	9	0.720	0.427	0.116	0.532	-8.513	-0.846	-1.593	1266.2
	10	0.706	0.412	0.100	0.517	-8.974	-0.985	-1.896	1129.0
	11	0.690	0.396	0.083	0.501	-8.907	-0.858	-1.737	1073.7
	12	0.659	0.365	0.053	0.470	-8.844	-0.725	-1.532	1218.8
	13	0.669	0.374	0.061	0.479	-8.094	-0.446	-1.047	1012.6
	14	0.552	0.258	-0.053	0.363	-7.828	-0.071	-0.539	1050.1
	15	0.353	0.058	-0.256	0.163	-9.088	-0.597	-1.574	541.3
West Kettle River	6	0.821	0.528	0.218	0.633	-12.260	-1.366	-2.587	1205.0
	16	0.872	0.577	0.264	0.682	-7.895	-0.544	-0.950	1861.3
	17	0.860	0.566	0.254	0.671	-7.466	-0.525	-0.891	1518.8
	18	0.876	0.580	0.267	0.685	-6.966	-0.495	-0.812	1064.9
	19	0.860	0.564	0.250	0.669	-7.102	-0.810	-1.336	681.9
	20	0.854	0.558	0.244	0.663	-7.606	-0.926	-1.563	774.1
	21	0.807	0.512	0.197	0.616	-7.053	-0.983	-1.689	395.9
	22	0.772	0.477	0.162	0.582	-4.791	-0.723	-1.115	134.2

Table B-1b: Surface water samples from June 2010: Geochemical Modeling Results

Sub-catchment	ID	Saturation Indices [log(Q/K)]							
		Quartz	**Chalcedony**	**Cristobalite**	**Tridymite**	**Chrysotile**	**Calcite**	**Dolomite**	***p*CO$_2$ (ppmv)**
Below the Confluence	28	0.581	0.293	-0.012	0.398	-8.347	-1.360	-2.557	485.6
	27	0.578	0.289	-0.015	0.394	-8.297	-1.285	-2.419	534.6
	35	0.551	0.264	-0.039	0.369	-8.592	-1.384	-2.577	632.3
	26	0.588	0.299	-0.006	0.404	-8.089	-1.311	-2.455	444.6
	29	0.573	0.284	-0.020	0.390	-8.845	-1.451	-2.789	513.6
	30	0.563	0.274	-0.030	0.379	-8.599	-1.469	-2.812	421.2
	31	0.555	0.266	-0.038	0.371	-9.591	-1.658	-3.225	541.7
	32	0.572	0.282	-0.023	0.387	-10.020	-1.712	-3.326	642.0
Kettle River	34	0.507	0.217	-0.088	0.323	-10.350	-1.748	-3.439	637.3
	36	0.511	0.221	-0.085	0.326	-11.560	-1.996	-3.944	873.2
	39	0.476	0.186	-0.120	0.291	-9.650	-1.651	-3.291	351.7
	40	0.481	0.191	-0.116	0.296	-9.659	-1.683	-3.332	339.3
	41	0.478	0.187	-0.120	0.292	-8.861	-1.433	-2.888	283.4
	42	0.485	0.194	-0.112	0.300	-8.199	-1.115	-2.300	325.1
	43	0.458	0.167	-0.140	0.272	-9.293	-1.584	-3.217	253.5
	44	0.432	0.143	-0.162	0.248	-5.978	-0.004	-0.306	464.6
	45	0.305	0.020	-0.280	0.125	-7.823	-0.681	-1.676	450.3
West Kettle River	33	0.643	0.354	0.050	0.459	-8.956	-1.541	-2.875	634.1
	38	0.608	0.321	0.020	0.427	-7.562	-1.314	-2.441	400.0
	37	0.609	0.321	0.019	0.427	-7.603	-1.380	-2.512	388.4
	25	0.654	0.365	0.059	0.470	-9.640	-1.768	-3.332	600.8
	24	0.647	0.357	0.051	0.462	-9.688	-1.944	-3.653	425.9
	71	0.619	0.331	0.027	0.436	-9.553	-2.011	-3.703	448.8
	47	0.554	0.264	-0.043	0.369	-10.090	-2.105	-4.010	299.9
	46	0.520	0.229	-0.079	0.334	-9.548	-2.212	-4.166	150.1

Table B-1c: Surface water samples from October 2010:Geochemical Modeling Results

Sub-catchment	ID	Saturation Indices [log(Q/K)]							
		Quartz	**Chalcedony**	**Cristobalite**	**Tridymite**	**Chrysotile**	**Calcite**	**Dolomite**	***p*CO$_2$ (ppmv)**
Below the Confluence	100	0.714	0.423	0.115	0.528	-6.109	-0.392	-0.550	917.2
	101	0.704	0.413	0.105	0.518	-5.438	-0.376	-0.533	539.0
	109	0.727	0.435	0.127	0.540	-4.200	-0.047	0.138	455.4
	108	0.738	0.446	0.137	0.551	-5.547	-0.303	-0.379	677.5
	107	0.789	0.495	0.183	0.600	-7.866	-0.669	-1.155	1425.1
	106	0.670	0.382	0.078	0.487	-6.928	-0.576	-0.946	1305.7
	105	0.702	0.412	0.105	0.517	-5.056	-0.282	-0.388	480.0
	104	0.720	0.429	0.121	0.534	-6.102	-0.453	-0.738	701.0
Kettle River	102	0.698	0.406	0.098	0.511	-6.749	-0.630	-1.096	707.0
	117	0.788	0.492	0.178	0.597	-10.420	-1.252	-2.382	2093.2
	118	0.779	0.484	0.170	0.589	-10.140	-1.251	-2.406	1566.2
	119	0.750	0.454	0.140	0.559	-10.090	-1.235	-2.398	1387.6
	120	0.743	0.447	0.133	0.552	-9.586	-1.067	-2.136	1134.9
	121	0.718	0.422	0.108	0.527	-9.526	-0.903	-1.898	1231.7
	122	0.651	0.356	0.041	0.461	-10.140	-1.403	-2.759	781.5
	123	0.607	0.312	-0.001	0.417	-7.998	-0.129	-0.643	1014.5
	124	0.337	0.045	-0.264	0.150	-9.131	-0.719	-1.761	643.5
West Kettle River	103	0.835	0.542	0.232	0.647	-4.709	-0.149	-0.132	483.2
	110	0.892	0.597	0.282	0.701	-11.070	-1.207	-2.262	5228.6
	116	0.864	0.569	0.257	0.674	-6.510	-0.458	-0.731	897.5
	115	0.874	0.578	0.265	0.683	-7.970	-0.728	-1.282	134.6
	114	0.875	0.579	0.265	0.684	-8.876	-1.283	-2.305	897.1
	113	0.871	0.575	0.261	0.680	-8.796	-1.278	-2.277	882.6
	112	0.671	0.383	0.080	0.488	-8.559	-1.505	-2.633	850.1
	111	0.800	0.504	0.190	0.609	-9.319	-1.600	-2.889	611.4

Table B-2a: Groundwater samples from June 2010: Geochemical Modeling Results

Sub-catchment	ID	Saturation Indices [log(Q/K)]							
		Quartz	Chalcedony	Cristobalite	Tridymite	Chrysotile	Calcite	Dolomite	pCO_2 (ppmv)
Below the Confluence	53	0.791	0.503	0.200	0.608	-7.009	-0.059	0.214	8247.5
	59	0.828	0.539	0.235	0.644	-8.485	-0.613	-0.827	8520.9
	52	0.895	0.607	0.304	0.712	-7.764	-0.401	-0.456	8124.2
	54	0.637	0.351	0.050	0.456	-2.327	0.374	1.330	948.8
	57	0.802	0.512	0.205	0.617	-7.180	-0.137	0.084	6665.5
	62	0.889	0.601	0.296	0.706	-5.925	0.253	1.013	11754.0
	60	0.752	0.462	0.157	0.567	-3.535	0.394	1.178	1383.6
	61	0.684	0.397	0.096	0.503	-4.214	0.083	0.572	1457.7
	51	0.752	0.467	0.167	0.572	-4.236	0.259	0.945	2777.1
	58	0.854	0.563	0.257	0.668	-9.728	-1.009	-1.610	8568.3
	55	0.834	0.545	0.241	0.650	-6.570	0.244	0.536	5934.2
	56	0.795	0.507	0.205	0.613	-5.640	-0.028	0.491	5101.3
	70	0.910	0.620	0.314	0.725	-5.334	0.422	1.010	4446.0
	66	0.806	0.517	0.213	0.623	-8.443	-0.314	-0.509	8110.3
Kettle River	67	0.911	0.623	0.318	0.728	-6.514	0.253	0.669	8643.3
	63	0.889	0.598	0.292	0.703	-11.500	-1.333	-2.402	13520.5
	65	0.767	0.478	0.173	0.583	-11.760	-1.230	-2.489	9190.0
	64	0.830	0.543	0.241	0.648	-11.290	-1.220	-2.184	18839.9
West Kettle River	69	0.837	0.548	0.244	0.653	-11.340	-1.148	-2.156	15060.1
	68	0.698	0.412	0.111	0.517	-6.070	-0.073	0.087	3043.6
	48	0.865	0.576	0.271	0.681	-9.133	-0.525	-0.869	10747.3
	49	0.870	0.579	0.272	0.684	-10.050	-0.664	-1.151	14369.3
	50	0.827	0.538	0.233	0.643	-8.868	-0.571	-0.869	9176.2

Table B-2b: Groundwater samples from October 2009 and 2010: Geochemical Modeling Results

Sub-catchment	ID	Saturation Indices [log(Q/K)]							
		Quartz	**Chalcedony**	**Cristobalite**	**Tridymite**	**Chrysotile**	**Calcite**	**Dolomite**	***p*CO$_2$ (ppmv)**
Below the Confluence	23	0.852	0.566	0.265	0.671	-6.583	0.139	0.778	18376.1
	130	0.810	0.521	0.216	0.626	-7.684	-0.169	-0.033	9655.8
	143	0.835	0.545	0.239	0.650	-7.808	-0.467	-0.539	6223.4
	141	0.908	0.620	0.318	0.726	-7.402	-0.295	-0.229	9055.8
	142	0.658	0.371	0.069	0.476	-2.071	0.389	1.361	746.8
	138	0.807	0.516	0.209	0.621	-6.253	0.010	0.374	4272.3
	144	0.854	0.568	0.268	0.673	-5.302	0.316	1.172	11527.0
	136	0.767	0.477	0.170	0.582	-3.567	0.392	1.168	1319.8
	134	0.725	0.436	0.133	0.542	-5.134	-0.015	0.479	2643.9
	137	0.717	0.428	0.124	0.533	-4.461	0.097	0.611	1550.4
	135	0.762	0.475	0.173	0.580	-2.760	0.331	1.022	799.1
	133	0.860	0.569	0.261	0.674	-9.288	-0.933	-1.463	6661.6
	132	0.856	0.567	0.262	0.672	-6.875	0.084	0.351	7102.7
	140	0.787	0.500	0.197	0.605	-6.096	-0.066	0.432	7122.5
	150	0.875	0.587	0.283	0.692	-7.416	-0.004	0.190	10441.4
	139	0.784	0.496	0.193	0.601	-7.629	-0.133	-0.187	6170.1
Kettle River	131	0.944	0.654	0.348	0.759	-6.741	0.213	0.595	9130.8
	152	0.901	0.610	0.301	0.715	-12.060	-1.477	-2.645	15523.9
	153	0.818	0.526	0.218	0.631	-10.470	-0.741	-1.514	8013.6
	151	0.877	0.587	0.282	0.692	-11.560	-1.254	-2.231	18997.8
West Kettle River	149	0.709	0.420	0.115	0.525	-6.811	-0.209	-0.294	2596.5
	145	0.857	0.566	0.258	0.671	-9.557	-0.531	-0.903	11615.8
	146	0.873	0.583	0.276	0.688	-10.910	-0.901	-1.612	18208.3
	147	0.837	0.547	0.240	0.652	-10.500	-0.826	-1.433	15573.3
	148	0.789	0.502	0.199	0.607	-8.733	-0.812	-1.376	4774.6

APPENDIX C:

Equations from Telmer and Veizer (1999) used to determine DIC concentrations

$$K_{CO2} = -2.22 \times 10^{-6}(T^3) - 1.91 \times 10^{-5}(T^2) + 1.63 \times 10^{-2}(T) + 1.11$$

$$K_1 = 1.67 \times 10^{-4}(T^2) - 1.34 \times 10^{-2}(T) + 6.58$$

$$K_2 = -2.22 \times 10^{-6}(T^3) + 2.29 \times 10^{-4}(T^2) + 1.62 \times 10^{-2}(T) + 10.6$$

Sample calculation for the equilibrium line shift between albite and Na-smectite in Figure 8-2c.)

Albite + **0.858** H^+ = **0.858** Na^+ + **0.429** Na-smectite + **1.425** SiO_2(aq)

Step 1: Write the logK formula

logK = **0.858** log a[Na^+] + **0.429** log a[Na-smectite] + **1.425** log a[SiO_2(aq)]

- **0.858** log a[H^+]

Step 2: Re-arrange

log a [Na^+]/[H^+] = **1.170** logK – **0.500** log a[Na-smectite] – **1.660** log a[SiO_2(aq)]

logK at 5 °C = 0.2083 (Calculated in GWB)

log a[Na^+]/[H^+] = **0.244** – **0.500** log a[Na-smectite] – **1.660** log a[SiO_2(aq)]

The '0.244 term' is the y-intercept and '-1.66loga[SiO2(aq)]' is the slope. The maximum and minimum values for the activity of Na-smectite were put into the above formula and as a result, the line moved up along the y-axes, which caused the line on the graph to shift to the right.

APPENDIX D:

Table D-1: Percent of volcanic varieties upstream of each surface water site. Data is from the BC Geologial Survey (2005).

	Rock Type	**undivided**	**undivided**	**basaltic**	**basaltic**	**volcaniclastic**	
	Age (Ma)	**35.4 - 56.5**	**178 -235**	**1.64 - 23.3**	**208 - 408.5**	**245 - 362.5**	
	Group	**Penticton**	**Nicola**	**Chilcotin**	**Harper Ranch& Nicola**	**Harper Ranch**	
Section	**Sample**	**% of volcanic bedrock upstream of sampling locations**					**Total %**
Kettle River	Keef	-	20.98	-	-	-	21.0
	Hwy 6	-	21.0	-	-	-	15.7
	Bruer	-	9.7	-	6.0	-	11.9
	KRCross	-	2.4	8.0	1.5	-	8.9
	Goat	-	1.5	4.9	0.9	1.6	8.0
	Grano	1.3	1.0	3.9	0.6	1.1	13.6
	Dear	4.1	0.6	3.3	0.4	5.2	15.1
	Lost	6.2	0.6	3.2	0.4	4.8	16.9
	Fiva	8.9	0.5	3.0	0.3	4.2	17.9
West Kettle River	BW	10.9	0.4	2.6	0.3	3.7	10.9
	Trap	3.7	-	7.1	-	-	11.2
	Carmi	6.5	-	4.7	-	-	9.0
	Beaverdell	6.5	-	2.4	-	-	8.7
	Tuzo	6.3	-	2.3	-	-	7.9
	Rhone N	5.9	-	2.1	-	-	7.7
	Rhone S	5.9	-	1.8	-	-	8.4
	Westbridge	6.7	-	1.7	-	-	9.0
Below the Confluence	KVCamp	7.3	-	1.7	-	-	15.0
	Pub	10.8	0.2	2.0	0.1	1.8	15.0
	KVB	10.8	0.2	2.0	0.1	1.8	15.2
	Ingram	11.3	0.2	1.9	0.1	1.7	15.5
	Bugeaud	11.7	0.2	1.9	0.1	1.6	15.6
	Bick	11.8	0.2	1.9	0.1	1.6	16.9
	Midway	13.2	0.2	1.8	0.1	1.6	17.3
	Border	13.6	0.2	1.8	0.1	1.6	17.4

Table D-2: Percent of intrusive igneous varieties upstream of each surface sampling site. Data is from the BC Geological Survey (2005).

	Rock Type	**granodiorite**	**granite, K-feldspar granite**	**granite, K-feldspar granite**	**undivided**	**syenite to monzonite**	
	Age (Ma)	**157.1 - 178**	**157.1 - 178**	**35.4 - 65**	**65 - 145.6**	**35.4 - 56.5**	
	Group	-	-	-	**Okanagan Batholith**	**Coryell Plutonic Suite**	
Section	**Sample**	**% of intrusive igneous bedrock upstream of sampling locations**					**Total %**
Kettle River	Keef	17.0	-	-	-	-	-
	Hwy 6	42.5	19.7	-	-	-	17.0
	Bruer	25.9	40.7	-	-	-	62.2
	KRCross	17.8	32.6	-	5.0	-	66.6
	Goat	11.1	21.8	-	25.1	0.2	55.4
	Grano	10.2	20.7	-	27.9	0.1	58.2
	Dear	9.0	18.5	-	29.7	0.1	59.0
	Lost	7.8	16.6	-	33.8	0.1	57.3
	Fiva	-	17.6	-	25.5	-	58.2
West Kettle River	BW	-	6.1	-	54.4	0.2	43.1
	Trap	-	10.7	-	64.5	0.1	60.7
	Carmi	-	14.6	0.4	61.1	0.1	75.3
	Beaverdell	-	18.7	1.1	53.9	0.4	76.2
	Tuzo	-	17.5	0.9	58.0	0.4	74.1
	Rhone N	-	16.7	0.9	58.9	0.4	76.8
	Rhone S	-	16.6	0.9	58.5	0.4	76.8
	Westbridge	3.9	16.6	0.4	44.2	0.3	76.3
Below the Confluence	KVCamp	3.8	16.5	0.4	43.9	0.3	65.3
	Pub	3.5	16.5	0.4	41.1	0.4	64.9
	KVB	3.5	16.4	0.4	40.8	0.5	61.9
	Ingram	3.5	16.4	0.4	40.7	0.5	61.6
	Bugeaud	3.4	16.1	0.4	39.7	0.6	61.5
	Bick	3.4	16.0	0.3	39.5	0.7	60.2
	Midway	3.4	15.9	0.3	39.5	0.7	59.9
	Border	17.0	-	-	-	-	59.9

Table D-3: Percent of metamorphic varieties upstream of each surface sampling site. Data is from the BC Geologial Survey (2005).

	Rock Type	**undivided**	**orthogneiss**	**greenstone, greenschist**	
	Age (Ma)	**245 - 2500**	**245 - 2500**	**245 - 362.5**	
	Group	**Shuswap Assemblage**	**-**	**-**	
Section	**Sample**	**% of metamorphic bedrock upstream of sampling locations**			**Total %**
Kettle River	Keef	-	-	-	-
	Hwy 6	-	-	-	-
	Bruer	1.2	7.6	-	8.8
	KRCross	9.4	4.6	-	14.1
	Goat	26.2	3.2	-	29.4
	Grano	21.3	2.0	-	23.3
	Dear	19.6	1.8	-	21.5
	Lost	17.3	1.6	2.7	21.6
	Fiva	14.9	1.4	3.9	20.2
West Kettle River	BW	46.0	-	-	46.0
	Trap	27.5	-	0.6	28.1
	Carmi	13.5	-	2.1	15.5
	Beaverdell	12.7	-	2.3	15.0
	Tuzo	10.2	-	7.7	17.8
	Rhone N	8.7	-	6.6	15.3
	Rhone S	8.2	-	6.4	14.6
	Westbridge	8.1	-	6.4	14.5
Below the Confluence	KVCamp	11.2	0.7	5.6	17.5
	Pub	11.1	0.7	6.1	17.9
	KVB	10.2	0.6	9.3	20.1
	Ingram	10.2	0.6	9.2	20.0
	Bugeaud	10.1	0.6	9.2	19.9
	Bick	9.9	0.6	9.2	19.7
	Midway	9.8	0.6	9.1	19.6
	Border	9.8	0.6	9.1	19.5

APPENDIX E:

Table E-1: Weight percent oxides of smectites used to determine average mole proportions

Source	Sample name	CaO	MgO	Na_2O	K_2O	Fe_2O_3
Wolters et al. (2009)	2LP	0.04	2.84	2.81	0.05	4.45
	3, 7th Mayo	0.01	3.08	2.76	0.42	6.91
	4JUP	0.05	1.86	2.7	0.28	7.52
	5MC	0.01	3.4	2.9	0.12	6.36
	6GPC	0.04	3.29	2.62	1.41	6
	7EMC	0.01	2.48	2.7	0.05	2.61
	8UAS	0.01	4.16	3.31	0.07	3.1
	12TR01	0.01	3.35	2.76	0.07	1.11
	13TR02	0.01	5.16	3.43	0.1	3.24
	14TR03	0.01	5.59	3.67	0.03	1.73
	16GR01	0.01	3.56	3.16	0.05	1.74
	17GR02	0.01	2.33	2.38	0.03	1.45
	18USA01	<0.005	3.13	3.03	0.08	4.11
	19USA02	0.07	3.13	3.05	0.04	5.86
	21D01	<0.005	3.42	2.85	0.39	6.16
	24Beid**	0.03	2.31	4.12	0.03	0.13
	25Volclay**	0.05	2.21	3.26	0.08	3.41
	26-27 Valdol C14**	0.07	3.15	2.83	1.49	7.43
	28SB	0.03	4.73	3.08	0.6	4.55
	31BAR3	0.04	3.7	2.73	0.47	5.56
	32Volclay	0.03	2.32	2.99	0.1	3.78
	33CA	0.05	3.19	2.67	0.96	5.85
	36M650	0.08	2.7	2.16	0.25	8.47
	37BB	0.01	2.69	2.98	0.11	11.16
	38MW	0.02	2.75	2.81	0.07	8.34
	39G Q-1	0.01	4.42	3.05	0.25	4.57
	41Val C-18	0.15	3.55	2.51	1.11	8.65
	42Linden**	0	4.08	2.97	0	3.86
Robert and Goffe (1992)	Coirons-1	3.4	14.78	0.1	0.4	12.62
	Coirons-2	1.66	0.63	0.01	0.55	3.24
	Coirons-3	1.24	3.83	0.41	0.62	30.66
	Cantal-1	0.75	22.26	0.02	0.11	5.12
	Cantal-2	1.1	15.87	0.1	0.35	8.84
	Riffe-1	1.68	16.37	0.05	0.56	15.71
	Riffe-2	1.36	9.1	0.12	1.53	25.28
Christidis (2001)	1-zone5	0.71	4.06	0.57	0.75	1.66
	2-zone5	0.85	4.21	0.53	1.03	1.68
	3-zone5	1.62	3.62	0.42	0.27	2.06

Table E-1 (continued):

Source	Sample name	CaO	MgO	Na_2O	K_2O	Fe_2O_3
Christidis and Dunham (1997)	SM136	0.58	2.18	0.69	0.46	1.45
	SM155	0.78	1.39	0.53	1	1.67
	SM176	0.45	2.16	0.72	0.58	1.05
	SM235	0.86	2.48	0.81	0.9	1.04
Nadeau and Bain (1986)	WMB	0.01	2.74	0.12	0.01	4.01
	LJB	0.01	1.94	0.09	0.46	4.07
	RIB	0.01	3.5	0.03	0.01	3.46
	CRb	0.1	3.45	0.18	0.14	4.39
	HVB	0.02	3.82	0.09	0.28	2.06
	MCB	3.15	3.07	0.07	0.01	3.66
	GCB	3.55	3.76	0.06	0.05	2.74
	C3B	0.02	3.93	0.14	0.27	2.07
	VLB	3.26	3.18	0.07	0.04	3.23
	JNB	0.01	4.11	0.08	0.03	2.94
	RPB	3.57	3.35	0.11	0.4	2.6

Table E-2a: Groundwater samples from the Sera Geral basalt aquifer: Sample details and field measurements (Hutcheon pers. comm.)

Sample			Location (UTM)		Field Measurements		
ID	**Name**	**Date**	**X**	**Y**	**pH**	**Temp. (°C)**	**Cond. (µS/cm)**
1	Pref.UFMS	08.11.99	748689	7731917	6.28	27.0	77.0
3	Perkal	08.11.99	750930	7733707	5.59	26.0	101.0
4	Hidrosomat	08.11.99	749525	773197	5.59	27.0	120.0
5	João Pedro	08.11.99	751980	7737310	5.99	27.0	169.0
8	J.V.	09.11.99	753398	7735271	7.19	27.0	83.0
9	C.G.Diesel I	09.11.99	749108	7732157	6.61	24.0	65.0
11	Horta Com.	09.11.99	747229	7735510	6.3	26.0	28.0
12	C.G.Diesel II	09.11.99	750109	7730024	6.99	27.0	154.0
13	Horto Flor.	09.11.99	748186	7734695	7.38	28.0	147.0
17	UFMS.D.Q.	17.11.99	748624	7730651	8.51	32.0	93.0
23	Maracaju-1	19.11.99	690728	7607501	7.97	28.0	126.0
25	Anhanduí-1	20.11.99	759141	7676558	7.08	28.0	88.0
30	Ar.Moreira 1	22.11.99	639941	7461938	7.28	28.0	108.0
31	P.Porã-5	22.11.99	631227	7508012	7.97	28.0	164.0
32	Ant.João-2	23.11.99	607838	7545441	7.68	28.0	112.0
33	Dourados 9	23.11.99	724961	7537717	7.78	28.0	391.0
35	F.Sul-3	24.11.99	755037	7523484	7.97	28.0	217.0
37	R.Brilhante-5	24.11.99	753359	7586408	6.39	27.5	161.0
69	Ithaum-1	31.10.00	669858	7556940	6.38	30.0	48.0
70	N.America 1	31.10.00	719674	7510511	7.34	28.0	146.0
71	Caarapó-7	31.10.00	723836	7494948	7.59	26.3	88.0
73	Bocajá-1	31.10.00	680523	7485050	7.63	21.5	88.0
76	Dourados 9	06.03.01	724961	7537717	7.95	31.0	429.0

Table E-2b: Groundwater samples from the unconfined part of the GAS: Sample details and field measurements

Sample			Location		Field Measurements		
ID	**Name**	**Date**	**Latitude**	**Longitude**	**pH**	**Temp. (°C)**	**Cond. (µS/cm)**
ALC003	Alcinópolis	-	18°19'37"S	53°42'32"W	6.21	26.7°	124.0
SP066	Araraquara	-	21 46"59"S	48°11'00"W	7.85	23.0°	65.0
ARE 001	Areado	-	19°15'22"S	54°19'36"W	5.65	29.5°	44.3
SP162	Avaré	-	23°07'59"S	48°55'00"W	5.99	22.0°	16.0
BAI001	Baian polis	-	19°43'42"S	54°44'17"W	5.43	26.3°	44.0
BQR001	Boqueirão	-	21°41'27"S	56°16'40"W	6.07	25.6°	68.2
SP149	Botucatu	-	22°55'01"S	48°26'50"W	5.96	23.5°	23.0
SP150	Botucatu	-	22°55'01"S	48°26'50"W	5.94	24.0°	10.0
CAM 016	Camapuã	-	19°31'34"S	54°02'36"W	8.08	27.0°	289.0
CAM 004	Camapuã	-	19°32'07"S	54°02'29"W	7.89	28.0°	192.6
CAM018	Camapuã	-	19°32'09"S	54°02'28"W	7.67	26.8°	170.2
COR 001	Corguinho	-	19°49'59"S	54°49'45"W	6.4	28.5°	78.0
DIR 901	D. I. Buriti	-	20°38'15"S	55°18'02"W	5.9	26.4°	68.3
DIR001	D. I. Buriti	-	20°41'08"S	55°16'29"W	5.25	24.8°	20.6
SP085	Descalvado	-	21°51'58"S	47°38'00"W	7.48	22.0°	65.0
FIG 004	Figueirão	-	18°40'44"S	53°38'19"W	6.88	28.2°	135.6
SP049	Guatapará	-	21°30'00"S	48°02'00"W	6.58	23.0°	53.0
ITA 005	Itaporã	-	22°05'19"S	54°47'41"W	6.47	25.0°	112.0
SP104	Itirapina	-	22°18'00"S	47°48'00"W	5.45	23.4°	5.6
SP128	Itirapina	-	22°11'00"S	48°53'00"W	5.85	24.4°	12.0
JAD901	Jardim	-	21°40'48"S	56°09'08"W	5.82	27.9°	71.0
GO008	Jataí	-	17°48'31"S	52°12'45"W	6.27	24.6°	23.4
JAU001	Jauru	-	18°39'01"S	54°21'35"W	7.42	27.4°	286.0
GO004	Mineiros	-	18°05'04"S	54°53'38"W	6.19	21.6°	68.4
GO005	Mineiros	-	18°15'52"S	53°06'26W	4.85	24.2°	7.4

Table E-2b (continued):

Sample			Location		Field Measurements		
ID	**Name**	**Date**	**Latitude**	**Longitude**	**pH**	**Temp. (ºC)**	**Cond. (µS/cm)**
NIO 003	Nioaque	-	21º09'36"S	55º49'24"W	6.53	27.0	144.0
POL001	Pólvora	-	18º15'04"S	54º02'20"W	6.02	26.4	63.1
PCO001	Pont. do Coxo	-	19º00'55"S	53º54'05"W	7.61	28.9	141.3
RCO 010	Rochedo	-	20º18'04"S	54º46'02"W	6.94	27.0	92.6
ETA 001	S. G. Oeste	-	19º23'45"S	54º34'11"W	5.51	24.5	8.5
SP144	São Pedro	-	22º31'58"S	47º54'00"W	6.5	22.2	14.0
SP052	São Simão	-	21º18'58"S	47º33'00"W	6.3	25.0	60.0
SP054	São Simão	-	21º27'58"S	47º38'00"W	6.5	25.0	84.0
SP039	Serrana	-	21º12'00"S	47º37'00"W	6.38	26.0	129.0
GO009	Serranópolis	-	18º23'10"S	53º53'38"W	5.01	25.0	10.2
SID910	Sidrolândia	-	21º13'00"S	54º50'11"W	6.21	26.4	71.6
SP076	Sta.Rosa Vit.	-	21º31'34"S	47º27'22"W	6.6	24.0	33.0
CNV001	Terenos	-	20º20'05"S	54º54'30"W	5.89	26.8	79.8

Table E-2c: Groundwater samples from the confined part of the GAS: Sample details and field measurements (Gastmans et al., 2010a)

Sample			Location		Field Measurements		
ID	**Name**	**Date**	**Latitude**	**Longitude**	**pH**	**Temp. (°C)**	**Cond. (µS/cm)**
CGR 172	C. Grande	-	20°25'02"S	54°33'50"W	7.93	36.0	208.00
CGR 174	C. Grande	-	20°28'14"S	54°38'22"W	8.17	36.2	136.50
CGR 160	C. Grande	-	20°30'58"S	54°36'56"W	7.71	29.9	128.50
CGR 152	C. Grande	-	20°33'10"S	54°36'38"W	7.62	34.0	111.10
CGR 176	C. Grande	-	20°33'30"S	54°34'15"W	7.06	37.2	128.80
CGR 168	C. Grande	-	20°33'36"S	54°39'04"W	6.61	33.6	85.70
ETA 002	S. G. Oeste	-	19°24'06"S	54°34'35"W	5.80	24.3	20.70
CTR 095	Costa Rica	-	19°01'07"S	53°00'55"W	5.94	25.5	27.10
CTR 096	Costa Rica	-	19°01'43"S	53°00'52"W	6.47	26.0	48.80
CTR 004	Costa Rica	-	18°31'59"S	53°08'23"W	6.42	26.5	60.40
CTR 005	Costa Rica	-	18°33'02"S	53°07'39"W	6.42	27.5	48.20
SID 010	Sidrolândia	-	21°15'24"S	54°57'46"W	7.44	30.2	133.10
SID 007	Sidrolândia	-	20°56'26"S	54°57'37"W	7.88	29.0	180.70
MAR 004	Maracaju	-	21°03'13"S	55°09'55"W	7.96	27.0	156.00
MAR 008	Maracaju	-	21°36'00"S	55°09'37"W	7.48	28.9	148.80
CAS 001	Cassilandia	-	19°07'26"S	51°44'01"W	6.00	28.2	42.20

Table E-3a: Groundwater samples from the Sera Geral basaltic aquifer: Major anions, cations, SiO_2 and pCO_2 (Hutcheon pers. comm.)

	Anions (mg/L)				Cations (mg/L)					
ID	**HCO_3^-**	**NO_3^-**	**Cl^-**	**SO_4^{2-}**	**Ca^{2+}**	**Mg^{2+}**	**Na^+**	**K^+**	**SiO_2(mg/L)**	**pCO_2 (atm)**
1	51.58	-	1.00	-	7.94	3.58	2.18	0.71	25.6	0.0275
3	31.86	10.80	9.50	-	8.40	5.03	2.08	1.02	19.1	0.0822
4	27.38	20.20	12.40	-	9.59	4.81	3.40	1.24	19.9	0.0712
5	52.14	32.10	6.80	-	13.30	6.61	3.25	1.70	20.6	0.0536
8	62.57	-	0.00	-	7.73	3.14	3.30	3.24	17.5	0.0041
9	40.64	-	0.00	-	5.68	2.83	2.17	0.53	21.6	0.0104
11	15.38	-	0.00	-	2.28	1.06	0.70	0.32	10.3	0.0081
12	77.00	9.30	3.30	-	14.90	5.83	3.74	0.95	25.9	0.0040
13	78.57	13.50	3.55	-	2.91	4.71	2.00	1.25	41.4	0.0079
17	74.04	-	3.20	-	15.23	3.21	2.00	2.00	28.2	0.0033
23	47.39	-	3.55	-	3.45	3.75	2.00	1.25	31.0	0.0002
25	60.65	1.10	6.39	-	3.36	3.61	1.00	0.75	30.3	0.0005
30	102.50	-	8.52	-	10.90	8.78	2.00	2.25	38.7	0.0051
31	41.19	-	5.68	-	4.09	5.24	4.00	1.50	38.2	0.0053
32	118.30	11.10	67.45	-	34.54	10.70	16.00	1.00	40.9	0.0004
33	119.70	0.60	7.10	13.60	8.18	3.52	24.00	0.75	49.6	0.0024
35	100.90	0.70	4.97	-	11.36	2.52	18.00	0.50	34.0	0.0020
37	34.39	-	-	-	5.28	1.96	1.41	1.18	19.1	0.0010
69	84.15	10.40	2.90	-	18.30	4.31	4.45	0.55	22.8	0.0144
70	59.53	-	-	-	9.01	3.14	3.16	1.93	22.2	0.0355
71	61.27	-	-	-	10.50	0.95	6.50	0.68	17.5	0.0027
73	95.44	16.20	72.60	-	39.20	9.64	13.60	0.79	23.4	0.0016
76	118.10	-	4.97	-	18.20	4.71	3.00	1.75	36.0	0.0023

Table E-3b: Groundwater samples from the unconfined part of the GAS: Major anions, cations, SiO_2 and pCO_2 (Gastmans et al., 2010a)

	Anions (mg/L)				Cations (mg/L)					
ID	**HCO_3^-**	**NO_3^-**	**Cl^-**	**SO_4^{2-}**	**Ca^{2+}**	**Mg^{2+}**	**Na^+**	**K^+**	**SiO_2**	**pCO_2 (atm)**
ALC003	51.24	22.21	2.01	0.32	19.90	1.80	0.50	6.80	40.80	0.0325
SP066	33.46	< 0.05	1.00	< 0.50	6.80	2.90	2.90	4.20	3.00	0.0005
ARE 001	22.17	< 0.05	0.31	0.32	2.02	1.66	0.16	5.69	23.16	0.0537
SP162	6.99	< 0.05	0.40	< 0.50	1.00	1.60	0.30	1.90	14.00	0.0073
BAI001	21.08	< 0.05	0.52	0.30	2.70	0.50	0.30	6.90	30.64	0.0821
BQR001	37.77	1.02	0.52	0.25	7.30	1.60	1.30	5.30	32.23	0.0355
SP149	4.99	0.77	1.00	< 0.50	0.90	0.60	0.80	2.90	19.00	0.0056
SP150	3.00	0.38	1.20	< 0.50	0.80	0.40	0.30	0.80	11.40	0.0036
CAM 016	160.30	< 0.05	0.33	0.18	25.44	13.56	1.11	5.58	11.23	0.0013
CAM 004	100.80	< 0.05	0.54	0.31	15.30	9.97	0.50	4.57	11.55	0.0013
CAM018	112.90	0.45	0.65	0.36	22.80	8.50	1.70	4.70	14.71	0.0025
COR 001	41.64	0.05	1.30	1.00	5.71	2.26	0.53	6.29	27.43	0.0176
DIR 901	29.03	1.26	2.63	0.26	3.10	2.91	3.28	3.20	24.77	0.0381
DIR001	12.77	< 0.05	0.65	0.28	1.50	0.60	0.80	3.30	23.98	0.0013
SP085	32.64	0.14	1.00	< 0.50	7.50	6.50	2.10	4.60	4.00	0.0011
FIG 004	70.95	0.92	1.24	0.29	14.42	2.67	0.75	4.98	24.96	0.0098
SP049	21.94	0.05	1.00	< 0.50	4.40	1.90	1.30	3.30	3.00	0.0059
ITA 005	43.73	5.84	10.30	1.00	8.91	4.06	4.43	1.88	50.14	0.0151
SP104	1.99	< 0.05	0.50	< 0.50	0.30	0.60	0.00	0.10	7.30	0.0073
SP128	5.00	< 0.05	0.50	< 0.50	0.80	0.40	0.30	1.40	13.90	0.0073
JAD901	36.30	< 0.05	0.53	0.26	6.40	1.70	1.60	3.50	34.39	0.0580
GO008	12.14	< 0.05	< 3.00	< 3.00	7.80	1.00	0.57	3.00	29.79	0.0067
JAU001	1885.90	< 0.05	0.63	0.41	33.30	11.50	11.10	5.10	16.24	0.0072
GO004	7.29	0.13	< 3.00	5.00	0.24	0.08	0.10	0.03	9.21	0.0048

Table E-3b (continued):

	Anions (mg/L)				Cations (mg/L)					
ID	**HCO_3^-**	**NO_3^-**	**Cl^-**	**SO_4^{2-}**	**Ca^{2+}**	**Mg^{2+}**	**Na^+**	**K^+**	**SiO_2**	***p*CO_2 (atm)**
GO005	0.49	0.07	< 3.00	< 3.00	0.16	0.08	0.07	0.03	9.86	0.0074
NIO 003	77.89	2.56	3.20	1.00	19.80	2.21	3.57	2.30	41.79	0.0237
POL001	37.79	1.70	0.88	0.24	5.00	2.00	1.00	9.20	41.08	0.0375
PCO001	100.70	< 0.05	0.52	0.47	23.80	4.30	2.90	4.30	14.01	0.0026
RCO 010	35.39	0.29	0.35	0.23	7.10	4.33	2.22	1.11	37.48	0.0042
ETA 001	4.08	< 0.05	0.31	0.12	0.14	0.75	0.04	0.39	11.01	0.0132
SP144	6.00	0.32	1.50	< 0.50	1.30	1.00	0.00	0.70	12.40	0.0019
SP052	9.96	0.29	4.00	1.00	4.80	4.10	2.60	2.10	2.00	0.0051
SP054	28.85	0.32	4.00	< 0.50	10.90	3.70	1.90	1.70	2.00	0.0093
SP039	44.70	1.06	4.50	< 0.50	12.00	7.00	3.50	1.50	3.00	0.0191
GO009	3.90	0.76	< 3.00	< 3.00	0.42	0.23	0.25	0.29	10.71	0.0399
SID910	36.76	< 0.05	0.58	0.29	5.50	2.80	1.70	1.30	35.23	0.0236
SP076	13.95	< 0.05	< 0.50	< 0.50	3.40	0.60	0.00	2.00	9.80	0.0361
CNV001	48.77	4.51	1.39	0.31	8.80	3.80	4.50	1.20	64.86	0.0651

Table E-3c: Groundwater samples from the confined part of the GAS: Major anions, cations, SiO_2 and pCO_2 (Gastmans et al., 2010a)

	Anions (mg/L)				Cations (mg/L)					
ID	**HCO_3^-**	**NO_3^-**	**Cl^-**	**SO_4^{2-}**	**Ca^{2+}**	**Mg^{2+}**	**Na^+**	**K^+**	**SiO_2**	**pCO_2 (atm)**
CGR 172	102.2	< 0.05	0.24	0.14	18.02	7.73	6.55	4.56	17.68	0.0014
CGR 174	69.57	< 0.05	0.39	0.18	13.81	4.45	0.63	1.77	13.35	0.0005
CGR 160	69.7	< 0.05	0.35	0.38	13.01	4.21	0.81	1.49	32.87	0.0014
CGR 152	65.01	0.28	0.61	0.3	11.5	4.13	0.62	1.64	33.26	0.0017
CGR 176	62.78	< 0.05	0.3	0.13	11.54	4.68	0.9	1.74	38.36	0.0064
CGR 168	38.87	< 0.05	0.3	0.11	7.56	3.42	0.5	1.79	19.69	0.0106
ETA 002	9.883	< 0.05	0.27	0.08	0.91	1.52	0.25	0.44	21.34	0.0161
CTR 095	13.78	0.39	0.43	0.08	1.5	1.48	0.32	0.18	18.39	0.0164
CTR 096	13.74	0.31	0.36	0.26	4.26	3.44	0.41	0.59	14.83	0.0048
CTR 004	23.12	5.97	1.05	0.36	3	3.49	2.91	0.73	14.12	0.0091
CTR 005	14.34	0.26	0.62	0.33	2.96	2.82	1.3	1.63	18.71	0.0058
SID 010	63.88	0.3	0.37	0.3	9.56	4.99	6.71	1.66	19.52	0.0025
SID 007	96.13	< 0.05	0.39	0.11	17.3	6.91	5.17	0.94	23.1	0.0013
MAR 004	81.08	0.31	0.57	0.3	15.64	9.68	3.34	1.61	21.51	0.0009
MAR 008	71.06	0.31	0.39	0.29	37.18	5.92	3.94	1.14	32.91	0.0025
CAS 001	21.17	0.28	0.55	0.28	1.48	1.69	0.21	6.4	14.06	0.0224